Oil Shale Ash as a Source of Calcium for Calcium Carbonate: Process Feasibility, Mechanism and Modeling

OLGA VELTS

TUT
PRESS

TALLINN UNIVERSITY OF TECHNOLOGY
Faculty of Chemical and Materials Technology
Laboratory of Inorganic Materials

Dissertation was accepted for the defence of the degree of Doctor of Philosophy (Chemical and Materials Technology) on October 26, 2011

Supervisor: Lead Research Scientist, Rein Kuusik, Laboratory of Inorganic Materials, Tallinn University of Technology

Co-Supervisor: Senior Research Scientist, Professor Emeritus Juha Kallas, Laboratory of Inorganic Materials, Tallinn University of Technology; Department of Chemical Technology, Lappeenranta University of Technology, Finland

Opponents: Professor Thomas Van Gerven, Department of Chemical Engineering, Catholic University of Leuven, Belgium

Senior Research Scientist, Professor Emeritus Rein Munter, Department of Chemical Engineering, Tallinn University of Technology, Estonia

Defence of the thesis: December 6, 2011, at 11.00 Lecture hall: X-308
Tallinn University of Technology, Ehitajate tee 5, Tallinn

Declaration:
Hereby I declare that this doctoral thesis, my original investigation and achievement, submitted for the doctoral degree at Tallinn University of Technology has not been submitted for any academic degree.

Olga Velts

Põlevkivituhk kaltsiumkarbonaadi toormena: protsessi teostatavus, mehhanism ja modelleerimine

OLGA VELTS

TABLE OF CONTENTS

LIST OF PUBLICATIONS

The thesis is based on seven original articles in peer-reviewed international research journals (hereafter referred to as *Paper I – Paper VII*) and a patent.

I   *Velts, O.*, Uibu, M., Rudjak, I., Kallas, J., Kuusik, R. Utilization of oil shale ash to prepare PCC: leachibility dynamics and equilibrium in the ash–water system. – *Energy Procedia* 2009, 1(1), 4843–4850.

II   *Velts*, *O.*, Hautaniemi, M., Kallas, J., Kuusik, R. Modeling calcium dissolution from oil shale ash: PART 1. Ca dissolution during ash washing in a batch reactor. – *Fuel Processing Technology* 2010, 91(5), 486–490.

III   *Velts*, *O.*, Hautaniemi, M., Kallas, J., Kuosa, M., Kuusik, R. Modeling calcium dissolution from oil shale ash: PART 2. Continuous washing of the ash layer. – *Fuel Processing Technology* 2010, 91(5), 491–495.

IV   *Velts*, *O.,* Hautaniemi, M., Uibu, M., Kallas, J., Kuusik, R. Modelling of CO_2 mass transfer and hydrodynamics in a semi-batch reactor. – *Materials, Methods & Technologies* 2010, 4(2), 68–79.

V   *Velts*, *O.,* Uibu, M., Kallas, J., Kuusik, R. CO_2 mineral trapping: Modeling of calcium carbonate precipitation in a semi-batch reactor. – *Energy Procedia* 2011, 4, 771–778.

VI   *Velts*, *O.,* Uibu, M., Kallas, J., Kuusik, R. Prospects in waste oil shale ash sustainable valorization. – *World Academy of Science, Engineering and Technology* 2011, 76, 451–455.

VII   *Velts*, *O.,* Uibu, M., Kallas, J., Kuusik, R. Waste oil shale ash as a novel source of calcium for precipitated calcium carbonate: Process mechanism, modeling, and product characterization. – *Journal of Hazardous Materials* 2011, 195, 139–146.

Patent Kuusik, R., Uibu, M., Uus, M., *Velts, O.*, Trikkel, A., Veinjärv, R. Method for eliminating CO_2 from flue gases by calcium compounds containing industrial wastes. – *Patent EE05446B1* (2011), Joint Stock Company Narva Power Plants, Tallinn University of Technology

Copies of these publications are included in APPENDIX A.

Closely related publications

Uibu, M., *Velts, O.*, Kuusik, R. Developments in CO_2 mineral carbonation of oil shale ash. – *Journal of Hazardous Materials* 2010, 174(1-3), 209–214.

Uibu, M., *Velts, O.*, Trikkel, A., Kuusik. R. Reduction of CO_2 emissions by carbonation of alkaline wastewater. – *WIT Transactions on Ecology and the Environment* 116/Brebbia, C.A., Longhurst, J.W.S. (eds.). WIT Press, 2008, 311–320. doi:10.2495/AIR08321

Uibu, M., *Velts, O.*, Trikkel, A., Kallas, J., Kuusik, R. Developments in CO_2 mineral carbonation by oil shale ash. – *Proceedings of the 2nd International Conference on Accelerated Carbonation for Environmental and Materials Engineering,* Rome, Italy, Oct. 1-3, 2008/Baciocchi, R., Costa, G., Polettini, A., Pomi, R. (eds.). Rome, Italy: University of Rome "La Sapienza", 2008, 421–430.

Kuusik, R., Uibu, M., *Velts, O.,* Trikkel, A., Kallas, J. CO_2 trapping from flue gases by oil shale ash aqueous suspension: Intensification and modeling of the process. – *Proceedings of the Third International Conference on Accelerated Carbonation for Environmental and Materials Engineering: ACEME10,* Turku, Finland, Nov. 29 - Dec. 1, 2010/Zevenhoven, R. (ed.). Åbo Akademi University Printing Press, 2010, 227–235.

Velts, O., Kallas, J., Kuusik, R. Modeling of calcium leaching from lime-consisting oil shale combustion ash. – *Proceedings of the Third International Conferencee on Accelerated Carbonation for Environmental and Materials Engineering: ACEME10*, Turku, Finland, Nov. 29 - Dec. 1, 2010/Zevenhoven, R. (ed.). Åbo Akademi University Printing Press, 2010, 323–326.

Uibu, M., *Velts, O.*, Kuusik, R. Aqueous carbonation of oil shale wastes from Estonian power production for CO_2 fixation and PCC production. – *Proceedings of the Conference of Young Scientist on Energy Issues,* Kaunas, Lithuania, May 26-27, 2011, 415–424.

THE AUTHOR'S CONTRIBUTION

I   The author was responsible for conducting the experiments, the interpretation of the results, the calculation work and writing the paper.

II   The author carried out the experiments and wrote the manuscript. The applicant performed the kinetic analysis and process modeling in collaboration with M. Hautaniemi.

III   The author made a major contribution to writing the manuscript and was responsible for planning and conducting the experiments, the interpretation of the results and the calculation work. The applicant performed the kinetic analysis and process modeling in co-operation with M. Hautaniemi.

IV   The author was responsible for planning and conducting the experiments, the interpretation of the results, the calculation work and writing the paper. The applicant had the lead role in planning and performing the kinetic analysis and process modeling.

V   The author completed the experiments, analyzed the results, performed the calculation work and wrote the paper. The applicant had the lead role in planning and performing the kinetic analysis and process modeling.

VI   The author carried out the experiments and was responsible for interpretation of the results and writing the manuscript.

VII   The applicant had the lead role in planning and performing the kinetic analysis and process modeling. The author was responsible for planning and conducting the experiments, the interpretation of the results, the calculation work and writing the paper.

INTRODUCTION

Due to the ever-increasing demand for energy, fossil fuels will continue to be the dominant source of primary energy production globally in the coming decades. Environmentally safe disposal and/or reuse of solid wastes, as well as controlling atmospheric emissions of the greenhouse gas carbon dioxide (CO_2) are currently the key challenges related to the extensive use of fossil fuels (especially low-grade solid fuels) in heat and power production.

In Estonia, about 93% of locally excavated low-calorific fossil fuel - oil shale - is consumed by power plants, which produce over 95% of Estonian electricity and a great part of the nation's thermal power. Combustion of oil shale is characterized by elevated specific carbon emissions (29.1 tC/TJ) due to its high content of mineral carbonates. The power sector is also responsible for producing enormous amounts (~6 Mt annually) of calcium-rich ash, most of which is deposited in waste piles due to current lack of practical applications. This then becomes a source of solid and liquid pollutants.

In order to secure sustainable use of oil shale as a primary energy source, the environmental impacts of oil shale energetics, including CO_2 emissions, should be minimized. Unfortunately, no suitable geological formations are known to exist in Estonia for storing captured CO_2. A possible technology that can contribute to the reduction of CO_2 emissions is CO_2 sequestration by mineral carbonation, an artificial process mimicking the natural weathering of rock, in which metal oxide-bearing materials, for instance natural silicate minerals (serpentinite, olivine) react with gaseous CO_2 to form solid carbonates. Moreover, efforts in the direction of waste minimization have evoked a new strategy for achieving cost-effective CO_2 sequestration processes, *i.e.* upgrading Ca/Mg-containing industrial residues (metallurgical slags, combustion ashes, etc.) into products with high commercial value via the carbonation route. In the context of Estonia, special interest should be paid to oil shale ashes which contain a considerable amount of free lime (10-30 wt%, depending on the combustion technology) as the most active compound. It is our belief, that the usability of oil shale waste ash could be diversified by utilizing it as an inexpensive calcium (lime) source in an indirect carbonation process for producing precipitated calcium carbonate (PCC)-type material. PCC is currently produced in a multi-stage process that requires large amounts of energy and uses expensive high-quality raw material (limestone). PCC production using oil shale ash could have considerable commercial importance in the paint, plastics, rubber and paper industries. Other potential advantages of this approach are safer disposal of wastes, the long-term fixation/storage of CO_2 emissions and alkaline wastewater neutralization.

While implementation of oil shale ashes as sorbents for binding CO_2 from flue gases in direct aqueous carbonation has been found to be promising, this process produces a mixture of carbonation products and residual ash from which the separation of individual components is difficult. In indirect (or multi-step)

processes, the component of interest (Ca ion) is first extracted from the waste material into an aqueous solution, which is then reacted with flue gas CO_2 to form a solid precipitate in the next stage. The indirect aqueous process is currently considered as the most attractive route for producing separate streams of carbonates and other materials for further recovery. Despite the more complex reactor system, a major advantage compared to the direct process is that there is no need for balancing dissolution and precipitation reactions in a single vessel. This new and attractive alternative, however, requires basic and applied research to fully understand the mechanisms involved before this type of technology can be applied on an industrial scale.

Therefore, the objective of this work was to generate a knowledge base that can lead to the development of a new method for converting lime-containing oil shale waste ash into PCC, a valuable commodity, using ash as a source of calcium. In achieving this goal, the mechanisms, kinetics and dynamics of the multi-step process must be understood and the main stages mathematically described. A secondary target was to characterize the crystalline product of this process in terms of composition, particle size, morphology and textural properties over a wide range of operating conditions.

Acknowledgements

LIST OF ABBREVIATIONS AND SYMBOLS

Abbreviations

BET	Brunauer-Emmett-Teller particle surface area determination method
BSF	total sulfur and its bonding forms analysis
CCS	carbon dioxide capture and storage
DAC	direct aqueous carbonation
FBC	fluidized bed combustion
FT-IR	Fourier transform – infrared spectroscopy
IAC	indirect aqueous carbonation
PCC	precipitated calcium carbonate
PF	pulverized firing
SEM	scanning electron microscopy
SSA	specific surface area
TC	total carbon content
TA	thermoanalysis
XPS	X-ray photoelectron spectroscopy
XRD	X-ray diffraction

Chemical compounds, minerals

$CaCO_3$	calcium carbonate (calcite, aragonite, vaterite); limestone
$Ca_3Mg(SiO_4)_2$	merwinite
$Ca(OH)_2$	calcium hydroxide; hydrated lime; portlandite
$CaSiO_3$	calcium metasilicate; wollastonite
Ca_2SiO_4	calcium silicate
$CaSO_4$	calcium sulfate; anhydrite

Symbols

$c\ (c^*)$	specie (equilibrium) concentration in the liquid phase
c_{co2}	CO_2 content in the inlet gas
d_{mean}	mean diameter
D_s	the solid phase effective diffusion coefficient
E	mass transfer enhancement factor
I	ionic strength
$[i]$	molar concentration of the specie i
K	overall mass transfer coefficient
k_H	Henry's law constant
K_i	equilibrium constant
k_{ii}	reaction rate constant
k_L	liquid phase mass transfer coefficient

$k_L a$	volumetric mass transfer coefficient
k_s	solid phase mass transfer coefficient
K_w	water solubility product
M	molar mass
m	the slope of the equilibrium line $q^* = f(c^*)$
N	rotation speed of the stirrer
n	number of theoretical sections
N_i	molar flux of the specie i
P	atmospheric pressure
P_N	stirrer power consumption
Q	volumetric flow rate
$q\ (q^*)$	substance (equilibrium) concentration in the solid (ash) phase
R	radius
R^2	correlation coefficient
S	cross-sectional area
S_0	specific surface area (surface area/volume)
T	temperature
t	time
V	volume
v	average axial velocity of the fluid in the interstitial spaces
z_i	ion charge
Z	height coordinate

Greek symbols

ε	porosity
ρ	density
τ	time

1. LITERATURE REVIEW

The current thesis investigates the possibility of obtaining a precipitated calcium carbonate (PCC)-type material as a valuable by-product from Estonian oil shale waste ash for the long-term storage of carbon dioxide (CO_2) using a multi-step carbonation route.

In this Chapter, a short up-to-date overview of the various CO_2 capture and storage options, including mineral carbonation, is given with an emphasis on the advantages of the latter in general and particularly in the context of industrial residue and by-product utilization. The literature review also provides insight into the production methods for PCC, including alternative approaches to implementing industrial residues. Also, various factors affecting PCC characteristics in the precipitation process are discussed. Furthermore, the environmental issues of importance within the Estonian oil shale-based power production industry are highlighted.

1.1 Aspects of CO_2 capture and storage (CCS)

Today, approximately 85% of the world's energy consumption is based on fossil resources. Unfortunately, fossil fuel-based heat and power production has raised multiple environmental concerns worldwide, including vast amounts of atmospheric emissions of the greenhouse gas CO_2 released as a result of combustion. According to the International Energy Agency (IEA), the global annual energy-related CO_2 emissions were the highest in history in 2010, a record 30.6 Gt. Altogether, power and industrial plants emit more than half of global man-made CO_2 emissions, whereas the other half stem mainly from transportation and buildings. The level of CO_2 in the atmosphere has increased from 280 (1750) [1] to 394 ppm (2011) [2] since the beginning of the industrial revolution, with much of this rise being attributed to the increased use of fossil fuels such as coal, oil and natural gas for energy supply [3]. Carbon dioxide (CO_2) is one of the major atmospheric contributors to the greenhouse effect. The impact of climate change due to the assumed enhanced greenhouse effect is an ongoing problem facing scientists, governments and the general public at a global level. The potential future effects of global climate change include melting of polar ice caps and glaciers, increased extreme weather occurrences such as flooding and droughts, rising sea levels, spreading of diseases and extinction of endangered species [1]. According to the Intergovernmental Panel on Climate Change (IPCC), it is imperative that we prevent a global warming of more than 2ºC in order to stop the most dramatic consequences of climate change. As our standard of living improves, world energy consumption will increase significantly and drawing alone on measures such as (*i*) improving the efficiency of energy production and utilization, (*ii*) increasing the use of renewable (solar, wind, biomass) energy sources or nuclear energy and (*iii*) the

expansion of natural CO_2 sinks by forestation, will be insufficient to combat the greenhouse emissions challenge [1].

   Carbon dioxide capture and storage (CCS), also known as "*CO_2 sequestration*" is internationally considered to be one of the most promising emerging technological concepts for reducing atmospheric emissions of CO_2 in the relatively short term. In CCS technologies, instead of being discharged directly into the atmosphere, the flue gas from a stationary CO_2 source, such as a fossil fuel-powered energy plant, is directed to large tanks where the CO_2 is separated from a mixture of several different gas components to get the smallest possible volume for transport and storage as well as to eliminate possible corrosion problems. This separation process is often referred to as *CO_2 capture*. After capture, dried and compressed CO_2 is transported to a suitable storage location, either by pipeline or by ships, and subsequently stored for long-term isolation from the atmosphere [4]. The concept of CCS is portrayed in the Fig. 1, demonstrating CO_2 storage options.
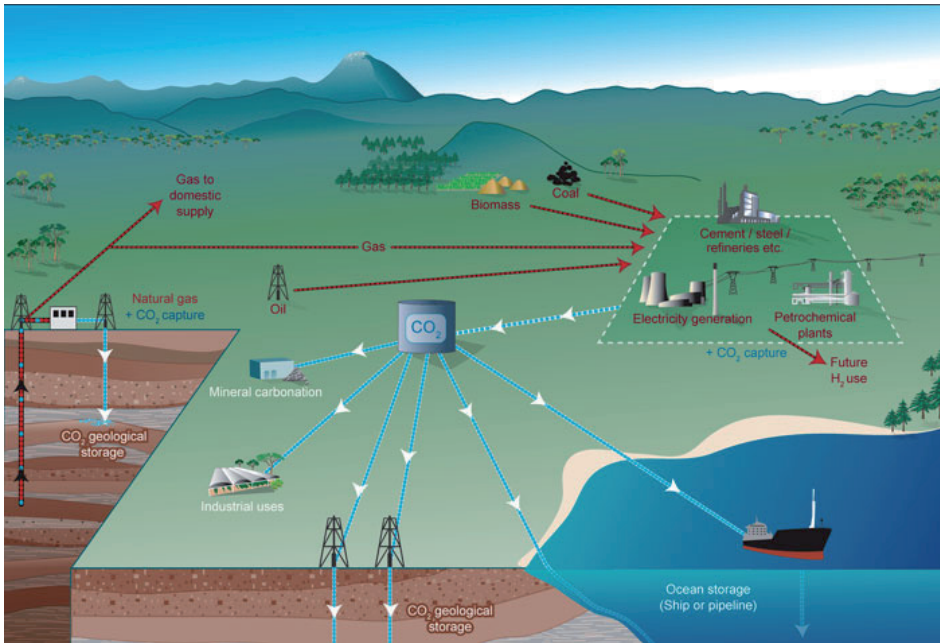
Figure 1. Schematic diagram of possible CCS systems [4, 5]

   There are three main types of ***CO_2 capture*** systems: post-combustion, pre-combustion and oxy-fuel combustion. In a *post-combustion process*, CO_2 is separated and captured from the flue gases after combustion. With *pre-combustion carbon capture* CO_2 is trapped before the fossil fuel is burned. In this case, the fossil fuel is partially oxidized, for instance in a gasifier, and the resulting syngas (CO and H_2) is converted into CO_2 and more H_2. The CO_2 is captured from a relatively pure exhaust stream before combustion takes place

and the H_2 is used as fuel. A third option (called *oxy-fuel combustion*) is to combust the fuel (coal, gas) with pure oxygen instead of air, resulting in a flue gas comprising mostly CO_2 and water vapor that are separated by cooling and compressing the gas stream. This promising technique is still under development as the challenge is to efficiently separate pure oxygen from air [4-6].

A number of separation methods exist for CO_2 capture, the most common commercially available technology being absorption with monoethanolamine (MEA) followed by stripping with steam [7]. This technology in its current state is energy-intensive and costly [4]. To overcome the limitations of the existing systems, numerous other technologies are being developed, including new absorption liquids [8, 9], adsorption systems [10], gas separation membranes [5, 11], cryogenic separation methods [12] and chemical-looping combustion [13, 14]. The available technology captures about 85–95% of the CO_2 processed in a capture plant. Many of the post-combustion capture systems have the advantage that they can become add-ons in existing fossil fuel burning power plants. The post-combustion process, however, requires a lot of energy to compress the gas enough for transport. The pre-combustion process is lower in cost, but cannot be retrofitted on older power plant generators [4].

Storage of CO_2 is envisaged either in deep geological formations [15-17], in deep ocean masses [18, 19], or in the form of mineral carbonates [20] (Fig. 1). *Geological storage* involves injecting CO_2, generally in supercritical form, directly into underground geological formations below the Earth's surface. Depleted oil and gas fields [21], saline formations [22] and unminable coal seams [23] have been suggested as storage sites. Various physical (*e.g.* highly impermeable caprock) and geochemical trapping mechanisms would prevent the CO_2 from escaping to the surface [24, 25]. From the proposed methods for CO_2 *deep ocean storage,* (*i*) CO_2 dispersal in a very dilute form at depths of 1000-2000 m is thought to be the most promising in the short-term. Other options include (*ii*) discharge at 3000 m to form a lake of liquid CO_2 on the seabed; (*iii*) formation of a sinking plume to carry most of the CO_2 into deeper water; (*iv*) release of solid CO_2 at depth [4].

Although the list of possible demonstration projects is growing, there are currently only four full-scale CO_2 projects in operation worldwide which are involved in removing CO_2 from natural gas and sequestering it in geological formations nearby [4, 6]: (*i*) the Sleipner project in the North Sea off the western coast of Norway [26]; (*ii*) the Snohvit project in the Barents Sea north of Norway; (*iii*) the In Salah project in Algeria and (*iv*) the Weyburn project in Canada, where CO_2 is injected into an oilfield for the purpose of enhanced oil recovery (EOR).

The largest potential for CCS as a strategy for reducing CO_2 emissions is fossil fuel power plants. However, current CCS technologies require a lot of energy to implement and run; up to 40% of a power station's capacity, most of which is for capture and compression [4, 27]. In addition to cost, a major environmental concern within the CCS scheme is the risk of CO_2 leakage from

underground or submarine storage into the atmosphere. In the case of deep ocean storage, there is also a risk of greatly increasing the problem of ocean acidification. Higher water acidity adversely affects marine life. Another issue is that dissolved CO_2 would eventually equilibrate with the atmosphere, so the storage would not be permanent [28, 29]. Geological storage would require infinite continuous monitoring of the large amounts of concentrated CO_2 present, because of possible leakage or accidental rapid release of CO_2 into the atmosphere, which may cause health risks due to asphyxiation and/or inflict measurable ecosystem damage [30, 31]. Furthermore, barriers such as public perception, regulatory issues and the risk of induced seismicity [4] will most likely slow down the implementation of subsurface CO_2 storage and will in turn attract interest towards alternative CCS sequestration techniques. Among these is *mineral carbonation* that can potentially store large amounts of CO_2 in a safe, permanent and environmentally benign manner. This topic is the subject of the following Section 1.2.

1.2 Mineral carbonation

1.2.1 Basic principles and advantages

Mineral carbonation was first mentioned as a CO_2 binding concept by Seifritz [20] and discussed further by Dunsmore [32]. However, Lackner *et al.* [33] were the first to provide the details and foundation for today's research efforts. In the context of CCS, the term "*mineral carbonation*" also known as "*mineral sequestration*" involves a process where a high concentration CO_2 from a capture step is brought into contact with a metal oxide-bearing material that contains alkaline-earth metals (such as calcium and magnesium) with the purpose of fixing the CO_2 as insoluble carbonates [4]. The basic idea behind mineral CO_2 sequestration is the imitation of natural weathering processes in which calcium or magnesium containing minerals react with gaseous CO_2 and form solid carbonates:

$$(Mg,Ca)_xSi_yO_{x+2y+z}H_{2z} + xCO_2 \rightarrow x(Mg,Ca)CO_3 + ySiO_2 + zH_2O \qquad (1)$$

Suitable raw materials are abundant primary Ca- and Mg-minerals such as olivine, serpentine and wollastonite. Also, several Ca-rich alkaline solid industrial residues seem particularly suitable for niche applications of CO_2 sequestration [34]. Mineral carbonation can be carried out either *ex situ* [35] (Fig. 2) in a chemical processing plant after mining and pretreating the material, or *in situ* [36] by injecting CO_2 into silicate-rich geological formations or in alkaline aquifers [4]. Furthermore, two main types of process routes for mineral carbonation can be distinguished, mainly *direct* and *indirect* (or *multi-step)* routes. Direct carbonation of a suitable feedstock takes place in a single-step process, either in a gas-solid or a gas-liquid-solid process [37, 38], whereas an

indirect (or multi-step) process comprises routes [33] in which the reactive components (Ca or Mg) are first extracted from the mineral matrix and subsequently carbonated in a separate process step [39].
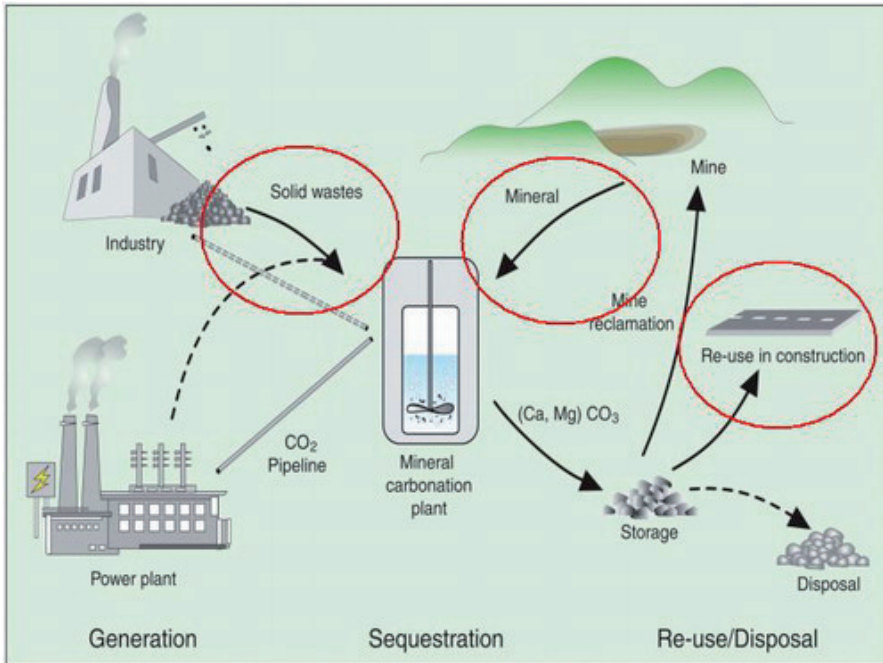
Figure 2. Schematic view of ex situ mineral CO_2 sequestration [4]

CO_2 sequestration by mineral carbonation has a myriad of unique advantages that motivate the need for mineral sequestration R&D, including:

- *Long-term stability:* Mineral carbonation is thermodynamically favorable because carbonates have a lower energy state than CO_2 [33]. The produced mineral carbonates are known to be environmentally safe and stable over geological time frames (millions of years);
- *Vast potential sequestration capacity:* The suitable raw materials are abundant across the globe. For instance natural Ca-Mg-silicate (serpentinite, olivine minerals) deposits are sufficient to fix the CO_2 that could be produced from the combustion of all fossil fuel resources [4];
- *Potential to be economically viable:* The overall process is exothermic. Nevertheless, the production of value-added by-products during the carbonation process may further compensate its costs.

In light of these features, mineral carbonation is attracting interest as an alternative CO_2 abatement technique in many countries, especially those without geological storage sites.

1.2.2 Carbonation of natural minerals (Ca/Mg-silicates)

1.2.2.1 Carbonation reaction engineering

Carbonation of naturally-occurring minerals is extremely slow in nature; therefore, the challenge is to speed up the reaction to be able to design an economically viable process. Various strategies have been explored to intentionally accelerate the weathering of Ca and Mg-containing minerals to precipitate carbonate [40]. The simplest process is *direct dry gas-solid* carbonation, *i.e.* the reaction of a particulate metal oxide-bearing material directly with gaseous CO_2 at suitable temperature and pressure levels. This path was initially thought to have high potential and has been studied extensively [*e.g.* 41]. However, it was concluded [42] that the slow reaction rates and thermodynamic limitations (high temperature favors gaseous CO_2 over precipitated carbonates [43]) make it at present not feasible for industrial purposes. While some investigations into *multi-step gas-solid* carbonation options continue [44], most research has focused on more attractive alternatives.

Significant attention has been dedicated to the *direct aqueous carbonation* process [*e.g.* 37, 45] in which a Ca/Mg silicate is carbonated directly in an aqueous suspension. One of the options suggested for maximization of the carbonation rate is raising the temperature, although the enhancement of reaction rates upon a temperature increase is counteracted by a decrease in the solubility of carbon dioxide in the water phase. Hence, an optimum temperature for olivine and serpentine is typically kept below 200°C in aqueous systems [37, 46].

Many researchers [*e.g.* 38, 47] have reported that metal oxide dissolution constitutes the rate-limiting step, which is thought to be controlled by the diffusion of Mg/Ca through a Mg/Ca-depleted silica-rich layer around the mineral particle. The release of metal ions from the solid raw materials could be accelerated by activating the mineral to make it more labile and reactive. Different methods of pre-treatment of the solid feedstock, aimed at an increase of the carbonation rate, have been investigated, including size reduction, heat activation, surface activation techniques, magnetic separation and other pre-treatment options [4, 34]. Some examples include high-energy attrition grinding for olivine and wollastonite to induce imperfections into the crystal lattice [46, 48], heat-treatment at 650ºC for serpentine to remove the hydroxyl groups and create an open structure [49], surface activation by treatment with acids, steam [50], supercritical water [49] and magnetic separation of the iron compounds prior to the carbonation process [50]. Although significant improvement of the carbonation rate has been obtained after some pretreatment options, the only available pre-treatment option that has proven to be energetically and potentially economically viable is conventional grinding [37].

Alternatively, the release of Ca^{2+}/Mg^{2+} ions from the mineral can be enhanced by the presence of additives or catalysts in solution, affecting ionic strength or forming complexes with dissolved Ca or Mg, *e.g.* Cl^- [4, 34]. Salt

additives that have been used in carbonation studies include NaCl, NaHCO$_3$, (Na/K)NO$_3$ and KHCO$_3$ [37, 49, 51]. Catalysts that can be added to the aqueous solution to enhance the dissolution of silicate minerals include strong and weak acids, bases and chelating agents [52-54].

In addition to the direct carbonation pathway, Lackner *et al.* [33] initiated research into *indirect carbonation* using hydrochloric acid as a leaching agent to extract Ca or Mg from a silicate matrix. Several process schemes, such as the acetic acid route [52], two-step aqueous carbonation [55] and the pH swing process [56], have been proposed and studied involving the extraction of the reactive compound (Ca or Mg), conversion to a (hydr)oxide and subsequent carbonation. In the case of the indirect route, the reaction rate is generally higher and the CO$_2$ pressure required for carbonation is lower than in direct process routes. However, cost-effective and energetically feasible recovery and recycling of the extraction agent is still a key hurdle associated with indirect process routes [4, 39].

1.2.2.2 Conclusions on aqueous carbonation of minerals

While the understanding of the potential reaction pathways has improved significantly based on research to date, there are several technical challenges hindering the industrial implementation of mineral carbonation. The process is currently too slow and energy-intensive for practical applications despite the abovementioned attempts to speed up the carbonation reaction. Demanding reaction conditions (high pressure and moderately elevated temperature) contribute to process expense. Another major hurdle that must be overcome is the complete recovery of all the chemical species involved. An important aspect to be considered as well is the environmental impact from mining minerals and carbonation processes [4]. Hence, the costs of CO$_2$ sequestration by mineral ore carbonation processes are relatively high compared to other CO$_2$ storage technologies and CO$_2$ market prices. However, the profitability of the mineral carbonation process can be made more attractive through applications based on the use of solid residues as feedstock and/or on upgrading industrial waste materials into valuable commercial products. These aspects are discussed in the following Section 1.2.3.

1.2.3 Carbonation of industrial residues and by-products

In addition to the use of natural mineral ores as feedstock for CO$_2$ mineralization, alkaline Ca- and Mg-containing waste residues, such as ashes from coal- and oil shale-fired power plants [57-63], steel slags (electric arc furnace slag, EAFS; basic oxygen furnace steel slag, BOFS; ladle furnace slag, LFS) [64-67], municipal solid waste incineration (MSWI) ashes [68-71], air pollution control (APC) residues [72], cement kiln dust (CKD) [73], ordinary Portland cement (OPC) [74], etc. [75] have risen into focus as particularly

promising CO_2 sorbents. These inexpensive materials are often associated with CO_2 point source emissions and tend to be chemically more active than geologically-derived minerals due to their (geo)chemical instability. Consequently, they do not require as much pre-treatment and less energy-intensive operating conditions (lower operating temperature and pressure) are appropriate to achieve sufficient carbonation rates [64]. Some examples of the CO_2 binding potentials as well as the process conditions (solid to liquid ratio, S/L; temperature, t; pressure, P; duration, τ) of alkaline waste materials are described in Table 1.

Table 1. Process conditions and CO_2 binding potentials of alkaline waste materials

Waste	CaO^{total} %	MgO^{total} %	$ThCO_2$ kg/t	Process	CO_2 bound kg/t	Ref.
Coal filter ash (FA)	5.00		35	DAC: 100% CO_2; S/L=0.05-0.15; t=20-60°C; P=10-40 bar	26	[62]
Oil shale ash (PF)	51.2	4.93	350	DAC: S/L=0.1; 15% CO_2; ambient t and P, τ=65min	290	[60]
Lignite FA	29.28	4.47	241	DAC: S/L=1.5; τ=520h	78	[63]
MSWI FA	53.02		337	SDC (semidry carbonation): S/L=25; 100% CO_2; τ=240h	125	[70]
APC	61.13	1.40	369	SDC: S/L=20; 100% CO_2; t=30°C; P=30 bar; τ=10min	250	[72]
CKD	48.03	1.39	319	DAC: S/L ≤ 0.8; 80% CO_2; ambient t and P; τ=1-8d	255	[73]
OPC	64.50	2.90	516	SDC: S/L=0.1; 100% CO_2; P=2bar; τ=24h	290	[74]
EAFS	32.80	10.00	366	DAC: S/L=0.1; 15% CO_2, t=20°C; τ=24h	17	[66]
LFS	58.10	6.20	522		247	
BOFS	49.9	7.7	437	IAC: extraction with 0.5M HNO_3; t=20°C; τ=60min	384	[67]
Red mud	7.77	0.68	129	DAC: S/L=0.1; 15% CO_2; t=20°C; P=1 bar	42	[75]

The theoretical extent of carbonation, $ThCO_2$ in Table 1 was calculated according to Huntzinger *et al*. [73]:

$$\%ThCO_2 = 0.785(\%CaO - 0.56 \cdot CaCO_3 - 0.7 \cdot \%SO_3) + 1.091 \cdot \%MgO + 0.71 \cdot \%Na_2O + 0.468(\%K_2O - 0.632 \cdot \%KCl)) \qquad (2)$$

Most studies have focused on direct residue carbonation conducted in the presence of water due to concerns with indirect routes attributed to heterogeneous composition of wastes (complicated solvent recovery, possible side-reactions and leaching of heavy metals) [34, 70]. Other proposed alternative routes include, according to [34], waste cement carbonation in a two-step aqueous pressure-swing process (*i.e.*, extraction at high CO_2 pressure and subsequent precipitation at low CO_2 pressure) [77], carbonation of waste concrete and steel and blast furnace slags in a two-step process based on aqueous extraction of Ca [76]. Studies on the *direct gas-solid* carbonation of alkaline residues have also been reported. To name a few, in pressurized thermogravimetric analysis experiments with fluidized bed combustion (FBC) ash performed by Jia *et al*. [61], CaO conversion efficiencies up to 60% were achieved when operating at temperatures above 400°C and in a 100% CO_2 atmosphere. In a study by Bachiochi *et al*. [78] on APC residue carbonation, a maximum conversion of 57% was measured at 400°C, implying a storage capacity of 0.12 kg of CO_2/kg of dry solid.

Even though the total amounts of waste materials are too small to substantially reduce CO_2 emissions [34], the possibility of simultaneously binding CO_2 and relieving the hazardous nature of alkaline residues makes this carbonation route attractive. After stabilization by carbonation, the leaching behavior of wastes is often improved, allowing for use in civil engineering applications or for safer final disposal to landfills [71]. Moreover, the production of valuable end-products (*e.g.* precipitated $CaCO_3$ or magnesium carbonate) by co-utilization of CO_2 and industrial residues has been the objective of many studies in recent years [55, 79, 80]. By upgrading these materials into useful green products with high commercial value, economically more feasible CO_2 sequestration processes may be achieved within the CCS value chain, so research in this area continues. This topic is discussed further in Section 1.3.2 in the context of PCC production.

1.3 Production of precipitated calcium carbonate (PCC)

1.3.1 Introduction to PCC and its applications

Calcium carbonate occurs abundantly in several natural minerals (limestone, marble and chalk), comprising approximately 4% of the earth's crust [81]. Natural ground calcium carbonate (*GCC*), obtained by the mechanical treatment of minerals, often does not meet market demand for high-quality product.

Conversely, *precipitated calcium carbonate* (*PCC*), which is produced under controlled conditions, provides the ability to manufacture a product with specific properties. First introduced in England in 1841, PCC, also known as purified, refined or synthetic calcium carbonate with the chemical formula $CaCO_3$, is a fine white powder without odor or taste and is considered non-toxic. PCC can be distinguished from GCC through its finer and more uniform particle size, narrower particle size distribution and higher degree of chemical purity [81-83]. Besides the amorphous phase (ACC), calcium carbonate has three anhydrous crystalline polymorphs (calcite, aragonite and vaterite) and several hydrated forms (monohydrocalcite and ikaite) [84-86]. The most common arrangement for PCC is the hexagonal form known as calcite. Because of its thermodynamic stability under standard conditions and its ability to appear in various morphologies (rhombohedral, scalenohedral, spheroidal, etc.), calcite has proven to be the most important polymorph in industrial applications [82, 87]. Less common is aragonite, which has a discrete or clustered needle orthorhombic crystal structure. Rare and generally unstable is the spherical vaterite calcium carbonate mineral [83]. The different shapes allow PCC to act as a functional additive in paper, adhesives, plastics, rubber, inks, pharmaceuticals, nutritional supplements and many other demanding applications [88, 89]. The global consumption of PCC is largely concentrated in Asia, while other major regions include Europe and North America. World consumption of PCC in 2007 was 13 Mt and is forecasted to grow to 16 Mt by 2012 [90].

PCC is well-established as a filler and coating pigment for premium quality *paper products*. PCC improves paper bulk, brightness, light scattering, fiber coverage and printability [91]. The mean particle size, size distribution and particle shapes are important factors which have an influence on the physical and optical properties of paper [92]. For instance, the particle size affects paper smoothness, gloss and printing characteristics. For filler pigments, 70% of the carbonate particles are smaller than 2 μm, the specific surface area (BET) is ~10 m^2/g and the brightness is greater than 93%. As a coating pigment, the average particle size is 0.4–2.0 μm with a refraction index of 1.49–1.67 and a specific surface area of 4–11 m^2/g. The high refraction index and narrow particle size distribution of PCC promotes sheet light scattering. The ISO brightness for a PCC coating pigment is 95%, which requires very pure limestone as the raw material [82, 93]. The *plastics industry* is another important consumer of calcium carbonate products. In addition to cost savings, the use of calcium carbonate provides improvements in modulus, heat resistance, hardness, shrinkage reduction, color fastness, impact strength and stability. Nano PCCs (less than 0.1 μm in size) control viscosity and sag in automotive and construction *sealants* [94]. Calcium carbonate is one of the most common filler/extenders used in the *paint* and *coatings industry*. Various paint formulas can include products from sub-micrometer sizes to coarse mesh sizes. Calcium carbonate acts as a low-cost extender in paint and is used to improve brightness, application properties, stability and exposure resistance. Coarse products help to

lower gloss and sheer or even provide textured finishes [81, 95]. The *printing ink industry* uses ultrafine PCCs in high-quality letter press and high quality ink [96]. High purity grades of precipitated calcium carbonate are used in *cosmetics, foods* and *pharmaceuticals*. For example, calcium carbonate is used medicinally as an inexpensive dietary calcium supplement, antacid and/or phosphate binder and in the pharmaceutical industry as a base material for tablets of other pharmaceuticals [81, 95].

A wide variety of applications require PCC to have a number of strictly defined parameters (*e.g.*, morphology, structure, size, brightness, oil adsorption and chemical purity). Control of these characteristics is fundamental from the viewpoint of technical application and is closely related to the method of PCC production and the process parameters [87, 89, 97]. This matter is the topic of Section 1.3.3.

1.3.2 Production methods of PCC

PCC can be produced by several methods such as [81] the lime-soda process, the calcium chloride process and the carbonation process. The method predominantly used by alkali manufacturers is the *lime-soda process,* in which a solution of sodium carbonate is treated with excess calcium hydroxide, producing a sodium hydroxide solution and coarse PCC as a by-product. In the *calcium chloride process,* calcium hydroxide is reacted with ammonium chloride, forming ammonia gas and a calcium chloride solution. After purification, this solution is reacted with sodium carbonate to form a calcium carbonate precipitate and a sodium chloride solution. This simple process, however, requires a low-cost source of calcium chloride to be economical and is usually carried out in a satellite facility adjacent to a Solvay process soda ash plant [93]. The most commonly used PCC process is the *carbonation route* (Fig. 3). In this process, crushed limestone is converted into calcium oxide and carbon dioxide by means of calcination in a lime kiln at temperatures in excess of 900°C. The raw material (limestone) used in the PCC process is required to have low manganese and iron content, since these elements have a very negative influence on the brightness of the product. It is also desirable that the limestone should contain above 52.0% CaO, below 4~5% $SiO_2+Al_2O_3+Fe_2O_3$ and 0.1~0.2% Na_2O+K_2O [92]. After calcination, the dry CaO is slaked (hydrated) with water at temperatures of 30-50°C, producing a calcium hydroxide slurry (milk-of-lime). Before carbonation, the process slurry is screened to remove impurities originating from the limestone and then fed to a three-phase stirred tank reactor (*"carbonator"*), either at atmospheric pressure or pressurized, where it reacts with CO_2 obtained from the calcination process [91].
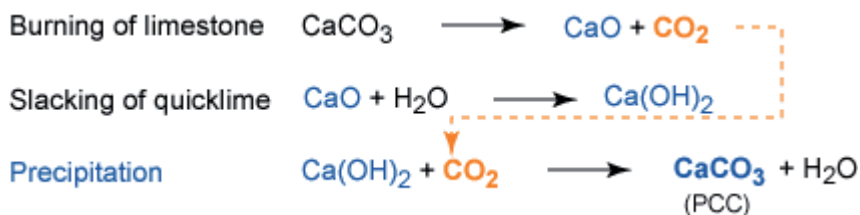
Figure 3. A schematic representation of the PCC production chain

As the calcium ions are consumed in the $CaCO_3$ precipitation reaction, more calcium hydroxide dissolves to equalize the concentration of calcium ions (Ca^{2+}). The rate of dissolution of $Ca(OH)_2$ into Ca^{2+} depends on the dissolution pressure and temperature, while the reaction rate of calcium ions combining with carbonate ions is instantaneous. Therefore, the rates of formation of calcium and carbonate ions are the primary limitations to the overall reaction rate [98].

Upon the completion of carbonation, the product can be further purified by screening followed by dewatering. Rotary vacuum filters, pressure filters or centrifuges are used in the mechanical removal of water. Final drying is accomplished in either a rotary, spray or flash dryer [81]. The required conditions are maintained in the reactor to obtain different grades of precipitated calcium carbonate. The particle size, particle size distribution, particle shape and changes in surface properties of the calcium carbonate particles are dictated by controlling the reaction time, temperature, agitation, pressure, rate of carbon dioxide addition and post-crystallization processing [83, 97]. These aspects are discussed in Section 1.3.3.

Alternative production processes for PCC

Several limitations associated with traditional PCC manufacturing methods (energy-intensive, multiple stages, expensive high-quality raw material) have raised interest in alternative raw materials and improved technological developments. A number of studies have explored the implementation of calcium-containing natural minerals as a lime replacement in PCC production. For instance, Kakizawa *et al*. [52] suggested an alternative method based on the extraction of calcium from a calcium-rich mineral (wollastonite) using acetic acid. A similar concept was investigated by Teir *et al*. [47, 99] aimed at producing a high-value PCC material from wollastonite. Teir *et al*. [99] showed that manufacturing PCC through traditional methods emits 0.21 kg CO_2/kg PCC (assuming oil combustion for lime calcination), whereas the acetic route using wollastonite provides net fixation of 0.34 kg CO_2/kg PCC [100].

Nowadays, the possibility of using industrial wastes as a feedstock for PCC is especially attractive. For example, Katsuyama *et al*. [55] studied the feasibility of producing $CaCO_3$ by first extracting calcium from pulverized waste cement in

a water slurry at high CO_2 pressure, followed by the precipitation of high purity $CaCO_3$ (up to 98% was achieved) from the extracted solution at lower CO_2 pressures. Compared to the commercial price (~7 700 €/m³) for ultra-high purity $CaCO_3$, the production costs using this method were estimated to be significantly lower (~250 €/m³). Kodama *et al.* [101] investigated the pH-swing process for $CaCO_3$ production on the basis of steelmaking slag, where at first the pH of the solution was lowered to enhance the extraction of calcium and then raised in the second step to enhance precipitation. In the patent by Geerlings *et al.* [102], a process utilizing paper bottom ash and steel slag for producing $CaCO_3$ is described, involving the extraction of calcium inside a water-filled stirred reactor for 15 minutes and solid-free hydroxide slurry (1.1 g L^{-1} of calcium hydroxide for paper bottom ash and 0.46 g L^{-1} for steel slag) carbonation with pure CO_2 at a rate of 25 ml min^{-1}. The research described in [79, 103] also focused on steel slag carbonation in the context of producing valuable PCC, additionally addressing problems related to heavy metal leaching during the Ca-extraction phase. Eloneva *et al.* [103] reported that 80–90% pure calcite was produced from blast furnace slag using acetic acid.

$CaCO_3$ obtained from the abovementioned processes is expected to be commercially useful if the properties of the obtained particles meet the requirements for practical applications. Still, as mentioned earlier, significant amounts of required reagents/additives and recycling complexity are major drawbacks of most proposed alternative methods.

1.3.3 Control over the precipitation process

1.3.3.1 Theoretical background

In order to obtain a product of the desired quality, effective control of the precipitation process is necessary. The complexity of the particle size distribution control in a precipitation process is inflicted by the high level of supersaturation generated by the fast reaction. According to Mersmann [104, 105], the important factors for sparingly soluble systems in isothermal precipitation are: (*i*) the concentration of the reactants; (*ii*) the rate of the chemical reaction; (*iii*) the intensity of macro- and micromixing; (*iv*) the dilution of the solution and (*v*) agglomeration. *Nanometer-scale crystals* can be obtained by applying very high primary nucleation rates, which require extremely strong supersaturations. Such high levels of supersaturation can be achieved through: (*i*) a high concentration of reactants; (*ii*) the avoidance of agglomeration (using surfactants, pH control, etc.); (*iii*) rapid quenching or diluting in order to halt growth (a combination of a T-mixer and a stirred vessel; the reactants are mixed in a T-mixer where the chemical reaction takes place, then the suspension is introduced into the vessel operating at a relatively low level of supersaturation); (*iv*) no dilution (T-mixer) in order to produce many nuclei; (*v*) rapid local micromixing and poor macromixing of the reactants; (*vi*) products with high

concentrations and low solubilities and (*vii*) rapid micromixing at the feed point of the reactants for a fast chemical reaction. If a *coarse product* is required, supersaturation must be kept at a low level through: (*i*) the use of low-concentration reactants; (*ii*) good macromixing in the entire precipitator and (*iii*) seeding by recycling the slurry at high rates in order to reduce local supersaturation peaks while keeping primary nucleation at a minimum and promoting crystal growth [106].

The basic factors affecting reactive crystallization have been discussed by Kind [107]. The primary precipitated particles are in the micro- or even nanometer size range. Interfacial forces govern the behavior of suspended particles in these size ranges, as a result of which fine particles are affected by colloidal interactions. Therefore, the final product particles are often secondary, built by the aggregation of fine primary ones. The final product morphology results from the action of aggregation, the rheological behavior of the suspensions and the shear rates present in the precipitator. The primary processes are mixing on the macro, micro and molecular scales, as well as the reaction, nucleation and growth of the particles. The formation of primary crystals depends mainly on the mixing conditions. If mixing does not control reactive crystallization, the crystallization reaction can be best controlled by initial supersaturation. Under ideal mixing conditions, the final primary particles in the nanometer size range are rapidly formed within a few milliseconds and remain unchanged, except in the case of long-term ripening and aging. Aggregation, aging and ripening are secondary processes [106]. The following section reviews the literature on the effect of various factors on the size and shape of PCC particles formed in a precipitation process.

1.3.3.2 Factors affecting PCC particle size and morphology in a precipitation process

In general, the polymorphism of crystalline calcium carbonate depends mainly on the precipitation conditions such as supersaturation [108], pH [109], temperature [110, 111], hydrodynamics [112], conductivity [113] or impurities and additives [114, 115], while the factors and conditions contributing to the change in the particle size of $CaCO_3$ are additives, initial concentration, temperature, initial pH level and (in the case of the carbonation route) CO_2 flow rate [116, 117].

Effect of supersaturation

The three solid phases of calcium carbonate, in order of increasing solubility, are calcite, aragonite and vaterite. The predominant phase to precipitate depends on the supersaturation conditions and the presence of foreign cations and impurities [104, 118].

The degree of supersaturation (S_I) with respect to calcite is defined as $[Ca^{2+}][CO_3^{2-}]/K_{sp}$, where $[Ca^{2+}]$ and $[CO_3^{2-}]$ are the activities of calcium and carbonate ions in the solution, respectively, and K_{sp} is the thermodynamic solubility product of calcite [119]. High supersaturation levels at nucleation and the initial stages of growth result in the formation of amorphous forms of $CaCO_3$ (ACC), vaterite and aragonite [120] which finally transform into the more stable calcite via dissolution–crystallization reactions of various degrees of complexity [121] in agreement with Ostwald's step rule [122]. For instance, Elfil and Roques [123] reported that under high supersaturation in relation to calcite, hydrated forms (ACC) constitute precursors to $CaCO_3$ precipitation, transforming within a few minutes to a mixture of anhydrous polymorphs; at low temperatures (14–30ºC), calcite and vaterite are formed, whereas at high temperatures (60–80ºC), a mixture of aragonite and calcite is obtained. Precipitation of $CaCO_3$ by the aqueous reaction of calcium nitrate and sodium carbonate in a continuous crystallizer was investigated by Chakraborty and Bhatia [124]. Polymorphic nuclei of calcite and vaterite were reportedly generated simultaneously and unstable vaterite tended to be transformed into stable calcite. Different growth rates and aggregation tendencies of calcite and vaterite affected the particle size distribution. These observations were explained in terms of homogeneous and heterogeneous nucleation, which depended on the supersaturation level and ionic ratio of $[Ca^{2+}]/[CO_3^{2-}]$ in solution [125].

In *gas–liquid* reactive crystallization processes, supersaturation of solutions is created by the processes of bubbling, absorption, mixing and chemical reaction, leading to precipitation during crystallization [126]. The most common morphologies of precipitated calcite, obtained via solution and carbonation routes, are rhombohedral and scalenohedral, respectively [113]. As a measure to achieve a morphological change from rhombohedral to scalenohedral shapes, García-Carmona *et al*. [113, 127] proposed an adjustment in electrical conductivity during the semicontinuous carbonation of a $Ca(OH)_2$ suspension. This transition was attributed to the increase of both supersaturation and the $[Ca^{2+}]/[CO_3^{2-}]$ ratio in solution.

Effect of surfactants and additives

Surfactants and additives (*e.g.* metal cations, polyphosphates and other anions and organic compounds) affect particle morphology and size by modifying the precipitation mechanism [128,129].

In the carbonation experiments performed by Xiang *et al*. [130], the diameter of $CaCO_3$ particles synthesized at room temperature decreased from 150 to 90–120 nm after the addition of 0.1–1.0 vol% terpineol due to the ability of terpineol to significantly reduce the surface tension of bubbles, thus preventing aggregation and improving the stability of small bubbles. Higher amounts of terpineol resulted in larger particle sizes with irregular shapes due to inhibition of the CO_2 mass transfer rate. The particle size decreased from 70 to 50 nm

when the EDTA concentration was increased from 0.25 to 1% [129]. However, Feng *et al.* [116] reported that the size of PCC particles obtained in direct aqueous carbonation were larger than previously reported for the additives used.

In a study by Xiang *et al.* [129], the addition of $MgCl_2$ resulted in micrometer-sized spherical and spindle-shaped particles, while spherical $CaCO_3$ particles 0.2 μm in diameter were formed when 1% (w/w) $ZnCl_2$ was used as an additive. According to Yu *et al.* [88], the formation of unusual dendrite-shaped $CaCO_3$ aggregates consisting of two dendrite-like heads composed of radially aligned crystals occurred at a temperature of 80ºC with the addition of polyvinyl alcohol (PVA). Wei *et al.* [131] and Agnihotri *et al.* [132] found that with the addition of a suitable surfactant, the surface area of the $CaCO_3$ prepared through the reaction between $Ca(OH)_2$ suspensions and CO_2 in a bubble column could be increased to a very high value (61 m^2/g). The additives caused the aggregation of fine $CaCO_3$ crystals by neutralizing the charge on the particle surface, thus forming secondary particles with a high surface area and porosity [132]. Also, using the carbonation route, Yang and Shih [133] found that the $CaCO_3$ surface area was markedly increased when sodium polyacrylate (PAAS) at pH 11.4–11.1 and sodium phosphate at pH 6.5–6.2 were used as additives.

Different foreign ions in the fluid during $CaCO_3$ crystallization can potentially be incorporated into the structure of the crystal during the growth process or adsorbed onto specific sites on crystal surfaces which may in turn modify the solvent structure [134] or promote the formation of metastable phases. For example, iron and magnesium have been reported [135] to be effective inhibitors of calcite growth as well as being able to change the dominant precipitated phase from calcite to aragonite [118, 136, 137]. Furthermore, high Mg:Ca ratios seem to play a role in stabilizing ACC [138].

Effect of temperature

It has been observed by Reddy and Nancollas [139] that the proportion of calcite, aragonite and vaterite particles depends on the initial supersaturation and temperature of the solution. Han *et al.* [140] synthesized calcium carbonate by bubbling a CO_2/N_2 gas stream into a $CaCl_2$ solution. Under specified operating conditions, pure aragonite was precipitated at 60ºC while a vaterite/calcite mixture was produced at ambient temperature. In experiments carried out by Yu *et al.* [88], regular plate-like shaped particles in the size range of 6-12 μm were formed at 25ºC, whereas slightly smaller (about 4–10 μm) rhombohedral shaped $CaCO_3$ crystals were observed at 80ºC. This was attributed to the fact that higher temperature altered the solubility of $CaCO_3$ and the increased solubility changed the morphology of the particles. Cheng *et al.* [89] also noted that when the temperature was increased from 25 to 80ºC, particle size decreased from approximately 6–12 to 4–8 μm. On the contrary, Vucak *et al.* [141] reported the formation of particles with coarser particle size at higher temperatures.

Effect of initial concentration

The findings of Wei *et al*. [131] correlate well with those of Agnihotri *et al*. [132] in terms of lower $Ca(OH)_2$ suspension concentrations during carbonation leading to much larger $CaCO_3$ particles with wider particle size distributions. This was attributed to nucleation predominating over crystal growth at higher suspension levels leading to a decrease in particle size.

Effect of the pH level

The influence of the initial pH level of the solution in the $CaCO_3$ precipitation process was investigated by Cheng *et al*. [89]. The authors attributed the loss of control over $CaCO_3$ particle morphology (formation of irregular aggregates) at high pH levels (over 12) to the high supersaturation levels of the initial solution. The size of the primary particles decreased with increasing pH as a result of an increase in the nucleation rate of primary particles. Hostomsky and Jones [142] reported that the morphology of calcium carbonate could be controlled by the pH of the solution in a continuous crystallizer. According to their study, the formation of vaterite in the precipitation reaction of calcium nitrate and sodium carbonate occurs at pH>9.5, but calcite is obtained at pH<8.5. Similarly, Tai and Chen [143] attributed the morphological change of calcium carbonate as being related to the supersaturation level and the pH of the solution.

Other variables

The *CO_2 flow rate* during carbonation can be seen from the literature as one of the main factors in controlling the reaction rate which in turn influences particle size [116]. In a study by Agnihotri *et al*. [132], the particle size was found to decrease with increasing the CO_2 gas flow rate due to the increased shear stress effects as dictated by the gas flow rate and solids concentration [144]. Feng *et al*. [116] studied the influence of *CO_2 bubble size* (with a frit pore size of 17–40 or 101–160 μm) and *CO_2 concentration* (25 and 100 vol%), observing a slight decrease in the size of carbonated particles when smaller CO_2 bubble sizes and lower CO_2 concentrations were used. Xiang *et al*. [129] reported that the use of a *radial sparger* for bubbling CO_2 gas through a $Ca(OH)_2$ slurry improved gas dispersion, leading to a higher carbonation rate and the formation of superfine $CaCO_3$ particles. A recent study by G. Montes-Hernandez *et al*. [117] on the aqueous carbonation of calcium hydroxide in contact with *compressed CO_2* at moderate temperatures demonstrated the synthesis of fine particles of calcite. The particle size of $CaCO_3$ was reported [104] to decrease remarkably with an increase in the *specific power input* due to a strong increase in the nucleation rate and increased probability of breakage and attrition of the crystals.

It can be concluded based on the literature overview discussed here that the relationship between the precipitation conditions and the morphology/size of PCC particles has received a significant attention. Still, there are many unanswered questions and inconsistences among authors. In order to meet demand in terms of practical applications, more effort is needed to understand the combined effects of the operating parameters on $CaCO_3$ characteristics, especially in the case of precipitation from a novel crystallization medium.

1.4 Environmental concerns within the Estonian oil shale-based energy sector

In Estonia, the largest utilization in the world of local oil shale for energy and shale oil production has assured the nation's energetic independence and some of the lowest electricity prices in the European Union. In the first half of 2010, the price of electricity, including taxes, was lower only in Bulgaria [145]. Oil shale gained its leading role in the energy balance of Estonia before the Second World War and although total energy consumption has grown remarkably since that time, oil shale has remained the dominant fuel [146]. The production divisions of the Eesti Energia Narva power plants produce a total of about 9 TWh of electricity each year. Two of the world's largest oil shale-fired power plants in Estonia are Eesti Elektrijaam (1615 MWel per h, 84 MWth) and Balti Elektrijaam (765 MWel per h, 400 MWth). The current technology of processing the oil shale is the combustion of the pulverized fuel (PF) and new fluidized bed combustion (FBC) technology implemented in 2004 [145, 147].

Estonian oil shale is characterized by a high ash content (45-50%), a moderate content of moisture (11-13%) and sulfur (1.4-1.8%), a low net calorific value (8–12 MJ/kg) and a high content of volatile matter in the combustible part. Of the 13–15 million tonnes (Mt) of calcareous kerogenous oil shale mined annually in Estonia, about 93% is consumed by power plants to generate over 95% of Estonian electricity and a great part of its thermal power, with a production of approximately 6 Mt of waste ash annually [145]. Only a small portion of the ash is used for construction materials, road construction and agricultural purposes [147]. The present waste ash management strategy of the national energy company Eesti Energia implements transportation of most of the residue (in the form of a slurry) for deposition in ash fields. The Balti and Eesti power plant ash fields near Narva are Estonia's largest waste handling sites and cover a total of 13 km^2. It is estimated that Estonian power plants have produced ~280 Mt of ash to date [145].

The presence of a considerable amount of free CaO (10-30 wt%, depending on the combustion technology) as the most active compound (Table 2) gives combustion waste ash a high alkalinity [58, 59]. Consequently, the main environmental concern with respect to the disposal of oil shale ash is the formation of highly alkaline leachates (pH 12–13) as a result of leaching processes. These pose a potential long-term environmental risk as neutralization

of ash fields under natural conditions may take hundreds of years [149]. Since Estonia is situated in the Baltic Sea catchment basin, the major issue is that, in the case of leakage, this wastewater might contaminate soil, groundwater and surface water or reach the sea [150, 151].

Table 2. Chemical and phase composition of oil shale ashes

Chemical composition [148]					
Component, % (average value in brackets)					
CaO^{total}	30–60 (41.5)	SiO_2^{total}	20–50 (30)	$Al_2O_3^{total}$	5–15 (9.5)
MgO^{total}	1-6 (3)	$Fe_2O_3^{total}$	2–9 (5.5)	K_2O	2–6 (3.5)
SO_3	3.0–6.5 (4.5)	TiO_2	0.2–1.2 (0.7)	Na_2O	0.1–0.5 (0.2)
Phase composition on the basis of PF ash [60]					
Component, %		α-Ca_2SiO_4			1.99
Calcite, $CaCO_3$	9.55	β-Ca_2SiO_4			16.92
Dolomite, $CaMg(CO_3)_2$	3.34	Melilite, $(Ca,Na)_2(Mg,Al)(Si,Al)_3O_7$			4.99
Portlandite, $Ca(OH)_2$	1.42	Merwinite, $Ca_3Mg(SiO_4)_2$			6.81
Lime, CaO	29.52	Wollastonite 2M, $CaSiO_3$			3.88
Periclase, MgO	4.27	Hematite, Fe_2O_3			1.19
Anhydrite, $CaSO_4$	4.48	Quartz, SiO_2			7.38
Gypsum, $CaSO_4*2H_2O$	0.76	Orthoclase, $KAlSiO_3$			3.51

Combustion of oil shale is also characterized by high CO_2 emissions. Due to the extensive use of oil shale for energy production, per capita CO_2 emissions in Estonia (15.2 metric tonnes in 2007) are about twice the European average and rank 13th worldwide [152]. The export of energy to Finland, Latvia and Lithuania leads to the additional discharge of a large amount of CO_2 emissions. As Estonia is located in the northern, shallow part of the Baltic sedimentary basin possessing potable water, its CO_2 geological storage capacity has been estimated as zero [153, 154]. Thus, alternative techniques for curtailing atmospheric emissions of CO_2 from oil shale-fired power plants are required in hopes of tackling global climate change issues.

Hence, it is imperative that proper management of the solid/liquid/gaseous wastes streams associated with oil shale-based energetics is devised so as to continue the exploitation of oil shale in an environmentally sustainable manner.

1.5 Summary of the literature review and objectives of the thesis

It may be concluded based on the discussion presented in the literature review that a balance is needed between energy security and growing concerns over the impact of increasing concentrations of greenhouse gases in the atmosphere, particularly CO_2. For countries without geological storage sites, such as Estonia, mineral carbonation could be considered as a CO_2 fixation option. Since carbonation securely traps CO_2, there would be little need to monitor the disposal sites and the environmental risks would be very low. Moreover, upgrading industrial wastes into commercial products via the carbonation route is an interesting alternative for Estonia, where the technology used in oil shale processing for heat and power production exerts strong environmental effects. In this context, an idea of implementing lime-containing oil shale ash as a low-cost source of water-soluble calcium in an indirect carbonation process for producing precipitated calcium carbonate (PCC)–type material is of great environmental and commercial interest.

The aim of this thesis was to study the feasibility, mechanism and kinetics of the aforementioned novel process for the long-term storage of CO_2 and the beneficiation of a potentially hazardous inorganic waste material of complicated composition in the form of a valuable commodity. The second equally important goal was to propose mathematical models describing the major stages of the multi-step process, including leaching of the main water-soluble ash components, followed by CO_2 absorption along with precipitation of the solid product in a complex system of ash leachates and CO_2-containing model flue gas. Moreover, such models may also be suitable for other Ca-containing wastes. In order to achieve these tasks, the following steps were taken.

First, leaching (dissolution) dynamics and equilibrium investigations were performed to evaluate the potential of ash (leachates) as an alternative calcium source and to create mathematical models describing Ca^{2+}, SO_4^{2-} and OH^- dissolution from oil shale ash (*Papers I–III*). In addition to calcium, extra attention was drawn to the entire complex of different substances leached from ash in terms of environmental safety as well as possible co-crystallization effects which could influence the quality of the final product.

After establishing the dissolution behavior of the lime-containing ash, the mechanism of CO_2 absorption into an alkaline model solution was experimentally examined (*Paper IV*). The goal was to develop a mathematical description of this stage to improve our understanding of the chemistry and specifics of the CO_2 mass transfer process into alkaline wastewaters such as leaching waters of oil shale ash in used reactor.

Finally, the study proceeded to investigating the precipitation process of calcium carbonate in the gas-liquid system under various operating conditions (*Papers V–VII*). In the comparative laboratory carbonation experiments, ash leachates and $Ca(OH)_2$ model solutions were used as liquid agents. The purpose was:

- to create a mathematical model for the description of changes in the composition of the gaseous, liquid and solid phases in the heterogeneous system of oil shale ash leachate – CO_2-containing flue gas;
- to propose the mechanism of $CaCO_3$ precipitation from alkaline oil shale ash leachates of complex multi-ionic composition;
- to provide a comprehensive characterization (composition, morphology, surface area and particle size) of the precipitates crystallized from oil shale ash leachates under various conditions;
- to determine the influence of operating parameters (gas flow rate, mixing intensity, CO_2 concentration, residence time, pH of the final solution, etc.) on the characteristics of the solid product for process optimization;
- to compare the products obtained on the basis of ash and conventional raw materials in PCC production;
- to provide a preliminary technological evaluation for using oil shale ash and its leaching waters as a precursor in the manufacture of PCC.

2. MATERIALS AND METHODS

2.1 Experimental methods and procedures

An outline of the processes experimentally studied in this work is given in Table 3. The investigations on the *leaching* behavior of the main water-soluble species (primary focus on Ca ions) in oil shale ashes were performed in *batch* and *continuous* modes. The *carbonation* experiments were divided into three series (SET I–III, Table 3) depending on the alkaline liquid agent used. The CO_2 absorption by alkaline *model* solutions was investigated in SET I and II, whereas the ash leachate – CO_2-containing model flue gas system was examined in SET III. The experimental set-ups of the studied systems are described in more detail in the following sub-sections 2.1.2 and 2.1.3.

Table 3. Outline of the systems under investigation

Investigated processes	**Paper**
I. *Leaching/dissolution behavior in the ash – water system*	
i. batch mode leaching of water-soluble species (Ca) from ash	*I, II*
ii. continuous mode washing process of the stagnant ash layer	*III*
II. *Carbonation (precipitation regime) in the gas-liquid system*	
SET I: CO_2 absorption by an NaOH solution representing the Ca^{2+} and SO_4^{2-}-free alkaline model solution	*IV*
SET II: CO_2 absorption by a $Ca(OH)_2$ solution representing the Ca^{2+}-rich and SO_4^{2-}-free alkaline model solution	*V, VI*
SET III: CO_2 absorption by Ca^{2+} and SO_4^{2-}-rich alkaline ash leachates	*VI, VII*

2.1.1 Characterization methods

The characteristics (composition, morphology, surface area, particle size, etc.) of solid samples (ash and carbonation products) as well as the composition and parameters of the liquid phase were determined according to methods briefly described in Table 4.

Table 4. Applied characterization methods

Properties	Characterization method
Solid phase	
Chemical composition[1]	Total CaO (slightly modified EVS-EN 196-2:1997); free CaO [155]; CO_2 (total carbon TC; ELTRA CS-580 Carbon/Sulfur Determinator); total S and its bonding forms (BSF; EVS 644:1995)
Elemental composition (Ca/Mg/Fe/Al/S/K/ MnNa/Zn/Si/Cr/Cu /Ni/PbV/Co/Cd)	IRIS Intrepid II Inductive Coupled Plasma (ICP) Spectrometer (Thermo Electron Corporation, software: thermo elemental validated analysis); solid material initially dissolved in 65% nitric acid in a pre-treatment module (GWB Pressurized Microwave Decomposition)
Particle size distribution	Laser diffraction Multi-Wavelength Particle Size Analyzer (Beckman Coulter, LS 13320); ash samples measured in an ethanol solution
Morphology[2]	SEM (Jeol JSM-8404A)
Specific surface area, total and micropore volume[3]	BET and BJH nitrogen dynamic desorption analysis methods (Sorptometer KELVIN 1042, Costech Microanalytical SC)
Phase composition	Quantitative powder XRD[4] (Bruker D8 Advanced), (diffractograms were analyzed by Siroquant code [156] using full-profile Rietveld analysis [157]); FT-IR spectrometer Interspec 2020 (samples prepared as KBr pellets); Thermoanalyzer (Setaram Setsys 1750) coupled to a FT-IR spectrometer (Nicolet 380)
Brightness[5]	Brightness of PCC samples: ISO 2470:1999
Surface analysis (chemical composition)[6]	X-Ray Photoelectron Spectroscopy (XPS): The XPS spectra were recorded with a Kratos Axis Ultra DLD electron spectrometer using a monochromated Al Kα source operated at 150 W, a hybrid lens system with magnetic lens providing an analysis area of 0.3 x 0.7 mm^2, and a charge neutralizer
Liquid phase	
Chemical analysis	Ca^{2+} (titrimetric method ISO 6058:1984), SO_4^{2-}, Cl^-, K^+, PO_4^{3-} (Lovibond SpectroDirect spectrophotometer), CO_3^{2-}, HCO_3^- and OH^- (titrimetric method ISO 9963-1:1994(E)), pH (Mettler Toledo GWB SG2), conductivity (HI9032 microprocessor), Na/Si/Al/Fe/Mg/Mn/Co/Cr/Cu/Ni/Pb/V/ Zn/Cd (ICP Thermo IRIS Intrepid II XDL)
Gas phase	
CO_2 content	infrared CO_2 analyzer (Duotec)

[1] Performed by H. Ehala at the Laboratory of Inorganic Materials, TUT
[2] Performed by Dr. V. Mikli at the Center of Material Research, TUT
[3] Performed by Dr. M. Uibu at the Laboratory of Inorganic Materials, TUT
[4] Performed by Prof. K. Kirsimäe at the Institute of Geology, UT
[5] Performed by the UPM-Kymmene Corporation (Finland)
[6] Performed by Dr. A. Shchukarev at the Department of Chemistry, Umeå University

2.1.2 Experimental set-ups for leaching behavior studies

Characterization of the oil shale ashes (Papers I, II: Materials and Methods chapter)

The oil shale ash samples used in investigations of the leaching behavior of the main water-soluble species of oil shale ashes (*Papers I-III*) were collected from different points of pulverized firing (PF) or fluidized bed combustion (FBC) boilers at Estonian power plants. The main characteristics of ashes and the average content of the basic elements are given in *Paper I (Tables 1* and *2)* and *Paper II (Table 1)*.

Batch mode (Papers I, II: Materials and Methods chapter)

The leaching dynamics and equilibrium experiments of Ca^{2+} and other ions from oil shale ash were carried out in a laboratory-scale batch reactor with a volume of 800 mL using ash-Millipore water suspensions by varying the solid/liquid (S/L) mass ratios from 1:1250 to 1:10. Depending on the objective, suspensions were well-mixed at a controlled temperature for up to 180 minutes, which was considered sufficient to reach equilibrium. Samples were taken with a syringe and filtered (0.45 μm). The resulting liquid phase was analyzed for chemical composition including the content of heavy metals (see Section 2.1.1; Table 4).

Continuous-flow reactor (Paper III: Experimental chapter)

The leachability of Ca ions from a stagnant oil shale ash layer was investigated in a specially designed continuous mode leaching column *(Paper III: Fig. 1a)*. Ash samples in portions of 60 g (PF1) or 35 g (FBC1) were placed in a column inside a plastic cylinder (height = 3 cm; inner diameter = 4.9 cm) and secured with a filter cloth and metallic mesh in order to obtain a fixed packing area for each sample. Water (10 L) was passed through the ash layer from the bottom of the column and subsequently collected in the solution (leachate) collection container (collector). Samples were taken from the outlet flow of the column and the collector, filtered (0.45 μm) and analyzed for Ca^{2+} content. Experiments were repeated at various flow rates (58-350 mL min^{-1}).

2.1.3 Experimental set-up for the carbonation of alkaline liquid agents

2.1.3.1 Preparation of parental alkaline solutions

Model solutions (SET I and II) (*Papers IV, V: Materials and Methods chapter*)

In SET I, the initial concentration of the NaOH solution and the pH were fixed at 0.01 M and 12.0, respectively. The pH level was chosen to be equal to that of the saturated water – lime-containing ash system. For SET II, initial $Ca(OH)_2$ solutions with various concentrations (350, 600 and 850 mg Ca^{2+} L^{-1})

were prepared by slaking chemically pure lime (Sigma-Aldrich) and filtering the suspension in order to remove any inert or non-dissolved solids.

Alkaline wastewater: ash leachates (SET III) *(Paper VII: Experimental chapter)*

The oil shale PF cyclone ash (8.0% of CaO_{free}, BET 0.26 m^2 g^{-1}) was chosen for the preparation of ash leachates as the most typical PF ash (it amounts to 60% of the total PF ash produced). The ash was dispersed in distilled water (a liquid to solid mass ratio of 10:1 w/w) under atmospheric pressure and room temperature for 15 minutes in a 15 L reactor equipped with a turbine-type impeller (Fig. 4a). The alkaline suspension was filtered from the solid ash residue. The preparation of the alkaline mother solution from waste ash is schematically represented in Fig. 4a.

2.1.3.2 Conditions of aqueous carbonation (Papers IV-VII: Materials and Methods chapter)

All carbonation tests (SET I-III) were performed in a semi-batch barboter-type reactor equipped with a turbine-type impeller to provide effective mechanical mixing of the gas and liquid phases and to increase the interfacial contact area (Fig. 4b). The respective alkaline liquid agents (10 L) were treated with a model gas mixture containing pre-determined concentrations of CO_2 in air (c_{CO2}). The flow rate (Q_G) and composition of the inlet gas were controlled using calibrated rotameters and an infrared CO_2 analyzer. For SET I and III, a 2^3 full-factorial experimental plan was designed in which the process variables were maintained near the center of the operating range (Table 5; *Papers IV* and *VII: Table 1*). Operating variables potentially influencing the absorption/precipitation conditions were varied:

- air–CO_2 gas mixture flow rate, Q_G
- CO_2 concentration in the inlet gas, c_{CO2}
- stirring rate, N

In SET II, the carbonation process was conducted under the same conditions as Regime 1 (Table 5) by varying the Ca^{2+} initial concentration in the solution.

The reactor was operated batch-wise with respect to the liquid phase and continuously with respect to the gas phase. Samples of the suspension were collected through a valve on the reactor body. In each experiment, the volume of the gas phase in the gas-liquid mixture (V_G) and above it (V_{G2}) (Fig. 4b) was registered. During the carbonation, the concentrations of relevant ions in the liquid phase, the pH and the conductivity of the suspension as well as the CO_2 content of the outlet gas flow (see Section 2.1.1; Table 4) were continuously monitored. To elucidate nucleation-growth (morphogenesis) of PCC crystals, the morphological development of the precipitate particles in the course of the experiments in SET II and III was examined.

Table 5. Parameters of the oil shale ash leachates carbonation experiments

TEST nr	Q_G, L h^{-1}	Air flow rate, L h^{-1}	CO_2 flow rate, L h^{-1}	c_{CO2}, vol.%	N[a], rpm
1	1000	950	50	5	400
2	1000	950	50	5	1000
3	1000	850	150	15	400
4	1000	850	150	15	1000
5	2000	1900	100	5	400
6	2000	1900	100	5	1000
7	1500	1350	150	10	700
8	2000	1700	300	15	400
9	2000	1700	300	15	1000

[a]the stirring rate, measured experimentally, corresponds to a specific mixing power consumption 1.1, 2.0 and 3.7 W L^{-1} to provide N = 400, 700 and 1000 rpm, respectively.

When the pH of the solution had stabilized and the CO_2 concentration in the outlet gas became equal to the inlet values, CO_2 addition was stopped. In SET II and III, after the carbonation, the suspension was filtered (using Whatman "blue ribbon" filter paper) and the resulting solid was dehydrated at 105ºC. The solid materials were analyzed for chemical composition, surface properties and particle size distribution (see Section 2.1.1; Table 4) as received with no subsequent washing. The data obtained in the carbonation experiments was used among others in the kinetics evaluation and model validation.

2.2 Modeling software

Kinetic calculations and leaching/precipitation process simulations in this work were performed using the MODEST 6.1 software package [158] designed for various tasks of model building such as simulation, parameter estimation, sensitivity analysis and optimization. The software consists of a FORTRAN 95/90 library of objective functions, solvers and optimizers linked to model problem-dependent routines and the objective function. The differential equations were solved by means of linear multi-step methods implemented in ODESSA, which is based on LSODE software [159]. The partial differential equations were solved numerically and integrated by the method of lines presented in [160] with the appropriate initial and boundary conditions.

a.)

Stirrer

Oil shale ash

H₂O

L/S 10:1 w/w
Mixing time: 15min

Filtration

Leachate

Residual ash

Figure 4. Principal experimental scheme: a) Leaching step; b) Carbonation step
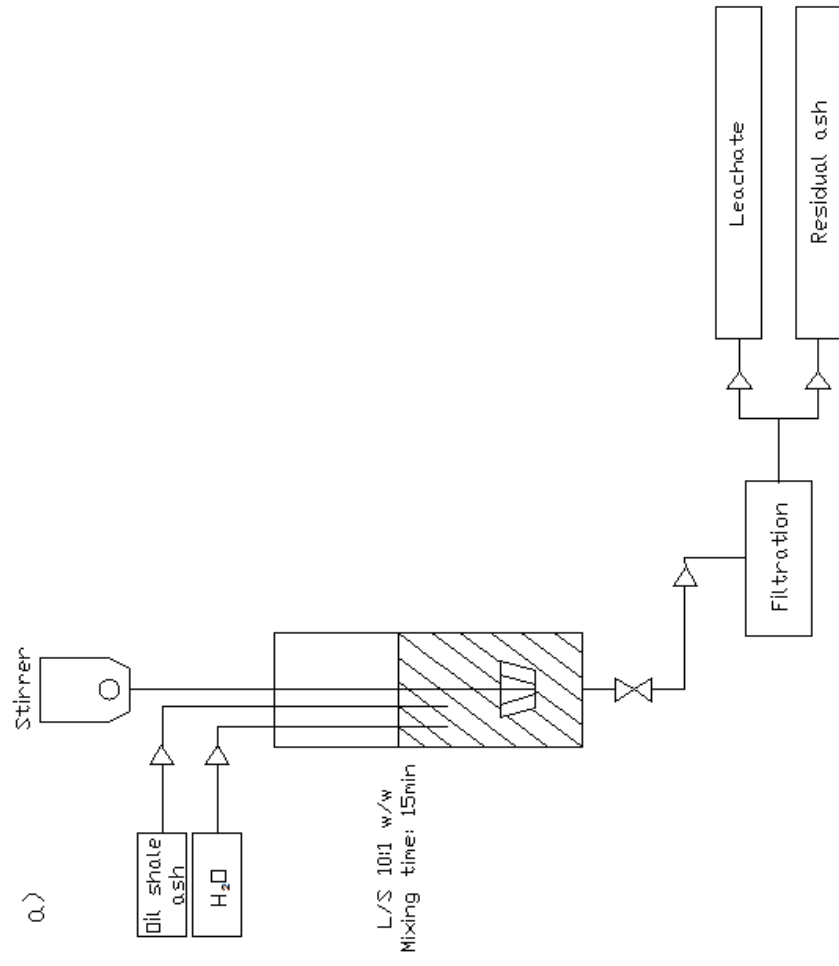
Figure 4. Principal experimental scheme: a) Leaching step; b) Carbonation step

3. RESULTS AND DISCUSSION

3.1 Leachability dynamics, equilibrium and mass transfer in the ash – water system

In the context of PCC production on the basis of oil shale ash, the availability of lime for hydration and carbonation reactions is of prime importance. The complexity of the process is exacerbated by the complicated and significantly variable chemical and phase composition of various types of oil shale ashes. Consequently, different leaching behavior is expected during ash-water contact. For this reason, as a tool for simplifying the first step of the process under discussion, a generalized mathematical dissolution model for the evaluation of changes in calcium (or any other water-soluble substance) concentration upon leaching from ash was composed. Moreover, as calcium-rich ash leachates can be obtained either in a batch reactor *(Papers I, II)* by mixing an ash-water suspension or by washing a stagnant ash layer (leaching column; *Paper III*), calcium dissolution models for both process modes were developed in order to design the appropriate PCC process. Furthermore, understanding the behavior of the main water-soluble compounds in oil shale ashes in the course of leaching also has significance in the field of environmental protection. These aspects are discussed in detail in *Papers I-III* and a brief overview is given in this section.

3.1.1 Dissolution behavior of lime-containing ash

The leaching behavior of the main water-soluble constituents of oil shale ash was investigated in a batch reactor (Section 2.1.2) with a liquid to solid (L/S) mass ratio 10:1 to imitate the hydraulic ash transportation system. When ash is immersed into water, lime slaking, dissociation of portlandite and dissolution of different salts occur. During the first minutes of ash-water contact, the solution becomes deeply alkaline (pH ~12.2) and oversaturated with Ca^{2+} ions (Ca^{2+} = 1.4–1.5 g L^{-1}; *Paper I: Fig. 1*) as in addition to free lime ash also contains other water-soluble Ca-compounds ($Ca(OH)_2$, anhydrite etc.), thus allowing the solution to exceed the equilibrium solubility limit for Ca ions with respect to pure CaO. The latter is an important positive factor in the context of the PCC production process. At the same time, the resulting elevated content of sulfate (SO_4^{2-}) as well as the presence of additional ions characteristic of ash leachates, such as K^+, Cl^-, PO_4^{3-} etc. (*Paper I: Table 3, Paper VII: Experimental chapter)*, could potentially play major roles in the precipitation process. This aspect is discussed in Section 3.2.1, where the average composition of ash leachates obtained in the aqueous extraction step for subsequent carbonation is given. Most importantly, the toxic heavy metals have very low leachability in these conditions (*Paper I: Section 3.1*).

The effect of temperature on the leaching behavior of Ca was also examined (*Paper I: Section 3.3*). Favorable conditions for batch dissolution of calcium

compounds from ash could be achieved at room temperature, which simplifies the first stage of the PCC production process.

Furthermore, for the purpose of Ca dissolution process kinetics evaluation and model validation, a set of Ca leaching dynamics and equilibrium experiments was performed with different ash/water ratios in a batch reactor according to the procedure described in Section 2.1.2. The implementation of the obtained experimental data is discussed in the following Section 3.1.2.

3.1.2 Modeling of Ca and the main water-soluble species dissolution process from ash

The mechanism of Ca leaching from ash was investigated in a batch reactor as well as during a continuous washing process performed in a leaching column. This analysis is mostly reflected in *Papers II* and *III*. As a result, the mathematical models for predicting the outcome of the Ca (or any other water-soluble substance) leaching process from different kinds of Ca-containing ashes were composed *(Papers II, III)*. The models are a set of (partial) differential equations that mathematically describe the changes in Ca content in the solid (ash) and liquid phases in the course of the process. Furthermore, these models allow for estimating the period of time necessary for the species of interest to reach the pre-determined value, a highly relevant aspect in the context of the PCC process and in the field of environmental protection. Moreover, efficient environmental implementation of the developed model for the simulation of large-scale estimations of Ca leaching from ash was also demonstrated *(Paper III)*.

3.1.2.1 Batch process

The leaching (dissolution) of a substance (Ca) from a solid particle into a solution is mathematically similar to the diffusion which takes place during the desorption process. The dynamics of calcium dissolution from ash involves a rate-controlling step of mass transfer inside a spherical ash particle *(Paper I: Fig. 3)*. A mathematical model consisting of differential equations *(Paper II: Eq. 10, 11)* was proposed to describe the leaching mechanism of Ca from ash. Accordingly, in order to predict Ca (or any water-soluble substance) concentration profiles during the batch dissolution process from ash, the following steps of the modeling procedure must be carried out:

1. Determination of Ca (substance) solubility

2. Evaluation of the internal mass transfer coefficient of Ca in the ash particle, k_s

3. Process simulation

The first task implies establishing the equilibrium apportioning of the substance of interest (*e.g.* Ca^{2+}, SO_4^{2-} etc.) between the solid-liquid phases in the form of an equilibrium equation $q^*=f(c^*)$ based on data from the leaching

equilibrium experiments described in Section 2.1.2. A detailed description and the results of this step were reported on the basis of Ca in *Papers I* and *II*. For an estimation of the solid phase mass transfer and effective diffusion coefficients of Ca, k_s and D_s, data on the leaching dynamics obtained from the batch experiments was used to compare with the model predictions. The parameters k_s and D_s were estimated by two different approaches, by Crank's solution given in the literature [161] (*Papers I, II*) and by a numerical solution of the differential equations describing the mass transfer in the ash-water system (*Paper II*). A comparison of both approaches is given in *Paper II (Section 3.2.2)*. The latter was used in further modeling as it is a more precise approach.

As the liquid phase in the batch process is well-mixed, the mass transfer resistance is concentrated in the solid phase and the estimated values of the mass transfer coefficient, k_s, should be the same for one ash in experiments with different dilutions. Thus, considering the k_s values, Ca leaching kinetics from ashes with different characteristics (ash particle size, Ca content) can be evaluated or compared as well as the process simulated for various L/S ratios of the suspension. The details on Ca dissolution process modeling are reported in *Paper II*, where it was shown on the basis of two types of ashes differing notably in their chemical (content of CaO_{free}) and physical structure (BET-surface area, particle mean diameter etc.) that proposed modeling algorithms can be implemented for different ashes.

Furthermore, the Ca dissolution model was later amended according to the modeling algorithm elucidated in this section to allow for the simulation of concentration profiles for other major species participating in the leaching process. The addition of SO_4^{2-} and OH^- ions into a Ca^{2+} system was found to be sufficient to fulfill the electroneutrality constraint of ash leachates at any moment in time during leaching:

$$\sum_i N_i \times z_i = (+2) \times N_{Ca^{2+}} + (-1) \times N_{OH^-} + (-2) \times N_{SO_4^{2-}} \approx 0, \qquad (3)$$

where N_i and z_i are the molar flux and charge of the ith specie. The constraint offers an effective simplification for the solution of many ion-transport problems [162, 163] and has been applied widely.

Consequently, the set of differential equations describing the changes in Ca content in the solid and liquid phase of the perfectly mixed ash-water suspension during leaching *(Paper II)* was complemented by considering the leaching mechanisms of SO_4^{2-} and OH^- ions. The following system of equilibrium relations and model equations (Eq. 4-10) for the solid (ash) and liquid phase was proposed to describe the leaching behavior of the main water-soluble species (Ca^{2+}, SO_4^{2-}, OH^-) from multi-component oil shale ashes:

$$\frac{dc_{Ca^{2+}}(t) \times V \times \varepsilon}{dt} = k_s^{Ca^{2+}} \times V \times (1-\varepsilon) \times S_0 \times (q_{Ca^{2+}} - q_{Ca^{2+}}^*) \qquad (4)$$

$$\frac{dq_{Ca^{2+}} \times V \times (1-\varepsilon)}{dt} = k_s^{Ca^{2+}} \times V \times (1-\varepsilon) \times S_0 \times (q_{Ca^{2+}}^* - q_{Ca^{2+}}) \qquad (5)$$

$$q_{Ca^{2+}}^* = f(c_{Ca^{2+}}^*) \qquad (6)$$

$$\frac{dc_{SO_4^{2-}}(t) \times V \times \varepsilon}{dt} = k_s^{SO_4^{2-}} \times V \times (1-\varepsilon) \times S_0 \times (q_{SO_4^{2-}} - q_{SO_4^{2-}}^*) \qquad (7)$$

$$\frac{dq_{SO_4^{2-}} \times V \times (1-\varepsilon)}{dt} = k_s^{SO_4^{2-}} \times V \times (1-\varepsilon) \times S_0 \times (q_{SO_4^{2-}}^* - q_{SO_4^{2-}}) \qquad (8)$$

$$q_{SO_4^{2-}}^* = f(c_{SO_4^{2-}}^*) \qquad (9)$$

$$\frac{dc_{OH^-}(t) \times V \times \varepsilon}{dt} = 2 \times \frac{k_s^{Ca^{2+}} \times V \times (1-\varepsilon) \times S_0 \times (q_{Ca^{2+}} - q_{Ca^{2+}}^*)}{M_{Ca^{2+}}}$$
$$-2 \times \frac{k_s^{SO_4^{2-}} \times V \times (1-\varepsilon) \times S_0 \times (q_{SO_4^{2-}} - q_{SO_4^{2-}}^*)}{M_{SO_4^{2-}}} \qquad (10)$$

where k_s is the solid phase mass transfer coefficient of a substance; $c(t)$ and c^* are the species current and equilibrium concentration in the liquid phase; q and q^* are the species average and equilibrium concentration in the solid phase; V is the suspension volume; S_0 (surface area/volume of particle) is the specific surface area of a spherical particle (calculated as $3/R$, where R is the average radius of the particle); ε is the fluid (water) fraction in suspension and M is the molar mass.

The accuracy of the proposed extended dissolution model was confirmed by comparing the results of a Ca^{2+}, SO_4^{2-} and OH^- ion leaching process simulation (performed using the MODEST 6.1 software package (see Section 2.2)) for different ash-water ratios with experimental data (not used in parameter k_s evaluation) obtained in batch leaching experiments on the basis of selecting a PF ash sample as the example, characterized by a high free lime content (~30 %) and initial calcium and sulfate content 0.425 and 0.0317 g/g ash, respectively (Fig. 5).
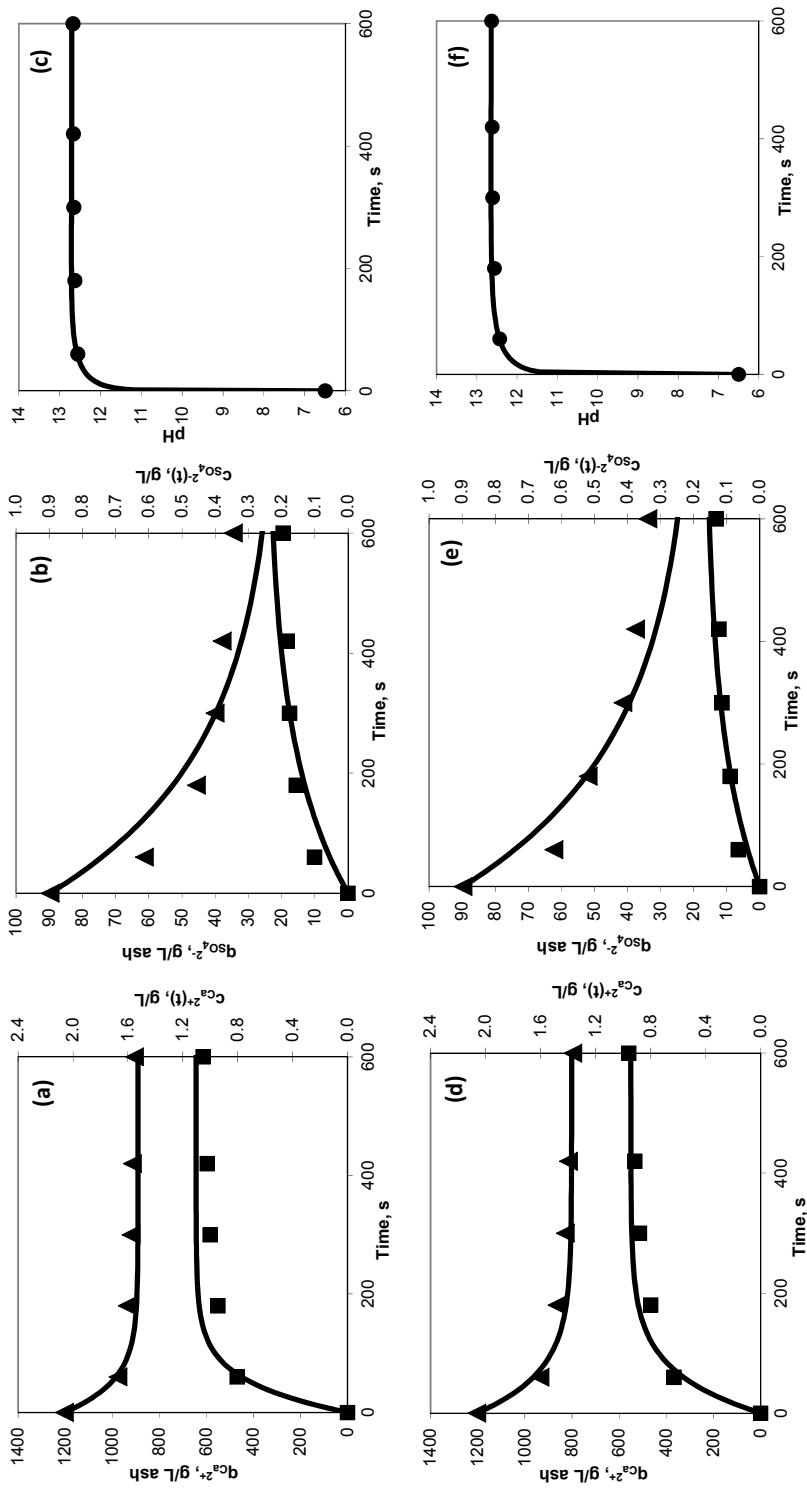
Figure 5. Modeling of Ca^{2+}, SO_4^{2-} dissolution and pH changes during PF ash washing in a batch reactor: experimental vs. simulated (—) concentration profiles: species content in ■ liquid phase c(t), g/L and in ▲ solid phase (ash) q, g/L ash; ● pH value; S/L ratio (a)-(c) 1:100; (d)-(f) 1:150

3.1.2.2 Continuous washing process of the ash layer (Paper III: Section 3.1)

The mechanism of Ca mass transfer phenomena in a fixed ash layer leaching unit was described by the differential mass balance equations, derived through consideration of a short length ΔZ of a reactor of cross-sectional area S, as shown in *Paper III: Fig. 1b*. The following system of model equations (Eq. 11-14; *Paper III: Eq. 2-5*) was proposed assuming that heat effects and axial dispersion can be neglected:

$$v \times \frac{\partial C}{\partial Z} + \frac{\partial C}{\partial t} + \frac{1-\varepsilon}{\varepsilon} \times K \times S_0 \times (q^* - \overline{q}) = 0 \qquad (11)$$

$$\frac{\partial \overline{q}}{\partial t} + K \times S_0 \times (\overline{q} - q^*) = 0 \qquad (12)$$

$$\frac{1}{K} = \frac{m}{k_L} + \frac{1}{k_s} \qquad (13)$$

$$Q = \varepsilon \times v \times S \qquad (14)$$

where K is the overall mass transfer coefficient; k_L and k_s are, respectively, the liquid and the solid phase mass transfer coefficients; C is the concentration of Ca in the water; $\overline{q}$ is the average concentration of Ca in ash; ε is the fluid (water) fraction in the layer (estimated from the volumes of the ash layer and the empty column); v is the average axial velocity of the flowing fluid in the interstitial spaces; Z is the ash layer height coordinate, from the bottom ($Z=0$) to the top ($Z=L$); m is the slope of the equilibrium line $q^*=f(c^*)$; Q is the volumetric flow rate of the liquid phase; S is the cross-sectional area of the empty column and S_0 (surface area/volume of particle) is the specific surface area of a particle.

In addition to steps 1 and 2 presented for the batch process in the previous Section 3.1.2.1, the modeling procedure in this case involved the task of determining the Ca overall and liquid phase mass transfer coefficients, K and k_L. For this purpose, continuous leaching experiments were conducted in a semi-batch washing column at various liquid flow rates as described in Section 2.1.2. Because the same types of ash samples as in batch dissolution modeling were used as an example material for the continuous mode process, previously obtained data from steps 1 ($q^*=f(c^*)$) and 2 (values of k_s) *(Paper II: Eq. 3-4, Table 3)* was applied in the modeling. The kinetics calculations and process simulation were performed using the MODEST 6.1 software package (Section 2.2). The system of model equations above was solved numerically and integrated by the method of lines with the following initial and boundary conditions:

at $Z=0$: $C=0$ for every moment of time $t= 0 \ldots t= \infty$ (15)

at $t=0$: $\bar{q} = q_0$ for every length coordinate $Z= 0 \ldots Z=L$ (16)

The solution of Eq. 11-12 and 15-16 gives the concentration distributions in the layer, $\bar{q}\,(Z,t)$ and $C(Z,t)$. The values of the overall mass transfer coefficient, K were evaluated using a parameter estimation procedure. The results presented in *Paper III* were in good agreement with theoretical knowledge: as the flow rates increase, the turbulence of the flow increases and consequently reduces the mass transfer resistance. Furthermore, the liquid phase mass transfer coefficient, k_L was calculated according to Eq. 13, based on the values of the overall mass transfer coefficient, K *(Paper III: Table 1)* and the solid phase mass transfer coefficient, k_s estimated from the batch dissolution experiments (using very intensive mixing) presented for different ash types in *Paper II (Table 3)*. Slope m of the equilibrium line $q^*=f(c^*)$ was calculated as the derivative of the equilibrium equation (presented in *Paper II: Eq. 3, 4*) for the argument value equal to the average Ca concentration in the liquid phase within the experimental range. As a result, an empirical function for the estimation of the liquid phase mass transfer coefficient, k_L at different liquid flow rates (Q) was built up *(Paper III: Eq. 9, 10)*.

Simulations of the Ca dissolution process during continuous washing of various types of oil shale ash layers with different flow rates are presented in *Paper III: Fig. 2*, where it has been shown by a comparison of experimental data and results of the process simulation that the developed model was able to provide an accurate estimation of the changes in Ca content in the leaching fluid as well as in the stagnant layer of ash. The results and discussion on this subject are given in more detail in *Paper III*.

3.1.2.3 Simulation scenario of the ash deposit leaching process (Paper III: Section 3.3)

In order to demonstrate the versatility of application of the developed Ca dissolution model, an example was designed to simulate a scenario of an industrial ash layer washing process in a natural environment over an extended period of time *(Paper III)*. The goal was to imitate the current situation in Estonia, where every year about 6 Mt of oil shale ash produced by power plants is transported to nearby ash fields.

Overview of the initial parameters of the simulation
In the simulation, seventy tons of dry PF ash formed in a power plant are considered as having been distributed uniformly over an area of 5 x 13 m^2, creating a theoretical 1 meter high ash layer (cross-sectional area of 65 m^2). The average annual amount of precipitation in Estonia was taken as about 757 mm. The objective of the simulation was to estimate changes in the Ca concentration in the solid (ash) phase and in the leaching water during industrial ash layer

washing by natural precipitation and therefore to predict the outcome of the process.

Results and discussion

For the simulation, the set of model equations *(Paper III: Eqs. 2-5, 9)* was solved using estimates for the ash parameters obtained from the study on the kinetics of batch and continuous dissolution processes described in *Papers II and III*. The calculations details and results are presented in *Paper III*. As can be seen from *Fig. 3* in *Paper III*, the calcium concentration level where only the insoluble part of free lime is left in the ash layer was estimated by the model as being reached in approximately 500 years. The results indicate that the Ca content in the leaching fluid will be at a level of about 1.51 g L^{-1} and maintain this high value for hundreds of years to come. Therefore, it was demonstrated that oil shale ash can be viewed, without the implementation of any constraints, as a source of environmental damage for a long time.

3.2 From waste to value: calcium carbonate precipitation on the basis of oil shale ash

Based on our investigations relating to the leaching behavior of oil shale ash *(Papers I-III)*, the latter could be qualified as a source of calcium which is easily and rapidly extractable by water. The possibility of obtaining PCC on the basis of alkaline wastes from oil shale energetics was first introduced in our earlier paper [164] where the preliminary results of alkaline ash-transportation water neutralization experiments with a CO_2-containing model gas carried out in a small-size (0.6 L) laboratory absorber were reported. As the next step, the feasibility, specifics and mechanism of calcium carbonate precipitation in the *ash leachate – CO_2-containing model flue gas* system were systematically investigated in a ~15 L semi-batch stirred barboter-type reactor and the main characteristics (composition, morphology, surface area and particle size) of the resulting solid product were examined over a wide range of operating conditions. These aspects are discussed in *Papers VI* and *VII*. Complimentary carbonation experiments with commercial CaO fine powder were conducted for a comparative characterization of the final products obtained on the basis of two different Ca-rich raw materials. This analysis is mostly reflected in *Paper VI*.

The mathematical tasks of the study focused on the main challenges in indirect mineral carbonation, including establishing a quantitative understanding of heterogeneous gas-liquid-solid system kinetics and dynamics. To elucidate the specifics and to estimate the performance of the CO_2 mass transfer process into alkaline wastewaters such as leaching waters of oil shale ash, kinetics studies on the phenomena of CO_2 absorption in a model gas – liquid system in the absence *(Paper IV)* and presence of a precipitation reaction *(Papers V and VII)* were performed in a stirred semi-batch reactor.

Based on the results of a multifaceted study, a consistent set of model equations and physical-chemical parameters was finally proposed to describe the $CaCO_3$ precipitation process from oil shale ash leachates of complex composition *(Paper VII)*.

Furthermore, aspects such as CO_2 sequestration and PCC production capacity of ash and its leachates were discussed. Consequently, technological concepts for continuous mode co-utilization of waste streams from oil shale energetics in the production of synthetic calcium carbonate were worked out and a pilot-scale reactor system was proposed.

3.2.1 Feasibility and specifics of ash indirect carbonation (Papers VI and VII)

The investigation into multi-step PCC formation on the basis of waste ash was comprised of two major stages: aqueous extraction and a precipitation regime. Similar to the process described in this work, in the conventional PCC production method, dry CaO, an expensive high quality raw material, is slaked (hydrated) with water to form a calcium hydroxide slurry which is then screened to remove impurities originating from the limestone and fed into a stirred tank reactor where it reacts with CO_2 [83]. Unlike the lime solution, leachates contain different salts leached from the heterogeneous composition of oil shale ashes, as was elaborated in Section 3.1.1 where the dissolution behavior of the lime-containing ash was discussed. In order to systematically investigate calcium carbonate precipitation in the ash leachate – CO_2-containing flue gas system, a set of carbonation experiments was conducted in a semi-batch stirred reactor according to the procedure described in Section 2.1.3. In the primary aqueous extraction step, oil shale ash leachates (pH ~12.65) with the following average ion concentrations were obtained: (in g L^{-1}) Ca^{2+} ~1.23, SO_4^{2-} ~0.75, K^+ ~0.076, Cl^- ~0.038, PO_4^{3-} ~0.011; (in mol L^{-1}) OH^- ~0.047. In the subsequent carbonation step, neutralization of ash leachates (pH ~7) was accompanied by the formation of solid precipitates. These experiments indicated that alkaline ash leachates react readily with a CO_2-containing model gas, radically decreasing the content of Ca^{2+} ions and the pH value (Fig. 6) of the solution. Contact between Ca^{2+}-ions and dissolved CO_2 led to the precipitation of $CaCO_3$ (PCC), which is practically insoluble in water with a pH>9. As the pH was lowered, the increased content of H^+ ions triggered the re-dissolution of $CaCO_3$, liberating calcium ions into the solution (Fig. 6). The concentration of SO_4^{2-} ions decreased moderately (from ~0.75 to 0.57 g L^{-1} depending on the process conditions). The content of background ions such as K^+, Cl^-, etc. remained unchanged during the experiment, which indicates that they do not participate in the precipitation reaction and remain in solution. This finding is important in the context of product purity.
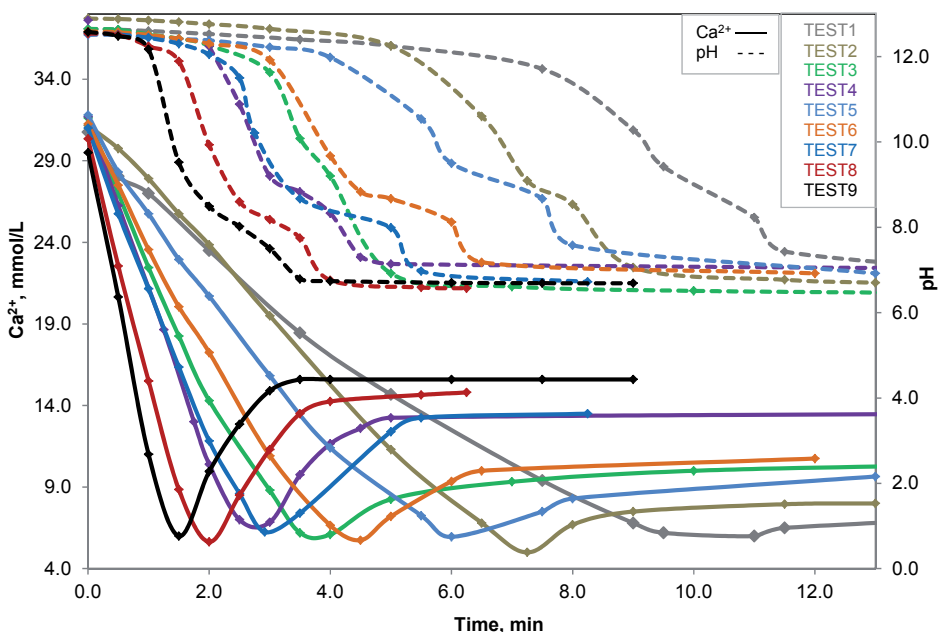
Figure 6. Process-induced changes in Ca^{2+} concentration and pH profiles

The influence of precipitation conditions on the main characteristics of the resulting crystalline product is discussed in the following Section 3.2.2, whereas the mechanism of calcium carbonate precipitation during the gas-liquid reaction in the ash leachate – CO$_2$-containing gas system is elaborated in Section 3.2.3.

3.2.2 Characterization of PCC crystallized in the ash leachate – CO$_2$-containing flue gas system (Papers VI and VII)

It is evident that among the other parameters, the shape, size and texture of the crystals play a crucial role in determining the properties and application suitability of the material. In precipitation processes, especially the hydrodynamic conditions in the system strongly influence the result of the reaction, *i.e.* the characteristic features of the precipitate. Nevertheless, the impact of a complex composition of ash leachates on the quality of the resulting crystalline product is a matter of importance. Consequently, a detailed examination of the precipitates which formed during ash leachate carbonation (until a solution pH ~7) under different conditions was performed. The characteristics of the solid products were determined using numerous characterization techniques (see Section 2.1.1, Table 4) and are presented in Table 6 *(Paper VII: Table 3)*.

Table 6. Synthesis conditions and main characteristics of oil shale ash leachate carbonation products

Sample	Operating variables			Solid product characteristics								
	Q_G, L h⁻¹	c_{CO2}, vol.%	N, rpm	$CaCO_3^{av}$, % XRD			$CaSO_4^{av}$, %	SSA, m²/g	V_{tot}, mm³/g	V_{micro}, mm³/g	d_{mean}, μm	Brightness ISO, %
				TC	calcite	vaterite						
PCC1	1000	5	400	94.5	100.0	-	5.7	2.28	3.38	-	4.1	93.2
PCC2	1000	5	1000	94.5			5.8	2.56	3.51	0.11	5.1	
PCC3	1000	15	400	94.6			5.5	3.15	4.03	-	4.8	
PCC4	1000	15	1000	94.4			5.9	1.33	1.93	-	7.8	
PCC5	2000	5	400	94.4			5.9	1.35	1.74	-	6.5	
PCC6	2000	5	1000	95.1	97.3	2.6	5.0	2.38	3.77	-	8.1	92.7
PCC7	1500	10	700	95.6	77.2	21.9	4.4	4.70	11.05	0.01	7.7	92.3
PCC8	2000	15	400	96.2	63.2	36.3	4.0	7.29	17.44	0.43	8.0	
PCC9	2000	15	1000	95.4	95.7	3.6	4.5	1.95	3.44	-	9.9	

The unwashed precipitates (Table 6: PCC1–PCC9) were characterized by their bright white color and fine powdery texture. Total carbon- and thermoanalysis indicated that the solid samples predominantly contained $CaCO_3$ (~94.4−96.2%), with minor amounts of $CaSO_4$ (~4−6% TA and BSF analyses; Table 6; *Paper VII: Table 3*), evidently adsorbed on the surface of the $CaCO_3$ crystals as implied by XPS analysis. Only traces of other constituents were detected (XPS) on the crystal surface, confirming conclusions drawn based on the liquid phase composition analysis. Washing of the precipitate cake would be expected to improve the purity of the product by a few percentage points *(Paper VI)*. The phase composition was also confirmed using FT-IR spectroscopy.

The morphology of the precipitated particles was examined using scanning electron microscopy (SEM). SEM images of the final precipitates PCC1-PCC9 crystallized under various carbonation conditions are shown in *Paper VII: Fig. 3*. Under the conditions of TEST 1-5 (Table 5), well-defined rhombohedral crystals with a mean size ranging from ~4−8 μm were produced (Table 6; *Paper VII: Fig. 3(a-e))*. X-ray powder diffraction analysis (XRD) of these samples identified calcite as the only crystal form of calcium carbonate detected. Carbonation under intensified hydrodynamic conditions (TEST 6-9, Table 5) resulted in the formation of distinctly spherical particles of vaterite in the precipitates along with rhombohedral crystals of calcite *(Paper VII: Fig. 3(f-i))*. The coexistence of calcite and vaterite in the product (PCC6-PCC9) was confirmed using XRD measurements (Table 6; *Paper VII: Table 3*), which enabled us to distinguish different polymorphic modifications of calcium carbonate. The XRD results indicated that samples PCC6 and PCC9 contained relatively small amounts of the vaterite phase (2.6 and 3.6%), while the relative mass percentages of vaterite in samples from TESTS 7 and 8 were ~22 and 36% (Table 6; *Paper VII: Table 3*). The presence of a significant amount of spherical vaterite explains the greater surface area and pore volume (V_{tot}) of samples PCC7 and PCC8. Precipitation under the most rapid conditions (TEST 9, Table 5) significantly decreased the amount of vaterite in the final product compared to sample PCC8, leading to the formation of pseudo-cubic or randomly aggregated rhombohedral *(Paper VII: Fig. 3i)* and spherical structures with a mean diameter of ~10 μm and a calcite content of ~96% (Table 6; *Paper VII: Table 3*).

The particle size distribution analysis revealed that the PCC particle size was influenced by the operating conditions, especially the hydrodynamics of the system (flow rate, mixing intensity). For instance, in the experiments with 15% CO_2 in the flue gas, increasing the gas flow rate from 1000 to 2000 L h^{-1} increased the mean diameter of the particles from ~4.8 to 8.0 μm and from ~7.8 to 9.9 μm at 400 rpm and 1000 rpm, respectively. A similar effect was observed upon increasing the rotation speed from 400 to 1000 rpm (d_{mean} increased from ~4.8 to 7.8 μm and from ~8.0 to 9.9 μm at 1000 and 2000 L h^{-1}, respectively). Based on the gathered experimental data, applicable to barboter-type reactors, a simplified empirical dependence ($R^2 = 0.94$) relating the mean particle size, d_{mean} (in μm) to the process parameters was constructed:

$$d_{mean} = 0.16685 \times \left(\frac{Q_G}{V_L}\right)^{0.609} \left(\frac{P_N}{V_L}\right)^{0.234} c_{CO_2}^{0.231}, \tag{17}$$

where Q_G/V_L is the specific gas flow rate (h^{-1}) and P_N/V_L is the stirrer specific power consumption (W L^{-1}).

It was evident that elevated values of the operating parameters (gas mixture flow rate or/and CO_2 content as well as mixing intensity in the reactor) lead to more rapid precipitation accompanied by a faster pH decline. The results, therefore, indicate that by prolonging the carbonation process, the mean particle size decreases (Table 6). This trend was also observed in the additional experiments described in *Paper VI* were CO_2 gas flow was switched off either prior to reaching the pronounced re-dissolution region or after the pH of the solution had stabilized *(Paper VI: Table 1)*. In the same study, the effect of the extent of carbonation on the textural properties of PCC particles was observed: by prolonging carbonation below pH ~8 (the re-dissolution region), the initially smooth surface of the crystal faces of PCC particles *(Paper VI: Fig. 2(c, e))* appeared to become rougher *(Paper VI: Fig. 2d)*. This observation was confirmed by surface area measurements *(Paper VI: Table 1)*.

Furthermore, the results suggest that faster precipitation due to intensified hydrodynamic conditions provoked the formation of the usually metastable vaterite in the final product. Consequently, a closer examination of the morphological development of the $CaCO_3$ crystals in the course of carbonation under the conditions of TESTS 8 and 9 was undertaken (Fig. 7). The morphogenesis of the PCC crystals in the course of carbonation is illustrated in sub-figures (a) - (d) and (e) - (h) in Fig. 7 during TESTS 8 and 9, respectively. It can be observed from sub-figures (b) and (f) in Fig. 7 that by the time the Ca^{2+} content in the solution reached its lowest value, only *regularly-shaped rhombohedral calcite* crystals precipitated. At this point, all the calcium potential of the solution was utilized and equilibrium between the processes of $CaCO_3$ precipitation and dissolution was established. Moreover, agglomeration of particles was not detected during this period. Further addition of CO_2 initiated PCC re-dissolution due to a decline in the pH (pH<9) (Fig. 6). At this stage, parallel crystallization of vaterite, a $CaCO_3$ polymorph, took place (Fig. 7(c, g)). By the end of carbonation (pH ~7), presumably due to an excess of Ca^{2+} in the solution as a result of PCC re-dissolution, vaterite was partially replaced by more stable calcite, whereas the remaining amount stabilized under these experimental conditions (Fig. 7(d, h)). In addition to the influence of hydrodynamics on the system, the formation of the metastable phase might have been promoted by the presence of specific accompanying ions in the leachates. According to a study by Fernández-Díaz *et al.* [165], a significant role in the stabilization of vaterite may be attributed to the presence of sulfate in the system. Hence, elaborated observations are of great interest in the context of PCC production on the basis of oil shale ash.
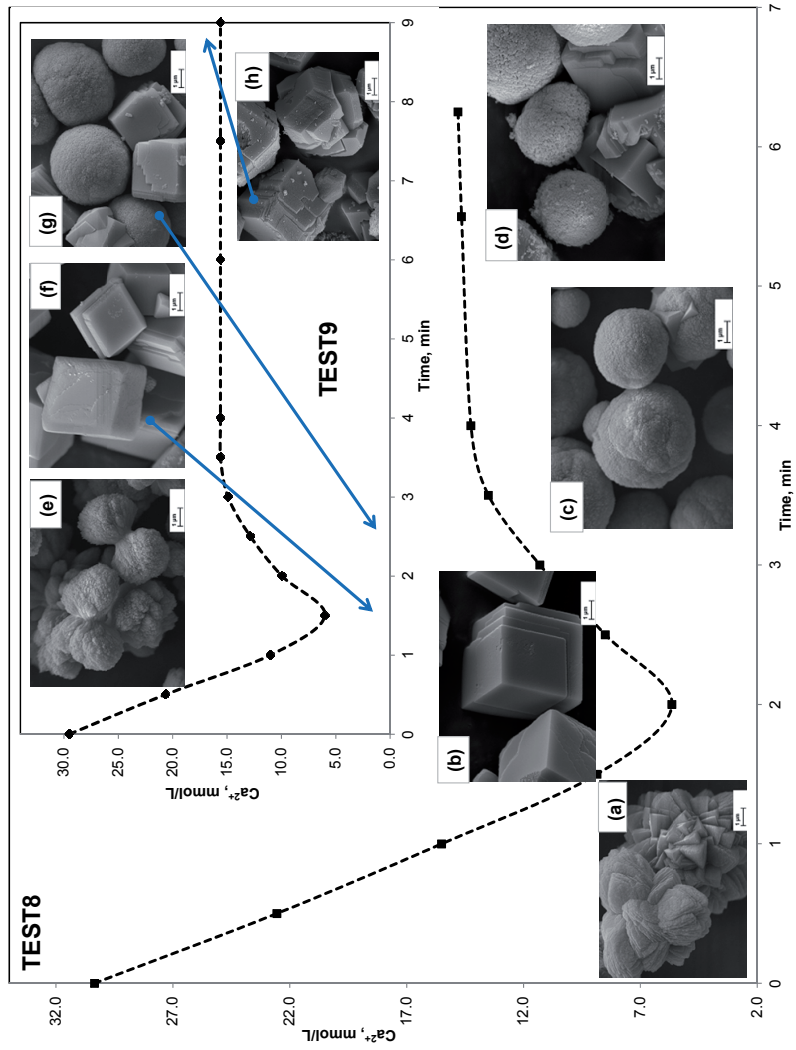
Figure 7. Morphological development of the CaCO₃ crystals and Ca²⁺ concentration change in the course of ash leachate carbonation under the conditions of TEST 8: (a) after 1.5 min, pH= 11.89, Ca²⁺ =8.85 mmol/L; (b) after ~2 min, pH=9.93, Ca²⁺ =5.65 mmol/L; (c) after 3.5 min, pH=7.75, Ca²⁺ =13.5 mmol/L; (d) PCC8; and TEST 9: (e) after 1.0 min, pH=12.17, Ca²⁺ =11.0 mmol/L; (f) after 1.5 min, pH=9.52, Ca²⁺ =6.0 mmol/L; (g) after 2.5 min, pH=8.02, Ca²⁺ =12.85; (h) PCC9.

Additionally, precipitation experiments were conducted under the same conditions as in TEST 1 (Table 5) with commercial CaO fine powder according to the procedure described in Section 2.1.3 for comparative characterization of the final products. Interestingly, the precipitates obtained under the identical conditions, yet on the basis of different raw materials, contained crystals with the same order of particle size and similar morphology, whereas the brightness value (~93%) of particles crystallized from ash leachates exceeded that of PCC obtained from a pure $Ca(OH)_2$ solution (~89%) *(Paper VI: Table 1)*. More details, including SEM images for the respective types of PCC, can be found in *Paper VI*.

3.2.3 Reaction mechanism and modeling of PCC formation in the ash leachate – CO_2-containing flue gas system

3.2.3.1 CO_2 absorption kinetics and mass transfer into the alkaline model solution (Paper IV)

A vital part of the carbonation process is the transfer of CO_2 from the gas phase to the aqueous phase, since only the dissolved molecules of CO_2 take part in the reactions. Furthermore, the concentrations of the various carbonate species depend on the pH of the solution. As shown in previous Sections, ash leaching waters are characterized by high pH levels; however, the data on the rate of CO_2 transfer from air bubbles into the aqueous alkaline solution has rarely been reported in the literature [166, 167]. Consequently, a study on CO_2 uptake kinetics in hydroxide solution in the absence of precipitation reaction was undertaken *(Paper IV)*. The performance of the CO_2 mass transfer process in a stirred semi-batch reactor was evaluated under various conditions in absorption experiments with an NaOH solution representing the Ca^{2+} and SO_4^{2-}-free alkaline model solution. The experimental setup and conditions are presented in Section 2.1.3 and in more detail in *Paper IV*. Considering information on all of the main factors involved in the mass transfer of CO_2 from the gas phase to an aqueous solution of hydroxides and the subsequent reactions (hydrodynamics, kinetics etc.), a mathematical model *(Paper IV: Eq. 4-10)* for description of CO_2 mass transfer in a stirred semi-batch reactor was composed, allowing for simulating the concentration profiles of reactive species (CO_2, CO_3^{2-}, HCO_3^-, OH^-, H^+) in the gas and liquid phase. The detailed description of the model is elaborated in *Paper IV*. Under the conditions prevailing in the reactor, the rate of CO_2 transfer is governed by the liquid phase mass transfer coefficient, k_L and is usually characterized by the volumetric mass transfer coefficient, $k_L a$. Based on the experimental data and proposed CO_2 mass transfer model, an estimation of the volumetric mass transfer coefficient of CO_2 for the system in the absence of a precipitation reaction, $k_L a^0_{CO2}$, was made under different conditions of gas flow rate, mixing speed and CO_2 partial pressure. The calculations were performed using the MODEST 6.1 software package (Section 2.2). Based on the obtained

data, the effects of hydrodynamics on the rate of CO_2 mass transfer were described in a form of an empirical correlation of $k_L a^0_{CO2}$ (s^{-1}) as a function of the main operating variables, allowing for the estimation of CO_2 absorption performance per unit volume of gas-liquid mixture in barboter-type reactors under different conditions *(Paper IV: Eq. 16)*. The implementation of the obtained mathematical data into the algorithm of the $CaCO_3$ precipitation model on the basis of ash leachates is acknowledged in Section 3.2.3.3.

3.2.3.2 Calcium carbonate precipitation kinetics in a model gas – liquid system (Paper V)

In order to design the PCC formation process and to optimize CO_2 elimination from flue gas using alternative CaO-containing materials, such as oil shale ash and its leachates, mathematical models describing the outcome of the precipitation process of $CaCO_3$ in a model gas–liquid system must be developed using at first chemically pure lime as a Ca source. For this purpose, a kinetics study on chemical absorption of CO_2 into an aqueous solution of $Ca(OH)_2$, representing the Ca^{2+}-rich and SO_4^{2-}-free alkaline model water, was carried out in a stirred semi-batch reactor. The experimental setup and conditions are given in Section 2.1.3. The mathematical model described in the previous section was extended to account for the $CaCO_3$ precipitation reaction kinetics and a resulting set of model equations is presented in *Paper V (Eq. 8-16)*. On the basis of the modified model and the obtained experimental data, the volumetric mass transfer coefficient of CO_2 in the presence of a precipitation reaction, $k_L a_{CO2}$, was estimated under the conditions of various initial concentrations of the $Ca(OH)_2$ solution. According to the same procedure and considering the value of the solubility product of $CaCO_3$, the reaction rate constants of the $CaCO_3$ precipitation reaction were evaluated *(Paper V: Table 2)*. The calculations were performed using the MODEST 6.1 software package (Section 2.2). Details of the determination can be found in *Paper V*. Furthermore, the influence of the precipitation reaction on the rate of CO_2 mass transfer was investigated. This analysis is described in *Paper V*. The reactions of CO_2 with a $Ca(OH)_2$ solution enhance the rate of absorption and increase the capacity of the liquid solution to dissolve the solute, when compared with physical absorption systems. The effect of the precipitation reaction on process performance can be expressed by introducing the CO_2 mass transfer enhancement factor, E [168, 169], defined here as the ratio of the volumetric mass transfer coefficients for CO_2 absorption for both cases with ($k_L a_{CO2}$) and without the precipitation reaction ($k_L a^0_{CO2}$), $E=k_L a_{CO2}/k_L a^0_{CO2}$. By considering the results of the study for the system in the absence of a precipitation reaction described in Section 3.2.3.1, values of the enhancement factor E for CO_2 absorption were determined *(Paper V: Table 2)* and the empirical Eq. *(Paper V: Eq. 19)* of E as a function of the initial Ca^{2+} concentration was proposed. It was shown that an increase in the Ca concentration produces a continuous increase in the enhancement factor. This

fact along, with the kinetics data described in this section, was later accounted for in the Ca^{2+}-rich ash leachates system.

3.2.3.3 Modeling of the CO_2 absorption and $CaCO_3$ precipitation in the ash leachate – CO_2-containing flue gas system (Paper VII)

The mechanism expressed by Cents *et al.* [170] for the reaction of CO_2 with aqueous solutions of hydroxides was considered as a starting point and extended by us based on the theoretical considerations and obtained data to be applicable for description of the CO_2 absorption and $CaCO_3/CaSO_4$ precipitation in the system of ash leachate – CO_2-containing flue gas. The reactions occurring upon contact of ash leachate, characterized by an excess amount of Ca^{2+} and SO_4^{2-} ions, with CO_2 present in the gas are presented in Fig. 8 *(Paper VII: Eq. 1-9)*.

Physical dissolution of gaseous CO_2 into solution:
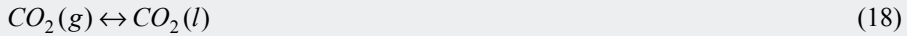
$$CO_2(g) \leftrightarrow CO_2(l) \tag{18}$$

Formation of bicarbonate:

$$CO_2(l) + OH^- \underset{k_{12}}{\overset{k_{11}}{\rightleftarrows}} HCO_3^- \tag{19}$$

Dissociation of bicarbonate:

$$HCO_3^- + OH^- \underset{k_{22}}{\overset{k_{21}}{\rightleftarrows}} CO_3^{2-} + H_2O \tag{20}$$

Ionization of water:

$$OH^- + H^+ \underset{k_{32}}{\overset{k_{31}}{\rightleftarrows}} H_2O \tag{21}$$

CO_2 hydration:

$$CO_2(l) + H_2O \underset{k_{42}}{\overset{k_{41}}{\rightleftarrows}} HCO_3^- + H^+ \tag{22}$$
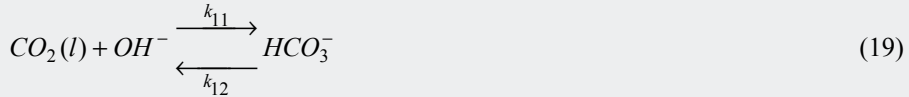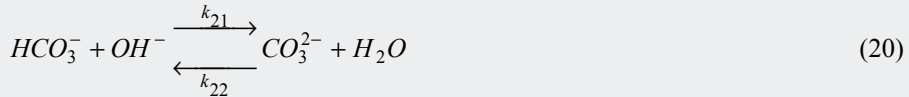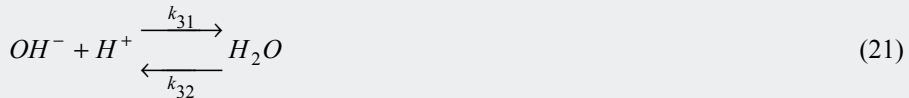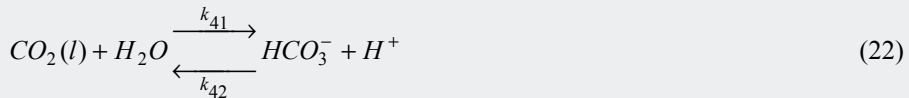
Precipitation of $CaCO_3$ crystals:

$$Ca^{2+} + CO_3^{2-} \underset{k_{52}}{\overset{k_{51}}{\rightleftarrows}} CaCO_3 \tag{23}$$
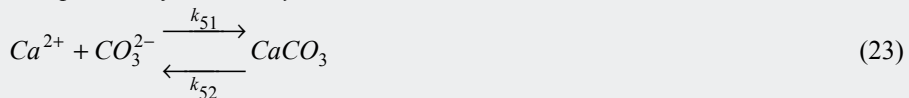
Formation of the anhydrite phase:

$$Ca^{2+} + SO_4^{2-} \leftrightarrow CaSO_4 \tag{24}$$

Back-dissolution of $CaCO_3$ crystals at lower pH:

$$CaCO_3 + H^+ \underset{k_{62}}{\overset{k_{61}}{\rightleftarrows}} Ca^{2+} + HCO_3^- \tag{25}$$
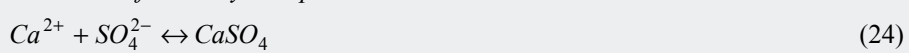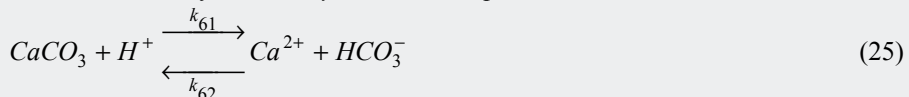
Figure 8. A set of reactions occurring in the ash leachate–CO_2-containing gas system

As indicated by the experimental data described in Section 3.2.1, it can be assumed that the background ions in the leachate, such as K^+, Cl^- etc., do not take part in the precipitation process in significant amounts.

Based on the results of a multifaceted kinetics study *(Papers IV, V* and *VII)*, the mathematical process model was developed *(Paper VII)* incorporating the mechanisms and modeling algorithms composed for intermediate stages *(Papers IV* and *V)* and accounting for the absorption and reaction kinetics taking place in the liquid phase, including $CaCO_3$ and $CaSO_4$ precipitation, as well as the hydrodynamic conditions within the system. According to our proposal, assuming the ash leachate – CO_2-containing flue gas system is operated isothermally at 25°C, the concentration profiles of characteristic species participating in the precipitation process may be modeled as a function of time using differential Eq. 26-36 *(Paper VII: Eq. 10-20)*:

- For CO_2 dissolved in the liquid phase:

$$\frac{d[CO_2(l)]}{dt} = \frac{k_L a_{CO_2}^0 \times E \times \sum_{i=1}^{n} \left(\left(\frac{k_H \times M_{CO_2} \times P \times [CO_2^i(g)]}{\rho_{CO_2}} - [CO_2(l)] \right) \times \frac{V_L + V_G}{n} \right)}{V_L}$$
$$- k_{11}[CO_2(l)][OH^-] + k_{12}[HCO_3^-] - k_{41}[CO_2(l)] + k_{42}[HCO_3^-][H^+]$$

(26)

- For Ca^{2+}, OH^-, SO_4^{2-}, HCO_3^-, CO_3^{2-} and H^+ ions:

$$\frac{d[Ca^{2+}]}{dt} = k_{52} - k_{51}[Ca^{2+}][CO_3^{2-}] + k_L a_{CaSO_4} \times \left([SO_4^{2-}]^* - [SO_4^{2-}] \right)$$
$$+ k_{61}[H^+] - k_{62}[Ca^{2+}][HCO_3^-]$$

(27)

$$\frac{d[OH^-]}{dt} = -k_{11}[CO_2(l)][OH^-] + k_{12}[HCO_3^-] - k_{21}[HCO_3^-][OH^-]$$
$$+ k_{22}[CO_3^{2-}] + k_{32} - k_{31}[OH^-][H^+]$$

(28)

$$\frac{d[SO_4^{2-}]}{dt} = k_L a_{CaSO_4} \times \left([SO_4^{2-}]^* - [SO_4^{2-}] \right)$$

(29)

$$\frac{d[HCO_3^-]}{dt} = k_{11}[CO_2(l)][OH^-] - k_{12}[HCO_3^-] - k_{21}[HCO_3^-][OH^-]$$
$$+ k_{22}[CO_3^{2-}] + k_{41}[CO_2(l)] - k_{42}[HCO_3^-][H^+] + k_{61}[H^+] - k_{62}[Ca^{2+}][HCO_3^-]$$

(30)

$$\frac{d[CO_3^{2-}]}{dt} = k_{21}[HCO_3^-][OH^-] - k_{22}[CO_3^{2-}] + k_{52} - k_{51}[Ca^{2+}][CO_3^{2-}]$$

(31)

$$\frac{d[H^+]}{dt} = k_{32} - k_{31}[OH^-][H^+] + k_{41}[CO_2(l)] - k_{42}[HCO_3^-][H^+]$$
$$- k_{61}[H^+] + k_{62}[Ca^{2+}][HCO_3^-]$$

(32)

- For CO_2 exiting the *i*th section of the reaction mixture:

$$\frac{d[CO_2^i(g)]}{dt} = \left(\begin{array}{c} Q_G\left([CO_2(g)]_{IN} - [CO_2^i(g)]\right) \\ -k_L a_{CO_2}^0 \times E \times \left(\dfrac{k_H \times M_{CO_2} \times P \times [CO_2^i(g)]}{\rho_{CO_2}} - [CO_2(l)] \right) \times \dfrac{(V_L + V_G)}{n} \end{array} \right) \Bigg/ \frac{V_G}{n}$$

(33)

- For CO_2 exiting the reactor headspace (V_{G2} above the mixture; Fig. 4b):

$$\frac{d[CO_2(g)]_{OUT}}{dt} = \left(Q_G\left([CO_2(g)] - [CO_2(g)]_{OUT}\right) \right) / V_{G_2}$$

(34)

- For $CaCO_3$ forming during the carbonation process:

$$\frac{d[CaCO_3]}{dt} = k_{51}[Ca^{2+}][CO_3^{2-}] - k_{52} - k_{61}[H^+] + k_{62}[Ca^{2+}][HCO_3^-]$$

(35)

- For $CaSO_4$ forming during the carbonation process:

$$\frac{d[CaSO_4]}{dt} = k_L a_{CaSO_4} \times \left([SO_4^{2-}] - [SO_4^{2-}]^* \right)$$

(36)

In Eqs. 26-36, the concentrations are expressed in molar units, Q_G is the gas volumetric flow rate in L s^{-1}, $k_L a_{CO_2}^0$ is the volumetric mass transfer coefficient of CO_2 in the absence of a precipitation reaction in s^{-1}, E is the CO_2 mass transfer enhancement factor, V_L is the solution volume in L, V_G is the volume of gas in the gas-liquid mixture in L, V_{G2} is the gas volume in the reactor headspace in L, k_H is the Henry's law constant in mol·(L atm)$^{-1}$, P is the atmospheric pressure in atm, M_{CO2} is the CO_2 molar mass in g mol^{-1} and ρ_{CO2} is the CO_2 gas density in g L^{-1}.

The gas phase in the reaction mixture was divided into a number of theoretical sections n with a volume V_G/n (gas phase in approximately plug flow, liquid phase in perfectly mixed flow due to solution recirculation). Each of these sections (high correlation coefficient observed at n=10) was treated as a non-equilibrium stage governed by Eq. 33.

Considering the near infinite-dilution ionic strength of the leachate (I=0.1), the value of the second-order rate constant, k_{11} (in L·(mol s)$^{-1}$) in Eq.19 in Fig. 8 was calculated as a function of temperature T (K) using a relationship proposed by Pohorecki and Moniuk [171]:

$$\log(k_{11}) = 11.916 - \frac{2382}{T} \tag{37}$$

The backward reaction rate, k_{12} in Eq. 19 is defined by the value of the equilibrium constant for this reaction $(k_{12}=k_{11}K_w/K_1)$. The value of the solubility product, K_w (mol^2 m^{-6}) is given by Tsonopoulos [172]:

$$\log\left(\frac{K_w}{\rho_w^2}\right) = -\frac{5839.5}{T} - 22.4773\log(T) + 61.2062 \tag{38}$$

The value of the equilibrium constant, K_1 (mol m^{-3}) is given as a function of temperature by Edwards et al. [173]:

$$K_1 = \exp\left(-\frac{12092.1}{T} - 36.786\ln(T) + 235.482\right)\rho_w, \tag{39}$$

where ρ_w is the density of water (kg m^{-3}). The reaction rate constant, k_{21} in Eq. 20 was reported as 6×10^6 $m^3\cdot(mol\ s)^{-1}$ by Eigen [174]. The equilibrium constant, K_2 (m^3 mol^{-1}) at infinite dilution, which determines the value of the backward reaction rate, $k_{22}=k_{21}/K_2$, is given by Hikita et al. [175]:

$$\log(K_2) = \frac{1568.9}{T} - 2.5866 - 6.737\times10^{-3}T \tag{40}$$

The neutralization rate constant, k_{31}, was determined by Eigen [174] to be 1.4×10^8 $m^3\cdot(mol\ s)^{-1}$. The rate constant, k_{41} for the reaction between CO_2 and water is 0.024 s^{-1} [176]. The values of the backward reaction rate constants, k_{32} and k_{42} may be calculated from the equilibrium constants and are equal to k_{31}/K_W and k_{41}/K_1. The value of the Henry's law constant k_H ($mol\cdot(L\ bar)^{-1}$) may be expressed as a function of temperature using the equation of Pohorecki and Moniuk [177]:

$$\log(k_H) = 9.1229 - 5.9044\times10^{-2}T + 7.8857\times10^{-5}T^2 \tag{41}$$

Based on our study on CO_2 uptake kinetics in hydroxide solutions under various process conditions described in Section 3.2.3.1 *(Paper IV)*, the volumetric CO_2 mass transfer coefficients for the system in the absence of a precipitation reaction $k_L a_{CO_2}^0$ (s^{-1}) were calculated using an empirical equation (R^2=0.91) applicable to barboter-type reactors *(Paper IV: modified Eq. 16)* :

$$k_L a_{CO_2}^0 = 2.953\times10^{-3}\left(\frac{Q_G}{V_L}\right)^{0.386}\left(\frac{P_N}{V_L}\right)^{0.330} c_{CO_2}^{0.114}, \tag{42}$$

in which P_N is the power consumed by the stirrer in watts.

The average values of the reaction rate constants, k_{51} and k_{52} in Eq. 23 were estimated in our study on $CaCO_3$ precipitation kinetics in the model gas–liquid system *(Paper V)* described in Section 3.2.3.2 to be 1.88×10^6 $L\cdot(mol\ s)^{-1}$ and 0.009 $mol\cdot(L\ s)^{-1}$. The value of the CO_2 mass transfer enhancement factor, E (introduced in Section 3.2.3.2), was determined using an empirical equation

(R^2=0.97) proposed by us in the same study *(Paper V: Eq. 19)*, where E is a function of the initial Ca^{2+} concentration (mmol L^{-1}):

$$E = 0.0027 \times \left[Ca^{2+}\right]_0^2 + 0.0224 \times \left[Ca^{2+}\right]_0 + 1.0 \tag{43}$$

Based on the experimental data obtained for the ash leachate–CO_2-containing flue gas system (Section 2.1.3), the SO_4^{2-} dynamic equilibrium concentration, $[SO_4^{2-}]^*$ (mmol L^{-1}), was calculated using an empirical equation (R^2=0.98) dependent on the operating parameters and the initial concentrations of Ca^{2+} and SO_4^{2-} ions (mmol L^{-1}) in the leachate *(Paper VII: Eq. 28)*:

$$\left[SO_4^{2-}\right]^* = 0.761 \times \left[SO_4^{2-}\right]_0^{0.976} \left[Ca^{2+}\right]_0^{-0.073} \left(\frac{Q_G}{V_L}\right)^{0.066} c_{CO_2}^{0.038} \left(\frac{P_N}{V_L}\right)^{-0.012} \tag{44}$$

The kinetic calculations were performed using the MODEST 6.1 software package (Section 2.2). Additionally, a program feature accounting for changes in V_L, V_G and V_{G2} due to sample collection was implemented in the modeling algorithm. The volumetric mass transfer coefficient of anhydrite, $k_L a_{CaSO_4}$ and the reaction rate constants, k_{61} and k_{62} in Eq. 25 were evaluated from differential Eqs. 26-36. A parameter estimation procedure was carried out on the basis of the proposed model and some of the experimental data. The correlation coefficients for all data sets were greater than 0.93. The average values of the reaction rate constants, k_{61} and k_{62}, were estimated to be $0.1(\pm0.021)\times10^7$ s^{-1} and $0.4(\pm0.013)\times10^3$ L·(mol s)$^{-1}$, respectively *(Paper VII)*. Based on the evaluated values of $k_L a_{CaSO_4}$ (s^{-1}), an empirical equation (R^2=0.8) applicable to barboter-type reactors was proposed as a function of the main process parameters *(Paper VII: Eq. 29)*:

$$k_L a_{CaSO_4} = 1.95 \times 10^{-7} \times \left(\frac{Q_G}{V_L}\right)^{1.702} c_{CO_2}^{1.134} \left(\frac{P_N}{V_L}\right)^{0.126} \tag{45}$$

Table 7. Parameters used in the modeling of oil shale ash leachate carbonation at 298K

Parameter	Value	Parameter	Value
k_{11}, L·(mol s)$^{-1}$	8.4×10^3	k_{42}, L·(mol s)$^{-1}$	5.7×10^4
k_{12}, s^{-1}	2.0×10^{-4}	k_{51}^{av}, L·(mol s)$^{-1}$	1.9×10^6
k_{21}, L·(mol s)$^{-1}$	6.0×10^9	k_{52}^{av}, mol·(L s)$^{-1}$	9.0×10^{-3}
k_{22}, s^{-1}	1.2×10^6	k_{61}^{av}, s^{-1}	0.1×10^7
k_{31}, L·(mol s)$^{-1}$	1.4×10^{11}	k_{62}^{av}, L·(mol s)$^{-1}$	0.4×10^3
k_{32}, mol·(L s)$^{-1}$	1.3×10^{-3}	k_H, mol·(L atm)$^{-1}$	3.5×10^{-2}
k_{41}, s^{-1}	2.4×10^{-2}	ρ_{CO2} (25ºC), kg m^{-3}	1.8×10^0

The developed model was used to simulate the carbonation/precipitation process in the ash leachate – CO_2-containing flue gas system. The procedure was accomplished with the MODEST 6.1 software package (Section 2.2). The reaction rate constants and the main parameters applied for process simulation are summarized in Table 7 *(Paper VII: Table 2)*.

The model was verified by comparing the dynamic response of the concentrations of the reactive species (Ca^{2+}, OH^-, SO_4^{2-}, $CaCO_3$, $CaSO_4$, HCO_3^-, CO_2, H^+ and CO_3^{2-}) to variable operational conditions with the experimental data obtained according to the procedure described in Section 2.1.3. Plots of experimental and model-predicted concentration profiles corresponding to TESTS 4, 6, 7 and 8 (Table 5) are provided in *Paper VII (Fig. 2)*. The proposed model supports the assumed reaction scheme and describes with high certainty the process course including the re-dissolution of PCC due to increased solubility of $CaCO_3$ at lower pH. The model also enables the prediction of pH values *(Paper VII: Fig. 2a)*, which suggests potential applications in wastewater neutralization process design. Additional details can be found in *Paper VII*.

3.2.4 Continuous mode process concept and scale-up

A conceptual process flow diagram for the beneficiation of waste streams from oil shale energetics via the production of synthetic calcium carbonate-type material and simultaneous CO_2 mineral sequestration and residual material stabilization/neutralization was proposed (Fig. 9) for continuous mode operation. The suggested process concept does not require the use of chemicals (acid for extraction or alkali for precipitation) and the liquid phase is recycling in the system. For improved performance of the process, the PCC production route is envisaged to be implemented (according to Fig. 9) with the new method recently proposed by us for eliminating CO_2 from flue gases by Ca-containing industrial wastes (*Patent*). The process includes contacting the aqueous suspensions of Ca-containing waste material with a CO_2-containing flue gas in two steps: in the first step (Reactor 1), the suspension is bubbled with flue gas, maintaining pH levels in the range of 10–12, and in the second step (Reactor 2) maintaining the pH levels in the range of 7–8 (Fig. 9b). The water-soluble components such as free lime are carbonated in the first step and the components with low solubility, in which Ca is generally contained in the form of silicates ($CaSiO_3$, Ca_2SiO_4, $Ca_3Mg(SiO_4)_2$), are carbonated in the second step. This enables optimal conditions for treating different phases of multicomponent waste materials.

A simplified technological scheme of a potential continuous-flow pilot-scale installation including the units of oil shale ash leachate preparation, carbonation and solid product separation is given in Fig. 10.
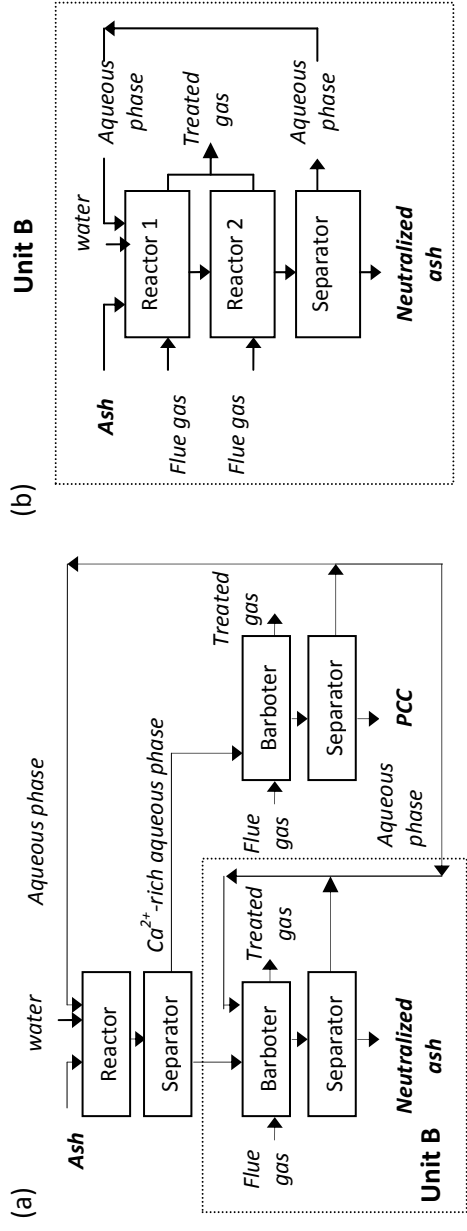
Figure 9. Process diagrams for continuous mode aqueous carbonation of Ca-containing waste materials
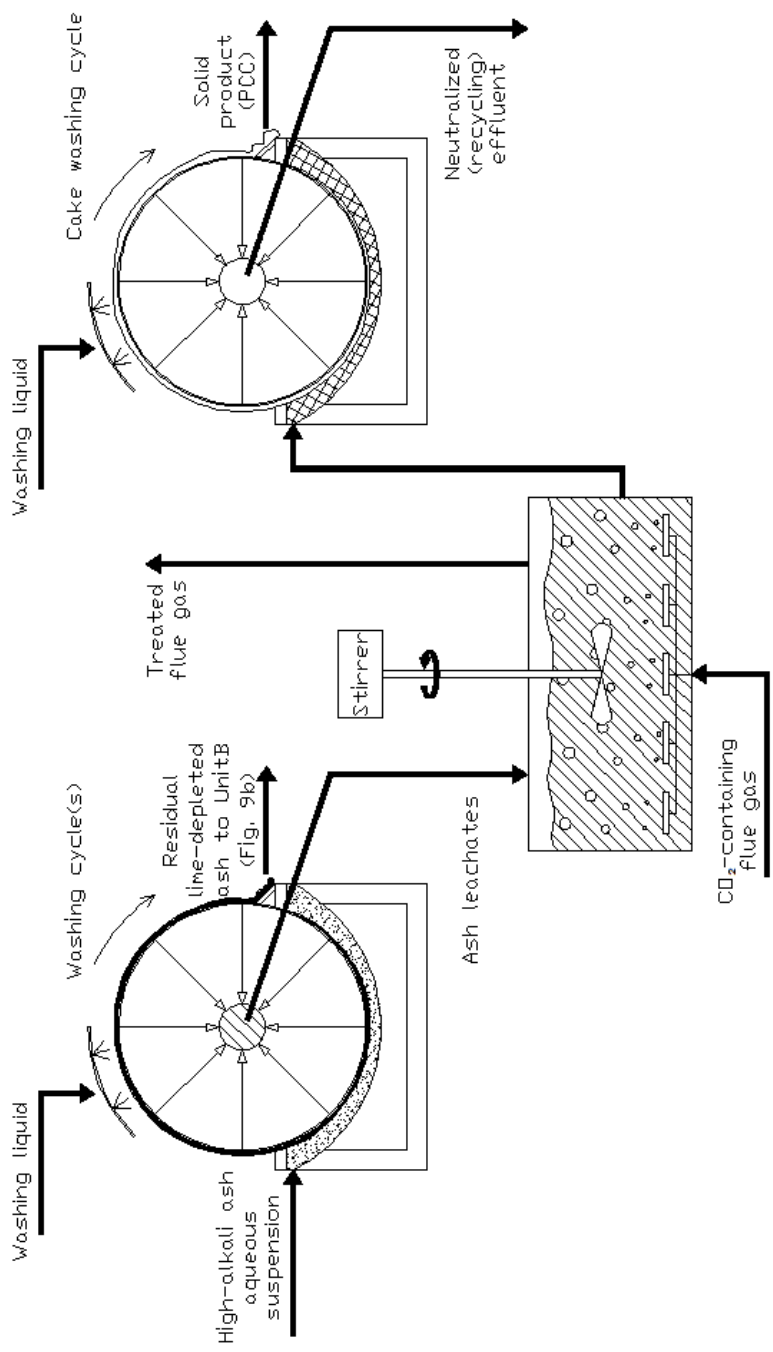
Figure 10. Simplified schematic of the continuous PCC production process on the basis of waste oil shale ash

According to intended design, a highly alkaline ash-water suspension from the power plant ash hydraulic transportation system is directed to the rotary drum filter, where the solid residue is separated under vacuum from the parental Ca-rich solution. The alkaline liquid phase is then treated with the CO_2-containing flue gas injected by nozzles (for improved mixing) located at the bottom of the barboter-type reactor where neutralization of the ash leaching water and formation of the solid precipitate ($CaCO_3/CaSO_4$ composite) takes place. In the final stage, the solid material is washed and separated by means of a drum filter from the stabilized wastewater exiting the barboter-basin. The neutralized effluent is recirculated in the system. Alternatively, as a more robust version of the process, the oversaturated with Ca ions alkali wastewater from the settling ponds of the ash transportation system could be used directly as a feedstock. In this case, the load on the first filter will drop considerably, consequently lowering its dimensions.

Preliminary technological evaluation and recommendations

From the point of view of PCC production via the carbonation route, there are two major pH regions to be considered. Because CO_2 dissolution into water is pH-dependent (CO_2 is found in the solution mainly as CO_3^{2-} at pH>9 and as HCO_3^- around pH<9.0), the highest concentration of PCC is expected at pH>9. Furthermore, at lower pH values, H^+ ions will initiate the re-dissolution of $CaCO_3$. At the same time, alkaline wastewater (such as ash leachate) has to be neutralized to a pH level accepted by environmental regulations (pH<9) before directing it into nature. Taking into account the above specifics and assuming a wastewater flow rate of 3600 L h^{-1}, evaluation of the important parameters (Table 8) in the design of the continuous mineralization process of CO_2 accompanied by the formation of PCC on the basis of oil shale ash was made by implementing the proposed model (Section 3.2.3.3) for two possible objectives: maximum CO_2 mineralization (highest $CaCO_3$ content) or wastewater neutralization (effluent pH~7). The results are given in Table 8. Furthermore, the following recommendations could be given to come to an optimal process design or optimal crystalline product quality:

- The appropriate end-point of carbonation will need to be selected depending on the desired purity grade and textural properties (influenced by the precipitation conditions) of the product determined by its application field and/or the primary environmental objective of the process.
- The composition of the effluent will depend on the duration of carbonation. The alkalinity of the leachates could be decreased to an accepted pH level in the precipitation step or in the next stage after PCC separation at pH>9. In any case, the resulting effluent can be recirculated in the system.
- After the extraction of water-soluble calcium from ash, the lime-depleted residue is able to bind an additional amount of CO_2 on account of residual lime and Ca/Mg silicates. Following the stabilization route proposed in Fig.

9, waste material can be utilized or safely deposited at an environmentally suitable location without the need for monitoring programs.

- As the next step, an estimation of final product suitability for various applications must be undertaken.

CO$_2$ binding and PCC production capacity of oil shale energetics waste streams

In addition to a considerable amount of free CaO (10-30 wt%), oil shale ashes contain up to 30% Ca/Mg silicates as potential CO$_2$ binders. Our recent developments involving ash–water suspension carbonation demonstrated that oil shale ashes are able to bind up to 290 kg CO$_2$ per ton of ash or as much as ~15 and 73% of the oil shale's total and mineral carbon content, respectively [60]. Moreover, beneficiation of 1 million ton of ash (containing ~20% free lime on average) would allow for producing close to 360 kt of CaCO$_3$, while via the carbonation of 1 million m^3 of leachates, at least 1.3 kt of CO$_2$ could be captured and up to 3 kt of PCC formed.

Table 8. Process scale-up: design parameters estimation results

Process parameters	Process objective	Contact time t, min	Liquid volume in reactor V_L, L	Flue gas flow rate $Q_G \times 10^{-3}$, L/h	Stirrer power consumption, W	Ca^{2+}	SO_4^{2-}	$CaSO_4$	$CaCO_3$	$CaSO_4$	$CaCO_3$	solid product total	$CaSO_4$	$CaCO_3$	Amount CO_2 bond, g/min
						mmol/L				g/min			%		
$Q_{wastewater}$=60 L/min Q_G/V_L=200 h^{-1} c_{CO2}=15% P_N/V_L=3.7 W/L	max miner-on (Ca^{2+}_{min} point)	1.58	94.7	18.9	350.5	4.2	6.9	0.95	26.7	7.75	160.0	167.8	4.6	95.4	70.4
Liquid phase composition Ca^{2+}=31.80 mmol/L SO_4^{2-}=7.85 mmol/L pH=12.89	Solution neutralization (pH~7)	3.13	187.7	37.5	694.5	14.2	6.8	1.05	16.6	8.57	99.5	108.1	7.9	92.1	43.8

4. CONCLUSIONS

This thesis elucidates the feasibility, specifics and mechanisms of a novel route for CO_2 sequestration and utilization/beneficiation of a potentially hazardous waste into valuable product. It demonstrated that free lime could without difficulty be rapidly separated from oil shale ash by leaching it into aqueous solutions. The resulting leachates could then serve as a novel medium for the crystallization of a precipitated calcium carbonate-type material applicable to several industrial applications.

Treatment of ash leachates with a CO_2-containing model flue gas in a batch reactor under ambient operating conditions (room temperature and atmospheric pressure) resulted in the precipitation of high brightness PCC containing up to ~96% $CaCO_3$ with a mean particle size ranging from 4−10 μm. Variation in the process parameters had a profound influence on PCC characteristics: the crystal size, surface area and morphology of the calcium carbonate crystals were controlled by the hydrodynamic conditions (gas flow rate and mixing intensity) which affected the duration of precipitation and the pH of the crystallization medium.

The mechanisms and modeling algorithms for the main stages of the process, including leaching of the main water-soluble substances from ash, dissolution of gaseous CO_2 into the alkaline liquid phase and $CaCO_3$/$CaSO_4$ co-precipitation from ash leachates of complex composition, have been suggested. The mathematical models introduced here can be used to predict the dissolution behavior of the main water-soluble species from oil shale ashes in the course of leaching in terms of concentrations; moreover, these models can be used to forecast changes in the composition of the liquid (Ca^{2+}, SO_4^{2-}, CO_3^{2-}, HCO_3^-, OH^-, H^+, CO_2), gaseous (CO_2) and solid ($CaCO_3$, $CaSO_4$) phases during the precipitation regime of calcium carbonate from oil shale ash leachates treated with CO_2. Additionally, the necessary residence time or pH profile can be estimated. The proposed algorithms may also be applied to design PCC production from other lime-containing wastes or calcium-rich alkaline wastewaters used as the feedstock. This flexibility makes the developed models a valuable tool in the field of environmental protection in different industrial sectors.

The process was found to have a great potential for reducing the environmental burdens associated with oil shale-based power production, while simultaneously enhancing economic benefit. The neutralization of the alkalinity of ash (leachates) offers a possibility for environmentally sound disposal of waste residue.

REFERENCES

1. IPCC fourth assessment report: Climate change 2007 (AR4)/Pachauri, R.K., Reisinger, A. (eds.). Geneva, Switzerland. 104 p.

2. Tans, P. Trends in atmospheric carbon dioxide: Mauna Loa Observatory, NOAA/ESRL. www.esrl.noaa.gov/gmd/ccgg/trends, 01.11.2011

3. Keeling, C.D., Whorf, T.P., Wahlen, M., Van der Plicht, J. Interannual extremes in the rate of rise of atmospheric carbon dioxide since 1980. – *Nature* 1995, 375(1), 666–670.

4. IPCC special report on carbon dioxide capture and storage/Metz, B., Davidson, O., Coninck, H., Loos, M., Meyer, L. (Eds.). UK: Cambridge University Press, 2005. 431 p.

5. The Cooperative Research Centre for Greenhouse Gas Technologies: About CCS, http://www.co2crc.com.au/, 01.11.2011

6. Bellona CCS web: Introduction to CCS, http://bellona.org/ccs/, 01.11.2011

7. Kohl, A.O., Nielsen, R.B. Gas purification. Houston, TX, USA: Gulf Publishing Co., 1997. 1439 p.

8. Wappel, D., Gronald, G., Kalb, R., Draxler, J. Ionic liquids for post-combustion CO_2 absorption. – *Int. J. Greenhouse Gas Control* 2010, 4(3), 486–494.

9. Freeman, S.A., Dugas, R., Van Wagener, D.H., Nguyen, T., Rochelle, G.T. Carbon dioxide capture with concentrated aqueous piperazine. – *Int. J. Greenhouse Gas Control* 2010, 4, 119–124.

10. Zhao, Z., Cui, X., Ma, J., Li, R. Adsorption of carbon dioxide on alkali-modified zeolite 13X adsorbents. – *Int. J. Greenhouse Gas Control* 2007, 1, 355–359.

11. Nguyen, P.T., Lasseuguette, E., Medina-Gonzalez, Y., Remigy, J.C., Roizard, D., Favre, E. A dense membrane contactor for intensified CO_2 gas/liquid absorption in post-combustion capture. – *J. Membr. Sci.* 2011, 377(1-2), 261–272.

12. Tuinier, M.J., Van Sint Annaland, M., Kramer, G.J., Kuipers, J.A.M. Cryogenic CO_2 capture using dynamically operated packed beds. – *Chem. Eng. Sci.* 2010, 65(1), 114–119.

13. Wolf, J., Anheden, M., Yan, J. Comparison of nickel- and iron-based oxygen carriers in chemical looping combustion for CO_2 capture in power generation. – *Fuel* 2005, 84(7-8), 993–1006.

14. Naqvi, R., Bolland, O. Multi-stage chemical looping combustion (CLC) for combined cycles with CO_2 capture. – *Int. J. Greenhouse Gas Control* 2007, 1(1), 19–30.

15. Baes, C.F., Beall, S.E., Lee, D.W., Marland, G. The collection, disposal and storage of carbon dioxide. – *Interaction of Energy and Climate* /Bach, W., Pankrath, J., William, J. (eds.). D. Reidel Publishing Co., 1980, 495–519.

16. Van der Meer, L.G.H. The CO_2 storage efficiency of aquifers. – *Energy Convers. Manage.* 1995, 36(6–9), 513–518.

17. The underground disposal of carbon dioxide: Final report of Joule 2 Project No. CT92-0031/Holloway, S. (ed.). UK: British Geological Survey, 1996. 355 p.

18. Marchetti C. On geoengineering and the CO_2 problem. – *Clim. Change* 1977, 1, 59–68.

19. Cole, K.H., Stegen, G.R., Spencer, D. The capacity of the deep ocean to absorb carbon dioxide. – *Energy Convers. Manage.* 1993, 34(9–11), 991–998.

20. Seifritz, W. CO_2 disposal by means of silicates. – *Nature* 1990, 345, 486.

21. Stevens, S.H., Gale, J. Geologic CO_2 sequestration. – *Oil Gas J.* 2000, 98(20), 40–44.

22. Koide, H., Tazaki, Y., Noguchi, Y., Nakayama, S., Iijima, M., Ito, K., Shindo, Y. Subterranean containment and long-term storage of carbon dioxide in unused aquifers and in depleted natural gas reservoirs. – *Energy Convers. Manage.* 1992, 33(5–8), 619–626.

23. Gunter, W.D., Gentzis, T., Rottengusser, B.A., Richardson, R.J.H. Deep coalbed methane in Alberta, Canada: a fuel resource with the potential of zero greenhouse gas emissions. – *Energy Convers. Manage.* 1997, 38, 217–222.

24. Bachu, S., Gunter, W.D., Perkins, E.H. Aquifer disposal of CO_2: hydrodynamic and mineral trapping. – *Energy Convers. Manage.* 1994, 35(4), 269–279.

25. Gunter, W.D., Bachu S., Benson, S. The role of hydrogeological and geochemical trapping in sedimentary basins for secure geological storage for carbon dioxide. – *Geological Storage of Carbon Dioxide: Technology* 233/Baines, S., Worden, R.H. (eds.). UK: Special Publication of Geological Society, 2004, 129–145.

26. Korbol, R., Kaddour, A. Sleipner Vest CO_2 disposal - injection of removed CO_2 into the Utsira formation. – *Energy Convers. Manage.* 1995, 36(3–9), 509–512.

27. Davison, J. Performance and costs of power plants with capture and storage of CO_2. – *Energy* 2007, 32, 1163–1176.

28. Huesemann, M.H. Can advances in science and technology prevent global warming? – *Mitigation and Adaption Strategies for Global Change* 2006, 11, 539–577.

29. Armor, J.N. Addressing the CO_2 dilemma. – *Catal. Lett.* 2007, 114, 115–121.

30. Sorey, M.L., Farrar, C.D., Evans, W.C., Hill, D.P., Bailey, R.A., Hendley, J.W., Stauffer. P.H. Invisible CO_2 gas killing trees at Mammoth Mountain, California. US Geological Survey, 1996.

31. Overview of monitoring requirements for geological storage projects: Report Ph4/29. UK: IEA greenhouse gas R&D programme, 2004.

32. Dunsmore, H.E. A geological perspective on global warming and the possibility of carbon dioxide removal as calcium carbonate mineral. – *Energy Convers. Manage.* 1992, 33(5–8), 565–572

33. Lackner, K.S., Wendt, C.H., Butt, D.P., Joyce, E.L., Sharp, D.H. Carbon dioxide disposal in carbonate minerals. – *Energy* 1995, 20, 1153–1170.

34. Huijgen, W.J.J. Thesis: Carbon dioxide sequestration by mineral carbonation. The Netherlands: Energy research Centre of the Netherlands, 2007.

35. Gerdemann, S.J., O'Connor, W.K., Dahlin, D.C., Penner, L.R., Rush, H. Ex situ aqueous mineral carbonation. – *Environ. Sci. Technol*. 2007, 41, 2587–2593.

36. Matter, J. M., Keleman, P.B. Permanent storage of carbon dioxide in geological reservoirs by mineral carbonation. – *Nat. Geosci*. 2009, 2, 837–841.

37. O'Connor, W.K., Dahlin, D.C., Rush, G.E., Gerdemann, S.J., Penner, L.R., Nilsen, R.P. Aqueous mineral carbonation: Mineral availability, pretreatment, reaction parametrics, and process studies. DOE/ARC-TR-04-002. USA: Albany Research Center, 2005.

38. Huijgen W.J.J, Witkamp G.-J., Comans R.N.J. Mechanisms of aqueous wollastonite carbonation as a possible CO_2 sequestration process. **–** *Chem. Eng. Sci.* 2006, 61, 4242–4251.

39. Sipilä, J., Teir, S., Zevenhoven, R. Carbon dioxide sequestration by mineral carbonation: Literature review update 2005–2007. Report 2008-1. Finland: Abo Akademi University, 2008.

40. Lackner, K.S., Butt, D.P., Wendt, C.H. Progress on binding CO_2 in mineral substrates. – *Energy Convers. Manage.* 1997, 38, S259–264.

41. Koljonen, T., Siikavirta, H., Zevenhoven, R., Savolainen, I. CO_2 capture, storage and reuse potential in Finland. – *Energy* 2004, 29, 1521–1527.

42. Huijgen, W.J.J., Comans, R.N.J. Carbon dioxide sequstration by mineral carbonation: Literature review update 2003-2004. ECN-C-05-022. The Netherlands: Energy Research Centre of The Netherlands, 2005.

43. Zevenhoven, R., Kavaliauskaite, I. Mineral carbonation for long-term CO_2 storage: An exergy analysis. – *Int. J. Thermodyn.* 2004, 7, 22–31.

44. Zevenhoven, R., Teir, S., Eloneva, S. Heat optimisation of a staged gas–solid mineral carbonation process for long-term CO_2 storage. – *Energy* 2008, 33, 362–370.

45. Schulze, R.K., Hill, M.A., Field, R.D., Papin, P.A., Hanrahan, R.J., Byler, D.D. Characterization of carbonated serpentine using XPS and TEM. – *Energy Convers. Manage.* 2004, 45(20), 3169–3179.

46. Gerdemann, S.J., Dahlin, D.C., O'Connor, W.K. Carbon dioxide sequestration by aqueous mineral carbonation of magnesium silicate minerals. – *Proceedings of the 6th International Conference on Greenhouse Gas Control Technologies* 1/Gale, J., Kaya, Y. (eds.). Elsevier Ltd., 2003, 677–682.

47. Teir, S., Revitzer, H., Eloneva, S., Fogelholm, C.-J., Zevenhoven, R. Dissolution of natural serpentinite in mineral and organic acids. – *Int. J. Miner. Process.* 2007, 83, 36–46.

48. Kim, D.J., Chung, H.S. Effect of grinding on the structure and chemical extraction of metals from serpentine. – *Part. Sci. Technol.* 2002, 20(2), 159–168.

49. O'Connor, W.K., Dahlin, D.C., Nilsen, D.N., Walters, R.P., Turner, P.C. Carbon dioxide sequestration by direct mineral carbonation with carbonic acid. – *Proceedings of the 25th International Technical Conference on Coal Utilization and Fuel Systems*. Clearwater, FL, USA, 2000.

50. National Energy Technology Laboratory (NETL): Carbon sequestration; reference shelf, www.netl.doe.gov/technologies/carbon_seq/refshelf/refshelf.html/, 01.11.2011

51. Geerlings, J.J.C., Mesters, C.M.A.M., Oosterbeek, H. Process for mineral carbonation with carbon dioxide. – *Patent nr WO02085788*, 2002.

52. Kakizawa, M., Yamasaki, A., Yanagisawa, Y. A new CO_2 disposal process using artificial rock weathering of calcium silicate accelerated by acetic acid. – *Energy* 2001, 26, 341–354.

53. Blencoe, J.G., Anovitz, L.M., Palmer, D.A., Beard, J.S. Carbonation of metal silicates for long-term CO_2 sequestration. – *US20040213705*, 2004.

54. Park, A.-H., Jadhav, R.A., Fan, L.-S. CO_2 mineral sequestration: chemical enhanced aqueous carbonation of serpentine. – *Canadian J. Chem. Eng.* 2003, 81, 885–890.

55. Katsuyama, Y., Yamasaki, A., Iizuka, A., Fujii, M., Kumagai, K., Yanagisawa, Y. Development of a process for producing high-purity calcium carbonate (CaCO3) from waste cement using pressurized CO_2. – *Environ. Prog.* 2005, 24, 162–170.

56. Kodama, S., Nishimoto, T., Yogo, K.,Yamada, K. Design and evaluation of a new CO_2 fixation process using alkaline-earth metal wastes. – *Proceedings of 8-th International Conference of Greenhouse Gas Control Technologies.* Trondheim, Norway: Elsevier ltd., 2006, pp 5 p. on CD-ROM.

57. Kuusik, R., Uibu, M., Toom, M., Muulmann, M.-L., Kaljuvee, T., Trikkel, A. Sulphation and carbonization of oil shale CFBC ashes in heterogeneous systems. – *Oil Shale* 2005, 22(4S), 421–434.

58. Uibu, M., Uus, M., Kuusik, R. CO_2 mineral sequestration in oil shale wastes from Estonian power production. – *J. Environ. Manage.* 2009, 90, 1253–1260.

59. Kuusik, R., Uibu, M., Kirsimäe, K. Characterization of oil shale ashes formed at industrial scale boilers. – *Oil Shale* 2005, 22(4S), 407–420.

60. Uibu, M., Velts, O., Kuusik, R. Aqueous carbonation of oil shale wastes from Estonian power production for CO_2 fixation and PCC production. – *Proceedings of the Conference of Young Scientist on Energy Issues* (Kaunas, Lithuania, May 26-27, 2011), 415–424.

61. Jia, L., Anthony, E.J. Pacification of FBC ash in a pressurized TGA. – *Fuel* 2000, 79, 1109–1114.

62. Montes-Hernandez, G., Perez-Lopez, R., Renard, F., Nieto, J.M., Charlet, L. Mineral sequestration of CO_2 by aqueous carbonation of coal combustion fly-ash. – *J. Hazard. Mater.* 2009, 161, 1347–1354.

63. Uliasz-Bocheńczyk, A., Mokrzycki, E., Piotrowski, Z., Pomykał, R. Estimation of CO_2 sequestration potential via mineral carbonation in fly ash from lignite combustion in Poland. – *Energy Procedia* 2009, 1, 4873–4879.

64. Huijgen, W.J.J., Comans, R.N.J. Carbonation of steel slag for CO_2 sequestration: Leaching of products and reaction mechanisms. – *Environ. Sci. Technol.* 2006, 40, 2790–2796.

65. Eloneva, S., Teir, S., Salminen, J., Fogelholm, C.-J., Zevenhoven, R. Fixation of CO_2 by carbonating calcium derived from blast furnace slag. – *Energy* 2008, 33, 1461–1467.

66. Bonenfant, D., Kharoune, L., Sauve, S., Hausler, R., Niquette, P., Mimeault, M., Kharoune, M. CO_2 sequestration potential of steel slags at ambient pressure and temperature. – *Ind. Eng. Chem. Res*. 2008, 47, 7610–7616.

67. Doucet, F.J. Effective CO_2-specific sequestration capacity of steel slags and variability in their leaching behaviour in view of industrial mineral carbonation. – *Miner. Eng.* 2009, 23, 262–269.

68. Rendek, E., Ducom, G., Germain, P. Carbon dioxide sequestration in municipal solid waste incinerator (MSWI) bottom ash. – *J. Hazard. Mater.* 2006, B128, 73–79.

69. Van Gerven, T., Van Keer, E., Arickx, S., Jaspers, M., Wauters, G., Vandecasteele, C. Carbonation of MSWI-bottom ash to decrease heavy metal leaching, in view of recycling. – *Waste Manage*. 2005, 25, 291–300.

70. Wang, L., Jin, Y., Nie, Y. Investigation of accelerated and natural carbonation of MSWI fly ash with a high content of Ca. – *J. Hazard.Mater*. 2010, 174, 334–343.

71. Costa, G., Baciocchi, R., Polettini, A., Pomi, R., Hills, C.D., Carey, P.J. Current status and perspectives of accelerated carbonation processes on municipal waste combustion residues. – *Environ. Monit. Assess.* 2007, 135, 55–75.

72. Baciocchi, R., Costa, G., Polettini, A., Pomi, R., Prigiobbe, V. Comparison of different reaction routes for carbonation of APC residues. – *Energy Procedia* 2009, 1, 4851–4858.

73. Huntzinger, D.N., Gierke, J.S., Kawatra, K., EIsele, T.C., Sutter, L.L. Carbon dioxide sequestration in cement kiln dust through mineral carbonation. – *Environ. Sci. Technol*. 2009, 43, 1986–1992.

74. Gunning, P.J., Hills, C.D., Carey, P.J. Production of lightweight aggregate from industrial waste and carbon dioxide. – *Waste Manage.* 2009, 29, 2722–2729.

75. Bonenfant, D., Kharoune, L., Sauve, S. B., Hausler, R., Niquette, P., Mimeault, M., Kharoune, M. CO_2 Sequestration by Aqueous Red Mud Carbonation at Ambient Pressure and Temperature. – *Ind. Eng. Chem. Res*. 2008, 47, 7617–7662.

76. Stolaroff, J.K., Lowry, G.V., Keith, D.W. Using CaO- and MgO rich industrial waste streams for carbon sequestration. – *Energy Convers. Manage. 2005,* 46, 687–699.

77. Iizuka, A., Fujii, M., Yamasaki, A.,Yanagisawa, Y. Development of a new CO_2 sequestration process utilizing the carbonation of waste cement. – *Ind. Eng. Chem. Res.* 2004, 43(24), 7880–7887.

78. Baciocchi R., Polettini A., Pomi R., Prigiobbe V., v. Zedwitz V., Steinfeld A. CO_2 sequestration by direct gas-solid carbonation of air pollution control (APC) residues. – *Energy & Fuels* 2006, 20, 1933–1940.

79. Teir, S., Eloneva, S.,Fogelholm, C.-J., Zevenhoven, R. Dissolution of steelmaking slags in acetic acid for precipitated calcium carbonate production. – *Energy* 2007, 32, 528–539.

80. Gorset, O., Johansen, H., Kihle, J., Munz, I.A., Raaheim, A. Method for industrial manufacture of pure $MgCO_3$ from an olivine containing species of rock. – *Patent WO/2007/069902*, 2007.

81. Kirk, R.E., Othmer, D.F. Encyclopedia of chemical technology. Part: 4. 4th ed. USA: John Wiley & Sons Inc., 1992. 1117 p.

82. Imppola O. Precipitated calcium carbonate – PCC. *Pigment Coating and Surface Sizing of Paper*/Lehtinen, E. (ed.). Finland: Gummerus Printing, 2000, 141–151.

83. SMR: What is PCC, www.specialtyminerals.com/our-minerals/what-is-pcc/, 01.11.2011

84. Tlili, M.M., Ben Amor, M., Gabrielli, C., Joiret, S., Maurin, G., Rousseau, P. Characterization of $CaCO_3$ hydrates by micro-Raman spectroscopy. – *J. Raman Spectrosc.* 2001, 33, 10–16.

85. Chen, C.K., Tai C.Y. Competing effects of operating variables in the synthesis of $CaCO_3$ particles using the reverse microemulsion technique. – *Chem. Eng. Sci.* 2010, 65, 4761– 4770.

86. Lioliou, M.G., Paraskeva, C.A., Koutsoukos, P.G., Payatakes, A.C. Heterogeneous nucleation and growth of calcium carbonate on calcite and quartz. – *J. Colloid Interface Sci.* 2007, 308, 421–428.

87. Ukrainczyk, M., Kontrec, J., Babić-Ivančić, V., Brečević, L., Kralj D. Experimental design approach to calcium carbonate precipitation in a semicontinuous process. – *Powder Technol.* 2007, 171(3), 192–199.

88. Yu, J.G., Lei, M., Cheng, B., Zhao, X.J. Facile preparation of calcium carbonate particles with unusual morphologies by precipitation reaction. – *J. Cryst. Growth* 2004, 261, 566–570.

89. Cheng, B., Lei, M., Yu, J.G., Zhao, X.J. Preparation of monodispersed cubic calcium carbonate particles via precipitation reaction. – *Mater. Lett.* 2004, 58, 1565–1570.

90. Industrial minerals: The economics of precipitated calcium carbonate. 7th ed. Roskill, 2008. 194 p.

91. Koppinen, S., Riistama, K., Vuori, M. Suomen kemianteollisuus. Tampere, Finland: Tammer-Paino Oy, 2003.

92. Sang Hwan Cho, Jin Koo Park, Seung Kwan Lee, Sung Min Joo, Im Ho Kim, Ji Whan Ahn, Hwan Kim. Synthesis of precipitated calcium carbonate using a limestone and its application in paper filler and coating color. – *Mater. Sci. Forum* 2007, 544-545, 881–884.

93. Casey, J. Pulp and paper: Chemistry and chemical technology. 3rd ed. Wiley, 1983. 640 p.

94. National Lime Association: Precipitated calcium carbonate, www.lime.org/uses_of_lime/other_uses/precip_cc.asp#PCC2/, 01.11.2011

95. Myers, R.L. The 100 most important chemical compounds: A reference guide. London: Greenwood Press, 2007. 326 p.

96. Haskins, W.J., Osterhuber, E.J. Aragonitic precipitated calcium carbonate pigment for coating rotogravure printing papers. *US5861209,* 1999.

97. Mathur, K. High speed manufacturing process for precipitated calcium carbonate employing sequential pressure carbonation. – *Patent application WO 01/07365,* 2001.

98. Mohamed, Abdel-Mohsen Onsy et al. Method for treating particulate material. – *US Patent application 20110065854*, 2011

99. Teir, S., Eloneva, S., Zevenhoven, R. Production of precipitated calcium carbonate from calcium silicates and carbon dioxide. – *Energy Convers. Manage.* 2005, 46, 2954–2979.

100. Zevenhoven, R., Eloneva, S., Teir, S. Chemical fixation of CO_2 in carbonates: Routes to valuable products and long-term storage. – *Catal. Today* 2006, 115, 73–79.

101. Kodama, S., Nishimoto, T., Yamamoto, N., Yogo, K., Yamada, K. Development of a new pH-swing CO_2 mineralization process with a recyclable reaction solution. – *Energy* 2008, 33(5), 776–784.

102. Geerlings, J.J.C., Van Mossel, G.A.F., In't Veen, B.C.M. Process for sequestration of carbon dioxide. – *Patent PCT/EP2006/069796*, 2007.

103. Eloneva, S., Teir, S., Savolahti, J. Fogelholm, C.-J., Zevenhoven, R. Co-utilization of CO_2 and calcium silicate-rich slags for precipitated calcium carbonate production (part II). – *Proceedings of the ECOS2007* (Padova, Italy, 25-28 June, 2007), vol. II, 1389-1396.

104. Franke, J., Mersmann, A. The influence of the operational conditions on the precipitation process. – *Chem. Eng. Sci.* 1995, 50(11), 1737-1753.

105. Mersmann, A. Crystallization technology handbook. New York: Marcel Dekker Inc., 1995.

106. Palosaari, S., Louhi-Kultanen, M., Sha, Z. Industrial Crystallization. *Handbook of Industrial Drying*/ Mujumdar, A. (ed.). Taylor & Francis Group, LLC, 2007, 1203-1224.

107. Kind, M. Precipitation phenomena and their relevance to precipitation technology. – *Proceedings of the 14th International Symposium on Industrial Crystallization.* Cambridge, 1999.

108. Rodríguez-Navarro, C., Jiménez-Lopez, C., Rodríguez-Navarro, A., Gonzalez-Muñoz, M.T., Rodríguez-Gallego, M. Bacterially mediated mineralization of vaterite. – *Geochim. Cosmochim. Acta* 2007, 71(5), 1197–1213.

109. Ogino, T., Suzuki, T., Sawada, K.J. The rate and mechanism of polymorphic transformation of calcium carbonate in water. – *J. Cryst. Growth* 1990, 100(1–2), 159–167.

110. Altay, E., Shahwan, T., Tanoglu, M. Morphosynthesis of $CaCO_3$ at different reaction temperatures and the effects of PDDA, CTAB, and EDTA on the particle morphology and polymorph stability. – *Powder Technol*. 2007, 178(3), 194–202.

111. Chen, J., Xiang, L. Controllable synthesis of calcium carbonate polymorphs at different temperatures. – *Powder Technol*. 2009, 189, 64–69.

112. Han, Y.S., Hadiko, G., Fuji, M., Takahashi, M. Effect of flow rate and CO_2 content on the phase and morphology of $CaCO_3$ prepared by bubbling method. – *J. Cryst. Growth* 2005, 276, 541–548.

113. Carmona, J.G., Morales, J.G., Clemente, R.R. Rhombohedral–scalenohedral calcite transition produced by adjusting the solution electrical conductivity in the system $Ca(OH)_2$–CO_2–H_2O. – *J. Colloid Interface Sci*. 2003, 261, 434–440.

114. Wang, C.Y., Sheng, Y., Zhao, X., Zhao, J.Z., Ma, X.K. ,Wang, Z.C. A novel aqueous-phase route to synthesize hydrophobic $CaCO_3$ particles in situ. – *Mater. Sci. Eng*. 2007, C27, 42–45.

115. Yan, G., Wang, L., Huang, J. The crystallization behavior of calcium carbonate in ethanol/water solution containing mixed nonionic/anionic surfactants. – *Powder Technol*. 2009, 192(1), 58–64.

116. Feng, B., Yong A. K. Hui An. Effect of various factors on the particle size of calcium carbonate formed in a precipitation process. – *Mater. Sci. Eng.* 2007, 445-446, 170–179.

117. Montes-Hernandez, G., Renard, F., Geoffroy, N., Charlet L., Pironon J. Calcite precipitation from CO_2–H_2O–$Ca(OH)_2$ slurry under high pressure of CO_2. – *J. Cryst. Growth* 2007, 308(1), 228–236.

118. Baker, J.S., Judd, S.J. Review Paper: Magnetic Amelioration of Scale Formation. – *Water Res.* 1996, 30(2), 247.

119. Stumm, W., Morgan, J.J. Aquatic Chemistry. Wiley-Interscience, 1996.

120. Bolze, J., Peng, B., Dingenouts, N., Panine, P., Narayanan, T., Ballauff, M. Formation and growth of amorphous colloidal $CaCO_3$ precursor particles as detected by timeresolved SAXS. – *Langmuir* 2002, 18, 8364–8369.

121. Fernandez-Dıaz, L., Pina, C.M., Astilleros J.M., Sanchez-Pastor, N. The carbonatation of gypsum: pathways and pseudomorph formation. – *Am. Mineral*. 2009, 94, 1223–1234.

122. Söhnel, O., Garside, J. Precipitation. Oxford: Butterworth-Heinemann, 1992.

123. Elfil, H., Roques, H. Role of hydrate phases of calcium carbonate on the scaling phenomenon. – *Desalination* 2001, 137(1–3), 177–186.

124. Chakraborty, D., Bhatia, S.K. Formation and aggregation of polymorphs in continuous precipitation. 2. Kinetics of $CaCO_3$ precipitation. – *Ind. Eng. Chem. Res*. 1996, 35, 1995–2006.

125. Wang Mo Jung, Sung Hoon Kang, Woo-Sik Kim, Chang Kyun Choi. Particle morphology of calcium carbonate precipitated by gas–liquid reaction in a Couette –Taylor reactor. – *Chem. Eng. Sci.* 2000, 55(4), 733–747.

126. Chen, P.-C., Liu, S.M., Jang, C.J., Hwang, R.C., Yang, Y.L., Lee, J.S., Jang, J.S. Interpretation of gas–liquid reactive crystallization data using a size-independent agglomeration model. – *J. Cryst. Growth* 2003, 257, 333-343.

127. García-Carmona, J., Gómez-Morales, J., Rodrígrez-Clemente, R. Morphological control of precipitated calcite obtained by adjusting the electrical conductivity in the $Ca(OH)_2$–H_2O–CO_2 system. – *J. Cryst. Growth* 2003, 249, 561–571.

128. García-Carmona, J., Gómez-Morales, J., Rodrígrez-Clemente, R. Morphological characteristics and aggregation of calcite crystals obtained by bubbling CO_2 through a $Ca(OH)_2$ suspension in the presence of additives. – *Powder Technol*. 2003, 130, 307–315.

129. Xiang, L., Xiang, Y., Wang, Z.G., Lin, Y. Influence of chemical additives on the formation of super-fine calcium carbonate. – *Powder Technol*. 2002, 126, 129–133.

130. Xiang, L., Xiang, Y., Wen, Y., Wei, F. Formation of $CaCO_3$ nanoparticles in the presence of terpineol. – *Mater. Lett.* 2004, 58(6), 959–965.

131. Wei, S.H., Mahuli, S.K., Agnihotri, R., Fan, L.S. High surface area calcium carbonate: pore structural properties and sulfation characteristics. – *Ind. Eng. Chem. Res*. 1997, 36, 2114–2148.

132. Agnihotri, R., Mahuli, S.K., Chauk, S.S., Fan, L.S. Influence of surface modifiers on the structure of precipitated calcium carbonate. – *Ind. Eng. Chem. Res*. 1999, 38, 2283–2291.

133. Yang, J.H., Shih, S.M. Preparation of high surface area $CaCO_3$ by bubbling CO_2 in aqueous suspensions of $Ca(OH)_2$: effect of $(NaPO_3)_6$, $Na_5P_3O_{10}$, and Na_3PO_4 additives. – *Powder Technol*. 2010, 197, 230–234.

134. Sangwal, K. Additives and crystallization processes: From fundamentals to applications. Wiley, 2007.

135. Meyer, H. The influence of contaminants on the growth rate of calcite. – *J. Cryst. Growth* 1984, 66, 639.

136. Tai C.Y., Chen, F.B. Polymorphism of $CaCO_3$ precipitated in a constant-composition environment. – *AIChE J.* 1998, 44, 1790–1798.

137. Hu, Z., Deng, Y. Synthesis of needle-like aragonite from calcium chloride and sparingly soluble magnesium carbonate. – *Powder Technol.* 2004, 140, 10–16.

138. Loste, E., Wilson, R.M., Seshadri, R.M., Meldrum, F.C. The role of magnesium in stabilising amorphous calcium carbonate and controlling calcite morphologies. – *J. Cryst. Growth* 2003, 254, 206–218.

139. Reddy, M.M., Nancollas, G.H. The crystallization of calcium carbonate: Isotopic exchange and kinetics. – *J. Colloid Interface Sci.* 1971, 37, 166–172.

140. Han, Y.S., Hadiko, G., Fuji, M., Takahashi, M. Factors affecting the phase and morphology of $CaCO_3$ prepared by a bubbling method. – *J. Eur. Ceram. Soc.* 2006, 26, 843–847.

141. Vucak, M., Pons, M.N., Peric, J., et al. Effect of precipitation conditions on the morphology of calcium carbonate: quantification of crystal shapes using image analysis. – *Powder Technol.* 1998, 97, 1–5.

142. Hostomsky, J., Jones, A. G. Calcium carbonate crystallization, agglomeration and form during continuous precipitation from solution. – *J. Phys. D: Appl. Phys.* 1991, 24, 165–170.

143. Tai, C. Y., Chen, P. C. (1995). Nucleation, agglomeration and crystal morphology of calcium carbonate. – *AIChE J.* 1995, 41, 68–77.

144. Nieh, J.Y. M.S. Thesis: Role of the bubble wake in fine particle production in bubble column systems. USA: Ohio State University, Columbus, 1990.

145. Eesti Energia Annual Report 2010,

www.energia.ee/-/doc/pdf/concern/annual_report_2010_eng.pdf/, 01.11.2011

146. Paist, A., Kask, Ü., Kask, L., Vrager, A., Muiste, P., Padari, A., Pärn, L. Potential of biomass fuels to substitute for oil shale in energy balance in Estonian energy sector. – *Oil Shale* 2005, 22(4S), 369–380.

147. Ots, A. Oil shale fuel combustion. Tallinn: Eesti Energia AS, 2006. 833p.

148. Raukas, A., Teedumäe, A. (eds). Geology and Mineral Resources of Estonia. Tallinn: Estonian Academy Publishers, 1997. 436 p.

149. Mõtlep, R., Sild, T., Puura, E., Kirsimäe, K. Composition, diagenetic transformation and alkalinity potential of oil shale ash sediments. – *J. Hazard. Mater.* 2010, 184(1-3), 567–573.

150. Punning, J.M. Editor's Page: Oil shale and the environment. – *Oil Shale* 2000, 17(2), 77–79.

151. Kahru, A., Põllumaa, L. Environmental hazard of the waste streams of Estonian oil shale industry: an ecotoxicological review. – *Oil Shale* 2006, 23(1), 53–93.

152. US Carbon dioxide Information Analysis Center: CO_2 emissions – Estonia, http://data.worldbank.org/indicator/EN.ATM.CO2E.PC/countries/EE-7E-XR/, 01.11.2011

153. Sliaupa, S., Shogenova, A., Shogenov, K., Sliaupiene, R., Zabele, A., Vaher, R. Industrial carbon dioxide emissions and potential geological sinks in the Baltic States. – *Oil Shale* 2008, 25(4), 465–484.

154. Shogenova, A., Sliaupa, S., Shogenov, K., Sliaupiene, R., Pomeranceva, R., Uibu, M., Kuusik, R. Possibilities for geological storage and mineral trapping of industrial CO_2 emissions in the Baltic region. – *Energy Procedia* 2009, 1, 2753–2760.

155. Reispere, H.J. Determination of free CaO content in oil shale ash. – *Transact. Tallinn Polytechnical Institute* 1966, 245, 73–76.

156. Taylor, J.C. Computer programs for standardless quantitative analysis of minerals using the full powdered diffraction profile. – *Powder Diffr.* 1991, 6, 2–9.

157. Colin, R.W., Taylor, C.J., Cohen, D.R. Quantitative mineralogy of andstones by X-Ray diffractometry and normative analysis. – *J. Sedimentary Res.* 1999, 69, 1050–1062.

158. Haario, H. Modest user manual. Finland: Profmath Oy, 1994.

159. Hindmarsh, A.C. ODEPACK, a systematized collection of ODE solvers. – *Scientific Computing: IMACS Transactions on Scientific Computation* 1983, 1, 55–64.

160. Schiesser, W.E., Silebi, C.A. Computational transport phenomena. Cambridge: Cambridge University Press, 1997.

161. Cooney, D. Adsorption design in wastewater treatment. USA: Lewis Publishers, 1998.

162. Newman, J. Electrochemical systems. USA: Prentice-Hall, 1973.

163. Lightfoot, E.N. Transport phenomena and living systems. New York: Wiley, 1974.

164. Uibu, M., Velts, O., Kuusik, R. Developments in CO_2 mineral carbonation of oil shale ash. – *J. Hazard. Mater.* 2010, 174(1-3), 209–214.

165. Fernández-Díaz, L., Fernández-González, Á., Prieto, M. The role of sulfate groups in controlling $CaCO_3$ polymorphism. – *Geochim. Cosmochim. Acta* 2010, 74, 6064–6076.

166. Astarita, G. Absorption of carbon dioxide into alkaline solutions in packed towers. – *Ind. Eng. Chem. Fundam.* 1963, 2(4), 294–297.

167. Danckwerts, P.V., Kennedy, A.M., Roberts, D. Kinetics of CO_2 absorption in alkaline solutions- II absorption in a packed column and tests of surface renewal models. – *Chem. Eng. Sci.* 1963, 18, 63–72.

168. Nijsing, R.A.T.O., Hendriksz, R.H., Kramers, H. Absorption of CO_2 in jet and falling films of electrolyte solutions, with and without chemical reaction. – *Chem. Eng. Sci.* 1959, 10, 88–104.

169. Van Swaaij, W.P.M., Versteeg, G.F. Mass transfer accompanied with complex reversible reactions in gas-liquid systems: An overview. – *Chem. Eng. Sci.* 1992, 47, 3181–3196.

170. Cents, A.H.G., Brilman, D.W.F., Versteeg, G.F. CO_2 absorption in carbonate/bicarbonate solutions: The Danckwerts-criterion revisited. – *Chem. Eng. Sci*. 2005, 60, 5830–5835.

171. Pohorecki, R., Moniuk, W. Calculation of the rate constant for the reaction of carbon dioxide with hydroxyl ions in mixed electrolyte solutions. – *Rep. Inst. Chem. Engng. Warsaw. Tech. Univ*. 1976, 5, 179–192.

172. Tsonopoulos, C. Ionization constants of water pollutants. – *J. Chem. Eng. Data*. 1976, 21, 190–193.

173. Edwards, T.J., Maurer, G., Newman, J., Prausnitz, J.M. Vapor-liquid equilibria in multicomponent aqueous solution of volatile weak electrolytes. – *A.I.Ch.E. J.* 1978, 24, 966–976.

174. Eigen, M. Protonenübertagung, säure-base-katalyse und enzymatische hydrolyse. teil I: Elementarvorgänge. – *Angew. Chem*. 1963, 75, 489–508.

175. Hikita, H., Asai, S., Takatsuka, T. Absorption of carbon dioxide into aqueous sodium hydroxide and sodium bicarbonate solutions. – *Chem. Eng. J.* 1976, 11, 131–141.

176. Danckwerts, P.V., Sharma, M.M. Absorption of carbon dioxide into solutions of alkalis and amines. – *Chem. Eng. (London)* 1966, 10, 244–280.

177. Pohorecki, R., Moniuk, W. Kinetics of reaction between carbon dioxide and hydroxyl ions in aqueous electrolyte solutions. – *Chem. Eng. Sci*. 1988, 43, 1677–1684.

ABSTRACT

The current thesis reports the results of a multifaceted study on the utilization/valorization possibilities of waste streams originating from oil shale-based power production. A simplified approach for CO_2 capture and beneficiation of alkaline oil shale ash (or its leaching wastewaters) in the form of a precipitated calcium carbonate (PCC)-type material is proposed, with relevant implications on CO_2 mitigation and the recycling of industrial waste materials.

Ash was successfully converted via a multi-step carbonation route into high brightness calcium carbonate (~96% $CaCO_3$ in the unwashed product) with a mean particle size in the range of 4−10 μm and various controllable by process conditions polymorphic forms at room temperature and atmospheric pressure using water for the dissolution of Ca-containing compounds. Several characteristics of the obtained solid materials suggest high potential for a wide range of industrial applications.

The mathematical aspects of the work included the development of models describing the main stages of the process, including leaching of the main water-soluble compounds from ash, dissolution of gaseous CO_2 into the alkaline liquid phase as well as binding of gaseous CO_2 and $CaCO_3$/$CaSO_4$ precipitation in the heterogeneous system of flue gas – oil shale ash leachates. An estimation of the kinetic parameters of the species of interest upon dissolution from ash was made and the process simulated as well as model application illustrated in the field of environmental protection. The precipitation process model was built upon CO_2 absorption, reaction kinetics as well as hydrodynamic conditions, and allows for predicting the concentration profiles of the main reactive species in the liquid, gaseous and solid phases in the crystallization of calcium carbonate from oil shale ash leachates treated with CO_2. The model can be also implemented for the estimation of positive environmental impacts in terms of CO_2 abatement and diminishing wastewater alkalinity, and is transferable to Ca-containing solid and liquid wastes produced in different industrial sectors.

KOKKUVÕTE

Käesolev töö tutvustab põlevkivienergeetika näitel uut suunda tahkete jäätmete taaskasutamises, mis tugineb leeliseliste tööstusheitmete, põlevkivituha(-heitvete) ja süsihapegaasi (CO_2) utiliseerimisel sadestatud kaltsiumkarbonaadi (SKK) saamiseks. SKK on laialt kasutusel täite- ja pindamiseainena kummi-, plastmasside- ja paberitööstuses.

Rakendades põlevkivituhka kaltsiumi allikana kaheastmelises protsessis, mis hõlmas tuha leostusvee valmistamist ning viimase karboniseerimist pool-perioodilises barbotaažkolonnis 5-15% CO_2 sisaldava mudelgaasiga mahtkiirusel 1000-2000 L/tunnis ja reaktori segaja pöörlemiskiirusel 400-1000 p/min, õnnestus saada kõrge heledusastmega (93%) 4−10 µm keskmise diameetriga ja kontrollitava morfoloogiaga (romboeedriline kaltsiit ja/või sfääriline vateriit) SKK kristalle ($CaCO_3$ sisaldusega kuni 96%). Lisaks, arvutustulemused kinnitavad uuritud meetodi suurt potentsiaali põlevkivienergeetikaga kaasnevate tahkete jäätmete, leostusvete ja CO_2 emissioonide negatiivse keskonnamõju vähendamisel.

Töö oluline osa oli suunatud protsessi põhistaadiume (Ca ja teiste vees-lahustuvate ühendite väljaleostamine tuhast, gaasilise CO_2 lahustumine leelisesse vedelfaasi ja CO_2 sidumine ning $CaCO_3$ sadestamine heterogeenses süsteemis CO_2 sisaldav suitsugaas - tuha leostusvesi) kirjeldavate mudelite väljatöötamisele. Erilist tähelepanu pöörati kaltsiumi leostusele põlevkivituhast vedelfaasi, hinnates kaltsiumi leostusprotsessi kineetikat iseloomustavaid parameetreid. Samuti illustreeriti mudeli rakendust keskkonnakaitseliste aspektidega seotud küsimustes, simuleerides ioonide väljaleostamise stsenaariumi tööstuslikust põlevkivituhakihist sademete mõjul pikemal perioodil. Sadestusprotsessi mudel oli ülesehitatud arvestades CO_2 absorptsiooni, reaktsioonide kineetikat ning hüdrodünaamilisi tingimusi süsteemis, võimaldamaks vedel-gaas-tahke faaside peamiste ioonide ja ühendite kontsentratsiooniprofiilide ennustamist $CaCO_3$ kristallisatsiooni käigus tuha leostusvete töötlemisel CO_2 sisaldava suitsugaasiga. Lisaks, koostatud mudel on sobilik positiivsete keskkonnaeffektide hindamiseks CO_2 püüdmise ja reovee leelisuse vähendamise kontekstis ning on ülekantav ka teistele erinevates tööstussektorites tekkivatele Ca-sisaldavatele tahketele ja vedeljäätmetele.

APPENDIX A:
ORIGINAL PUBLICATIONS

PAPER I

Velts, O., Uibu, M., Rudjak, I., Kallas, J., Kuusik, R.

Utilization of oil shale ash to prepare PCC: leachibility dynamics and equilibrium in the ash–water system.

GHGT -9

Utilization of oil shale ash to prepare PCC: leachibility dynamics and equilibrium in the ash-water system

O. Velts [a]*, M. Uibu[a], I. Rudjak[a], J. Kallas[b], R. Kuusik[a]

[a]*Tallinn University of Technology, Laboratory of Inorganic Materials, 5 Ehitajate Str ., Tallinn 19086, Estonia*
[b]*Lappeenranta University of Technology, Laboratory of Separation Technology, Skinnarilankatu 34, Lappeenranta 53851, Finland*

Abstract

In current study the oil shale ash consisting free lime have been considered as a source of Ca in the precipitated calcium carbonate (PCC) production. In connection with this approach, a set of laboratory experiments was carried out in order to investigate the leach ibility dynamics and equilibrium of the main ions from oil shale ashes formed in boilers operating with different combustion technologies. The main characteristics of Ca distribution between phases have been established using different ash/water suspension ratios and diffusioncoefficients determined. The effect of t emperature on the Ca^{2+} equilibrium concentration was investigated. Data collected served as basis for modeling of the equilibrium and dynamics of leaching of Ca^{2+} ions.

1. Introduction

The use of oil shale as a fuel for power plant s is common in China, Germ any and Estonia. P ower production based on oil shale combustion is, however, accompanied by high CO_2 emissions and by the formation of alkaline waste ash [1-3]. In the modern world, environmental protection issues substantially influence the energy se ctor, making the above mentioned problems particularly relevant in Estonia, where over 90% [4] of the basic power supply is provided by oil shale -fired thermal power plants. Power plants are the biggest polluters in Estonia, emitting annually thousands of tons of gaseous additives into the atmosphere and contaminating the landscape with alkaline pollutants [5]. Also, Estonian oil shale is characterized by a high content of mineral matter, which leads to the formation of large amounts of ash during the combustion process, which makes it highly desirable to develop effective usage of this waste.

Oil shale energetic is also the main source of CO_2 emissions in Estonia. In 200 5, oil shale across all sectors of the economy was responsible for about 72 % of total Estonian energy - relat ed CO_2 emissions [4]. In this aspect, a new

---

* Corresponding author. Tel.: +372 -5283756; fax: +372.620 2801
E-mail address : olga.velts@ttu.ee (O. Velts) .

direction in reducing the negative environmental impact of emissions is CO_2 mineralization, which is based on the CO_2 binding capacity of oil shale ashes and its water suspension [6-8]. An advantage of this process is not only abatement of CO_2 emissions, but also the possibility of the utilization of oil shale waste ash for PCC production. Production of new materials from oil shale ash helps to reduce the ash amount to be deposited as well as reduce its environmental impact, and gives extra value to the combustion product.

Ash from oil shale power stations contains 45 -52% of Ca oxides (including free CaO up to 30 wt-%) [3, 7]. And therefore the separation of free lime from oil shale ash and its application in PCC production is of particular interest. Although the carbonation of lime is well known [9], data about the specific characteristics of the carbonation process of free lime in oil shale ash and of its reactivity towards CO_2 are incomplete. The latter depends on the chemical composition and physical properties of the ash as well as on the conditions of the heterogeneous interaction of the ash with CO_2. From multiple [3, 7, 10] studies it is known that the main part of the lime in oil shale ash can be neutralized by CO_2 from flue gases with the formation of calcium carbonate. Production of PCC from lime involves dissolving the Ca-ions (diffusion of Ca^{2+} ions into the solution), concentrating the lime milk and precipitation under controlled mixing and temperature conditions. Before this type of process can be applied on an industrial scale, basic and applied research must be carried out to fully understand the mechanisms involved.

Since accessibility of free CaO from ashes is essential for the carbonation process to take place, diffusion of Ca^{2+} ions into a solution is the primary stage. Consequently, leachability of other key ions and the effect of temperature on the Ca^{2+} equilibrium concentration are of importance and for this reason a set of laboratory experiments was carried out in order to investigate the leachability dynamics and equilibrium of Ca^{2+} and accompanying ions from oil shale ashes formed in boilers operating with different combustion technologies. Mathematical tasks of the present work included development of models for the description of Ca equilibrium distribution between phases and determination of an effective diffusion coefficient in the solid particle, which characterizes the resistance of mass transfer in Ca leaching.

2. Materials and Methods

The ashes studied were formed in boilers operating with different combustion technologies. The ashes and ash-mixes were collected from different points of pulverized firing (PF) or fluidized bed combustion (FBC) boilers at Estonian power plants. The main characteristics of ashes and the average content of the basic elements are presented in Table 1 and 2 respectively. Solid material composition was determined by IRIS Intrepid II Inductive Coupled Plasma Spectrometer (Thermo Electron Corporation, software: TEVA: thermo elemental validated analysis). Solid material was initially dissolved in 65% nitric acid in a pretreatment module (GWB Pressurized Microwave Decomposition). Particle size distribution was measured by LS 13 320 Multi-Wavelength Particle Size Analyzer with Aqueous Liquid Module System (Beckman Coulter, Miami, Florida) using ethanol solution.

Table 1. The main characteristics of oil shale ashes

PF ash	CaO_{total} %	CaO_{free}, %	CO_2, %	Particle mean diameter, µm
PF1 (TP6/EE/2Bl/BA/2K-A)	57.2	30.0	8.34	250.0
PF2 (TP6/EE/Bl/CA/K.2-A)	50.2	23.4	7.72	
PF3 (TP6/Mix)	-	23.2	4.23	
FBC ash				
FBC1 (KK6/EE/8Bl/EF1/K1)	27.9	8.0	3.50	26.5
FBC2 (KK6/EE/8Bl/Mix11-14)	38.1	7.6	16.15	
FBC3 (KK6/Mix12)	-	9.6	8.29	

Table 2. Average content of the basic elements present in oil shale ash (per g of ash)**

Ash type	Ca	Mg	Fe	Al	S	K	Mn	Na	Zn	Si	Cr	Cu	Ni	Pb	V
	g/g						µg/g								
PF1	0.425	0.038	0.03	0.015	0.018	0.007	545	540	155	70-100	25	20*	5	13	20
PF3	0.380	0.047	0.03	0.023	0.019	0.010	600	580	120	70-100	35	12	<5	38	30
FBC1	0.215	0.033	0.02	0.034	0.024	0.017	385	890	≈30	100-150	45	10	10	30	38
FBC3	0.265	0.037	0.02	0.026	0.033	0.013	445	640	≈30	80-120	40	12	5	20	30

*in some samples ≈100 µg/g; ** [Cd;Co]=0 µg/g

Experiments were carried out in a laboratory-scale batch reactor using ash/millipore water suspensions by varying solid/liquid mass ratios from 1/1250 to 1/10. Suspensions were mixed at fixed temperature during 1-180 minutes depending on the objective. Samples were taken with a syringe and filtered (0,45μm). Main parameters measured in filtrate (à 100 ml) were: pH (Precisa pH 900), TDS (total dissolved solids), conductivity (HI9032 Microprocessor Bench Conductivity/TDS/NaCl/Fertilizer/0C/0F meter with RS 232), Ca, K, Na, Mn, Mg, Al, Fe, several heavy metals (ICP Termo IRIS Intrepid II XDL), SO_4^{2-} (Ion chromatograph Dionex DX-120 Computer program: Peaknet DX -120), and SO_3^{2-}, S^{2-} (spectrophotometer SpectroDirect Lovibond).

3. Results and Discussion

3.1. Leachibility dynamics of Ca^{2+} and main ions at fixed temperature

Preliminary experiments with different ash types showed changes of Ca^{2+}, SO_3^{2-} and S^{2-} ion concentration (in terms of millipore water) in the first 10 minutes. Based on preliminary data, 1, 3, 5, 7, and 10 - minute periods were selected for more detailed investigation. Experiments were carried out at room temperature ($\approx$23 ℃) with an ash/millipore water mass ratio of 1/10.

Experiments with both types of ash showed that millipore water pH increased rapidly from 7.0 to 12.2 (Figure 1, a) during the first minute of ash-water contact and remained at this value through the entire process. Total dissolved solids content (*TDS*) (Figure 1, b) reached a value of 5.4 – 6.2 g/L by the end of the third minute in case of both ash types.

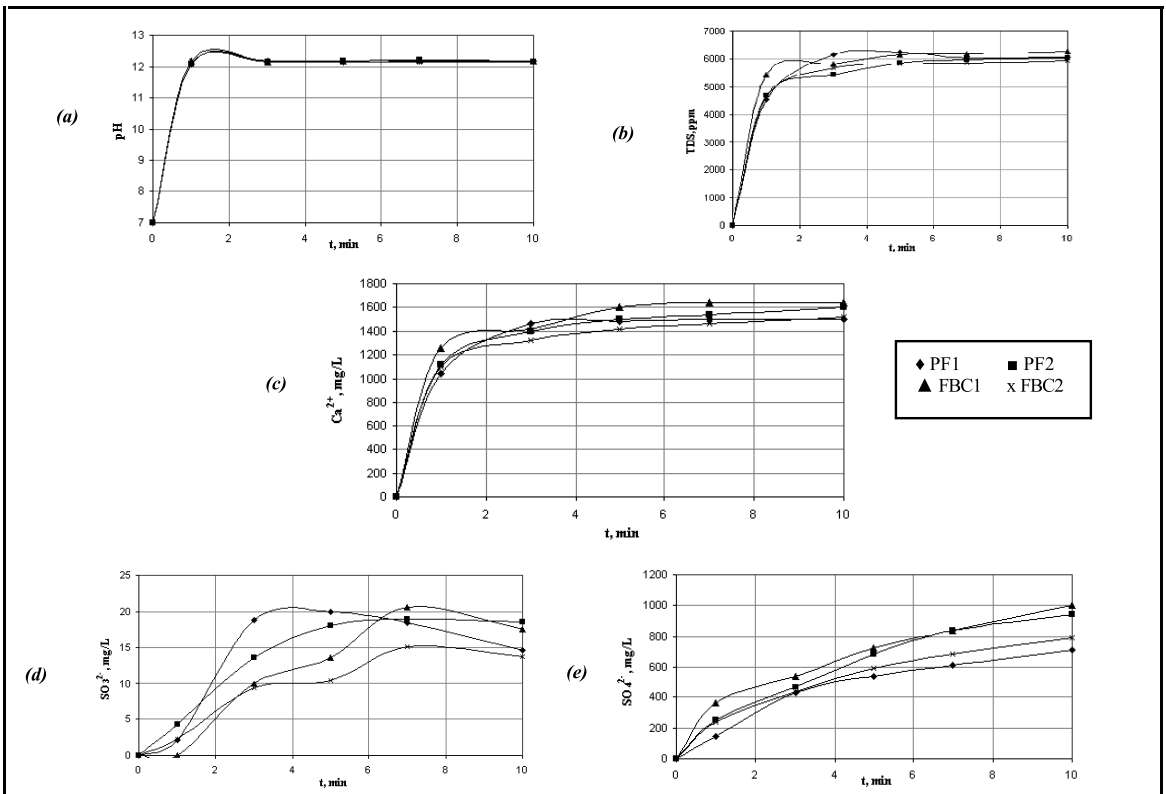Figure 1. Changing dynamics of *pH* **(a)** and *TDS* **(b)** values and concentration curves of Ca^{2+} **(c)**, SO_3^{2-} **(d)** and SO_4^{2-} **(e)** -ions during water contact with different kinds of ashes during the leachibility experiments

Ca^{2+} -ion equilibrium concentration (~860 mg/L depending on temperature) is reached rapidly during the first minute of oil shale ash-water contact (Figure 1, c). Extending the contact time by a few minutes resulted in a bout two times high supersaturation of the solution with Ca^{2+} ions: PF1–1500 mg/L, PF2–1600 mg/L, FBC1–1640 mg/L, FBC2–1520 mg/L. This finding is an important positive outcom e in the context of the PCC production process.

Although there was no significant difference in the Ca^{2+} concentration in filtrate from different kinds of ashes, a slightly lower Ca concentration (1500 mg/L) in case of coarse PF1 ash was observed, which indicates the influence of ash particle size on Ca^{2+} diffusion extent into the solution in a batch reactor.

For both ash types, the concentration curve of SO_3^{2-} ions (Figure 1, d) reached its maximum during a time span of 5-7 minutes and then started to decrease. A presence of S^{2-} ions in small concentrations was detected in the filtrat e after 10 minutes of contact time: ≈0.2 mg/L for samples PF1 and FBC2, and ≈0.5 mg/L for samples PF2 and FBC1. SO_4^{2-} content in the filtrate increased continuously through leachibility process (Figure 1, e).

As the environmental impact of ash disposal sys tems at oil shale combustion facilities is of particul ar interest nowadays, it is important to know which compounds could be released to the environment. However, data from the literature about the leaching of oil shale ashes are scarce. In order to invest igate the mobility of key ions and toxic metals from oil shale ashes after longer periods of contact with water, additional experiments were conducted with several oil shale ashes (PF1, PF3, FBC3) using an ash/water ratio of 1/10. A quantitative estimation of a wide spectrum of ions (incl. *Ca, K, Mg, Mn, Fe, Na, Si, Al*) and several heavy metals (*Cd, Co, Cr, Cu, Ni, Pb, V, Zn*) in final fluid was conducted after letting the experiment go to equilibrium in terms of overall oil shale ash leachibility (approximately 3 hours).

The results (Table 3) showed that after calcium, K is the second biggest cation present in the filtrate (70-94 mg/L). Other identified ions include Na (2.2 -3.4 mg/L), Al (<1 mg/L) and Si (<0.5mg/L). Ions like *Fe, Mg, Mn* were not present in the filtrate

Table 3. Concentration of ions in the final fluid after 3 -h contact

Ash sample name	Ca	K	Na	Si	Al	Fe, Mg, Mn, Co, Cr, Cu, Ni, Pb, V, Zn, Cd	SO_4^{2-}
						mg/L	
PF1	1523	70.1	3.4	<0.5	<1.0	0	2700
PF3	1716	91.2	2.2		<0.1	0	1276
FBC3	1781	93.7	2.5	<0.5	<0.1	0	1251

The m ain anion found in the filtrate was SO_4^{2-} (1300 -2700 mg/L). An important discovery from an environment al point of view is the fact that no trace of heavy metals was detected in any of the studied ash suspension filtrate s after 3-hou r contact.

3.2 Equilibrium distribution of Ca between phases

By varying ash/millipore water suspensions mass ratios from 1/1250 to 1/10 and letting the experiment in a stirred-batch go to equilibrium in terms of overall oil shale ash leachibility (approximately 3 hours), Ca equilibrium concentration in the final liquid-phase c^* was obtained for two ash samples with Ca content of 425 and 215 mg/g of ash, in PF and FBC ash, respectively (Table 4).

The equilibrium leachibility curves of the Ca^{2+} ash -water distribution were expressed as the equation:

$$q^* = A + B(c^*) + C(c^*)^2, \tag{1}$$

where coefficients A, B, C are evaluated by equilibrium experiments. To calculate the equilibrium concentration of Ca in ash q^* (unit in mass/mass of ash) (Table 4), the following mass balance was used:

$$W_0 q_0 = V(c^*) + W q^*, \tag{2}$$

where V – volume of liquid; W_0 – mass of ash in the beginning of the experiment; q_0 - initial concentration o f Ca in ash, unit mass/mass of ash; c^* – equilibrium concentration of Ca in water, mass/volum e of water; W – mass of ash at the end of experiment. It should be pointed out that the mass of ash is considered to be degreasing by the amount of CaO dissol ving into water.

Table 4. *Ca* equilibrium conce ntration in the final liquid and solid phases

Ash/water ratio	PF ash (PF1)		FBC ash (FBC1)	
	c*, g/L	q*, g Ca/g of ash	c*, g/L	q*, g Ca/g of ash
1/1250	0.210	0.257	0.066	0.150
1/500	0.440	0.296	0.164	0.150
1/250	0.805	0.312	0.291	0.158
1/100	-		0.45	0.163
1/150	1.006	0.348	0.648	0.165
1/50	1.265	0.397	1.085	0.174
1/20	1.350	0.414	1.45	0.194
1/10	1.523	0.419	1.653	0.203

The equilibrium leachibility curves of Ca^{2+} ash-water distribution (Figure 2) can be presented by the following equations:

$$q^*_{PF} = 0.2429 + 0.0808(c^*) + 0.0272(c^*)^2 \tag{3}$$

$$q^*_{F\,BC} = 0.15 + 0.0165(c^*) + 0.0091(c^*)^2 \tag{4}$$

for PF 1 and FBC 1 ashes studied, respectively .
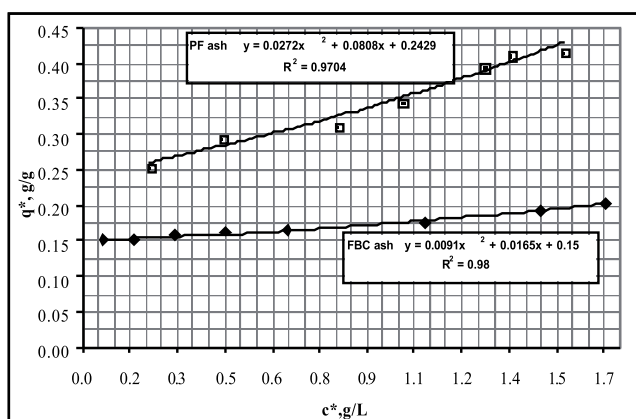
Figure 2. Equilibrium leachibility curves of Ca^{2+} ash-water distribution for PF (PF1) and FBC (FBC1) ashes

In leaching of *Ca* out fro m ash, the concentration q_{ins} (intersection of equilibrium line with q^*-axes) correspond s to the insoluble part of *Ca* in the ash (from eq. *(3)* and *(4)* 0.2429 and 0.15 g/g of ash for PF1 and FBC1 ashes respectively), the corresponding value of *CaO* is $q_{ins}*56/40$, by molar masses of *Ca* and *CaO*. In addition, equation:

$$CaO_{free},\ \% = (q_0 - q_{ins})*56/40 \tag{5}$$

should correspond to free *CaO* in ash. Therefore, for FBC1 ash eq. *(5)* gives a result of 0 .091 g CaO_{free}/g of ash or 9 .1 wt -%, while the corresponding analytically measured value is about 8% (Table 1).

It can be concluded that the above described approach works quite well and collected data can be used for simulation of processes of leaching/dissociation of Ca^{2+} - ions.

3.3 The effect of temperature on the Ca^{2+} equilibrium concentration

A PF bottom ash (PF1) was selected as the initial material in the temperature effect studies on the Ca^{2+} equilibrium concentration (after 3h -contact), because of its higher CaO_{free} content (≈30%). The ash suspension temperature variation range was from 15 to 45 ºC.

As expected, leachibility is greater at higher temperature, as conductivity increases with temperature increase (Table 5). In terms of *Ca*, however, increasing temperature c auses a decline in the *Ca* equilibrium concentration,

which is in good correlation with theoretical knowledge, as the highest levels of calcium hydroxide solubility are reached at the lowest temperatures [9].

Table 5. Effect of temperature on the Ca^{2+} equilibrium concentration and suspension conductivity value

T, ºC \ ash/water ratio	c*, mg/L				Conductivity, mS/cm		
	1/500	1/250	1/20	1/10	1/250	1/20	1/10
15	460	822	1371	1530	6.96	9.59	9.70
23	440	805	1350	1523	7.27	10.40	10.72
30	439	784	1291	1447	8.34	11.00	11.35
45	437	743	1124	1248	9.56	11.41	12.00
Theoretical max	429	857	10714	21429			

Based on the results (Table 5) there was no significant temperature effect on the *Ca* content when the ash suspension ratios 1/500 and 1/250 were used. However, use of more concentrated ash suspensions (1/20 and 1/10) showed a noticeable temperature effect. In the last case, conducting *Ca* dissolution below or at room temperature (15-23 ºC) had practically no effect on the *Ca* equilibrium concentration value in the final solution (about 1360 and 1525 mg Ca/L for ratios 1/20 and 1/10, respectively), increasing the suspension temperature from 30 to 45 ºC resulted, however, in a *Ca* content decline by 170-200 mg/L. At 30 ºC the Ca equilibrium concentration was only about 60-80 mg/L lower than that at room temperature. Therefore, favorable conditions for batch dissolution of ash could be achieved at room temperature, which simplifies the first stage of *PCC* production process.

3.4 Determination of effective diffusion coefficient in solid phase D_s

The dynamics of leaching (dissolving) of calcium from ash involves a rate controlling step of mass transfer inside an ash spherical particle. The equation describing homogeneous diffusion in a sphere, assuming a constant effective diffusivity, D_s, at all coordinates *r* in the particle, is (Figure 3):

$$\frac{\partial q}{\partial t} = \frac{D_s}{r^2}\frac{\partial}{\partial r}\left(r^2\frac{\partial q}{\partial r}\right) \qquad (6)$$
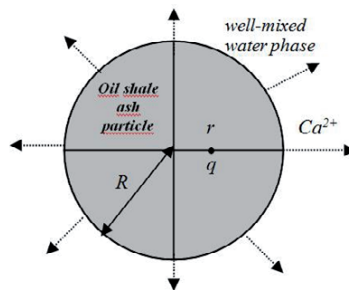
Figure 3. Leaching of *Ca* from an oil shale ash particle

For ash leaching, the *Ca* concentration in ash *q* in eq. *(6)* and later *q* is in grams per volume of ash.

As a solution of eq. *(6)*, Crank [11] developed the following analytical equation for the average concentration in the solid at any given time $\bar{q}(t)$, relative to the average concentration in the solid at infinite time q^*_∞:

$$\frac{\bar{q}(t)}{q^*_\infty} = 1 - \frac{6}{\pi^2}\sum_{n=1}^{\infty}\frac{1}{n^2}exp\left(\frac{-D_s n^2 \pi^2 t}{R^2}\right) \qquad (7)$$

For small times (beginning of the experiment), this equation may be written as:

$$\frac{\bar{q}(t)}{q^*_\infty} = 6\left(\frac{D_s t}{R^2}\right)^{\frac{1}{2}}\left[\pi^{\frac{1}{2}} + L\right] \qquad (8)$$

Thus, a plot of $\bar{q}(t)/q^*_\infty$ vs. the square root of time should give a straight line of slope (k):

$$k = 6(D_s/\pi R^2)^{1/2}, \qquad (9)$$

from which D_s can be determined.

Based on the above theoretical considerations and calculations, the values of the solute *Ca* concentration $c(t)$ in the liquid vs. time in stirred-batch leaching experiments with ash/water mass ratio of 1/500 and 1/250 for PF *(PF1: 0.425 g Ca/g of ash; $\rho_s = 2.83 g/cm^3$)* as well as 1/100 and 1/50 for FBC *(FBC1: 0.215 g Ca/g of ash; $\rho_s = 2.73 g/cm^3$)* ash were determined.

From the mass balance, $\bar{q}(t)$ values can be calculated:

$$\bar{q}(t) = \frac{W_0 q_0 - V c(t)}{V_s}, \qquad (10)$$

where q_o is the initial solid-phase concentration; $c(t)$ and $\bar{q}(t)$ are the values of the liquid and solid phase concentrations at any later time; V is the liquid volume; W_0 is the mass of solid material; V_s is the volume of solid material. The last volume is calculated by mass of solid: W_0/ρ_S, where ρ_s is the density of ash. The value of q^*_∞ is obtained from the same mass balance by letting the experiment go to equilibrium and measuring the final liquid-phase solute concentration. Equilibrium time was found to be about 10800 seconds (3h).

Although one must run a batch leaching experiment for a long time, in order to obtain q^*_∞ only short-time values are needed when plotting $\bar{q}(t)/q^*_\infty$ values vs. $t^{1/2}$ (Figure 4). Over such short times, the assumption of a constant surface concentration (on which the above equations are based) is reasonably good, and thus this approach works well.
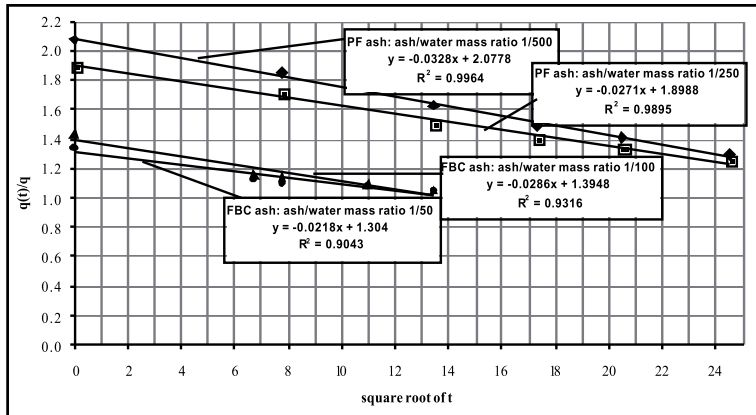
Figure 4. Plot of $\bar{q}(t)/q^*_\infty$ vs. the square root of time for different ashes

A plot of $\bar{q}(t)/q_\infty$ vs. the square root of time (Figure 4) for ash PF1 (ash/water ratio 1/500) gives a straight line:

$$\frac{\bar{q}(t)}{q^*_\infty} = -0.0328\sqrt{t} + 2.0778 \qquad (11)$$

of slope k eq. *(9)*, from which D_s can be determined:

$$-0.0328 = 6(D_s/\pi R^2)^{1/2} \Leftrightarrow D_s = 2.988 * 10^{-5} \pi R^2, \qquad (12)$$

where R is the particle average radius from size distribution measurement.

To estimate the reliability of the calculated effective diffusion coefficient value the experiments were performed with different ash/water ratios and results are given in Table 6 for both ashes studied.

Table 6.Values of effective diffusion coefficient for PF and FBC ashes

Ash sample name	D_s, m^2/s			
	Ash/water ratio			
	1/500	1/250	1/100	1/50
PF1 ash	$1.46*10^{-12}$	$1.0*10^{-12}$		
FBC1 ash			$1.25*10^{-14}$	$0.73*10^{-14}$

4. Conclusions

The main characteristics of Ca^{2+}-ion leachibility process in oil shale ash-water suspensions as of the first step of process utilizing oil shale for PCC production have been established. Mobility of different accompanying elements existing in ash was investigated and quantitative estimation of the solubility of a wide spectrum of ions ($Ca, K, Na, Al, Si, Fe, Mg, Mn, S^{2-}, SO_3^{2-}$ and SO_4^{2-}) including several heavy metals ($Co, Cr, Cu, Ni, Pb, V, Zn, Cd$) was made. The low leachibility of heavy metals in these conditions has been proved.

The leaching equilibrium equations of Ca for both types of oil shale ashes were obtained on the basis of the experiments. The single sphere diffusion model was used with determination of the effective diffusion coefficient characterizing the leaching process dynamics of Ca. This was the first step in modeling of the whole process, starting with Ca leaching, taking into account CO_2 mass transfer and finishing with calcium carbonate formation.

Acknowledgments

References

[1] A. Ots, Oil Shale Fuel Combustion. Tallinn University of Technology, Tallinn, 2006.

[2] Environmental Issues Associated with Narva Power Plants: Executive Summary. Narva Power, Estonia, 2001. [WWW] http://www.ebrd.com /projects/eias/narva.pdf (Retrieved on 10.10.2008)

[3] R. Kuusik, M. Uibu, K. Kirsimäe. Characterization of oil shale ashes formed at industrial-scale CFBC boilers. *Oil Shale* 22(4S) (2005) 407-420.

[4] I. Roos, O. Gavrilova. Greenhouse gas emissions in Estonia 1990–2005. National Inventory Report to the UNFCCC Secretariat, 2007. [WWW] http://www.envir.ee/kliima/files/c/ 0/0/1/85.pdf (Retrieved on 10.10.2008)

[5] M. Kaasik, T. Alliksaar, J. Ivask, J. Loosaar. Spherical fly ash particles from oil shale fired power plants in atmospheric precipitations: Possibilities of quantitative tracing. *Oil Shale* 22(4S) (2005) 547-562.

[6] J. M. Punning, A. Karindi. Composition of Estonian atmosphere: Estonia in the System of Global Climate Change. *Institute of Ecology : Publication s* No. 4 (1996) 26-34.

[7] R. Kuusik, H. Veskimäe, T. Kaljuvee, O. Parts. Carbon dioxide binding in the heterogeneous systems formed by combustion of oil shale: 1. Carbon dioxide binding at oil shale ash deposits. *Oil Shale* 18(2) (2001) 109-122.

[8] R. Kuusik, H. Veskimäe, M. Uibu. Carbon dioxide binding in the heterogeneous systems formed by combustion of oil shale:3. Transformations in the system suspension of ash – flue gases. *Oil S hale* 19(3) (2002) 277-288.

[9] J. A. H. Oates, Lime and Limestone: Chemistry and Technology, Production and Use. Weinheim etc. , Wiley - VCH, USA, 1998.

[10] M. Uibu, M. - L. Muulmann, R. Kuusik. CO_2 wet mineralization by oil shale ash and model compounds. Poster presented at the 4th Minisymposium on Carbon Dioxide Capture and Storage , Finland, Espoo, 2005. [WWW] www.eny.tkk.fi/minisym posium/proceedings/Uibu-poster.pdf (Retrieved on 10.10.2008)

[11] D. Cooney, Adsorption design in wastewater treatment. Lewis publishers, Boca Raton, USA, 1998.

Velts, *O*., Hautaniemi, M., Kallas, J., Kuusik, R.

Modeling calcium dissolution from oil shale ash: PART 1. Ca dissolution during ash washing in a batch reactor.

Modeling calcium dissolution from oil shale ash: Part 1. Ca dissolution during ash washing in a batch reactor

O. Velts [a,b,*], M. Hautaniemi [b], J. Kallas [a,b], R. Kuusik [a]

[a] Tallinn University of Technology, Laboratory of Inorganic Materials, 5 Ehitajate Str., Tallinn 19086, Estonia
[b] Lappeenranta University of Technology, Laboratory of Separation Technology, Skinnarilankatu 34, Lappeenranta 53851, Finland

ARTICLE INFO

ABSTRACT

Batch dissolution experiments were carried out to investigate Ca leachability from oil shale ashes formed in boilers operating with different combustion technologies. The main characteristics of Ca dissolution equilibrium and dynamics, including Ca internal mass transfer through effective diffusion coefficients inside the ash particle were evaluated. Based on the collected data, models allowing simulation of the Ca dissolution process from oil shale ashes during ash washing in a batch reactor were developed. The models are a set of differential equations that describe the changes in Ca content in the solid and liquid phase of the ash–water suspension.

© 2009 Elsevier B.V. All rights reserved.

1. Introduction

A considerable number of environmental problems result from oil shale based heat and power production, common in China, Germany and Estonia. The combustion of low-grade oil shale generates large quantities of waste material [1] as well as harmful atmospheric emissions, including carbon dioxide (CO_2), a major greenhouse gas. These environmental challenges are especially pertinent in the Republic of Estonia, where over 90% of the basic power supply is provided by the use of oil shale as a fuel for power plants. Furthermore, oil shale-based power production is responsible for about 72% of total Estonian energy-related CO_2 emissions [2].

Due to the high content of mineral matter in Estonian oil shale, a large amount of ash (5–6 millions tons/year) is formed during the combustion process. A main environmental concern with respect to final disposal or utilization of oil shale ash is associated with the high-alkali (pH = 12–13) water circulating in the ash removal system [3,4]. It is therefore highly desirable to develop effective usage of this waste ash.

In this context, a novel approach to reducing the negative environmental impact of emissions is CO_2 mineralization based on the CO_2 binding capacity of oil shale ashes [5,6]. In addition to abatement of CO_2 emissions, this approach permits the utilization of oil shale waste ash for precipitated calcium carbonate (PCC) production since the ashes contain a remarkable amount of Ca oxides (45–52% including free CaO

up to 30 wt.%) [6,7]. The separation of free lime from oil shale ash and its application in PCC production is, therefore, of considerable interest. Although the carbonation of lime is well known [8] and from multiple studies it is known that the main part of the lime in oil shale ash can be neutralized by CO_2 from flue gases with the formation of calcium carbonate [6,7,9,10], data about the specific characteristics of the different stages of the last process are incomplete.

In order for the carbonation to take place, access to free CaO from ashes is essential and, therefore, mass transfer of Ca^{2+} ions from ash particles into an aqueous solution is the primary stage of the carbonation process. For this reason, a set of laboratory experiments was carried out to investigate the Ca leachability equilibrium and dynamics during a batch dissolution process from oil shale ashes formed in boilers operating with different combustion technologies.

Mathematical modeling of the process focused on determination of the Ca equilibrium distribution equation between phases, estimation of the internal mass transfer through the evaluation of effective diffusion coefficients of Ca in the ash particle, and development of models allowing simulation of the dynamics of Ca dissolution process from oil shale ashes during ash leaching in a batch reactor. The models are a set of differential equations that describe the changes in Ca content in the solid phase and water phase of a well-mixed ash–water suspension.

2. Experimental

The oil shale ashes studied in the present work were collected from pulverized firing (PF: Sample PF1) and fluidized bed combustion (FBC: Sample FBC1) boilers at Estonian power plants. The main characteristics of the ashes including the average content of major elements are presented

* Corresponding author. Tallinn University of Technology, Laboratory of Inorganic Materials, 5 Ehitajate Str., Tallinn 19086, Estonia. Tel.: +372 5283756; fax: +372 620 2801.
 E-mail address: olga.velts@ttu.ee (O. Velts).

in Table 1. Solid material composition was determined by IRIS Intrepid II Inductive Coupled Plasma Spectrometer (Thermo Electron Corporation, software: TEVA: thermo elemental validated analysis). Solid material was initially dissolved in 65% nitric acid in a pre-treatment module (GWB Pressurized Microwave Decomposition). Particle size distribution was measured by Laser diffraction Multi-Wavelength Particle Size Analyzer LS 13320 (Beckman Coulter, Miami, Florida) using an ethanol solution. BET surface area, total- and micropore volume were determined by nitrogen dynamic desorption analysis method (Sorptometer KELVIN 1042).

The average content of dissolved solids (TDS) and the main ions of the leaching water formed after 3-h contact of PF and FBC ash suspensions with a solid/liquid mass ratio of 1/10 are presented in Table 1. For comparison, the average composition of the water circulating in the ash removal system at Estonian power plant is as follows (in g/L): Ca: 0.4–0.8, K: 3.0–4.7, Na: 0.1–0.2, Cl^-: 0.7–1.1, OH^-: 1.0–1.4, CO_3^{2-}: 0.2–0.36, SO_4^{2-}: 1.0–3.0 [3].

The modeling was carried out with the following steps:

(1) Determination of Ca solubility (empirical equilibrium equations).
(2) Evaluation of the internal mass transfer coefficient of Ca in the ash particle.

The experiments for the tasks (1) and (2) were carried out in a laboratory-scale batch reactor with volume 800 mL using ash-millipore water suspensions by varying solid/liquid mass ratios from 1/1250 to 1/10. Suspensions were well-mixed at a controlled temperature (25 °C) for 180 min, which was considered sufficient to reach equilibrium. Samples were taken with a syringe and filtered (0.45 μm). The main parameter measured in the filtrate was Ca content (ICP Thermo IRIS Intrepid II XDL).

3. Results and discussion

3.1. Equilibrium distribution of Ca between phases

The first step of the modeling procedure involved determination of the Ca equilibrium apportioning between the solid–liquid phases. The equilibrium leachability curves of the Ca^{2+} ash–water distribution were expressed as the empirical equation:

$$q* = A + B \times c* + C \times (c*)^2, \tag{1}$$

where q^* is the equilibrium concentration of Ca in ash; c^* is equilibrium concentration of Ca in water; coefficients A, B, C are evaluated by

equilibrium experiments. To calculate the equilibrium concentration of Ca in ash $q*$ (g Ca/L of ash), the following mass balance was used:

$$q* = \frac{W_0 \times q_0 - V \times c*}{V_s}, \tag{2}$$

where q_0 is the initial concentration of Ca in ash, g Ca/g of ash; V is the volume of liquid, L; W_0 is mass of ash at the beginning of the experiment, g; c^* is equilibrium concentration of Ca in water, g Ca/L; and V_s is the volume of solid material, L. The last volume is calculated by mass of solid: W_0/ρ_S, where ρ_S is the density of ash (Table 1).

Ca equilibrium concentration in liquid-phase c^* was obtained for ash samples PF1 and FBC1 by varying the ash/millipore water suspensions mass ratios from 1/1250 to 1/10 and letting the experiment in a stirred-batch go to equilibrium in terms of overall oil shale ash leachability (3 h). As a result, the equilibrium leachability curves ($R^2 = 0.97$) of Ca^{2+} ash–water distribution can be presented by the following empirical equilibrium equations for the PF1 and FBC1 ashes studied, respectively:

$$q^*_{PF} = 448.03 + 65.768 \times c* + 286.45 \times (c*)^2 \tag{3}$$

$$q^*_{FBC} = 363.71 + 42.771 \times c* + 37.967 \times (c*)^2 \tag{4}$$

3.2. Modeling of Ca dissolution process during ash washing in a batch reactor

3.2.1. Estimation of the Ca internal mass transfer and effective diffusion coefficients in the ash particle

Traditionally, solution of the diffusion equation for a spherical particle is used to evaluate the effective diffusion coefficient inside the particle during adsorption. In principle, the same solution is valid also to describe diffusion during the desorption process which is mathematically similar to the leaching of calcium out from the solid spherical particle. The solid phase mass transfer and effective diffusion coefficients, k_s and D_s were estimated by two different approaches, by Crank's solution given in the literature [11] and by numerical solution of the differential equations describing the mass transfer in the system. The volume of the particle is assumed to be constant.

3.2.1.1. Crank's solution. The dynamics of leaching (dissolution) of calcium from ash involves a rate controlling step of mass transfer

Table 1
Main characteristics of oil shale ashes and leaching water.

Main characteristics of oil shale ashes									
	CaO$_{total}$, %	CaO$_{free}$, %	CO$_2$, %	Ca content, g/g ash	Particle mean diameter, μm	Density, g/cm^3	BET surface area, m^2/g	Total pore volume, mm^3/g	Micropore volume, mm^3/g
PF1	57.2	30.0	8.34	0.425	250.0	2.83	5.26	14.75	0.23
FBC1	27.9	8.0	3.50	0.215	26.5	2.73	6.55	16.04	0.13

Average content of major elements present in oil shale ash (per g of ash)[a]														
	Ca	Mg	Fe	Al	S	K	Mn	Na	Zn	Si	Cr	Cu	Ni	Pb	V
	g/g						μg/g							
PF1	0.425	0.04	0.03	0.015	0.018	0.007	545	540	155	100	25	20[b]	5	13	20
FBC1	0.215	0.03	0.02	0.034	0.024	0.017	385	890	≈30	150	45	10	10	30	38

Concentration of total dissolved solids and main ions in the leaching water after 3-h contact (mg/L)								
	TDS	Ca	K	Na	Si	Al	Fe, Mg, Mn, Co, Cr, Cu, Ni, Pb, V, Zn, Cd	SO$_4^{2-}$
PF1	6900	1523	70.1	3.4	<0.5	<1.0	0	1360
FBC1	7000	1653	93.7	2.5		<0.1	0	1350

[a] [Cd; Co] = 0 μg/g.
[b] In some samples ≈ 100 μg/g.

inside a spherical ash particle. The equation describing homogeneous diffusion in a sphere, assuming a constant effective diffusivity, D_s, at all coordinates r in the particle, is:

$$\frac{\partial q}{\partial t} = \frac{D_s}{r^2}\frac{\partial}{\partial r}\left(r^2\frac{\partial q}{\partial r}\right) \tag{5}$$

In the ash leaching case, the Ca concentration in ash q in Eq. (5) and later is in grams per volume of ash.

As a solution of Eq. (5), Crank[11] developed the following analytical equation for the average concentration in the solid at any given time $\overline{q}(t)$, relative to the average concentration in the solid at infinite time q_∞^*, which for small contact times (beginning of the experiment) may be written as:

$$\frac{\overline{q}(t)}{q_\infty^*} = 6 \times \left(\frac{D_s \times t}{R^2}\right)^{1/2}[\pi^{-1/2} + L] \tag{6}$$

Thus, effective diffusivity D_s can be determined from a plot of $\overline{q}(t)/q_\infty^*$ vs. the square root of time, which should give a straight line of slope k:

$$k = 6 \times \left(\frac{D_s}{\pi \times R^2}\right)^{1/2}, \tag{7}$$

where R is the particle average radius from size distribution measurement (Table 1).

Based on the above theoretical considerations, the values of the Ca concentration in the liquid phase $c(t)$ vs. time in stirred-batch leaching experiments were determined, and $\overline{q}(t)$ values calculated according to the following mass balance:

$$\overline{q}(t) = \frac{W_0 \times q_0 - V \times c(t)}{V_s}, \tag{8}$$

where q_0 is the initial solid-phase concentration; $c(t)$ and $\overline{q}(t)$ are the values of the liquid and solid phase concentrations at any later time; V is the liquid volume; W_0 is the mass of solid material; and V_s is the volume of solid material. The value of q_∞^* is obtained from the same mass balance by letting the experiment go to equilibrium (estimated equilibrium time 3 h) and measuring the final liquid-phase solute concentration.

It should be pointed out that only short-time values are needed when plotting $\overline{q}(t)/q_\infty^*$ values vs. $t^{1/2}$, as over such short times the assumption of a constant surface concentration (on which the above equations are based) is more reasonable. To estimate the reliability of the calculated effective diffusion coefficient value, the experiments were performed with different ash/water ratios. The value of effective diffusivity should only be dependent on the ash type, not the fluid-ash ratio. Based on the solid phase diffusion coefficients, mass transfer coefficients k_s were calculated using the equation:

$$k_S = \frac{5 \times D_s}{R} \tag{9}$$

The values of mass transfer and diffusion coefficients obtained for different ashes and different ash–water ratios using Crank's solution are shown in Table 2.

3.2.1.2. Numerical solution of the mass balance differential equations. The solid phase mass transfer and effective diffusion coefficients were determined from Ca balances written for the solid phase and the water phase. The balances were written by considering a perfectly mixed volume of suspension V, which consists of a water phase with volume $\varepsilon \times V$ and a solid phase with volume $(1-\varepsilon) \times V$. The solid phase volume was calculated by the mass of solids W_s/ρ_S.

Table 2
Values of D_s and k_s coefficients for PF and FBC ashes estimated using Crank's solution.

Ash sample name (ash/water ratio)	k_s, m/s	D_s, m²/s
PF1 (1/500)	5.84×10^{-8}	1.46×10^{-12}
PF1 (1/250)	4.00×10^{-8}	1.00×10^{-12}
FBC1 (1/100)	4.72×10^{-9}	1.25×10^{-14}
FBC1 (1/50)	2.75×10^{-9}	0.73×10^{-14}

In the water phase:

$$\frac{dc(t)}{dt} = \frac{K \times (1-\varepsilon) \times S_0 \times (\overline{q} - q^*)}{\varepsilon}, \tag{10}$$

In the solid phase:

$$\frac{d\overline{q}}{dt} = K \times S_0 \times (q^* - \overline{q}), \tag{11}$$

where K is the overall mass transfer coefficient; ε is the fluid (water) fraction in suspension; $c(t)$ is the Ca concentration in the water phase; $\overline{q}$ is the average concentration of Ca in the solid phase; and q^* is the equilibrium concentration of Ca in the solid phase determined by empirical equilibrium Eq. (3) or (4) (see Section 3.1). The specific surface area S_0 (surface area/volume of particle) of a spherical particle was calculated as $3/R$, where R is the average radius of the particle.

The overall mass transfer coefficient K is defined according to the following well known equation:

$$\frac{1}{K} = \frac{m}{k_L} + \frac{1}{k_s}, \tag{12}$$

where m is the slope of equilibrium line $q^*=f(c^*)$, k_L is the liquid (fluid) phase mass transfer coefficient, and k_s the solid phase mass transfer coefficient. If the liquid phase is perfectly mixed, then $k_L = \infty$, and $K = k_s$.

The solid phase mass transfer coefficients k_s were estimated from the systems of differential Eqs. (10) and (11) using the least squares method. The differential equations were solved by means of linear multi-step methods implemented in ODESSA, which is based on the LSODE software [12]. The calculations were performed using the MODEST 6.1 software package [13] designed for various tasks of model building such as simulation, parameter estimation, sensitivity analysis and optimization. The software consists of a FORTRAN 95/90 library of objective functions, solvers and optimizers linked to model problem-dependent routines and the objective function.

Based on the mass transfer coefficients, the solid phase diffusion coefficients were calculated using Eq. (9). The values of k_s and D_s coefficients obtained for different ashes and different ash–water mass ratios are shown in Table 3.

Simulations of the Ca dissolution process during PF and FBC ash washing in a batch reactor for different ash–water ratios are presented in Fig. 1. The modeling and experimental results were also compared for experiments not used in parameter k_s evaluation. The results proved that the model describes quite well the Ca dissolution process during PF and FBC ash washing in a batch reactor.

Table 3
Values of D_s and k_s coefficients for PF and FBC ashes estimated by numerical solution ($R^2 = 99.8\%$).

Ash sample name (ash/water ratio)	k_s values (with their 95% confidence intervals), m/s	D_s, m²/s
PF1 (1/500)	$8.087 \pm 0.810 \times 10^{-8}$	2.02×10^{-12}
PF1 (1/250)	$7.723 \pm 0.835 \times 10^{-8}$	1.93×10^{-12}
FBC1 (1/100)	$7.078 \pm 1.393 \times 10^{-8}$	1.87×10^{-13}
FBC1 (1/50)	$5.771 \pm 0.772 \times 10^{-8}$	1.53×10^{-13}
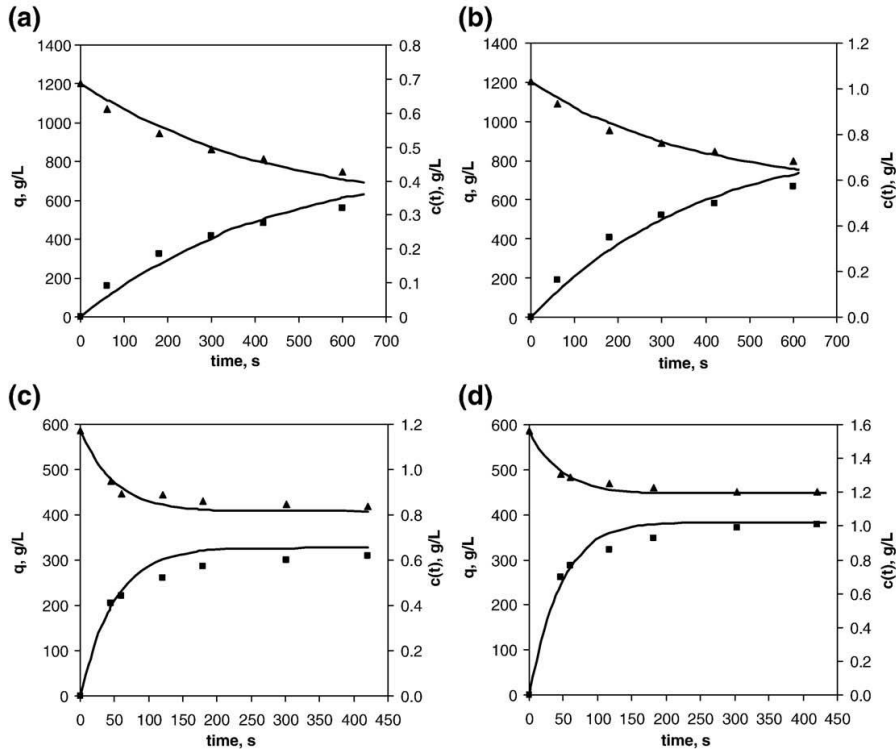
Fig. 1. Modeling of Ca dissolution during PF and FBC ash washing in a batch reactor: experimental (▲; ■) vs. simulated (—) Ca concentration profiles: ■ Ca concentration in liquid phase $c(t)$, g/L; ▲ Ca concentration in solid phase (ash) q, g Ca/L ash. (a) PF ash/water ratio 1/500; (b) PF ash/water ratio 1/250; (c) FBC ash/water ratio 1/100; (d) FBC ash/water ratio 1/50.

So, it has been shown on the basis of two types of oil shale ashes differing noticeably by their chemical (content of CaO_{free}) and physical structure (BET-surface, particle mean diameter etc) that proposed model can be implemented for different ashes having these characteristics in the range of parameters used in this work. This declaration has been proved on the basis of oil shale ash from electrostatic precipitator of FBC boiler (FBC1) and PF bottom ash (PF1), consisting 8.0 and 30.0% of CaO_{free} and having values of BET, 6.55 and 5.26 m²/g and particle mean diameter, 26.5 and 250.0 μm, respectively. Accordingly, the model is suitable to describe the Ca leaching process also from different kind of Ca-containing ashes.

3.2.2. Comparison of effective diffusion coefficients D_s calculated with different methods

The values of effective diffusion coefficients obtained for PF and FBC ashes with different ash–water ratios using two calculation approaches are shown in Tables 2 and 3. It can be seen that both methods worked quite well for PF ash, being able to give good correlation between the results of different approaches as well as within each method for different dilutions, and thus confirmed the reliability of the calculated coefficient. However, when comparing the results of the two methods for FBC ash, a significant deviation can be observed in the estimated values of D_s. Considering that the water phase in the experiments is well-mixed and the mass transfer resistance should be concentrated in the solid phase, the values of the estimated diffusion coefficients should be equal for one ash in experiments with different dilutions. As the estimated diffusion coefficients differ too much in estimations made using Crank's solution, it seems that Crank's model is not sufficiently accurate in the case of a Ca dissolution process from ash. Possible reasons may include the assumption of constant particle interface

concentration not being valid and the Ca balance in the water phase, accounting the fluid phase properties as phase fraction (volume of liquid phase/total volume of suspension), and specific surface area not being included in the Crank model, which uses directly only the balance of the ash phase. A numerical solution of the differential equations is consequently considered the more suitable approach for estimation of the effective diffusion and internal mass transfer coefficients in the case of the Ca dissolution process from oil shale ash, providing significantly more accurate results, and therefore values from Table 3 are used in further modeling.

4. Conclusion

In this part of the study of the dissolution process of Ca from oil shale ashes formed in boilers operating with different combustion technologies, the leachability dynamics and equilibrium of Ca were investigated during ash washing in a batch reactor using very intensive mixing.

The main characteristics of the Ca leachability process in oil shale ash–water suspensions as the first step of the process of utilizing oil shale ash for PCC production have been established. The empirical equilibrium equations of Ca for both types of oil shale ashes were obtained on the basis of leaching experiments and estimation of the Ca internal mass transfer and effective diffusion coefficients was done.

Models allowing simulation of the Ca dissolution process from oil shale ashes during ash washing in a batch reactor were developed and the dissolution process simulated. The accuracy of the developed models was confirmed by comparing experimental and simulated data of the changes in Ca content in the solid and liquid phase of ash–water suspensions.

In part 2 of the work, the dissolution process of Ca ions from oil shale ashes formed in boilers operating with different combustion technologies will be investigated and modeled for continuous washing of the oil shale ash layer in a packed-bed leaching column. These models will serve as the primary step in developing of the mathematical model of PCC formation process on the basis of Ca-containing waste ashes formed by utilization of oil shale as primary fuel in heat and power production.

Acknowledgments

References

[1] A. Ots, Oil shale fuel combustion, Tallinn University of Technology Press, Tallinn, 2006.
[2] Greenhouse gas emissions in Estonia 1990–2007, National inventory report to the UNFCCC secretariat, 2009. Available at: http://www.keskkonnainfo.ee/index.php?lan=EE&sid=336&tid=316&l3=334&l2=322&l1=320. Accessed 3 Sep 2009.
[3] H. Arro, J. Loosaar, A. Prikk, T. Pihu, Estonian oil shale power plants' ash handling problems, Energy and Sustainability, WIT Transactions on Ecology and the Environment 105 (2007) 247–255, doi:10.2495/ESUS070251.
[4] A. Hotta, R. Parkkonen, M. Hiltunen, H. Arro, J. Loosaar, T. Parve, T. Pihu, A. Prikk, T. Tiikma, Experience of Estonian oil shale combustion based on CFB technology at Narva Power Plants, Oil Shale 22 (4) (2005) 381–397.
[5] R. Kuusik, H. Veskimäe, M. Uibu, Carbon dioxide binding in the heterogeneous systems formed by combustion of oil shale: 3. Transformations in the system suspension of ash — flue gases, Oil Shale 19 (3) (2002) 277–288.
[6] R. Kuusik, M. Uibu, K. Kirsimäe, Characterization of oil shale ashes formed at industrial-scale CFBC boilers, Oil Shale 22 (4S) (2005) 407–420.
[7] R. Kuusik, H. Veskimäe, T. Kaljuvee, O. Parts, Carbon dioxide binding in the heterogeneous systems formed by combustion of oil shale: 1. Carbon dioxide binding at oil shale ash deposits, Oil Shale 18 (2) (2001) 109–122.
[8] J.A.H. Oates, Lime and limestone: chemistry and technology, production and use, Wiley - VCH, USA, 1998.
[9] M. Uibu, M. Uus, R. Kuusik, CO_2 mineral sequestration in oil-shale wastes from Estonian power production, Journal of Environmental Management 90 (2) (2009) 1253–1260.
[10] M. Uibu, R. Kuusik, Mineral trapping of CO_2 via oil shale ash aqueous carbonation: controlling mechanism of process rate and development of continuous-flow reactor system, Oil Shale 26 (1) (2009) 40–58.
[11] D. Cooney, Adsorption design in wastewater treatment, Lewis Publishers, USA, 1998.
[12] A.C. Hindmarsh, ODEPACK, a systematized collection of ODE solvers, Scientific Computing, IMACS Transactions on Scientific Computation 1 (1983) 55–64.
[13] H. Haario, Modest user manual, Profmath Oy, Finland, 1994.

Velts, *O*., Hautaniemi, M., Kallas, J., Kuosa, M., Kuusik, R.

Modeling calcium dissolution from oil shale ash: PART 2. Continuous washing of the ash layer.

Modeling calcium dissolution from oil shale ash: Part 2. Continuous washing of the ash layer

O. Velts [a,b,*], M. Hautaniemi [b], J. Kallas [a,b], M. Kuosa [b], R. Kuusik [a]

[a] Tallinn University of Technology, Laboratory of Inorganic Materials, 5 Ehitajate Str., Tallinn 19086, Estonia
[b] Lappeenranta University of Technology, Laboratory of Separation Technology, Skinnarilankatu 34, Lappeenranta 53851, Finland

ABSTRACT

In the present work a possible approach to the utilization of oil shale ash containing free lime in precipitated calcium carbonate (PCC) production is elucidated. This paper investigates the Ca (calcium) dissolution process during continuous washing of pulverized firing (PF) and fluidized bed combustion (FBC) oil shale ash layers in a packed-bed leaching column. The main characteristics of the Ca dissolution process from ash are established. The effect of water flow rate is investigated by conducting leaching experiments of oil shale ashes formed in boilers operating with different combustion technologies. The values of the overall and liquid phase mass transfer coefficients are evaluated based on experiments using the developed ash layer washing model. The model is a set of partial differential equations that describe the changes in Ca content in the stagnant layer of ash and in the water flowing through the ash layer. An example in which the model is applied to environmental assessment and estimation of Ca leaching from industrial oil shale ash fields is provided.

© 2009 Elsevier B.V. All rights reserved.

1. Introduction

As noted in the first part of the current study [1] oil shale-fired thermal power plants are considered to be major polluters [2]. In the Republic of Estonia, the processing of oil shale for heat and power production has created over 200 million tons of alkaline waste ash [3] which, due to the lack of possible applications, is deposited on so-called ash fields which become a source of alkaline liquid and solid pollutants. Because of the carbonaceous nature of oil shale (mineral CO_2 content is 16–19% [2]) CO_2 emission per capita in Estonia is one of the highest in the world, 14.5 tons in 2007 [4]. Controlling atmospheric emissions and finding environmentally safe disposal and/or reuse of solid wastes are among the most serious problems facing Estonian heat and power production.

The possibility of CO_2 mineral trapping based on Estonian oil shale ashes has been demonstrated [5,6]. In addition to abatement of CO_2 emissions, an advantage of this process is the possibility of utilizing oil shale waste ash, which would not only reduce the environmental impact of the ash but give extra value to the ash as a source of Ca for precipitated calcium carbonate (PCC) production. PCC formation from lime in oil shale ash is a complex multistage process. The first step of the process involves preparation of the Ca-rich leachate, which can be obtained either by mixing ash–water suspension (in a batch reactor) or by pumping water through stagnant ash layer (in reactor designed

for continuous washing process of the fixed ash layer). Therefore, special attention must be addressed towards the mass transfer of Ca^{2+} ions from ash particles into an aqueous solution and Ca dissolution models of both process variations are needed in order to design the optimal PCC process. In part 1 of the work [1], the batch dissolution process was investigated and the main characteristics of Ca leachability in ash–water suspensions have been established. Leaching equilibrium equations of Ca for two types of ash were obtained on the basis of experiments, and estimation of the Ca internal mass transfer and effective diffusion coefficients, k_s and D_s was made.

In connection with the above-mentioned study, present paper focused on the investigation of the Ca dissolution during continuous washing process. The aim of the current work was to develop models to simulate the Ca dissolution process during continuous washing of the ash layer and simultaneously to aid the choice of optimal washing conditions. Present paper also aimed to demonstrate efficient implementation of developed model for the simulation of large-scale estimations of Ca leaching from ash. The models are a set of differential equations that describe the changes in Ca content in the stagnant layer of ash and in the water flowing through the ash layer.

2. Experimental

The subject of the present research was oil shale ash collected from pulverized firing (PF) and fluidized bed combustion (FBC) boilers at Estonian power plants. The main characteristics of the ashes and the average content of major elements, as well as the analytical methods, are presented in detail in [1]. The PF ash sample, PF1 is characterized

* Corresponding author. Tel.: +372 5283756; fax: +372 620 2801.
  E-mail address: olga.velts@ttu.ee (O. Velts).

by a high amount of free CaO (30%), while the FBC ash sample, FBC1 contains 8% of free lime. Particle mean diameter is 250 and 26.5 μm, the *BET* surface area is 5.26 and 6.55 m^2/g for the PF1 and FBC1 ash samples, respectively.

The main parameter for estimating the leachability of Ca^{2+} from the ash was the CaO leachability degree (α):

$$\alpha = \frac{\beta}{W_{CaO}} \times 100\%, \tag{1}$$

where β is the amount of washed out free CaO, g; and W_{CaO} is the mass of free CaO in ash, g.

Modeling of mass transfer phenomena during ash layer washing was done with the following steps:

(1) Determination of Ca solubility (equilibrium equations)
(2) Estimation of the internal mass transfer coefficient of Ca in the ash particle
(3) Determination of the Ca overall mass transfer coefficient and mass transfer coefficient in the water phase.

Experimental design and data as well as results of the tasks (1) and (2) and the modeling procedure are presented in PART 1 of the work [1]. To carry out the task (3), continuous leaching experiments were conducted in a semi-batch washing column (Fig. 1a). Ash samples in portions of 60 g (PF1) or 35 g (FBC1) were placed in a column inside a plastic cylinder (height = 3 cm; inner diameter = 4.9 cm) and secured with a filter cloth and metallic mesh in order to attain the fixed packing area for each sample. Water (10 L) was led through the ash layer from the bottom of the column and after passing through the column collected in the solution (leachate) collection container (collector). Samples were taken from the outlet flow of the column and the collector, filtered (0.45 μm) and analyzed for Ca content using ICP. Experiments were repeated at various flow rates (58–350 mL/min).

Computations were performed using the MODEST 6.1 software package [7] designed for various tasks of model building such as simulation, parameter estimation, sensitivity analysis and optimization. The software consists of a FORTRAN 95/90 library of objective functions, solvers and optimizers linked to model problem-dependent routines and the objective function. The parameters were estimated from the systems of differential equations using the least squares method. The differential equations were solved by means of linear multi-step methods implemented in ODESSA, which is based on LSODE software [8]. The partial differential equations were solved numerically and integrated by the method of lines presented by [9]

with the initial and boundary conditions shown in Eqs. (6) and (7) in Section 3.1.

3. Results and discussion

3.1. Modeling of the Ca dissolution process during continuous washing of the ash layer

The differential mass balance equations in a fixed-ash layer leaching unit can be derived through consideration of a short length $\triangle Z$ of a reactor of cross-sectional area S, as shown in Fig. 1b. Assuming that heat effects and axial dispersion can be neglected gives the following equations:

$$v \times \frac{\partial C}{\partial Z} + \frac{\partial C}{\partial t} + \frac{1-\varepsilon}{\varepsilon} \times K \times S_0 \times (q^* - \overline{q}) = 0 \tag{2}$$

$$\frac{\partial \overline{q}}{\partial t} + K \times S_0 \times (\overline{q} - q^*) = 0 \tag{3}$$

$$\frac{1}{K} = \frac{m}{k_L} + \frac{1}{k_s}, \tag{4}$$

where K is the overall mass transfer coefficient, m/s; k_L and k_s are respectively the liquid (fluid) and the solid phase mass transfer coefficients, m/s; C is concentration of Ca in the water; $\overline{q}$ is the average concentration of Ca in ash; ε is fluid (water) fraction in the layer (estimated from the volumes of the ash layer and the empty column: for PF ash $\varepsilon = 0.625$ and for FBC $\varepsilon = 0.773$); v is the average axial velocity of the flowing fluid in the interstitial spaces, m/s; Z is the ash layer height coordinate, from the bottom ($Z = 0$) to the top ($Z = L$); and m is the slope of the equilibrium line $q^* = f(c^*)$. In Eqs. (2) and (3) concentrations are in units kg/m^3.

If Q is the volumetric flow rate of the fluid phase and S is the cross-sectional area of the empty column, then Q, S, and v are related by the equation:

$$Q = \varepsilon \times v \times S. \tag{5}$$

The equilibrium concentration q^* was calculated from the equations presented for each ash type in [1]. The specific surface area S_0 (surface area/volume of particle) of a spherical particle was calculated as $3/R$, where R is the average radius of the particle.
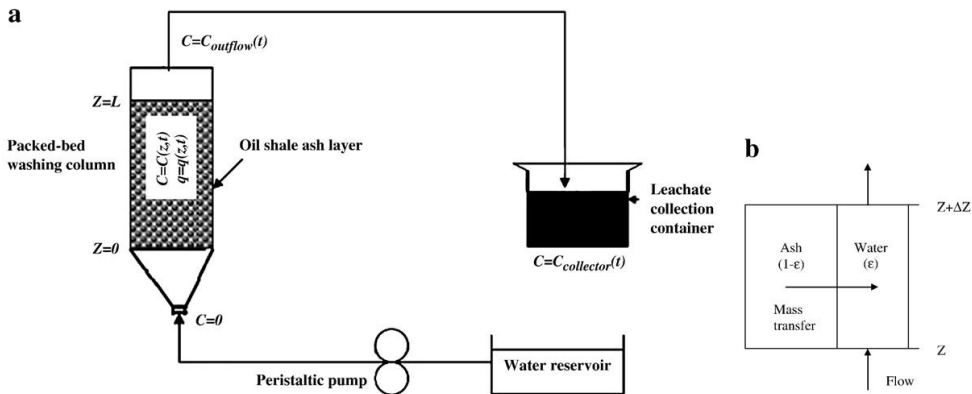

Fig. 1. Schematic design: (a) continuous leaching experiments conducted in a semi-batch washing column, (b) section of a fixed ash layer leaching unit.

The system of equations was solved with the following boundary and initial conditions:

At $Z = 0$: $C = 0$ for every moment of time $t = 0 \dots t = \infty$ (6)

At $t = 0$: $\overline{q} = q_0$ for every length coordinate $Z = 0 \dots Z = L$.   (7)

Solution of Eqs. (2)–(3) and (6)–(7) gives the concentration distributions in the layer, $\overline{q}$ (Z,t) and C (Z,t). The overall mass transfer coefficient K was obtained using a parameter estimation procedure in which the value of the Ca content in the solution collector was calculated from Eq. (8) and compared with the experimental results:

$$\frac{d(C_{collector} V_{collector})}{dt} = Q \times C_{z=L},$$ (8)

where $C_{collector}$ is the Ca concentration of the solution collected in the container; $V_{collector}$ is the volume of the solution collected in the container; Q is the liquid volumetric flow rate; and $C_{Z=L}$ is the Ca concentration in the outlet flow $C(t)$ at $Z=L$.

Table 1 shows the estimated values of the overall mass transfer coefficients K for different ashes at various water flow rates Q. As can be seen, the overall mass transfer coefficients increase with increasing flow rate in the range studied. This is in good agreement with theoretical knowledge: as the mass transfer coefficient in the fluid phase k_L depends on the flow rate, increasing the water flow rate results in increase of k_L and consequently of the overall mass transfer coefficient K. Therefore, as the flow rates increase, the turbulence of the flow increases and consequently reduces the mass transfer resistance.

The liquid phase mass transfer coefficient k_L was calculated according to Eq. (4), based on the values of the overall mass transfer coefficient K (Table 1) and the solid phase mass transfer coefficient k_s estimated from batch ash dissolution experiments (using very intensive mixing) presented for each ash type in [1]. Slope m of the equilibrium line $q^* = f(c^*)$ was calculated as the derivative of the equilibrium equation (presented for each ash type in [1]) for the argument value equal to the average Ca concentration in the liquid phase within the experimental range. The empirical function for estimation of the liquid phase mass transfer coefficient k_L at different flow rates Q was built up, for PF and FBC ash respectively, as:

$$k_L^{PF}(\text{m/s}) = 0.0015 \times Q(\text{L/s})$$ (9)

$$k_L^{FBC}(\text{m/s}) = 6 \times 10^{-5} \times Q(\text{L/s}).$$ (10)

Simulations of the Ca dissolution process during continuous washing of the PF and FBC ash layers with different flow rates are presented in Fig. 2. It can be seen that the developed model is able to provide quite accurate estimations of the changes in Ca content in the water flowing through the ash layer (at $Z=L$) and in the solution collector, as well as the average Ca content in the solid phase, i.e. in the ash layer $\overline{q}$ at every moment of time and, therefore, describes quite

Table 1
Values of the overall mass transfer coefficients K obtained for PF and FBC ashes during washing of the ash layer.

Ash sample name	Q, mL/min	K values (with their 95% confidence intervals), m/s
PF1	58	$2.23 \pm 0.12 \times 10^{-9}$
	146	$5.49 \pm 0.18 \times 10^{-9}$
	247	$1.05 \pm 0.04 \times 10^{-8}$
FBC1	58	$1.06 \pm 0.04 \times 10^{-10}$
	250	$2.27 \pm 0.23 \times 10^{-9}$
	350	$3.36 \pm 0.19 \times 10^{-9}$

well the Ca dissolution process during continuous washing of the PF and FBC ash layer.

It should be pointed out that additionally to the simulation presented in Fig. 2, the Ca dissolution model developed in the present work can also be used to describe the Ca concentration distributions inside the layer ($Z=Z_0 \dots Z_0 + \Delta Z$), in the solid $\overline{q}$ (Z, t), and in the liquid phase $C(Z, t)$ at any time period.

3.2. Characterization and selection of the conditions of the Ca washing process from the ash layer

Experiments in a semi-batch washing column showed that during the initial ash - water contact the concentration of Ca^{2+} ions increased rapidly (achieving saturation concentration of ~860 mg/L in the case of PF ash and Ca content of 200–450 mg/L in the case of FBC ash in 3 min). After ~0.5–0.75 L of water had been led through the ash layer, the concentration started to decrease in the outlet flow and consequently in the solution collector. However, by the end of the experiment (after 10 L of water had been pumped through the ash layer) Ca concentration in the outlet flow had decreased only ~1.5–2 times in the case of PF ash, and ~5.5 times in the case of FBC ash, compared to the highest concentration at the beginning of the process. Further remarkable differences in the leachability process of different ashes were noticed, like a stronger decline in Ca^{2+} content in the case of FBC ash characterized by finer fractional composition and lower CaO_{free} content, compared to PF ash, which maintained higher Ca concentration in the outlet flow through entire process.

The influence of water flow rate Q upon the Ca leaching process efficiency was significant in the case of FBC ash: increasing the flow rate from 58 to 95 mL/min resulted in a two times higher CaO leachability degree α (see Eq. (1)) of 60%. Value of $\alpha = 100\%$ was reached at a flow rate of 350 mL/min after about 30 min. In the experiments with PF ash, however, increasing the water flow rate did not seem to affect the results as substantially as in the case of FBC ash and resulted in only a slight increase of α from 45 to about 50%.

Although α value was significantly higher for FBC ashes at higher flow rates, it should be pointed out that Ca content and, consequently, the amount of washed out free CaO (β) in the final collected solution was 3–10 times higher for PF ash (about 600 mg Ca/L or 8.6 g CaO) than for FBC ash (60 - 200 mg Ca/L or 0.85–2.84 g CaO). Consequently, the specific water amount at the end of the experiments was lower for PF ash, 1.2 L/g CaO, while being as high as 3.5–12 L/g CaO for FBC ash. This finding is mainly due to the about four times higher CaO free content in PF ashes. Therefore, from the point of view of the first stage of the PCC production process, which aims to achieve a solution with the highest possible Ca concentration, PF ash could be considered as a better source of Ca in a continuous washing process of the ash layer. Furthermore, taking into account process time, the optimal conditions for Ca washing from the PF ash layer could be achieved at higher water flow rate, which simplifies the first stage of the PCC production process. Based on the collected data, the appropriate ash type and washing conditions (flow rate and the amount of the washing water, process time, etc) can nevertheless be selected depending on the objective of a washing process.

3.3. Simulation of the Ca washing process by natural precipitation from ash deposit

The following example was designed to simulate a scenario of an industrial ash layer washing process in a natural environment over an extended period of time. Such situation exists, for instance, in Estonia, where every year about 5.5 million tons of oil shale ash formed in power plants is transported to nearby ash fields [10]. Understanding the leaching process of Ca^{2+} and, consequently, OH^- ions from oil shale ash is crucial in predicting its impact on the quality (pH level, alkalinity) of the leaching water. As mentioned in Section 3.1, the

Fig. 2. Modeling of the Ca washing process for PF and FBC ash layers: experimental (♦; ▲; ■) vs. simulated (—) results of the changes in Ca content: in the water flowing through the ash layer (♦ Ca concentration in the outlet flow at $Z=L$, g/L), in the solution collector (▲ mass of Ca in the collector, g) and in the solid phase (■ average Ca concentration in the ash $\overline{q}$, g Ca/L ash): (a) PF1, water flow rate $Q=58$ mL/min; (b) PF1, $Q=146$ mL/min; (c) PF1, $Q=247$ mL/min; (d) FBC1, $Q=58$ mL/min; (e) FBC1, $Q=250$ mL/min; and (f) FBC1, $Q=350$ mL/min.

model introduced in the present work can be used to describe the Ca concentration distributions in the ash layer, in the solid $\overline{q}$ (Z, t) phase, and in the liquid phase $C(Z, t)$ at any time period. This example demonstrates the versatility of application of the developed model.

o *Overview of the initial parameters of the simulation*

In the simulation, seventy tons of dry PF ash formed in a power plant is considered as having been distributed uniformly over an area of 5×13 m², creating a theoretical 1 meter high ash layer (cross-sectional area of 65 m²). The average annual amount of precipitation in Estonia is about 757 mm (2.075 mm/day) [11]. The goal of the simulation is to estimate changes in the Ca concentration in the solid (ash) phase and in the leaching liquid phase during industrial ash layer washing by natural precipitation and therefore to predict and describe the outcome of the washing process.

o *Results and discussion*

The water fraction in the ash layer ε was estimated from the volumes of the ash layer and the field sector on which the ash is distributed. The volumetric flow rate of the fluid phase Q was calculated based on an average rain velocity v of 2.075 mm/day, a cross-sectional area of a field sector S of 65 m², and a water fraction in the ash layer ε of 0.619. The overall mass transfer coefficient K was calculated according to Eq. (4): the value of the liquid phase mass transfer coefficient k_L was estimated from the empirical function presented in Eq. (9); the average value of the solid phase mass transfer coefficient k_s from batch ash dissolution experiments was found to be 7.91×10^{-8} m/s [1]; the value of the average slope m of the equilibrium line was taken as 538.4.

The results of the simulation are presented in Fig. 3. As can be seen, even after 100 years, the average Ca concentration in the ash q will
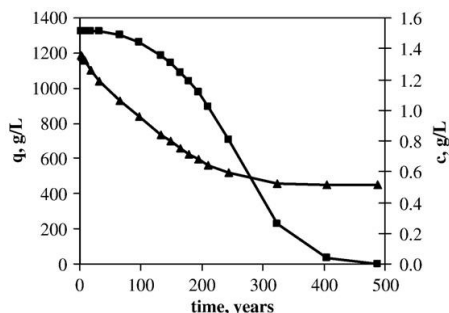
Fig. 3. Simulation of the Ca washing process for a 1 m high PF industrial ash layer by the average annual amount of precipitation: simulated results of the changes in Ca content in the leaching water (■ c, g/L) and in the ash (▲ average Ca concentration in the ash q, g Ca/L ash).

decrease by only 30% compared to its initial value (1203 g Ca per L of ash). Additionally, a Ca concentration level where only the insoluble part of the free lime is left in the ash layer was estimated by the model as being reached in approximately 500 years. The results indicate that the Ca concentration in the leaching fluid will be at a level of about 1.51 g/L and maintain this high value for hundreds of years to come.

It is well known that the main cause of the environmental impact of ash fields is the high-alkali water ($pH = 12 - 13$) circulating in the ash removal system [10]. The high alkalinity of the water is caused by contact between water and the oil shale ash containing free lime. At such contact $Ca(OH)_2$ produces Ca and hydroxide ions according to reaction R1:

$$Ca(OH)_2 \leftrightarrow Ca^{2+} + 2OH^- \tag{R1}$$

In the current simulation, Ca concentration in the leaching fluid was estimated by the model to be about 1.51 g/L or 0.03775 M, and according to R1 the molar concentration of the hydroxide ions is therefore $[OH^-] = 0.0755$ M. A pH of the solution can be found using the following equation:

$$pH = 14 + \log_{10}(\gamma_{OH^-} \times [OH^-]), \tag{11}$$

where γ_{OH^-} is the ionic activity coefficient of the hydroxide ions.

Therefore, taking into account ionic strength I of the 0.03775 M Ca $(OH)_2$ solution ($I = 0.11325$), the ionic activity coefficient of the hydroxide ions γ_{OH^-} is 0.748, and the pH value predicted by the model is 12.75, which confirms knowledge about the high alkalinity of the leaching waters from oil shale ash fields. So, the example demonstrates that oil shale ash can be viewed as a source of possible environmental damage since even some tons of ash may theoretically contaminate all rainwater falling onto the ash fields over a long period.

4. Conclusion

In the present work, the dissolution process of Ca ions from oil shale ashes formed in boilers operating with different combustion technologies was investigated for continuous washing of the oil shale ash layer in a packed-bed leaching column.

The main characteristics of the Ca dissolution process from ash were established and significant differences in the leachability process of Ca^{2+} from PF and FBC oil shale ashes were noted. Based on experiments and a parameter estimation procedure, values of the overall and liquid phase mass transfer coefficients K and k_L were evaluated. A simulation model was used for modeling of the Ca dissolution process from oil shale ashes during continuous ash washing processes. Comparison of experimental data and results of the process simulation confirmed that the developed models were able to provide accurate estimation of the changes in Ca content in the leaching fluid as well as in the stagnant layer of ash and therefore describe quite well the Ca dissolution process during continuous washing of PF and FBC ash layers.

Additionally, an example of the application of the developed model for environmental assessment and estimation of Ca^{2+} ion leaching from industrial oil shale ash fields was provided. Oil shale ash was shown to be without implementation of any constraints a source of environmental damage for long time.

Models described in this part 2 and in part 1 of the paper will serve as the first steps in developing of the mathematical model of PCC formation process on the basis of Ca-containing waste oil shale ashes. In the next step of this study the dissolution models will be combined with models of calcium carbonate precipitation reaction taking place in heterogeneous gas-liquid-solid system.

References

[1] O. Velts, M. Hautaniemi, J. Kallas, R. Kuusik, Modeling calcium dissolution from oil 368 shale ash: PART 1, Ca dissolution during ash washing in a batch reactor, Fuel Process Tech 91 (5) (2010) 486–490.
[2] A. Ots, Oil shale fuel combustion, Tallinn University of Technology Press, Tallinn, 2006.
[3] A. Kahru, L. Põllumaa, Environmental hazard of the waste streams of Estonian oil shale industry: an ecotoxicological review, Oil Shale 23 (1) (2006) 53–93.
[4] Greenhouse gas emissions in Estonia 1990–2007, National inventory report to the UNFCCC secretariat, 2009 http://www.keskkonnainfo.ee/index.php?lan=EE&-sid=336&tid=316&l3=334&l2=322&l1=320 Accessed 3 Sep 2009.
[5] M. Uibu, M. Uus, R. Kuusik, CO_2 mineral sequestration in oil–shale wastes from Estonian power production, J. Environ. Manage. 90 (2) (2009) 1253–1260.
[6] M. Uibu, R. Kuusik, Mineral trapping of CO_2 via oil shale ash aqueous carbonation: controlling mechanism of process rate and development of continuous-flow reactor system, Oil Shale 26 (1) (2009) 40–58.
[7] H. Haario, Modest user manual, Profmath Oy, Finland, 1994.
[8] A.C. Hindmarsh, ODEPACK, a systematized collection of ODE solvers, Scientific Computing, IMACS Transactions on Scientific Computation 1 (1983) 55–64.
[9] W.E. Schiesser, C.A. Silebi, Computational transport phenomena, Cambridge University Press, Cambridge, 1997.
[10] H. Arro, A. Prikk, T. Pihu, Reducing the environmental impact of Baltic power plant ash fields, Oil Shale 20 (3) (2003) 375–382.
[11] Estonica - Encyclopedia about Estonia: Nature, Climate, 2009 http://www.estonica.org/eng/lugu.html?menyy_id=422&kateg=10&alam=70&leht=2 Accessed 3 Sep 2009.

Velts, *O.,* Hautaniemi, M., Uibu, M., Kallas, J., Kuusik, R.

Modelling of CO_2 mass transfer and hydrodynamics in a semi-batch reactor.

Reprinted with permission from:

MODELLING OF CO$_2$ MASS TRANSFER AND HYDRODYNAMICS IN A SEMI-BATCH REACTOR

Olga Velts[1,2], Marjaana Hautaniemi[2], Mai Uibu[1], Juha Kallas[1,2], Rein Kuusik[1]

[1]Tallinn University of Technology, Laboratory of Inorganic Materials,

5 Ehitajate Str., Tallinn 19086, Estonia

[2]Lappeenranta University of Technology, Laboratory of Separation Technology,

Skinnarilankatu 34, Lappeenranta 53851, Finland

E-mail: olga.velts@ttu.ee Fax: (372) 620 2801

Abstract

Present study is considered to be a part of modelling the process for removal of CO$_2$ from industrial gas streams by carbonation of alkaline leachates of oil shale ash formed at Estonian power production. In current paper the chemical phenomena of CO$_2$ absorption into aqueous alkaline solution has been investigated and a mathematical model for description of CO$_2$ mass transfer in a stirred semi-batch reactor presented. The model was built upon the kinetics of absorption phenomena as well as reaction kinetics and hydrodynamic conditions. Based on the experimental data and the developed model, the volumetric mass transfer coefficient, $k_L a$ of the process was evaluated for a wide range of operating parameters. The model allows simulating the concentration profiles of reactive species and ions (CO$_2$, CO$_3^{2-}$, HCO$_3^-$, OH$^-$, H$^+$) in the gas and liquid phase. Additionally, the influence of hydrodynamics on the mass transfer rate of CO$_2$ was described and empirical functions for estimation of $k_L a$ and gas fraction ε in the liquid-gas mixture proposed.

Key words: *absorption, carbon dioxide, mass transfer, hydrodynamics, modelling*

1. INTRODUCTION

Carbon dioxide (CO$_2$) emissions, inevitably created by burning fossil fuels, are considered the main cause of global climate change. Due to the environmental concerns over greenhouse gas emissions, the removal of CO$_2$ from industrial gas streams has become especially important (Rubin, 2001; Weart, 2003). Particularly in the Republic of Estonia, where local carbonaceous fossil fuel - oil shale - is used as a fuel in electricity production, CO$_2$ emissions reduction is a high priority.

The removal of CO$_2$ from gas streams can be achieved by a number of separation techniques including absorption into a liquid solvent. Binding CO$_2$ from flue gases by alkaline wastewaters such as oil shale ash leachates circulating in the hydraulic ash-transportation system at Estonian oil shale firing power plants is a promising method for CO$_2$ safe disposal. CO$_2$ mineral trapping based on Estonian oil shale ash and on other lime-containing wastes is a novel approach (Uibu et al., 2009; 2010), which could be economically viable due to availability of large amounts of alkaline wastewater in the proximity of CO$_2$ emission source. The chemical binding of CO$_2$ in the form of stable carbonates permits CO$_2$ emissions reduction as well as utilization of Ca-rich ash alkaline leaching water for precipitated calcium carbonate (PCC) production (Uibu et al., 2010).

However, oil shale ash based PCC production is a complex multistage process, which requires modelling of each stage in order to predict the optimum conditions. In our previous work, the process of mass transfer of *Ca^{2+}* ions from oil shale ash particles into aqueous solution was mathematically described (Velts et al., 2010a; 2010b). Nevertheless, vital part of the carbonation process is the transfer of CO$_2$ from the gas phase to the aqueous phase, since only the dissolved molecules of CO$_2$ take part in the reactions. However, the data on the rate of CO$_2$ transfer from air bubbles into the aqueous alkaline solution has rarely been reported in the literature (Astarita, 1963; Danckwerts et al., 1963). Thus, as the next step of the study, present paper aimed to provide an insight into the chemical

phenomena of CO_2 absorption into aqueous alkaline solution as well as to develop a mathematical model for predicting mass transfer of CO_2 in a semi-batch reactor, while taking into account the kinetics, hydrodynamics and specifics of the process. Furthermore, the influence of the operating variables such as inlet gas flow rate and CO_2 concentration as well as mixing intensity of the stirrer on the CO_2 mass transfer rate was under attention.

2. MATERIAL AND METHODS

The experiments in a pilot-scale stirred semi-batch reactor were performed by bubbling a gas mixture of CO_2 and air through a recirculating NaOH solution representing the alkaline wastewater (Fig. 1). Gas mixture flow rate and composition was controlled using rotameters and CO_2 analyzer. Reactor was equipped with a gas sampling system connected to CO_2 IR-analyzer (Duotec) to allow measurements of CO_2 concentration in the gas stream exiting the reactor. The pH-value in reactor was continuously monitored by pH meter (Mettler Toledo GWB SG2). Collection of the liquid phase samples was performed by means of sampling valve on the reactor body.
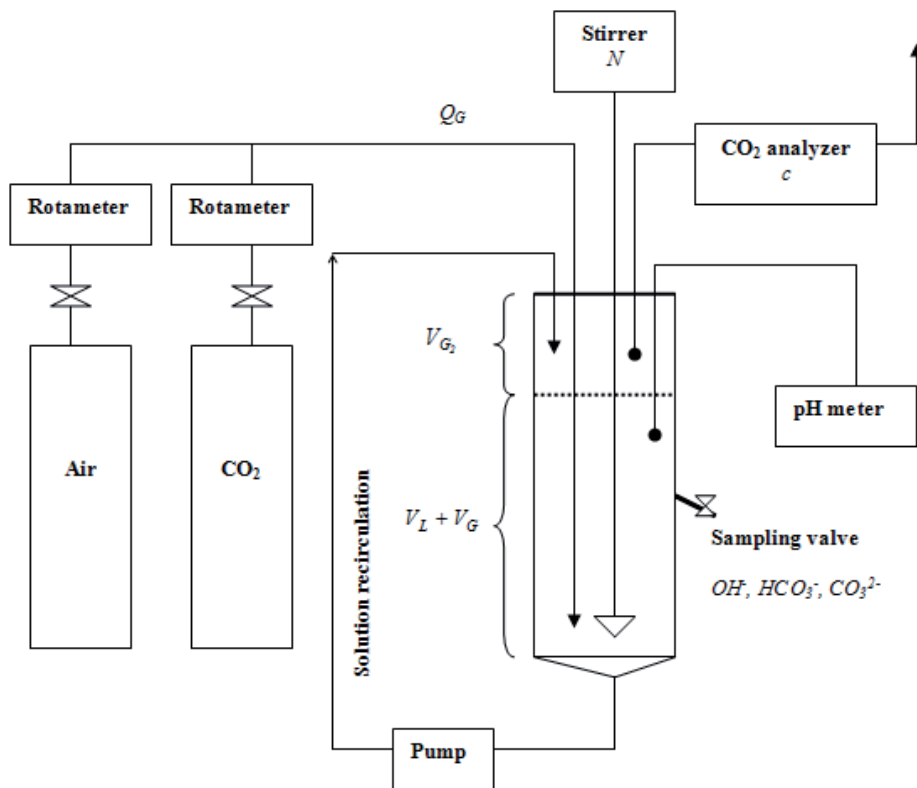
Fig. 1 Principal scheme of the experimental setup

NaOH solution initial volume, concentration and pH were fixed at 10 L, 0.01 M and 12.0 respectively. The pH-level was chosen to be equal to this characteristic for saturated system water − lime containing ash. According to full-factorial experimental plan with additional experimental point in the "middle" (Table 1) the following parameters were varied one at a time while keeping the others constant:

- CO$_2$-air gas mixture flow rate, Q_G

- CO$_2$ concentration in the inlet, c

- Stirrer rotation speed, N

Table 1. Experimental plan for investigation of the CO$_2$ mass transfer

№	Air/CO$_2$ flow rate			CO$_2$ concentration in the inlet gas	Stirrer rotation speed
	Total (Q_G, L/h)	Air	CO$_2$	c, vol. %	N, rpm
1	2000	1700	300	15	1000
2	2000	1700	300	15	400
3	2000	1900	100	5	1000
4	2000	1900	100	5	400
5	1000	850	150	15	1000
6	1000	850	150	15	400
7	1000	950	50	5	1000
8	1000	950	50	5	400
9	1500	1350	150	10	700

In the experiments the pH value, concentration of OH$^-$, CO$_3^{2-}$, HCO$_3^-$ ions (titrimetric method ISO 9963-1:1994(E)) in the liquid phase as well as CO$_2$ content in the outflow gas were continuously measured. In each experiment the volume of gas phase in the gas-liquid mixture (V_G) and above it (V_{G2}) was registered. Experiments were conducted until the solution pH reached a value of 7.

3. RESULTS AND DISCUSSION

3.1 Modelling of CO$_2$ mass transfer in a stirred semi-batch reactor

3.1.1 Distribution of carbonate species in an aqueous solution of hydroxides

Carbon dioxide is a volatile weak electrolyte of great industrial importance. CO$_2$ is sparingly soluble in an aqueous phase (CO$_2$ solubility in water is 1.45 g/L at 25°C, 100kPa), however the system is somewhat complex (Lide, 1990-1991; Lower, 1999; Reid et al., 1987). Reaction 1 (R1) represents the process of physical dissolution of gaseous CO$_2$ into liquid solution:

$$CO_2(q) \leftrightarrow CO_2(l) \tag{R1}$$

At pressures up to about 5 atm, the solubility equilibrium follows Henry's law:

$$\left[CO_2(l)\right]_{eq} = k_H \times P_{CO_2}, \tag{1}$$

where k_H is the Henry constant, P$_{CO_2}$ is the CO$_2$ partial pressure.

Once CO$_2$ has dissolved, equilibrium is established between the dissolved CO$_2$ and forming carbonic acid. Furthermore, rate of dissolution of CO$_2$ into water depends on pH with formation of CO$_3^{2-}$ and HCO$_3^-$ ions. Therefore, the reactions occurring during absorption of CO$_2$ into aqueous solutions of hydroxides can be expressed as follows (Cents et al., 2005):

$$CO_2(l) + OH^- \underset{k_{12}}{\overset{k_{11}}{\rightleftharpoons}} HCO_3^- \tag{R2}$$

$$HCO_3^- + OH^- \; \underset{k_{22}}{\overset{k_{21}}{\rightleftarrows}} \; CO_3^{2-} + H_2O \tag{R3}$$

$$OH^- + H^+ \; \underset{k_{32}}{\overset{k_{31}}{\rightleftarrows}} \; H_2O \tag{R4}$$

$$CO_2(l) + H_2O \; \underset{k_{42}}{\overset{k_{41}}{\rightleftarrows}} \; HCO_3^- + H^+ \tag{R5}$$

Accordingly, the overall concentration of dissolved carbon increases together with the amount of the HCO_3^- and CO_3^{2-} ions formed. Dissolved CO_2 consists thus of the three species:

$$C_{CO_2} = [CO_2(l)] + [HCO_3^-] + [CO_3^{2-}] \tag{2}$$

Therefore, when CO_2 gas is bubbled through a solution containing a strong base such as NaOH, the electro-neutrality balance (in molar concentration units) for such a mixture can be written as follows:

$$[H^+] + [Na^+] = [HCO_3^-] + 2[CO_3^{2-}] + [OH^-] \tag{3}$$

3.1.2 Estimation of the volumetric mass transfer coefficient $k_L a$ for CO_2

Based on the above considerations, the applicability of reactions (R1) - (R5) to describe CO_2 mass transfer from gas phase into the aqueous solutions of sodium hydroxide was studied. In addition to kinetics of the reactions taking place in the liquid phase, the modelling procedure accounted for kinetics of absorption phenomena as well as hydrodynamic conditions of the process.

When CO_2 is bubbled through a perfectly mixed aqueous alkaline solution, the CO_2 mass transfer process can be modelled according to our proposal by the following differential equations for the different species, assuming that the volume remains essentially constant, and that the system is operated isothermally at 25° C:

- *For CO_2 dissolved in water:*

$$\frac{d[CO_2(l)]}{dt} = \frac{k_L a \times \sum_{i=1}^{n} \left(\left(\frac{k_H \times M_{CO_2} \times P \times [CO_2^i(g)]}{\rho_{CO_2}} - [CO_2(l)] \right) \times \frac{V_L + V_G}{n} \right)}{V_L} -$$

$$k_{11}[CO_2(l)][OH^-] + k_{12}[HCO_3^-] - k_{41}[CO_2(l)] + k_{42}[HCO_3^-][H^+] \tag{4}$$

- *For OH^-, HCO_3^-, CO_3^{2-} and H^+ ions:*

$$\frac{d[OH^-]}{dt} = -k_{11}[CO_2(l)][OH^-] + k_{12}[HCO_3^-] - k_{21}[HCO_3^-][OH^-] +$$

$$k_{22}[CO_3^{2-}] + k_{32} - k_{31}[OH^-][H^+] \tag{5}$$

$$\frac{d[HCO_3^-]}{dt} = k_{11}[CO_2(l)][OH^-] - k_{12}[HCO_3^-] - k_{21}[HCO_3^-][OH^-] +$$
$$k_{22}[CO_3^{2-}] + k_{41}[CO_2(l)] - k_{42}[HCO_3^-][H^+]$$
(6)

$$\frac{d[CO_3^{2-}]}{dt} = k_{21}[HCO_3^-][OH^-] - k_{22}[CO_3^{2-}]$$
(7)

$$\frac{d[H^+]}{dt} = k_{32} - k_{31}[OH^-][H^+] + k_{41}[CO_2(l)] - k_{42}[HCO_3^-][H^+]$$
(8)

- *For CO_2 exiting the* i*th section of the reaction mixture:*

$$\frac{d[CO_2^i(g)]}{dt} = \left(\begin{array}{c} Q_G([CO_2(g)]_{IN} - [CO_2^i(g)]) - \\ k_L a\left(\frac{k_H \times M_{CO_2} \times P \times [CO_2^i(g)]}{\rho_{CO_2}} - [CO_2(l)] \right) \times \frac{(V_L + V_G)}{n} \end{array} \right) \Big/ \frac{V_G}{n}$$
(9)

- *For CO_2 exiting the reactor e.g. headspace V_{G2} above the reaction mixture* (see Fig. 1):

$$\frac{d[CO_2(g)]_{OUT}}{dt} = (Q_G([CO_2(g)] - [CO_2(g)]_{OUT}))/V_{G_2}$$
(10)

In equations (4) - (10) molar concentrations are used. Q_G is the gas volumetric flow rate, L/s; $k_L a$ is the volumetric mass transfer coefficient, s^{-1}; V_L is the water volume, L; V_G is the gas volume in the gas-liquid mixture, L; V_{G2} is the gas volume in the empty space above the reaction mixture, L; k_H is the Henry's constant, mol L^{-1} atm^{-1}; P is the atmospheric pressure, atm; M_{CO2} is the CO_2 molar mass, g/mol; ρ_{CO2} is the CO_2 gas density, g/L.

The gas phase in the reaction mixture was divided into a number of theoretical sections n with a volume V_G/n (gas phase in close to the plug flow regime, liquid phase in the perfectly mixed flow regime as solution was recirculated). Each of these sections (high correlation coefficient observed at n=10) was treated as a non-equilibrium stage, governed by the equation 9.

The value of the Henry's constant, k_H (mol L^{-1} bar^{-1}) was determined as a function of temperature, T (K) from the relation (Pohorecki and Moniuk, 1988):

$$\log k_H = 9.1229 - 5.9044 \times 10^{-2} T + 7.8857 \times 10^{-5} T^2$$
(11)

The rate constant k_{11} of reaction 2 (R2) has been correlated as a function of temperature and ionic strength by Pohorecki and Moniuk (Pohorecki and Moniuk, 1988). However, considering near to infinite dilution ionic strength of the 0.01 M NaOH solution, the value of the second-order rate constant k_{11} (L mol^{-1} s^{-1}) can be calculated as only a function of temperature from a relationship (Pohorecki and Moniuk, 1976):

$$\log k_{11} = 11.916 - \frac{2382}{T}$$
(12)

The backward reaction rate of reaction 2 (R2), k_{12}, is defined by the value of the equilibrium constant for this reaction $(k_{12}=k_{11}K_w/K_1)$. K_1 (mol/m^3) is given as a function of temperature by Edwards et al. (Edwards et al., 1978):

$$K_1 = \exp\left(-\frac{12092.1}{T} - 36.786\ln(T) + 235.482\right)\rho_w,$$ (13)

where ρ_w is the density of water (kg/m^3). The value of the solubility product K_w (mol^2/m^6) is given by Tsonopoulos (Tsonopoulos, 1976):

$$\log\left(\frac{K_w}{\rho_w^2}\right) = -\frac{5839.5}{T} - 22.4773\log(T) + 61.2062$$ (14)

Reaction 3 (R3) is fast as it involves only a proton transfer. The reaction rate constant, k_{21}, was determined to be 6×10^6 m^3 mol^{-1} s^{-1} (Eigen, 1963). The equilibrium constant K_2 (m^3/mol) at infinite dilution that determines the value of the backward reaction of reaction 3 (R3), $k_{22}=k_{21}/K_2$, is given by Hikita et al. (Hikita et al., 1976):

$$\log(K_2) = \frac{1568.9}{T} - 2.5866 - 6.737\times 10^{-3}T$$ (15)

The neutralization rate constant, k_{31}, was determined by Eigen (Eigen, 1963) to be 1.4×10^8 m^3 mol^{-1}s^{-1}. The reaction rate between CO_2 and water, k_{41}, is very slow (0.024 s^{-1}, Danckwerts and Sharma, 1966). The values of the backward reactions, k_{32} and k_{42} can be calculated from the equilibrium constants and are k_{31}/K_W and k_{41}/K_1, respectively.

Values of the reaction rate constants used in this paper (T=298.15K) in the modelling of CO_2 absorption are summarized in Table 2.

Table 2. Values of the parameters for absorption of CO_2 in a NaOH solution at 298K

Parameter	k_{11}, $\dfrac{L}{mol\times s}$	k_{12}, s^{-1}	k_{21}, $\dfrac{L}{mol\times s}$	k_{22}, s^{-1}	k_{31}, $\dfrac{L}{mol\times s}$
Value	8.4×10^3	2.0×10^{-4}	6.0×10^9	1.2×10^6	1.4×10^{11}
Parameter	k_{32}, $\dfrac{mol}{L\times s}$	k_{41}, s^{-1}	k_{42}, $\dfrac{L}{mol\times s}$	k_H, $\dfrac{mol}{L\times atm}$	ρ_{CO2}, $\dfrac{kg}{m^3}$
Value	1.3×10^{-3}	2.4×10^{-2}	5.7×10^4	3.5×10^{-2}	1.8

In this paper, the volumetric mass transfer coefficient, k_La, was determined numerically from the differential equations (4) - (10) using the least squares method. The set of model equations were solved by means of linear multi-step methods implemented in ODESSA, which is based on the LSODE software (Hindmarsh, 1983). The calculations were performed using the MODEST 6.1 software package (Haario, 1994) designed for various tasks of model building such as simulation, parameter estimation, sensitivity analysis and optimization. The software consists of a FORTRAN 95/90 library of objective functions, solvers and optimizers linked to model problem-dependent routines and the objective function.

Estimated values of k_La (R^2> 90 %) with their 95% confidence intervals are presented in Table 3 for various absorption conditions in compliance with experimental plan presented in Table 1.

Table 3. Estimated values of volumetric mass transfer coefficient for various absorption conditions

Air/CO$_2$ flow rate, L/h	CO$_2$ concentration in the inlet gas, vol. %	Stirrer rotation speed, rpm	$k_L a$, s^{-1}
2000	15	400	$3.27 \pm 0.09 \times 10^{-2}$
2000	15	1000	$4.87 \pm 0.90 \times 10^{-2}$
2000	5	1000	$4.07 \pm 0.25 \times 10^{-2}$
2000	5	400	$2.92 \pm 0.08 \times 10^{-2}$
1000	15	1000	$3.34 \pm 0.21 \times 10^{-2}$
1000	15	400	$2.68 \pm 0.01 \times 10^{-2}$
1000	5	1000	$3.71 \pm 0.14 \times 10^{-2}$
1000	5	400	$1.94 \pm 0.07 \times 10^{-2}$
1500	10	700	$3.23 \pm 0.21 \times 10^{-2}$

The verification of the model was carried out by comparing the simulated and experimental concentration profiles and, in general, a good agreement between them was found.
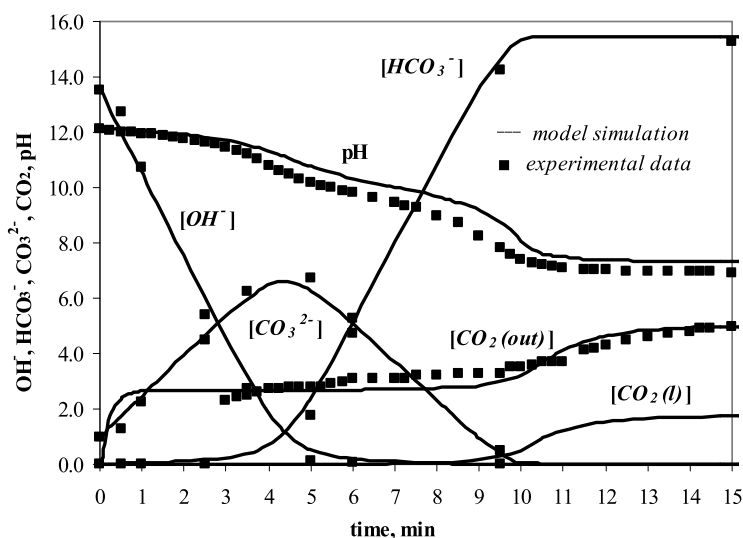
Fig. 2 Modelling of CO$_2$ absorption at $Q_G = 1000$ L/h, $N = 400$ rpm, $c = 5\%$: experimental (■) vs. simulated (—) OH^-, HCO_3^-, CO_3^{2-}, $CO_2(l)$ (mmol/L), $CO_2(out)$ (%) concentration and pH profiles

Examples of the plots of experimental and simulated concentration profiles of the reactive species and ions (CO$_2$, CO$_3^{2-}$, HCO$_3^-$, OH$^-$) in the gas and liquid phase are shown in Figures 2-4 for various conditions of CO$_2$ absorption.
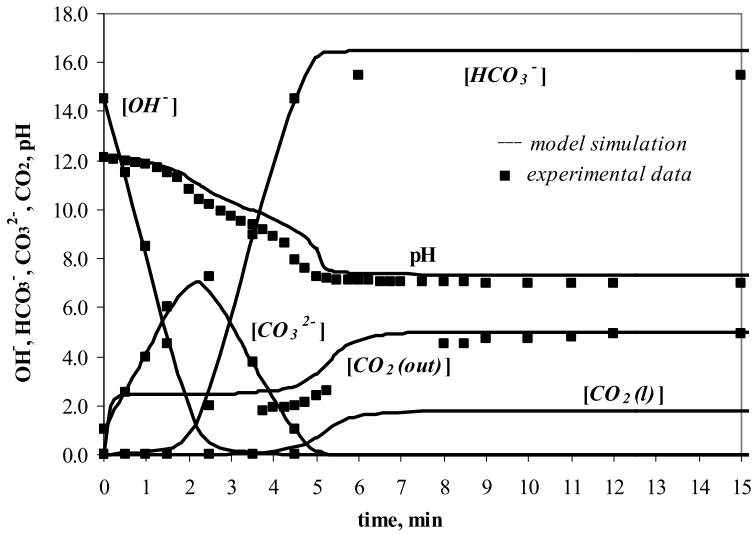
Fig. 3 Modelling of CO_2 absorption at $Q_G = 2000$ L/h, $N = 1000$ rpm, $c = 5\%$: experimental (■) vs. simulated (—) OH^-, HCO_3^-, CO_3^{2-}, $CO_2(l)$ (mmol/L), $CO_2(out)$ (%) concentration and pH profiles

Developed model allows also the prediction of pH during the neutralization of NaOH solution as graphically represented by Figures 2-4.
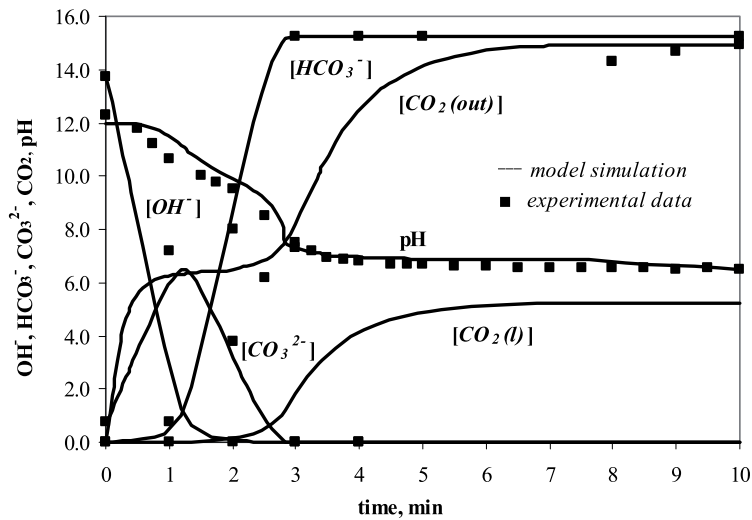
Fig. 4 Modelling of CO_2 absorption at $Q_G = 1000$ L/h, $N = 400$ rpm, $c = 15\%$: experimental (■) vs. simulated (—) OH^-, HCO_3^-, CO_3^{2-}, $CO_2(l)$ (mmol/L), $CO_2(out)$ (%) concentration and pH profiles

The results show (see Figures 2-4 above) that the model equations correspond to the experimental data quite well. Thus, the developed model is able to accurately predict the performance of CO_2 absorption into alkali aqueous model solutions in a stirred semi-batch reactor.

3.2 The effects of hydrodynamics and CO_2 partial pressure on the rate of CO_2 mass transfer

The rate of CO_2 transfer (under the conditions prevailing in the reactor) is governed by the liquid phase mass transfer coefficient, k_L and is usually characterized by the volumetric mass transfer coefficient, $k_L a$. A number of equipment and operational parameters interact to influence the efficiency and rate of CO_2 transfer. Hydrodynamic conditions of the process such as gas flow rate and stirrer rotation speed, can be viewed as the main factors affecting the rate of CO_2 mass transfer. These parameters determine factors such as bubble size, degree of turbulence etc. Clearly, another parameter affecting the CO_2 mass transfer performance is the CO_2 concentration in the inlet gas (e.g. CO_2 partial pressure). Increasing the input values of the named operating parameters is known to enhance the mass transfer rate.

As it may be observed from Table 3, the behavior of the volumetric mass transfer coefficient, $k_L a$ of CO_2 is in good agreement with the latter statement. Within the ranges of variables studied, it was observed that the mixing speed had the greatest effect on the mass transfer coefficient followed by the gas flow rate. Furthermore, based on the collected data, an empirical correlation ($R^2=90\%$) for estimation of the volumetric mass transfer coefficient $k_L a$ (s^{-1}) of carbon dioxide was built up as a function of the operating variables:

$$k_L a = 9.6218 \times 10^{-5} \times N^{0.4316} Q_G^{0.3840} c^{0.1117} , \tag{16}$$

where Q_G is the gas flow rate, L/h; N is the stirrer rotation speed, rpm; c is CO_2 content in the inlet gas, vol. %.

The effect of the stirring speed, gas flow rate and CO_2 partial pressure on the neutralization of NaOH is demonstrated by the experimental pH plots presented in Fig. 5.
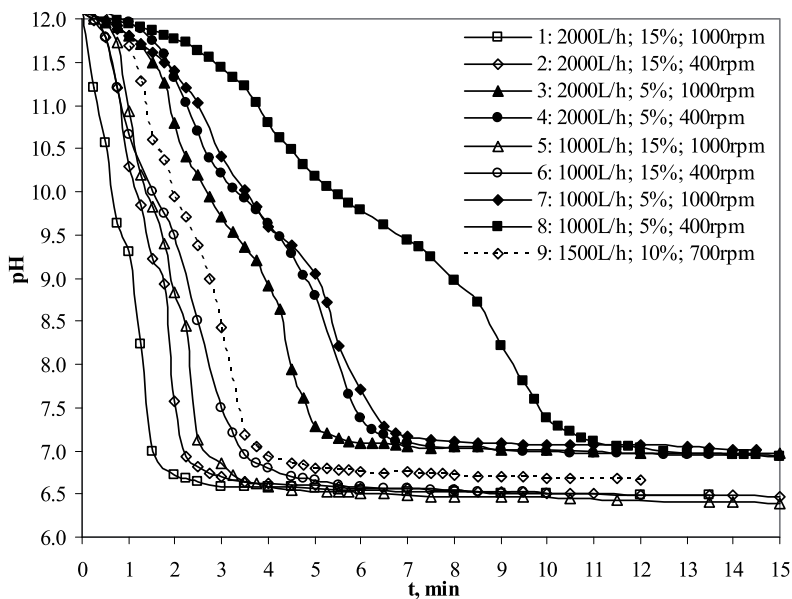
Fig. 5 The experimental pH plots for various conditions of CO_2 absorption

Examination of the curves 1-9 in Fig. 5 shows that the pH value corresponding to a neutral solution (6.5 < pH < 7.0) is reached in a shorter time as at least one of the operational variables Q_G, N or c is increased. Furthermore, increasing the stirring speed to 1000 rpm (curve 7) or the gas flow rate to 2000 L/h (curve 4) from the lower boundary conditions, characterized by the curve 8, resulted in a similar pH neutralization performance accompanied by a time reduction of about 4 minutes. In the experiments conducted in the upper boundary conditions of the CO_2 partial pressure, neutral pH region was reached after 3.5 minutes. Combined effect of the simultaneous increase of all three operating variables is demonstrated by the curve 1, whereas pH level 7.0 is reached in about 1.5 minutes.

Clearly, the decrease in CO_2 partial pressure elongates the duration to reach neutral pH, which can be compensated to some extend through the increase of gas flow rate or mixing intensity of the stirrer. Therefore, curve 9 represents the optimum conditions of operating. However, based on the collected data, the appropriate conditions (gas flow rate, stirrer rotation speed, CO_2 partial pressure, process time, etc) can be nevertheless selected depending on the objective of the absorption process (wastewater neutralization, carbonation/precipitation, gas purification) as well as equipment specifics.

It is also worth noting, that the volumetric ratio between the gas and liquid phases in the reaction mixture is mostly determined by the input value of the gas flow rate and stirring speed. Consequently, empirical function ($R^2=99\%$) for estimation of the gas fraction ε in the liquid-gas mixture was constructed as presented below:

$$\varepsilon = 2.047 \times 10^{-5} \times N^{0.579} Q_G^{0.630} \tag{17}$$

4. CONCLUSION

In this paper, the conditions of experimental work and the results of modelling of CO_2 absorption process into aqueous alkaline solution in a semi-batch reactor have been presented. For the conditions studied, a mathematical model was developed to simulate, design and optimize the CO_2 absorption process. The model includes information on all of the main factors involved in mass transfer of CO_2 from the gas to the liquid phase and the subsequent reactions (e.g. hydrodynamics, kinetics etc). Based on the experimental data and CO_2 mass transfer model, estimation of the volumetric mass transfer coefficient, $k_L a$, was made under different conditions of gas flow rate, mixing speed and initial CO_2 partial pressure. Finally, an empirical correlation for the volumetric mass transfer coefficient of carbon dioxide was proposed as a function of the main operating variables, allowing estimation of absorption performance per unit volume of gas-liquid mixture in the reactor.

As the concentrations of the various carbonate species depend on the pH of the solution, the results of this study lead to a better understanding of the chemistry and specifics of the CO_2 mass transfer process into the alkaline wastewaters such as leaching waters of oil shale ash and other lime-containing waste materials. In the next step of the study the CO_2 mass transfer model described here will be combined with models of calcium carbonate precipitation reaction taking place in heterogeneous gas-liquid-solid system. Furthermore, volumetric mass transfer coefficients, $k_L a$ evaluated in this paper, will be used to estimate the enhancement factor due to chemical reaction.

REFERENCES

1. Astarita G. Absorption of carbon dioxide into alkaline solutions in packed towers. Ind Eng Chem Fundamen 1963; 2 (4): 294-7.

2. Cents AHG, Brilman DWF, Versteeg GF. CO_2 absorption in carbonate/bicarbonate solutions: The Danckwerts-criterion revisited. Chem Eng Sci 2005; 60: 5830-5.

3. Danckwerts PV, Kennedy AM, Roberts D. Kinetics of CO_2 absorption in alkaline solutions- II absorption in a packed column and tests of surface renewal models. Chem Eng Sci 1963; 18: 63-72.

4. Danckwerts PV, Sharma MM. Absorption of carbon dioxide into solutions of alkalis and amines. Chem Eng (London) 1966; 10: 244-80.

5. Edwards TJ, Maurer G, Newman J, Prausnitz JM. Vapor-liquid equilibria in multicomponent aqueous solution of volatile weak electrolytes. AIChE J 1978; 24: 966-76.

6. Eigen M. Protonenübertagung, säure-base-katalyse und enzymatische hydrolyse. teil I: Elementarvorgänge. Angew Chem 1963; 75: 489-508.

7. Haario H. Modest user manual. Finland: Profmath Oy, 1994.

8. Hikita H, Asai S, Takatsuka T. Absorption of carbon dioxide into aqueous sodium hydroxide and sodium bicarbonate solutions. Chem Eng J 1976; 11: 131-41.

9. Hindmarsh AC. ODEPACK, a systematized collection of ODE solvers. Scientific computing, IMACS Transactions on scientific computation 1983; 1: 55-64.

10. Lide DR. CRC Handbook of chemistry and physics. 71 ed. Boca Raton, Ann Arbor, Boston: CRC Press, 1990-1991.

11. Lower SK. Environmental chemistry: Carbonate equilibria in natural waters. [online] Simon Fraser University, 1999. Available at: http://www.chem1.com/acad/pdf/c3carb.pdf

12. Pohorecki R, Moniuk W. Calculation of the rate constant for the reaction of carbon dioxide with hydroxyl ions in mixed electrolyte solutions. Rep Inst Chem Engng Warsaw Tech Univ 1976; 5: 179-92.

13. Pohorecki R, Moniuk W. Kinetics of reaction between carbon dioxide and hydroxyl ions in aqueous electrolyte solutions. Chem Eng Sci 1988; 43: 1677-84.

14. Reid RC, Prausnitz JM, Poling BE. The properties of gases and liquids. 4th ed. New York: McGraw-Hill, 1987.

15. Rubin ES. Introduction to engineering and the environment. 1st ed. New York: McGraw-Hill, 2001.

16. Tsonopoulos C. Ionization constants of water pollutants. J Chem Eng Data 1976; 21: 190-3.

17. Uibu M, Uus M, Kuusik R. CO_2 mineral sequestration in oil-shale wastes from Estonian power production. J Environ Manage 2009; 90(2): 1253-60.

18. Uibu M, Velts O, Kuusik R. Developments in CO_2 mineral carbonation of oil shale ash. J Hazard Mater 2010; 174(1-3): 209-14.

19. Velts O, Hautaniemi M, Kallas J, Kuusik R. Modeling calcium dissolution from oil shale ash: PART 1. Ca dissolution during ash washing in a batch reactor. Fuel Process Tech 2010a; in press, doi:10.1016/j.fuproc.2009.12.008

20. Velts O, Hautaniemi M, Kallas J, Kuosa M, Kuusik R. Modeling calcium dissolution from oil shale ash: PART 2. Continuous washing of the ash layer. Fuel Process Tech 2010b; in press, doi:10.1016/j.fuproc.2009.12.009

21. Weart SR. The discovery of global warming. Cambridge, MA: Harvard University Press, 2003.

PAPER V

Velts, *O.,* Uibu, M., Kallas, J., Kuusik, R.

CO_2 mineral trapping: Modeling of calcium carbonate precipitation in a semi-batch reactor.

Reprinted with permission from:

Energy Procedia 2011, 4, 771–778.

GHGT-10

CO$_2$ mineral trapping: Modeling of calcium carbonate precipitation in a semi-batch reactor

O. Velts[a, b, 1]*, M. Uibu[a], J. Kallas[a, b], R. Kuusik[a]

[a]*Tallinn University of Technology, Laboratory of Inorganic Materials, 5 Ehitajate Str., Tallinn 19086, Estonia*
[b]*Lappeenranta University of Technology, Laboratory of Separation Technology, Skinnarilankatu 34, Lappeenranta 53851, Finland*

Abstract

In the current paper, CaCO$_3$ precipitation process via CO$_2$ absorption into aqueous solution of Ca(OH)$_2$ was investigated in a stirred semi-batch reactor. Mathematical model describing the precipitation process was developed by considering the absorption and reaction kinetics as well as hydrodynamic conditions in the system. The model allows to simulate the concentration profiles of reactive species (CO$_2$, Ca^{2+}, OH$^-$, CaCO$_3$, HCO$_3^-$, H$^+$, CO$_3^{2-}$) in the gas and liquid phase as well as to predict the rate of CaCO$_3$ formation. The volumetric mass transfer coefficient, $k_L a_{CO2}$ characterizing CO$_2$ transfer performance from gas phase into Ca(OH)$_2$ solution as well as rate constant of the CaCO$_3$ precipitation reaction, k_{51} were estimated based on the experimental data and the developed model. The CO$_2$ mass transfer enhancement factor E due to chemical reaction was also estimated.
ⓒ 2011 Published by Elsevier Ltd.

Keywords: CaCO$_3$; CO$_2$; precipitation; mass transfer; modeling

1. Introduction

There is a considerable concern about the impact of greenhouse gases including carbon dioxide (CO$_2$) emissions on the global climate [1]. In spite of years of legislation and emission reduction, particularly in the Republic of Estonia, where local carbonaceous fossil fuel - oil shale - is used as a fuel in electricity production, remarkable CO$_2$ emissions are still one of the major environmental issues.

Among the options under consideration to help mitigate anthropogenic CO$_2$ emissions is carbon mineral trapping - the chemical binding of CO$_2$ by calcium (Ca) and magnesium (Mg) compounds to form stable carbonates [2]. In this context, the feasibility of CO$_2$ safe disposal in the form of precipitated calcium carbonate (PCC) by gas-liquid reaction is of considerable importance due to applicability of PCC in a wide range of products including paper, paints, plastics, rubber, textiles etc. Although PCC is traditionally produced from lime of natural limestone [3], the efforts in the direction of waste minimization have evoked designing of new production methods for PCC. A very promising one among them is related to the reusability of lime-containing wastes, including oil shale ash formed

---

* Corresponding author. Tel.: +372-528-3756; fax: +372-620-2801.
E-mail address: olga.velts@ttu.ee

during heat and power production in Estonia. It has been proven by our earlier studies, that due to high content of free lime (up to 30% of CaO) this residue could be considered as a low-cost source of water-soluble calcium [4].

In the preliminary stage, modeling of the process of CaO leaching/slacking from ash [5, 6] as well as dissolution of gaseous CO_2 into the liquid phase [7] have been worked out and described by the authors. Furthermore, in order to design the PCC formation process and to optimize CO_2 elimination from exhaust gas using alternative CaO containing materials, such as oil shale ash, mathematical models describing the precipitation process of calcium carbonate in a model gas – liquid system must be developed using at first chemically pure lime as a Ca source. Thus, the main goal of the current study was to develop a mathematical description of the multi-step PCC formation process in a model gas – liquid system by conducting chemical absorption experiments of CO_2 into an aqueous Ca-ion rich solution of calcium hydroxide $Ca(OH)_2$ with various initial concentrations. The scope of the study was extended to investigate the influence of precipitation reaction on the rate of CO_2 mass transfer.

2. Materials and methods

Experimental work was carried out in a pilot-scale stirred PCC semi-batch reactor by bubbling a gas mixture of CO_2 and air through a recirculating $Ca(OH)_2$ solution of 10 L volume. Gas flow rate (Q_G) and composition (c) was controlled using rotameters and CO_2 IR-analyzer (Duotec). The pH value in reactor was continuously monitored by pH meter (Mettler Toledo GWB SG2). Collection of the liquid phase samples was performed by means of sampling valve on the reactor body (Figure 1).
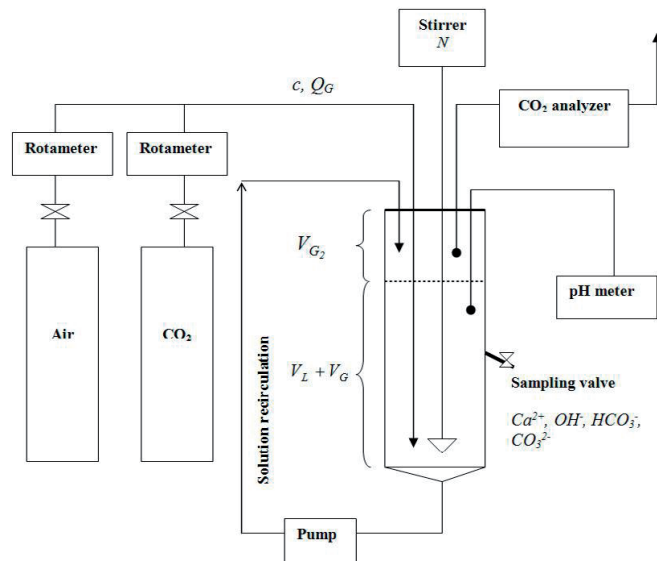
Figure 1 Principal scheme of the experimental setup

Initial $Ca(OH)_2$ solutions with various concentrations (350, 600 and 850 mg Ca^{2+} L^{-1}) were prepared by slaking chemically pure lime (Sigma-Aldrich) and filtering the suspension in order to remove any inert or non-dissolved solids. The carbonation process took place at a constant gas feed rate of 1000 L hr^{-1} with a gas mixture containing 5.0 vol.-% of CO_2 in air and stirrer rotation speed of 400 rpm. In the coarse of experiments, the pH value, concentration of Ca^{2+} (titrimetric method ISO 6058:1984), CO_3^{2-}, HCO_3^-, OH^- ions (titrimetric method ISO 9963-1:1994(E)) in the (filtered) liquid phase as well as CO_2 content in the gas stream exiting the reactor were continuously measured. Experiments were conducted until the solution pH reached a value of 7.0.

3. Results and discussion

3.1. Modeling of the CO_2 chemical absorption into aqueous $Ca(OH)_2$ solution

CO_2 transfer, the process by which CO_2 is transferred from the gaseous to the liquid phase, is a vital part of a number of industrial processes (gas purification, carbonation/precipitation, wastewater neutralization). The mechanism for the reaction of CO_2 with aqueous solutions of hydroxides has been expressed by Cents et al [8] and in the case of absorption into (under)saturated $Ca(OH)_2$ solution can be presented by the following reactions.

Formation of bicarbonate:

$$CO_2(l) + OH^- \underset{k_{12}}{\overset{k_{11}}{\rightleftarrows}} HCO_3^- \tag{1}$$

Dissociation of bicarbonate:

$$HCO_3^- + OH^- \underset{k_{22}}{\overset{k_{21}}{\rightleftarrows}} CO_3^{2-} + H_2O \tag{2}$$

Ionization of water:

$$OH^- + H^+ \underset{k_{32}}{\overset{k_{31}}{\rightleftarrows}} H_2O \tag{3}$$

CO_2 hydration:

$$CO_2(l) + H_2O \underset{k_{42}}{\overset{k_{41}}{\rightleftarrows}} HCO_3^- + H^+ \tag{4}$$

Formation of the $CaCO_3$ crystals:

$$Ca^{2+} + CO_3^{2-} \underset{k_{52}}{\overset{k_{51} = \frac{k_{52} \times [CaCO_3]_s}{Ksp}}{\rightleftarrows}} CaCO_3 \tag{5}$$

In addition to the above reactions, the process of physical dissolution of gaseous CO_2 into $Ca(OH)_2$ solution is represented by Eq. 6:

$$CO_2(q) \leftrightarrow CO_2(l) \tag{6}$$

The solubility equilibrium follows Henry's law (at pressures up to about 5 atm):

$$[CO_2(l)]_{eq} = k_H \times P_{CO_2} \tag{7}$$

where k_H is the Henry constant, P_{co2} is the CO_2 partial pressure.

The modeling procedure in this paper accounted for kinetics of absorption and reactions taking place in the liquid phase (Eq. 1-6) as well as hydrodynamic conditions in the system. According to our proposal [7], when CO_2 is bubbled through a perfectly mixed aqueous $Ca(OH)_2$ solution, the precipitation process of $CaCO_3$ can be modeled by the following differential equations for the different species, assuming that the system is operated isothermally at 25° C.

- For CO_2 dissolved in liquid phase:

$$\frac{d[CO_2(l)]}{dt} = \frac{k_L a_{CO_2} \times \sum_{i=1}^{n} \left(\left(\frac{k_H \times M_{CO_2} \times P \times [CO_2^i(g)]}{\rho_{CO_2}} - [CO_2(l)] \right) \times \frac{V_L + V_G}{n} \right)}{V_L}$$
$$- k_{11}[CO_2(l)][OH^-] + k_{12}[HCO_3^-] - k_{41}[CO_2(l)] + k_{42}[HCO_3^-][H^+] \tag{8}$$

- For Ca^{2+}, OH^-, HCO_3^-, CO_3^{2-} and H^+ ions:

$$\frac{d[Ca^{2+}]}{dt} = k_{52} - k_{51}[Ca^{2+}][CO_3^{2-}] = k_{52} - \frac{k_{52}[Ca^{2+}][CO_3^{2-}]}{K_{sp}} \tag{9}$$

$$\frac{d[OH^-]}{dt} = -k_{11}[CO_2(l)][OH^-] + k_{12}[HCO_3^-] - k_{21}[HCO_3^-][OH^-]$$
$$+ k_{22}[CO_3^{2-}] + k_{32} - k_{31}[OH^-][H^+] \tag{10}$$

$$\frac{d[HCO_3^-]}{dt} = k_{11}[CO_2(l)][OH^-] - k_{12}[HCO_3^-] - k_{21}[HCO_3^-][OH^-]$$
$$+ k_{22}[CO_3^{2-}] + k_{41}[CO_2(l)] - k_{42}[HCO_3^-][H^+] \tag{11}$$

$$\frac{d[CO_3^{2-}]}{dt} = k_{21}[HCO_3^-][OH^-] - k_{22}[CO_3^{2-}] + k_{52} - \frac{k_{52}[Ca^{2+}][CO_3^{2-}]}{K_{sp}} \tag{12}$$

$$\frac{d[H^+]}{dt} = k_{32} - k_{31}[OH^-][H^+] + k_{41}[CO_2(l)] - k_{42}[HCO_3^-][H^+] \tag{13}$$

- For CO_2 exiting the ith section of the reaction mixture:

$$\frac{d[CO_2^i(g)]}{dt} = \left(\begin{array}{l} Q_G \left([CO_2(g)]_{IN} - [CO_2^i(g)]\right) \\ - k_L a_{CO_2} \left(\frac{k_H \times M_{CO_2} \times P \times [CO_2^i(g)]}{\rho_{CO_2}} - [CO_2(l)] \right) \times \frac{(V_L + V_G)}{n} \end{array} \right) \Big/ \frac{V_G}{n} \tag{14}$$

- For CO_2 exiting the reactor e.g. headspace V_{G2} above the reaction mixture (see Figure 1):

$$\frac{d[CO_2(g)]_{OUT}}{dt} = \left(Q_G \left([CO_2(g)] - [CO_2(g)]_{OUT}\right) \right) / V_{G_2} \tag{15}$$

- For $CaCO_3$ forming in the carbonation process:

$$\frac{d[CaCO_3]}{dt} = k_{51}[Ca^{2+}][CO_3^{2-}] - k_{52} = \frac{k_{52}[Ca^{2+}][CO_3^{2-}]}{K_{sp}} - k_{52} \tag{16}$$

In equations (8) - (16) concentrations are expressed in molar units; Q_G is the gas volumetric flow rate, L s^{-1}; $k_L a_{CO2}$ is the CO_2 volumetric mass transfer coefficient, s^{-1}; K_{sp} is the solubility product of $CaCO_3$, mol^2/L^2, V_L is the solution volume, L; V_G is the volume of gas in the gas-liquid mixture, L; V_{G2} is the gas volume in the reactor

headspace, L; k_H is the Henry's constant, mol L^{-1} atm^{-1}; P is the atmospheric pressure, atm; M_{CO2} is the CO_2 molar mass, g mol^{-1}; ρ_{CO2} is the CO_2 gas density, g L^{-1}.

In our study, a program feature accounting for the changes in V_L, V_G, V_{G2} due to samples collection was implemented in the modeling algorithm. The gas phase in the reaction mixture was divided into a number of theoretical sections n with a volume V_G/n (gas phase in close to the plug flow regime, liquid phase in the perfectly mixed flow regime as solution was recirculated). Each of these sections (high correlation coefficient observed at n=10) was treated as a non-equilibrium stage, governed by the Eq. 14. Values of the reaction rate constants in Eq. 1-4 and parameters used in this paper (T=298.1K) in the modeling of $Ca(OH)_2$ solution carbonation process are summarized in Table 1 [7].

Table 1 Used parameters in the modeling of CO_2 absorption into $Ca(OH)_2$ solution at 298K

Parameter	Value	Parameter	Value
k_{11}, L mol^{-1} s^{-1}	8.4×10^3	k_{32}, mol L^{-1} s^{-1}	1.3×10^{-3}
k_{12}, s^{-1}	2.0×10^{-4}	k_{41}, s^{-1}	2.4×10^{-2}
k_{21}, L mol^{-1} s^{-1}	6.0×10^9	k_{42}, L mol^{-1} s^{-1}	5.7×10^4
k_{22}, s^{-1}	1.2×10^6	k_H, mol L^{-1} atm^{-1}	3.5×10^{-2}
k_{31}, L mol^{-1} s^{-1}	1.4×10^{11}	ρ_{CO2}, kg m^{-3}	1.8

The volumetric mass transfer coefficient of CO_2 in the presence of chemical reaction, $k_L a_{CO2}$ and the backward reaction rate constant of reaction 5 (Eq. 5), k_{52}, were determined numerically from the differential equations (8) - (16). The set of model equations was solved by means of linear multi-step methods implemented in ODESSA, which is based on the LSODE software [9].

The calculations were performed using the MODEST 6.1 software package [10] designed for various tasks of model building such as simulation, parameter estimation, sensitivity analysis and optimization. The software consists of a FORTRAN 95/90 library of objective functions, solvers and optimizers linked to model problem-dependent routines and the objective function.

Estimated values of $k_L a_{CO2}$ ($R^2 > 93$ %) with their 95% confidence intervals are presented in Table 2 for various concentrations of the initial $Ca(OH)_2$ solution. The average value of the backward reaction rate constant, k_{52} was estimated to be 9.0×10^{-3} s^{-1} and considering the value of solubility product of $CaCO_3$, K_{sp} =4.8×10^{-9} mol^2/L^2, rate constant of the $CaCO_3$ precipitation reaction, k_{51} is, thus, 1.88×10^6 L mol^{-1} s^{-1} (Table 2).

Table 2 Estimated parameters for carbonation of the $Ca(OH)_2$ solutions in a stirred semi-batch reactor at Q_G = 1000 L hr^{-1}, N = 400 rpm, c = 5%

$[Ca^{2+}]_0$, mol L^{-1}	$k_L a_{CO2}$, s^{-1}	E	Precipitation reaction kinetics	$Ca^{2+} + CO_3^{2-} \underset{k_{52}}{\overset{k_{51}=\frac{k_{52} \times [CaCO_3]_s}{Ksp}}{\rightleftarrows}} CaCO_3$
absent [7]	0.0194 ± 0.0007	1.0	$k_{51}{}^{av}$,	1.88×10^6
0.00863	0.0294 ± 0.0026	1.5	L mol^{-1} s^{-1}	
0.01500	0.0347 ± 0.0024	1.8	$k_{52}{}^{av}$,	9.00×10^{-3}
0.02125	0.0529 ± 0.0051	2.7	s^{-1}	

Proposed model allows to simulate the concentration profiles of reactive species (Ca^{2+}, OH^-, $CaCO_3$, HCO_3^-, CO_2, H^+, CO_3^{2-}) in the gas and liquid phase as well as to predict the rate of PCC formation. The model was verified by comparing the predictions of the species concentration changes in the course of carbonation with the experimental data. Examples of the plots of experimental and simulated concentration profiles are shown in Figure 2.
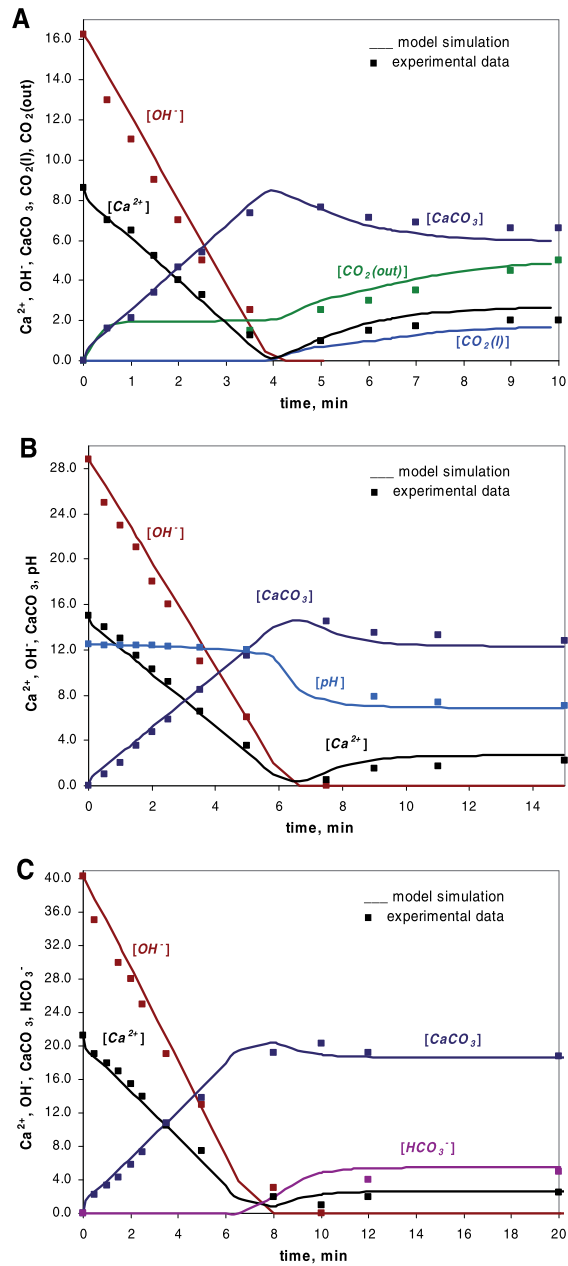
Figure 2 Modeling of CO_2 absorption at $Q_G = 1000$ L hr^{-1}, $N = 400$ rpm, $c = 5\%$, $[Ca^{2+}]_0 =$ (A) 0.00863; (B) 0.0150 and (C) 0.02125 mol L^{-1}: comparison of experimental (points) and simulated (solid lines) Ca^{2+}, OH^-, $CaCO_3$, HCO_3^-, CO_2(l) (mmol L^{-1}), CO_2(out) (%) concentration and pH profiles

It can be seen that the course of carbonation is quite well described. The correlation coefficients obtained for all sets of data were no less then 0.93. At lower pH values the solubility of the $CaCO_3$ increases, thus, the potentials of the presented model are manifested by the accurate prediction of the outcome of the final stage of the carbonation process, where the back-dissolution of PCC is starting to take place. Developed model allows also the prediction of pH during the neutralization of $Ca(OH)_2$ alkaline solution as graphically represented by Figure 2, B and can be used to design the precipitation as well as wastewater neutralization process.

3.2. The effect of precipitation reaction on the rate of CO_2 mass transfer

The volumetric mass transfer coefficient, k_La is a parameter that represents the absorption performance per unit volume of gas-liquid mixture in the reactor and depends fundamentally on the superficial gas velocity and on the physical properties of absorption phase. Furthermore, the presence of chemical reaction will, generally, enhance the mass transfer across the gas-liquid interface [11].

The reactions of CO_2 with $Ca(OH)_2$ solution enhance the rate of absorption and increase the capacity of the liquid solution to dissolve the solute, when compared with physical absorption systems. The effect of chemical reaction on the process performance can be expressed by introducing the CO_2 mass transfer enhancement factor, E [12, 13], defined here as the ratio of the volumetric mass transfer coefficients for CO_2 absorption for both cases with, k_La_{CO2} and without chemical reaction, $k_La^0_{CO2}$:

$$E = \frac{k_L a_{CO_2}}{k_L a^0_{CO_2}}$$ (17)

In our earlier study on the CO_2 absorption process into aqueous alkaline solution of hydroxides in a stirred semi-batch reactor, the volumetric mass transfer coefficient of CO_2 for the system in the absence of chemical reaction, $k_La^0_{CO2}$ (s^{-1}) was estimated for a wide range of operating parameters, including stirrer rotation speed (N, rpm), gas flow rate (Q_G, L hr^{-1}) and CO_2 content in the inlet gas (c, vol. %):

$$k_L a^0_{CO_2} = 9.6218 \times 10^{-5} \times N^{0.4316} Q_G^{0.3840} c^{0.1117}$$ (18)

Details of the $k_La^0_{CO2}$ determination can be found in [7]. For the same experimental conditions as applied in this work, $k_La^0_{CO2}$ was found to be 0.0194 s^{-1} (see Table 2). Thus, based on the results of these studies, values of the enhancement factor E for CO_2 absorption were determined (Table 2) and empirical equation of E (R^2=97.4%) as a function of $Ca(OH)_2$ solution initial concentration (unit mmol L^{-1}) was proposed as follows:

$$E = 0.0027 \times \left[Ca^{2+}\right]_0^2 + 0.0224 \times \left[Ca^{2+}\right]_0 + 1.0$$ (19)

Calculations indicate that in the case of absorption into $Ca(OH)_2$ solutions with up to the maximum solubility (saturation concentration ~850 mg Ca^{2+} L^{-1}), the enhancement factor is, as expected, noticeably (1.5 - 2.7 times) larger than unity. Chemical reaction keeps the concentration of CO_2 in the liquid phase nearly zero and, therefore, the driving force is remained high. Thus, an increase in the $Ca(OH)_2$ solution initial concentration produces a continuous increase in the enhancement factor.

4. Conclusion

This paper contributes to knowledge on the chemical absorption of CO_2 into aqueous $Ca(OH)_2$ solution performed in a stirred semi-batch reactor under different experimental conditions. As a result of the study, mathematical model for predicting $CaCO_3$ precipitation process was developed and the mass transfer parameters were determined. The presented carbonation model has been positively verified to find a good agreement between experimental data and modeling predictions. The proposed computational procedures may be effectively used to simulate and design precipitation or alkaline wastewater neutralization process at arbitrary conditions. To show the increasing rate of carbon dioxide transfer due to chemical reaction, the CO_2 mass transfer enhancement factor E was

evaluated and empirical equation of *E* as a function of solution initial concentration proposed. In the next step of the study the carbonation model described here will be applied in the modeling of oil shale ash leachates carbonation process taking place in the gas-liquid system.

Acknowledgements

References

[1] Weart SR. The discovery of global warming. Cambridge, MA: Harvard University Press; 2004.
[2] Carbon capture and storage: Trapping mechanisms, The cooperative research centre for greenhouse gas technologies (CO2CRC), 2010. Available at: http://www.co2crc.com.au/aboutccs/stor_trapping.html Accessed 3 Aug 2010
[3] What is PCC? Specialty Minerals Inc. (SMI), 2010. Available at: http://www.specialtyminerals.com/our-minerals/what-is-pcc/ Accessed 3 Aug 2010
[4] Velts O, Uibu M, Rudjak I, Kallas J, Kuusik R. Utilization of oil shale ash to prepare PCC: leachibility dynamics and equilibrium in the ash – water system. Energy Procedia 2009;1(1):4843-50.
[5] Velts O, Hautaniemi M, Kallas J, Kuusik R. Modeling calcium dissolution from oil shale ash: PART 1. Ca dissolution during ash washing in a batch reactor. Fuel Process Tech 2010;91(5):486-90.
[6] Velts O, Hautaniemi M, Kallas J, Kuosa M, Kuusik R. Modeling calcium dissolution from oil shale ash: PART 2. Continuous washing of the ash layer. Fuel Process Tech 2010;91(5):491-5.
[7] Velts O, Hautaniemi M, Uibu M, Kallas J, Kuusik R. Modelling of CO2 mass transfer and hydrodynamics in a semi-batch reactor. Journal of International Scientific Publications: Materials, Methods & Technologies 2010;4(2):68-79. Available at: http://www.science-journals.eu/mmt/index.html Accessed 3 Aug 2010
[8] Cents AHG, Brilman DWF, Versteeg GF. CO$_2$ absorption in carbonate/bicarbonate solutions: The Danckwerts-criterion revisited. Chem Eng Sci 2005;60:5830-5.
[9] Hindmarsh AC. ODEPACK, a systematized collection of ODE solvers. Scientific computing, IMACS Transactions on scientific computation 1983;1:55-64.
[10] Haario H. Modest user manual. Finland: Profmath Oy; 1994.
[11] Katoh S, Yoshida F. Biochemical Engineering: A Textbook for Engineers, Chemists and Biologists. Wiley-VCH; 2009.
[12] Nijsing RATO, Hendriksz RH, Kramers H. Absorption of CO$_2$ in jet and falling films of electrolyte solutions, with and without chemical reaction. Chem Eng Sci 1959;10:88-104.
[13] Van Swaaij WPM, Versteeg GF. Mass transfer accompanied with complex reversible reactions in gas-liquid systems: An overview. Chem Eng Sci 1992;47:3181-96.

PAPER VI

Velts, *O.,* Uibu, M., Kallas, J., Kuusik, R.

Prospects in waste oil shale ash sustainable valorization.

Prospects in Waste Oil Shale Ash Sustainable Valorization

Olga Velts, Mai Uibu, Juha Kallas, and Rein Kuusik

Abstract—An innovative approach utilizing highly alkaline oil shale waste ash and carbon dioxide gas (CO_2), associated with power production, as a resource for production of precipitated calcium carbonate (PCC) is introduced in this paper. The specifics and feasibility of the integrated ash valorization and CO_2 sequestration process by indirect aqueous carbonation of lime-consisting ash were elaborated and the main parameters established. Detailed description of the formed precipitates was included. Complimentary carbonation experiments with commercial CaO fine powder were conducted for comparative characterization of the final products obtained on the basis of two different raw materials. Finally, the expected CO_2 uptake was evaluated.

Keywords—Calcium Carbonate, Carbon Dioxide Sequestration, Oil Shale Ash, Waste Valorization.

I. INTRODUCTION

SAFE deposition/utilization of solid wastes is among the most serious problems in the world's heat-and-power production. In Estonia, oil shale type fossil fuel is an important resource for the national economy. About 85 % of oil shale is consumed by power plants, which produce over 95 % of Estonian electricity and a great part of thermal power. The power sector is the largest CO_2 emitter (15.2 metric tons per capita in 2007) in Estonia [1] as well as a source of enormous amounts of hazardous waste ash (about 6 Mt of ash annually). The oil shale based heat and power production has produced over the years about 280 million tons of alkaline waste ash which, due to the current lack of practical applications, is deposited on the waste plateaus nearby the power plants and is causing environmental problems as a source of alkaline pollutants [2]. Therefore, developing an effective usage of this waste ash would be a highly desirable outcome.

In this aspect, a conceptual approach of utilizing combustion waste ash as a low-cost source of water-soluble calcium (Ca) for production of precipitated calcium carbonate (PCC) is elucidated. In addition to obtaining a valuable commercial product, advantages of Ca-rich alkaline oil shale ash leachates carbonation include safer disposal of wastes,

O. Velts is with the Laboratory of Inorganic Materials, Tallinn University of Technology, Ehitajate Str. 5, Tallinn 19086 Estonia, as well as with the Laboratory of Separation Technology, Lappeenranta University of Technology, P.O.Box 20, Lappeenranta FI-53851 Finland (corresponding author: +372-528-3756; fax: +372-620-2801; e-mail: olga.velts@ttu.ee).

M. Uibu, J. Kallas and R. Kuusik are with the Laboratory of Inorganic Materials, Tallinn University of Technology, Ehitajate Str. 5, Tallinn 19086 Estonia (e-mail: maiuibu@staff.ttu.ee; Juha.Kallas@lut.fi; rein.kuusik@ttu.ee).

CO_2 emissions reduction and wastewater neutralization. The last aspects have been discussed earlier [3, 4]. Furthermore, in our previous papers, main characteristics and mechanisms for intermediate stages of the process, including Ca-leaching from ash [5, 6] and dissolution of gaseous CO_2 into alkaline liquid phase [7] have been reported. In current study, the feasibility of ash leachates carbonation accompanied by the formation of PCC was investigated experimentally in a semi-batch stirred barboter-type reactor. One of the tasks was to establish the impact of the complex composition of leachates on the main characteristics (chemical composition, morphology, surface area, particle size distribution etc) of the forming precipitate. Additionally, comparative calcium carbonate precipitation was performed on the basis of a pure lime based model solution. The scope of the study was extended to assessing the CO_2 sequestration and PCC production capacity of leachates.

II. MATERIALS AND METHODS

In this study, two types of solutions (à 10 L) were carbonated: *Solution I* (oil shale ash leachates) and *Solution II* (lime based model solution). *Solution I* was prepared by stirring oil shale ash (containing about 8.0 % of free CaO) - distilled water suspension (liquid to solid ratio of 10 w/w) in a 15 L reactor equipped with turbine type impeller for 15 minutes, and then filtering out the solid ash residue (Fig. 1, a). Oil shale ash leachates (pH=12.65) with the following average ion concentration were obtained: Ca^{2+}: 1.23 g/L, SO_4^{2-}: 0.73 g/L, K^+: 0.076 g/L, Cl^-: 0.038 g/L, OH^-: 0.047 mol/L. Saturated lime solution (*Solution II*) with Ca^{2+} equilibrium concentration of 0.85 g/L was produced by slaking chemically pure lime (Sigma-Aldrich) and filtering the suspension in order to remove any inert or non-dissolved solids. The carbonation process was conducted in a semi-batch stirred barboter-type reactor (Fig. 1, b) at a constant gas feed rate of 1000 L/h with a model gas containing 5.0 vol.% CO_2 in air and stirring rate of 400 rpm. In the carbonation experiments, concentration of Ca^{2+} (titrimetric method ISO 6058:1984), SO_4^{2-} (spectrophotometer SpectroDirect Lovibond), CO_3^{2-}, HCO_3^-, OH^- ions (titrimetric method ISO 9963-1:1994(E)) in the (filtered) liquid phase, pH (Mettler Toledo GWB SG2) and conductivity (HI9032) value in reactor as well as CO_2 content in the outgoing gas flow (CO_2 IR-analyzer, Duotec) were continuously measured. After carbonation, the suspension was immediately filtrated (Whatman filter paper "blue ribbon").

Fig. 1 Simplified schematic of the experimental setup: a) Leaching step; b) Carbonation step

The solid was dried and analyzed for its chemical composition by Total Carbon (TC; ELTRA Carbon/Sulfur Determinator CS-580) and X-Ray Diffraction (XRD; Bruker D8 Advanced) analyses. The surface morphology of precipitate particles was monitored in the course of experiment using a scanning electron microscope (Jeol JSM-8404A). The particle size distribution (PSD) of the final product was determined by laser diffraction analyzer (Beckman Coulter LS 13320) and BET-surface area by nitrogen dynamic desorption analysis method (Sorptometer KELVIN 1042).

Depending on the duration of CO_2 addition, two cases of carbonation experiments were performed: In *Experiment 1*, the CO_2 gas flow was switched off after the pH of the solution had stabilized, whereas in case of *Experiment 2* carbonation was stopped when conductivity of solution started to increase. Additionally, identical to *Experiment 1* carbonation procedure of the lime solution was conducted in order to compare the final precipitates obtained on the basis of different raw materials.

III. RESULTS AND DISCUSSION

A. Production of PCC on the Basis of Waste Oil Shale Ash

Despite of extensive knowledge of the carbonation of lime, producing PCC from oil shale ash is an unknown complex multistage process. Current production methods for PCC mainly use lime - an expensive high quality raw material. Similarly to ash leachates carbonation process described in this paper, in traditional PCC production method dry CaO is slaked (hydrated) with water to form calcium hydroxide slurry which is then screened to remove impurities originating from the limestone and fed to a stirred tank reactor where it reacts with CO_2 [8]. However, in addition to free lime, oil shale waste ash also contains other Ca-compounds such as anhydrite

etc that become additional sources of water-soluble Ca, thus allowing the solution to exceed the equilibrium solubility limit for Ca-ion in respect to pure CaO, which is an important positive factor in the context of oil shale ash based PCC production process. Thus, in this study, as a result of oil shale ash-water contact, Ca concentration in the ash leachates was higher (*Solution I*: 1.23 g/L) as compared to Ca-ion equilibrium concentration achieved by dissolving pure lime in water (*Solution II*: 0.85 g/L). Similarly to lime solution, ash leachates have a high pH (about 12-13), but consist in addition to Ca^{2+} and OH^- several other ions such as SO_4^{2-}, K^+, Cl^-, PO_4^{3-} etc. The latter could influence the precipitation process.

In this study, a set of ash leachates carbonation experiments was conducted. In *Experiment 1*, neutralization of ash leachates (pH = 6.8) accompanied by the formation of the solid precipitate *PCC1* (Table I) occurred. Considering the fact that CO_2 dissolution into water is pH-dependent (CO_2 is found in the solution mainly as CO_3^{2-} at pH >9 and as HCO_3^- around pH <9.0), the highest concentration of PCC is expected at pH >9. At lower pH values (pH<9) formation of HCO_3^--ions triggers re-dissolution of calcium carbonate. At the same time, alkaline wastewater (such as ash leachates) has to be neutralized to pH level accepted by environmental regulations (< 9) before directing it into the nature. Furthermore, in case of availability of large amounts of wastewater in the proximity of CO_2 emission source, it is also economically viable to sequester as much CO_2 as possible, yet still obtaining PCC of high quality as a by-product. Related to this, carbonation in *Experiment 2*, was stopped prior reaching the pronounce re-dissolution region (end-point pH value ~8.0) and precipitate *PCC2* was obtained as a result. It should be pointed out that no specific treatment (e.g. washing) of the final precipitates described above was done, thus purity of the product is expected to be higher after washing. In order to investigate how the washing affects the quality of the

precipitate, the *Experiment 2* was replicated (*Experiment 3*), but the precipitate was washed after the filtration by passing distilled water through precipitate cake (L/S ratio: 20 w/w) to remove possible water-soluble compounds, and the dried solid material (*PCC3*) was analyzed. Additionally, lime solution (*Solution II*), which is traditionally used for PCC production, was carbonated (*Experiment 4; PCC4*) at the same operational conditions as in *Experiment 1*. In the course of carbonation, depending on the duration of the process, Ca^{2+} and SO_4^{2-} concentration in the leachates decreased from about 1.23 and 0.74 g/L to 0.25-0.3 and 0.57-0.6 g/L respectively, and ~ 23-24 g of solid material precipitated from 10 L of solution. Furthermore, it was confirmed that the concentration of the background ions such as K^+, Cl^-, PO_4^{3-}, etc in the solution remained unchanged during carbonation. It can therefore be assumed that they do not take part in the precipitation process in detectible amount. This finding is important in the context of the PCC production process on the basis of oil shale ash. All formed precipitates (*PCC1–PCC4,* Table I) were in a form of calcite according to XRD analyses (100.0 wt-%) with bright white color, and fine and powdery texture. The TC analyze confirmed that the filtered solid samples *PCC1–PCC3* predominantly contained $CaCO_3$ (95-96 wt-%). The minor phase of the precipitates formed from ash leachates was gypsum (4-5 wt-%) deposited on the calcite matrix. Washed precipitate *PCC3* contained slightly higher amount of calcium carbonate (96.0 wt-%). More thorough washing would likely improve the purity of the solid product. At the conditions studied, the end-point pH value of the carbonation practically did not influence the calcium carbonate content in the precipitates, 95.2 and 95.4 wt-% in *PCC1* and *PCC2*, respectively. Nevertheless, carbonation extent is expected to have a significant effect on the product yield, especially in case of carbonation at higher CO_2 concentrations and flow rates. It has also been observed by comparing *PCC1* and *PCC2* samples formed from ash leachates, that the surface area and size of PCC particles were affected by the carbonation extent: surface area increased and mean particle size slightly decreased with increasing the carbonation duration. Main characteristics of the PCC obtained on the basis of ash and lime are presented in Table I.

indicate that the ash based PCC is characterized by higher brightness values as compared to traditional lime-based PCC. Samples *PCC1–PCC3* were also noticeably whiter in color then precipitate *PCC4* even without washing. Interestingly, samples *PCC1, PCC4* obtained in identical conditions, yet on the basis of different raw materials, contained particles with quite similar surface area and mean size values (Table I). Shape and surface observations confirmed the results of the particle size distribution analysis. Scanning electron microscopy images for respective types of PCC formed are shown in Fig. 2. The changes in the morphology of forming PCC particles in the course of carbonation of oil shale ash leachates are illustrated by sub-figures (a) to (d) in Fig. 2, whereas nucleation-growth of the lime-based PCC crystals by (g) and (h). Regardless of the raw material used as a calcium source, carbonation of *Solution I* and *II* obtained on the basis of ash and lime, respectively, leads via intermediate stages to formation of micrometric homogenous regularly structured particles of calcite with *rhombohedral* morphology (Fig. 2, c-e, h) at the conditions studied. SEM micrographs of samples *PCC1* and *PCC2* indicate that the shape of PCC particles is somewhat influenced by the extent of carbonation. By prolonging carbonation below pH ~8 (re-dissolution region), initially smooth surface of crystal faces of PCC particles (Fig. 2, c, e) appeared to become rougher (Fig. 2, d). This observation was confirmed by surface area measurements as can be seen from Table I. It should also be mentioned, that agglomeration of the formed PCC particles was not noticed at the precipitation conditions applied.

B. Estimation of CO_2 Sequestration Potential

In addition to ash valorization measure, this approach can be viewed as a method for CO_2 capture and storage. For this reason, the expected amounts of CO_2 bound were evaluated. CO_2 demand is calculated as the combination of CO_2 amounts needed for both precipitation of Ca^{2+}-ions and neutralization of OH^- ions. The pH value of the leachates under investigation is at the level of 12.65 and the concentration of Ca^{2+} ions is 1.23 g/L or 0.0308 mol/L. In this case, the stoichiometric amount of CO_2 needed for $CaCO_3$ precipitation is also sufficient for leachates neutralization.

TABLE I
MAIN CHARACTERISTICS OF THE CARBONATION PRODUCTS

Sample	Calcium source	Ca^{2+}, mg/L		end-point pH	$CaCO_3$, wt-%	BET surface area, m^2/g	Particles mean diameter, μm	Brightness ISO, %
		in AMS^a	in FS^b					
PCC1	oil shale ash	1230	310	6.8	95.2	2.28	4.05	93.2
PCC2	-"-	-"-	256	~8.0	95.4	1.61	4.46	-
PCC3	-"-	-"-	-"-	-"-	96.0	2.54	-	-
PCC4	lime	850	110	6.8	100.0	2.36	3.40	89.0

[a]AMS - alkaline mother solution
[b]FS – final solution

Results of the comparative experiments with lime solution
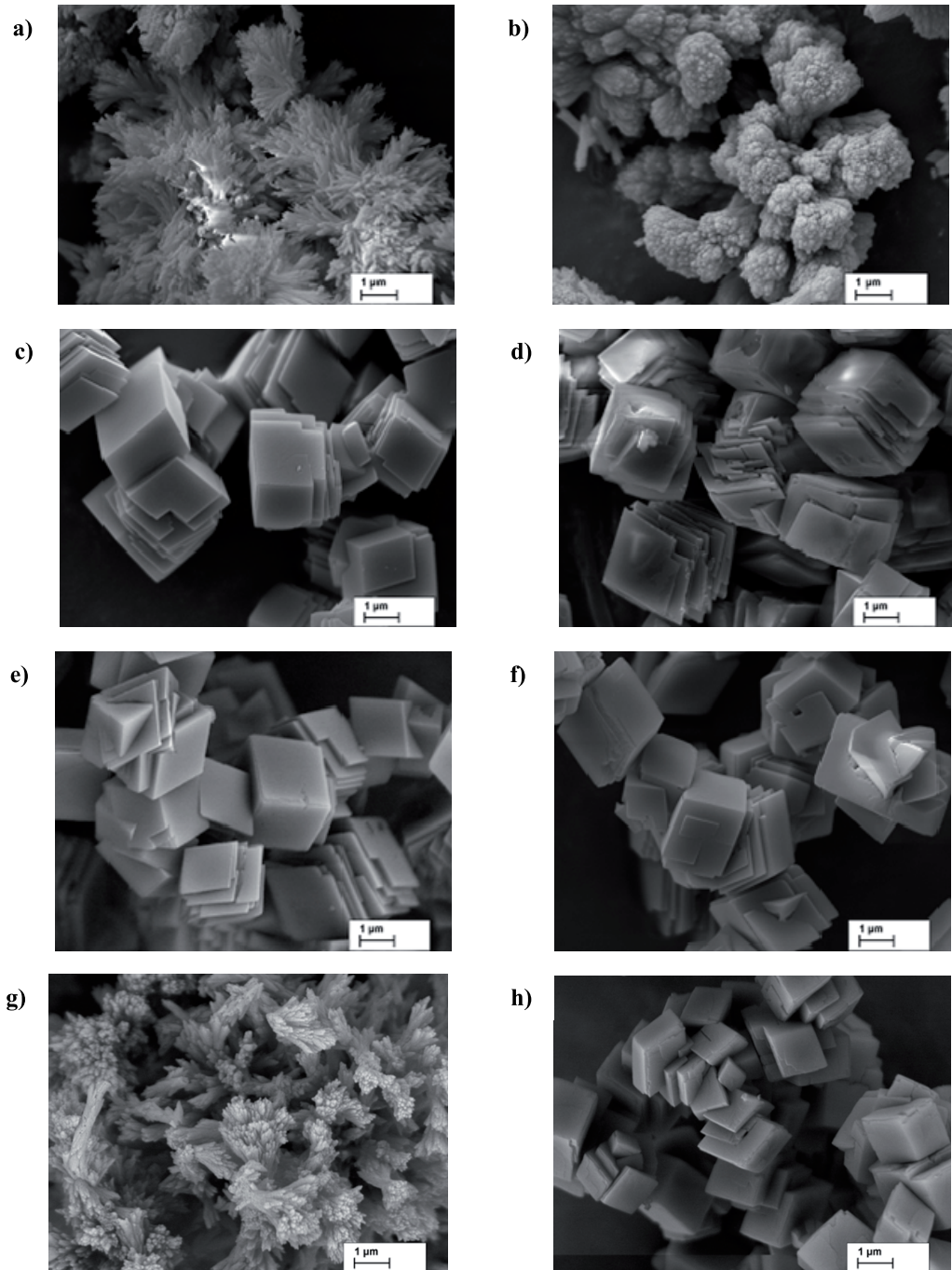
Fig. 2 SEM microphotographs of PCC particles obtained from oil shale ash leachates (Exp. 1: a - after 3.5 min; b - after 5 min; c - after 11.5 min; d - PCC1; Exp. 2: e - PCC2; Exp. 3: f - PCC3) and lime solution (Exp. 4: g - after 2 min; h - PCC4)

So, in order to neutralize this solution, 0.0308 moles or $0.0308 \times 22.4 = 0.69$ L of CO_2 must be added for every liter of solution, and CO_2 demand per 10 L of solution is, thus, about 7 liters. At pH 7.5-9.0 the binding capacity of liquid phase is almost utilized and the increase in CO_2 binding is mainly due to the increase in the amount of dissolved CO_2 and formed HCO_3^-. These results are in good agreement with the experimental data. Therefore, through carbonation of 1 million m^3 of leachates at least 1355 tons of CO_2 can be captured and up to 3080 tons of PCC produced. Considering the situation in Estonia, where the amount of ash leachates in the settling pounds is currently about 15-20 million m^3, oil shale energetics could benefit from this option by utilizing its own waste-products.

IV. CONCLUSION

According to the results presented in this paper, oil shale ash can be used as a calcium source for the production of PCC (containing ~96 % $CaCO_3$) at the carbonation conditions studied, and characterized by a distinctive regular rhombohedral crystalline structure with high brightness and the mean particle diameter of ~ 4 μm. The same order of particle size and the similar morphology of crystal faces for PCC were observed in carbonation experiments using chemically pure powdered lime as calcium source. Process conditions (pH, duration) have been found to have an influence on the PCC parameters. To avoid possible re-dissolution of PCC precipitation should be performed at pH>9. Furthermore, depending on the desired textural properties of the product, the residual alkalinity of the leachates could be decreased to acceptable pH levels in the precipitation step or in the next stage after PCC separation. Also, based on the end-application of PCC, washing of the precipitate is recommended. Gathered results provide data for estimating the potential of oil shale ash valorization option, which allows obtainment of a specific product, lowering the environmental impact of deposited waste material, alkaline leachates and CO_2 emissions associated with oil shale-based power production at the same time. The direct capture and storage of flue gas (10-15% CO_2) would further improve the feasibility of the technology, therefore, as of next, the impact of the flue gas composition and flow rate on the properties of PCC forming during carbonation of leachates will be investigated.

REFERENCES

[1] Carbon Dioxide Information Analysis Center, Environmental Sciences Division (US), "CO_2 emissions - Estonia," March 2011, http://data.worldbank.org/indicator/EN.ATM.CO2E.PC/countries/EE-7E-XR

[2] L. Savitskaja, "Man-made changes of groundwater quality," in *Geology and Mineral Resources of Estonia*, A. Raukas, A. Teedumäe, Eds. Tallinn: Estonian Academy Publishers, 1997, pp. 152–156.

[3] M. Uibu, M. Uus, and R. Kuusik, "CO_2 mineral sequestration in oil-shale wastes from Estonian power production," *J. Environ. Manage.,* vol. 90, no. 2, pp. 1253–1260, 2009.

[4] R. Kuusik, M. Uus, M. Uibu, et al, "Method for neutralization of alkaline waste water with carbon dioxide included in flue gas," Patent nr EE05349B1

[5] O. Velts, M. Hautaniemi, J. Kallas, and R. Kuusik, "Modeling calcium dissolution from oil shale ash: PART 1. Ca dissolution during ash washing in a batch reactor," *Fuel. Process. Tech.*, vol. 91, no. 5, pp. 486–490, 2010.

[6] O. Velts, M. Hautaniemi, J. Kallas, M. Kuosa, and R. Kuusik, "Modeling calcium dissolution from oil shale ash: PART 2. Continuous washing of the ash layer," *Fuel. Process. Tech.*, vol. 91, no. 5, pp. 491–495, 2010.

[7] O. Velts, M. Hautaniemi, M. Uibu, J. Kallas, and R. Kuusik, "Modelling of CO_2 mass transfer and hydrodynamics in a semi-batch reactor," *Materials, Methods & Technologies*, vol. 4, no. 2, pp. 68–79, 2010. Available at: http://www.science-journals.eu/mmt/index.html

[8] Specialty Minerals Inc. (SMI), "What is PCC?" March 2011, http://www.specialtyminerals.com/our-minerals/what-is-pcc/

Velts, *O.,* Uibu, M., Kallas, J., Kuusik, R.

Waste oil shale ash as a novel source of calcium for precipitated calcium carbonate: Process mechanism, modeling, and product characterization.

Reprinted with permission from:

Journal of Hazardous Materials 2011, 195, 139–146.

Journal of Hazardous Materials

Waste oil shale ash as a novel source of calcium for precipitated calcium carbonate: Carbonation mechanism, modeling, and product characterization

O. Velts [a,b,*], M. Uibu [a], J. Kallas [a], R. Kuusik [a]

[a] Laboratory of Inorganic Materials, Tallinn University of Technology, Ehitajate tee 5, Tallinn 19086, Estonia
[b] Laboratory of Separation Technology, Lappeenranta University of Technology, P.O. Box 20, Lappeenranta FI-53851, Finland

A B S T R A C T

In this paper, a method for converting lime-containing oil shale waste ash into precipitated calcium carbonate (PCC), a valuable commodity is elucidated. The mechanism of ash leachates carbonation was experimentally investigated in a stirred semi-batch barboter-type reactor by varying the CO_2 partial pressure, gas flow rate, and agitation intensity. A consistent set of model equations and physical–chemical parameters is proposed to describe the $CaCO_3$ precipitation process from oil shale ash leachates of complex composition. The model enables the simulation of reactive species (Ca^{2+}, $CaCO_3$, SO_4^{2-}, $CaSO_4$, OH^-, CO_2, HCO_3^-, H^+, CO_3^{2-}) concentration profiles in the liquid, gas, and solid phases as well as prediction of the PCC formation rate. The presence of $CaSO_4$ in the product may also be evaluated and used to assess the purity of the PCC product.

A detailed characterization of the PCC precipitates crystallized from oil shale ash leachates is also provided. High brightness PCC (containing up to ~96% $CaCO_3$) with mean particle sizes ranging from 4 to 10 μm and controllable morphology (such as rhombohedral calcite or coexisting calcite and spherical vaterite phases) was obtained under the conditions studied.

© 2011 Elsevier B.V. All rights reserved.

1. Introduction

In order to sustainably meet the ever-rising demand for energy, it is becoming necessary to exploit lower-quality fossil fuels such as oil shale. Well-explored oil shale reserves include the Green River deposits in the western United States, the Tertiary deposits in Queensland, Australia, the El-Lajjun deposit in Jordan, and deposits in Sweden, Estonia, France, Germany, Brazil, China, and Russia. In Estonia, large-scale combustion of calcareous kerogenous oil shale (8–12 MJ kg⁻¹) provides over 90% of the basic electric power supply. The technology used in oil shale processing for heat and power production exerts strong environmental effects. Due to the extensive use of oil shale, per capita CO_2 emissions in Estonia (15.2 metric tonnes in 2007) are about twice the European average and rank 13th worldwide [1]. In addition the process produces approximately 5–7 Mt of hazardous ash annually. A small portion of the waste ash is used for construction materials, road construction, and agricultural purposes [2], while most of the ash is transported as a slurry to be deposited on waste piles near the power plants. These ash dumps occupy an area of approximately 20 km². The

combustion waste ash is rich in free lime and anhydrite that under aqueous conditions produces highly alkaline leachates (pH 12–13). These pose a potential long-term environmental risk as neutralization of ash fields under natural conditions may take hundreds of years [3,4].

In the context of reducing the environmental burden and enhancing economic benefit, strategies for upgrading waste ashes into products of commercial value have arisen into focus, for instance [5–8]. Related to the aforementioned issues in Estonia, the authors recently introduced a novel approach for synthesizing precipitated calcium carbonate (PCC) crystals utilizing alkaline waste ash as an alternative low-cost source of water-soluble calcium [9]. PCC is currently produced from lime in a multi-stage process that requires large amounts of energy and uses expensive high-quality raw material. PCC production using oil shale ash could have considerable commercial importance in the paint, plastics, rubber, and paper industries. Other potential advantages of this process such as safer disposal of wastes, CO_2 emissions reduction, and wastewater neutralization were elaborated in our earlier studies [10,11]. Also, a new method for intensive heterogeneous gas–liquid processing was proposed [12]. One of the main challenges in this work was establishing a quantitative understanding of heterogeneous gas–liquid–solid system kinetics and dynamics. In this paper, the mechanism of calcium carbonate precipitation during gas–liquid reaction of oil shale ash leachates is discussed as well as a mathematical model describing the precipitation process reported. The

* Corresponding author at: Laboratory of Inorganic Materials, Tallinn University of Technology, Ehitajate tee 5, Tallinn 19086, Estonia. Tel.: +372 5283756; fax: +372 620 2801.
E-mail address: olga.velts@ttu.ee (O. Velts).

current study also examines the impact of the complex composition of ash leachates on the main characteristics (composition, morphology, surface area, and particle size) of the solid product over a wide range of operating conditions.

2. Experimental

2.1. Preparation of alkaline mother solutions (leachates)

The leaching of Ca^{2+} and other ions from oil shale ash was previously studied by the authors [3,13,14]. In this paper, oil shale (pulverized firing) combustion ash (containing ∼8.0% free CaO) was dispersed in distilled water (10:1 w/w liquid to solid ratio) under atmospheric pressure and room temperature for 15 min in a 15 L reactor equipped with a turbine-type impeller (Fig. 1(a)). The alkaline suspension was filtered from the solid ash residue. The solutions were analyzed for Ca^{2+} (titrimetric method ISO 6058:1984), SO_4^{2-}, Cl^-, K^+, PO_4^{3-} (using a Lovibond SpectroDirect spectrophotometer), CO_3^{2-}, HCO_3^-, and OH^- (titrimetric method ISO 9963–1:1994(E)). The oil shale ash leachates (pH ∼12.65) had the following average ion concentration: (in $g L^{-1}$) Ca^{2+}: ∼1.23, SO_4^{2-}: ∼0.75, K^+: ∼0.076, Cl^-: ∼0.038, PO_4^{3-}: ∼0.011 and (in $mol L^{-1}$) OH^-: ∼0.047.

2.2. Synthesis of PCC particles

Carbonation of oil shale ash leachates was performed in a semi-batch barboter-type reactor. A turbine-type impeller was used to provide effective mechanical mixing of the gas and liquid phases to increase the interfacial contact area (Fig. 1(b)). Recirculating alkaline mother solution (à 10 L) was treated with a model gas mixture containing pre-determined concentrations of CO_2 in air (c_{CO_2}). The CO_2 content was based on typical industrial flue gas compositions. The flow rate (Q_G) and composition of the inlet gas were controlled using calibrated rotameters and an infrared CO_2 analyzer (Duotec). The reactor was operated batch-wise with respect to the liquid phase and continuously with respect to the gas phase. A 2^3 full-factorial experimental plan was designed in which the process variables were maintained near the center of the operating range (Table 1). Operating variables potentially influencing the precipitation conditions were varied (base value and step in parenthesis):

(a) Air–CO_2 gas mixture flow rate, Q_G (b.v. = 1000 L h^{-1}, step 500)
(b) CO_2 concentration in the inlet gas, c_{CO2} (b.v. at 25 °C and 1 atm = 5 vol%, step 5)
(c) Stirring rate, N (b.v. = 400 rpm, step 300)

Samples of the suspension were collected through a valve on the reactor body. During the carbonation experiments, the concentrations of Ca^{2+}, SO_4^{2-}, Cl^-, K^+, PO_4^{3-}, CO_3^{2-}, HCO_3^-, OH^- in the (filtered) liquid phase samples, pH (Mettler Toledo GWB SG2) and conductivity (HI9032) in the reactor, and the CO_2 content of the outlet gas flow were continuously monitored. When the pH of the solution had stabilized and the CO_2 concentration in the outlet gas became equal to the inlet values, CO_2 addition was stopped. Immediately after carbonation, the suspension was filtered (Whatman "blue ribbon" filter paper) and the resulting solid was dehydrated at 105 °C. The solid material was analyzed as received with no subsequent washing. The synthesis of PCC particles (including the preparation of alkaline mother solution from waste ash) is schematically represented in Fig. 1.

2.3. Characterization of solid products

The solid product was analyzed to determine total carbon (TC; ELTRA CS-580 Carbon/Sulfur Determinator). Phase/composition identification was carried out using X-ray diffraction (XRD), FT-IR spectroscopy and thermal analysis techniques. XRD was performed using a Bruker D8 Advanced instrument. Fourier transform infrared (FT-IR) spectra (Interspec 2020) were acquired using samples prepared as KBr pellets and using a thermoanalyzer (Setaram Setsys 1750) coupled to a FT-IR spectrometer (Nicolet 380). Determination of total sulfur and its bonding forms was carried out according to EVS 664:1995. The crystal morphology of the precipitate particles was monitored during the course of the experiment using a scanning electron microscope (Jeol JSM-8404A). The particle size distribution (PSD) of the final product was determined using a laser diffraction analyzer (Beckman Coulter LS 13320). BET-surface area and total and micropore volume were measured using a nitrogen dynamic desorption analysis method (Sorptometer KELVIN 1042). The brightness of the PCC samples was measured according to ISO 2470:1999.

3. Results and discussion

3.1. Reaction mechanism of oil shale ash leachates carbonation process

Formation of PCC from lime-containing oil shale ash is an innovative yet complex multi-stage process. Recently, the mechanisms and modeling algorithms for intermediate stages of the process including calcium leaching [3,13], dissolution of gaseous CO_2 into the alkaline liquid phase [15], and calcium carbonate precipitation via CO_2 absorption into pure lime based model solutions [16] have been reported by the authors.

In the present study, a mechanism for the reaction of CO_2 with Ca^{2+} and SO_4^{2-} rich alkaline oil shale ash leachates is proposed. The carbonation process is described by Eqs. (1)–(9) beginning with the physical dissolution of gaseous CO_2 into solution:

$$CO_2(q) \leftrightarrow CO_2(l) \tag{1}$$

The solubility equilibrium follows Henry's law (at pressures below approximately 5 atm):

$$[CO_2(l)]_{eq} = k_H \times P_{CO_2} \tag{2}$$

where k_H is the Henry's law constant and P_{CO_2} is the CO_2 partial pressure.

Formation of bicarbonate:

$$CO_2(l) + OH^- \underset{k_{12}}{\overset{k_{11}}{\rightleftarrows}} HCO_3^- \tag{3}$$

Dissociation of bicarbonate:

$$HCO_3^- + OH^- \underset{k_{22}}{\overset{k_{21}}{\rightleftarrows}} CO_3^{2-} + H_2O \tag{4}$$

Ionization of water:

$$OH^- + H^+ \underset{k_{32}}{\overset{k_{31}}{\rightleftarrows}} H_2O \tag{5}$$

CO_2 hydration [17]:

$$CO_2(l) + H_2O \underset{k_{42}}{\overset{k_{41}}{\rightleftarrows}} HCO_3^- + H^+ \tag{6}$$

Nucleation and growth of $CaCO_3$ crystals:

$$Ca^{2+} + CO_3^{2-} \underset{k_{52}}{\overset{k_{51}}{\rightleftarrows}} CaCO_3 \tag{7}$$
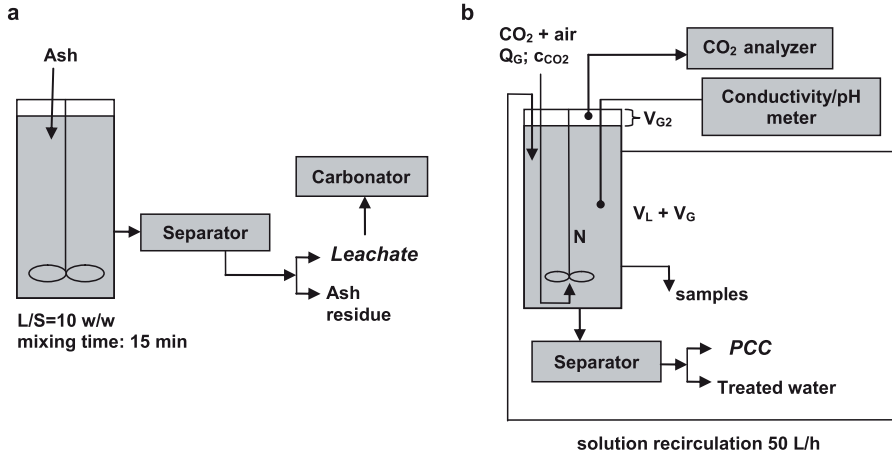
Fig. 1. Principal experimental scheme: (a) leaching step; (b) carbonation step.

Formation of anhydrate phase:

$$Ca^{2+} + SO_4^{2-} \leftrightarrow CaSO_4 \qquad (8)$$

Back-dissolution of CaCO$_3$ crystals at lower pH:

$$CaCO_3 + H^+ \underset{k_{62}}{\overset{k_{61}}{\rightleftharpoons}} Ca^{2+} + HCO_3^- \qquad (9)$$

The reactions of other ions present such as K^+, Cl^-, and PO_4^{3-} were neglected as their concentrations in the solution remained unchanged during carbonation. It is therefore assumed that they do not take part in the precipitation process in significant amounts.

3.2. Modeling of calcium carbonate precipitation from oil shale ash leachates

The model proposed in this paper accounts for absorption and reaction kinetics taking place in the liquid phase (Eqs. (1)–(9)), including formation of the solid product, as well as the hydrodynamic conditions within the system. The concentration profiles of all species participating in the precipitation process may be modeled as a function of time using the following differential equations (assuming that the system is operated isothermally at 25 °C):

• For CO_2 dissolved in the liquid phase:

$$\frac{d[CO_2(l)]}{dt} = \frac{k_L a_{CO_2}^0 \times E \times \sum_{i=1}^n \left(\left(\left(\frac{k_H \times M_{CO_2} \times P \times [CO_2{}^i(g)]}{\rho_{CO_2}} - [CO_2(l)] \right) \times \frac{V_L + V_G}{n} \right) \right)}{V_L}$$
$$-k_{11}[CO_2(l)][OH^-] + k_{12}[HCO_3^-] - k_{41}[CO_2(l)] + k_{42}[HCO_3^-][H^+] \qquad (10)$$

• For Ca^{2+}, OH^-, SO_4^{2-}, HCO_3^-, CO_3^{2-}, and H^+ ions:

$$\frac{d[Ca^{2+}]}{dt} = k_{52} - k_{51}[Ca^{2+}][CO_3^{2-}] + k_L a_{CaSO_4} \times ([SO_4^{2-}]^*$$
$$- [SO_4^{2-}]) + k_{61}[H^+] - k_{62}[Ca^{2+}][HCO_3^-] \qquad (11)$$

$$\frac{d[OH^-]}{dt} = -k_{11}[CO_2(l)][OH^-] + k_{12}[HCO_3^-] - k_{21}[HCO_3^-][OH^-]$$
$$+ k_{22}[CO_3^{2-}] + k_{32} - k_{31}[OH^-][H^+] \qquad (12)$$

$$\frac{d[SO_4^{2-}]}{dt} = k_L a_{CaSO_4} \times ([SO_4^{2-}]^* - [SO_4^{2-}]) \qquad (13)$$

$$\frac{d[HCO_3^-]}{dt} = k_{11}[CO_2(l)][OH^-] - k_{12}[HCO_3^-] - k_{21}[HCO_3^-][OH^-]$$
$$+ k_{22}[CO_3^{2-}] + k_{41}[CO_2(l)] - k_{42}[HCO_3^-][H^+]$$
$$+ k_{61}[H^+] - k_{62}[Ca^{2+}][HCO_3^-] \qquad (14)$$

$$\frac{d[CO_3^{2-}]}{dt} = k_{21}[HCO_3^-][OH^-] - k_{22}[CO_3^{2-}] + k_{52}$$
$$- k_{51}[Ca^{2+}][CO_3^{2-}] \qquad (15)$$

$$\frac{d[H^+]}{dt} = k_{32} - k_{31}[OH^-][H^+] + k_{41}[CO_2(l)]$$
$$- k_{42}[HCO_3^-][H^+] - k_{61}[H^+] + k_{62}[Ca^{2+}][HCO_3^-] \qquad (16)$$

Table 1
Parameters of the oil shale ash leachates carbonation experiments.

Nr	Q_G (L h^{-1})	Air flow rate (L h^{-1})	CO$_2$ flow rate (L h^{-1})	c_{CO_2} (vol%)	N^a (rpm)
1	1000	950	50	5	400
2	1000	950	50	5	1000
3	1000	850	150	15	400
4	1000	850	150	15	1000
5	2000	1900	100	5	400
6	2000	1900	100	5	1000
7	1500	1350	150	10	700
8	2000	1700	300	15	400
9	2000	1700	300	15	1000

[a] The stirring rate, as measured experimentally, corresponds to a power consumption 1.1, 2.0 and 3.7 W L^{-1} for N = 400, 700 and 1000 rpm, respectively.

- For CO_2 exiting the ith section of the reaction mixture:

$$\frac{d[CO_2{}^i(g)]}{dt} = \frac{Q_G([CO_2(g)]_{IN} - [CO_2{}^i(g)]) - k_La_{CO_2}^0 \times E \times ((k_H \times M_{CO_2} \times P \times [CO_2{}^i(g)]/\rho_{CO_2}) - [CO_2(l)]) \times (V_L + V_G)/n}{V_G/n} \quad (17)$$

- For CO_2 exiting the reactor e.g. headspace V_{G2} above the reaction mixture (see Fig. 1(b)):

$$\frac{d[CO_2(g)]_{OUT}}{dt} = \frac{Q_G([CO_2(g)] - [CO_2(g)]_{OUT})}{V_{G_2}} \quad (18)$$

- For $CaCO_3$ forming during the carbonation process:

$$\frac{d[CaCO_3]}{dt} = k_{51}[Ca^{2+}][CO_3{}^{2-}] - k_{52} - k_{61}[H^+]$$
$$+ k_{62}[Ca^{2+}][HCO_3{}^-] \quad (19)$$

- For $CaSO_4$ forming during the carbonation process:

$$\frac{d[CaSO_4]}{dt} = k_La_{CaSO_4} \times ([SO_4{}^{2-}] - [SO_4{}^{2-}]^*) \quad (20)$$

In Eqs. (10)–(20) concentrations are expressed in molar units, Q_G is the gas volumetric flow rate in L s^{-1}, $k_La_{CO_2}^0$ is the volumetric mass transfer coefficient of CO_2 in the absence of chemical reaction in s^{-1}, E is the CO_2 mass transfer enhancement factor, V_L is the solution volume in L, V_G is the volume of gas in the gas–liquid mixture in L, V_{G2} is the gas volume in the reactor headspace in L, k_H is the Henry's Law constant in mol·(L atm)$^{-1}$, P is the atmospheric pressure in atm, M_{CO_2} is the CO_2 molar mass in g mol^{-1}, and ρ_{CO_2} is the CO_2 gas density in g L^{-1}.

A program feature accounting for changes in V_L, V_G, and V_{G2} due to sample collection was implemented in the modeling algorithm. The gas phase in the reaction mixture was divided into a number of theoretical sections n with a volume V_G/n (gas phase in approximately plug flow, liquid phase in perfectly mixed flow due to solution recirculation). Each of these sections (high correlation coefficient observed at $n = 10$) was treated as a non-equilibrium stage governed by Eq. (17).

Considering the near infinite-dilution ionic strength of the leachates ($I = 0.1$), the value of the second-order rate constant k_{11} (in L (mol s)$^{-1}$) of reaction (3) was calculated as a function of temperature T (K) using a relationship proposed by Pohorecki and Moniuk [18]:

$$\log k_{11} = 11.916 - \frac{2382}{T} \quad (21)$$

The backward reaction rate k_{12} in Eq. (3) is defined by the value of the equilibrium constant for this reaction ($k_{12} = k_{11}K_w/K_1$). The value of the solubility product K_w (mol^2 m^{-6}) is given by Tsonopoulos [19]:

$$\log \left(\frac{K_w}{\rho_w^2}\right) = -\frac{5839.5}{T} - 22.4773 \log(T) + 61.2062 \quad (22)$$

The value of the equilibrium constant K_1 (mol m^{-3}) is given as a function of temperature by Edwards et al. [20]:

$$K_1 = \exp \left(-\frac{12092.1}{T} - 36.786 \ln(T) + 235.482\right) \rho_w \quad (23)$$

where ρ_w is the density of water (kg m^{-3}).

The reaction rate constant k_{21} of reaction (4) was reported as 6×10^6 m^3 (mol s)$^{-1}$ by Eigen [21]. The equilibrium constant K_2 (m^3 mol^{-1}) at infinite dilution that determines the value of the backward reaction rate, $k_{22} = k_{21}/K_2$, is given by Hikita et al. [22]:

$$\log(K_2) = \frac{1568.9}{T} - 2.5866 - 6.737 \times 10^{-3}T \quad (24)$$

The neutralization rate constant, k_{31}, was determined by Eigen [21] to be 1.4×10^8 m^3 (mol s)$^{-1}$. The rate constant k_{41} for the reaction between CO_2 and water is 0.024 s^{-1} [23]. The values of the backward reaction rate constants k_{32} and k_{42} may be calculated from the equilibrium constants and are equal to k_{31}/K_w and k_{41}/K_1.

The value of the Henry's law constant k_H (mol (L bar)$^{-1}$) may be expressed as a function of temperature using the equation of Pohorecki and Moniuk [24]:

$$\log k_H = 9.1229 - 5.9044 \times 10^{-2}T + 7.8857 \times 10^{-5}T^2 \quad (25)$$

The average values of the reaction rate constants k_{51} and k_{52} in Eq. (7) were estimated by Velts et al. [16] to be 1.88×10^6 L (mol s)$^{-1}$ and 0.009 mol (L s)$^{-1}$. Based on our study of CO_2 uptake kinetics in hydroxide solutions under various process conditions [15], the volumetric CO_2 mass transfer coefficients for the system in the absence of chemical reaction $k_La_{CO_2}^0$ (s^{-1}) were calculated using an empirical equation ($R^2 = 0.91$) applicable to barboter-type reactors:

$$k_La_{CO_2}^0 = 2.953 \times 10^{-3} \times \left(\frac{Q_G}{V_L}\right)^{0.386} \left(\frac{P_N}{V_L}\right)^{0.330} c_{CO_2}^{0.114} \quad (26)$$

in which P_N is the power consumed by the stirrer in watts.

The effect of chemical reaction on the process performance was accounted for by introducing the CO_2 mass transfer enhancement factor, E. This value was determined using an empirical equation ($R^2 = 0.97$) proposed by Velts et al. [16], where E is a function of the initial Ca^{2+} concentration (mmol L^{-1}):

$$E = 0.0027 \times [Ca^{2+}]_0^2 + 0.0224 \times [Ca^{2+}]_0 + 1.0 \quad (27)$$

Based on the experimental data obtained in this study, the $SO_4{}^{2-}$ dynamic equilibrium concentration $[SO_4{}^{2-}]^*$ (mmol L^{-1}) was calculated using an empirical equation ($R^2 = 0.98$) dependent on the operating parameters and the initial concentrations of Ca^{2+} and $SO_4{}^{2-}$ ions (mmol L^{-1}) in the leachate:

$$[SO_4{}^{2-}]^* = 0.761 \times [SO_4{}^{2-}]_0^{0.976}[Ca^{2+}]_0^{-0.073}$$
$$\times \left(\frac{Q_G}{V_L}\right)^{0.066} c_{CO_2}^{0.038} \left(\frac{P_N}{V_L}\right)^{-0.012} \quad (28)$$

The volumetric mass transfer coefficient of anhydrite, $k_La_{CaSO_4}$ and the reaction rate constants k_{61} and k_{62} in Eq. (9) were evaluated from the differential equations (10)–(20). The set of model equations was solved by means of linear multi-step methods implemented in ODESSA, which is based on the LSODE software [25]. The calculations were performed using the MODEST 6.1 software package [26] designed for various model-building tasks such as simulation, parameter estimation, sensitivity analysis, and optimization. The software consists of a FORTRAN 95/90 library of objective functions, solvers, and optimizers linked to model problem-dependent routines and the objective function.

Based on the estimated values of $k_La_{CaSO_4}$ (s^{-1}), an empirical equation ($R^2 = 0.8$) applicable to barboter-type reactors was proposed as a function of the main process parameters:

$$k_La_{CaSO_4} = 1.95 \times 10^{-7} \times \left(\frac{Q_G}{V_L}\right)^{1.702} c_{CO_2}^{1.134} \left(\frac{P_N}{V_L}\right)^{0.126} \quad (29)$$

The average values of the reaction rate constants k_{61} and k_{62} were estimated to be 0.1 (± 0.021)$\times 10^7$ s^{-1} and 0.4 (± 0.013)$\times 10^3$ L (mol s)$^{-1}$. The correlation coefficients for all data sets were greater than 0.93. The reaction rate constants used in Eqs. (3)–(9) and other parameters used in this paper ($T = 298.1$ K) are summarized in Table 2.
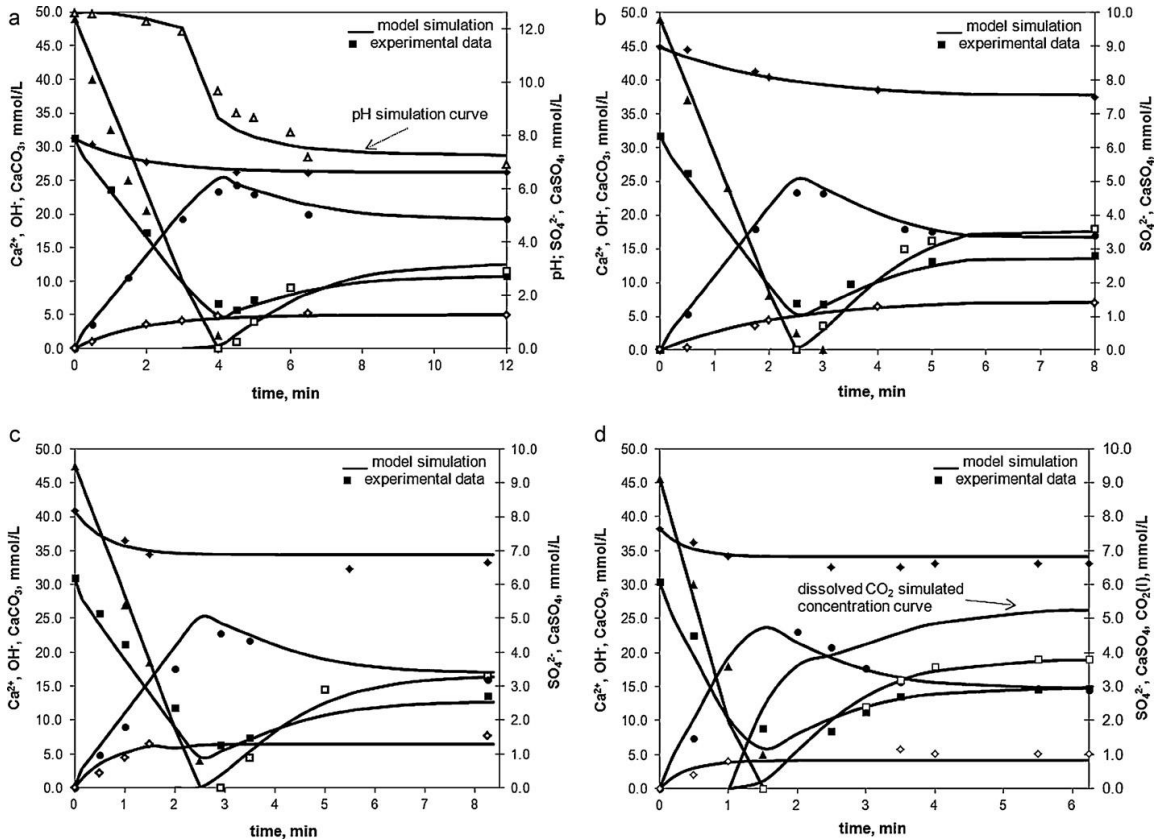
Fig. 2. Modeling of ash leachate carbonation process accompanied by the formation of PCC at (a): $Q_G = 2000 \, \mathrm{L \, h^{-1}}$, $c_{CO_2} = 5 \, \mathrm{vol\%}$; $N = 1000 \, \mathrm{rpm}$; (b): $Q_G = 1000 \, \mathrm{L \, h^{-1}}$, $c_{CO_2} = 15 \, \mathrm{vol\%}$; $N = 1000 \, \mathrm{rpm}$; (c): $Q_G = 1500 \, \mathrm{L \, h^{-1}}$, $c_{CO_2} = 10 \, \mathrm{vol\%}$; $N = 700 \, \mathrm{rpm}$; (d): $Q_G = 2000 \, \mathrm{L \, h^{-1}}$, $c_{CO_2} = 15 \, \mathrm{vol\%}$; $N = 400 \, \mathrm{rpm}$: experimental vs. simulated Ca^{2+} (■), SO_4^{2-} (♦), OH^- (▲), $CaCO_3$ (●), $CaSO_4$ (◊), HCO_3^- (□), $CO_2(l)$ concentration (mmol L^{-1}) and pH (△) profiles.

The model was verified by comparing the predictions of concentration changes for the reactive species (Ca^{2+}, OH^-, SO_4^{2-}, $CaCO_3$, $CaSO_4$, HCO_3^-, CO_2, H^+, and CO_3^{2-}) with the experimental data. Plots of experimental and simulated concentration profiles corresponding to experiments 4, 6, 7, and 8 (Table 1) are provided in Fig. 2. The relatively small deviations between the measured and estimated data confirm the ability of the proposed model to quite accurately describe the process course including re-dissolution of PCC due to increased solubility of $CaCO_3$ at lower pH. It is also worth emphasizing that the model enables the prediction of pH (Fig. 2(a)), which suggests potential applications in wastewater neutralization process design.

3.3. Characterization of PCC crystallized from oil shale ash leachates

Among other parameters, the shape, size, and texture of crystals play a crucial role in determining the properties and application suitability of a material. For this reason, a detailed characterization of the final precipitates formed during ash leachate carbonation under different conditions was performed. The characteristics of samples PCC1–PCC9 were determined using numerous characterization techniques (see Section 2.3) and are presented in Table 3. The unwashed precipitates were a bright white color with a fine and powdery texture. The brightness value (~93%) exceeded that of PCC (~89%) obtained from pure lime under the same conditions [9]. Total carbon (TC) analysis indicated that the solid samples predominantly contained $CaCO_3$ (~94.3–96.2%), with minor amounts of $CaSO_4$ (~4–6%), evidently adsorbed on the surface of the $CaCO_3$ crystals (Table 3). Washing of the precipitate cake would be expected to improve the purity of the solid product by a few percentage points. The phase composition was also confirmed using FT-IR spectroscopy.

The morphology of the precipitated particles was examined using scanning electron microscopy (SEM). Fig. 3 contains SEM images of the final precipitates PCC1–PCC9 crystallized under various carbonation conditions (Table 3). Under the conditions in experiments 1–5 (Table 1), well-defined rhombohedral

Table 2
Parameters used in the modeling of oil shale ash leachates carbonation at 298 K.

Parameter	Value	Parameter	Value
k_{11} (L(mol s)$^{-1}$)	8.4×10^3	k_{42} (L(mol s)$^{-1}$)	5.7×10^4
k_{12} (s^{-1})	2.0×10^{-4}	k_{51}^{av} (L(mol s)$^{-1}$)	1.9×10^6
k_{21} (L(mol s)$^{-1}$)	6.0×10^9	k_{52}^{av} (mol(Ls)$^{-1}$)	9.0×10^{-3}
k_{22} (s^{-1})	1.2×10^6	k_{61}^{av} (s^{-1})	0.1×10^7
k_{31} (L(mol s)$^{-1}$)	1.4×10^{11}	k_{62}^{av} (L(mol s)$^{-1}$)	0.4×10^3
k_{32} (mol·(Ls)$^{-1}$)	1.3×10^{-3}	k_H (mol(L atm)$^{-1}$)	3.5×10^{-2}
k_{41} (s^{-1})	2.4×10^{-2}	ρ_{CO_2} (25 °C) (kg m^{-3})	1.8×10^0

Fig. 3. SEM micrographs of PCC samples (a) PCC1, (b) PCC2, (c) PCC3, (d) PCC4, (e) PCC5, (f) PCC6, (g) PCC7, (h) PCC8, (i) PCC9 formed via oil shale ash leachate carbonation under experimental conditions presented in Table 1.

Table 3
Synthesis conditions and main characteristics of oil shale ash leachates carbonation products.

Sample	Operating variables			Solid product characteristics								
	Q_G (L h^{-1})	c_{CO_2} (vol%)	N (rpm)	CaCO$_3{}^{av}$ (%)			CaSO$_4{}^{av}$ (%)	SSA (m^2 g^{-1})	V_{tot} (mm^3 g^{-1})	V_{micro} (mm^3 g^{-1})	D_{mean} (μm)	Brightness ISO (%)
				TC	XRD							
					calcite	vaterite						
PCC1	1000	5	400	94.5			5.7	2.28	3.38	–	4.1	93.2
PCC2	1000	5	1000	94.5			5.8	2.56	3.51	0.11	5.1	
PCC3	1000	15	400	94.6	100.0		5.5	3.15	4.03	–	4.8	
PCC4	1000	15	1000	94.4			5.9	1.33	1.93	–	7.8	
PCC5	2000	5	400	94.4			5.9	1.35	1.74	–	6.5	
PCC6	2000	5	1000	95.1	97.3	2.6	5.0	2.38	3.77	–	8.1	92.7
PCC7	1500	10	700	95.6	77.2	21.9	4.4	4.70	11.05	0.01	7.7	92.3
PCC8	2000	15	400	96.2	63.2	36.3	4.0	7.29	17.44	0.43	8.0	
PCC9	2000	15	1000	95.4	95.7	3.6	4.5	1.95	3.44	–	9.9	

crystals with a mean size ranging from ∼4 to 8 μm were produced (Fig. 3(a–e)). X-ray powder diffraction analysis (XRD) of these carbonated samples (PCC1–PCC5) identified calcite as the only crystal form of calcium carbonate detected. Carbonation under the intensified hydrodynamic conditions (experiments 6–8, Table 1) resulted in formation of distinctly spherical particles in the precipitates along with the rhombohedral crystals of calcium carbonate (Fig. 3(f–h)). Initial analysis of these images indicated that the rhombohedral crystal was calcite, while the calcium carbonate microspheres were forms of vaterite. The coexistence of calcite and vaterite in the product (PCC6–PCC9) was confirmed using XRD measurements (Table 3), which enabled us to distinguish different morphologies of PCC. The XRD results indicated that sample PCC6 contained only small amount of the vaterite phase (2.6%), while the relative mass percentages of vaterite in samples from experiments 7 and 8 were ∼22 and 36% (Table 3). The presence of a significant amount of spherical vaterite could explain the greater surface area and pore volume in samples PCC7 and PCC8. The shape and surface observations 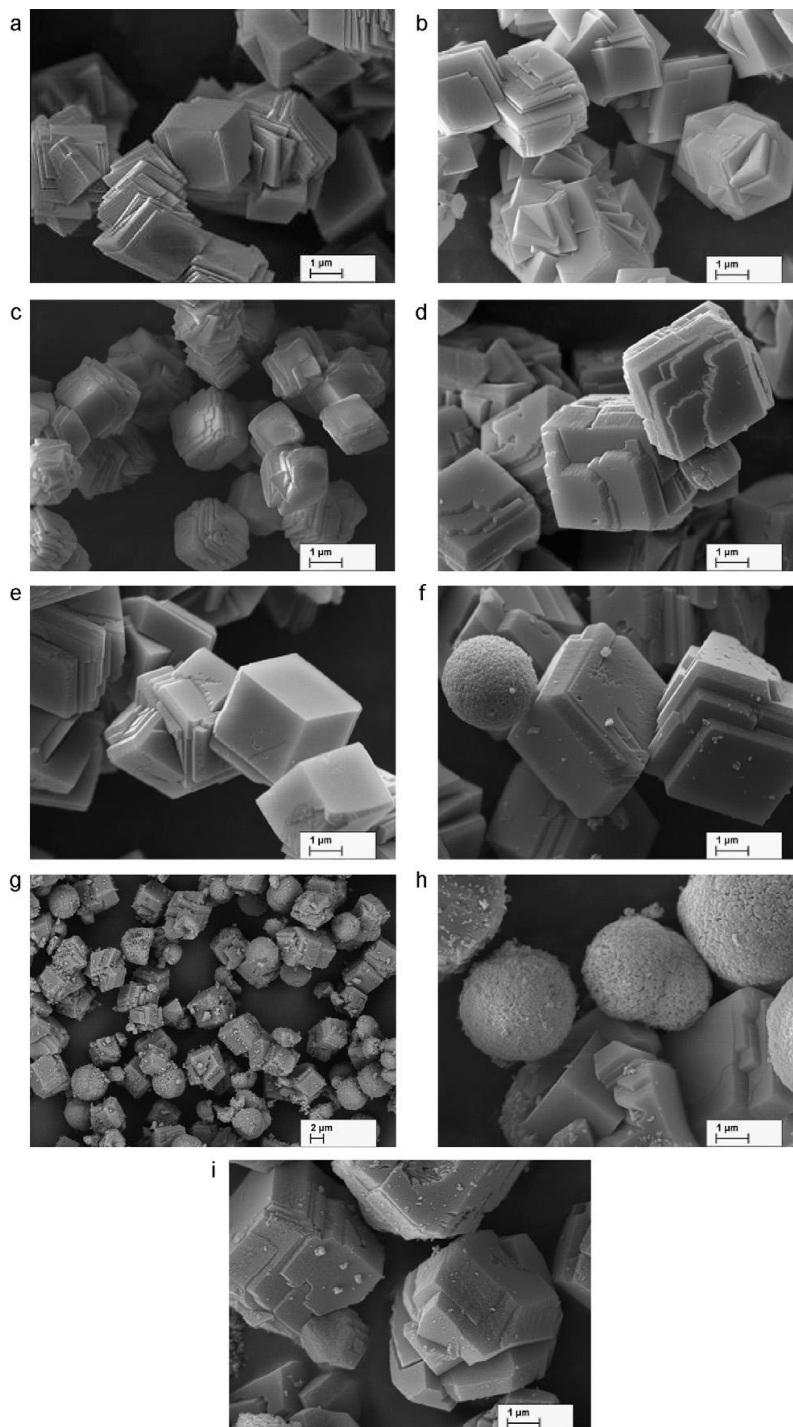confirmed the results of the particle size distribution analysis. Interestingly, precipitation under the most rapid conditions (experiment 9, Table 1) decreased the amount of vaterite in the product, leading to formation of pseudo-cubic or randomly aggregated rhombohedral (Fig. 3(i)) and spherical structures with a mean diameter of ∼10 μm and a calcite content of ∼96% (PCC9, Table 3).

The results suggest that the carbonation conditions may direct the morphology of the CaCO$_3$ crystals and indicate that the coexisting vaterite polymorph can be stabilized under specific experimental conditions. Whether the vaterite phase is formed prior to or during the PCC re-dissolution stage is a matter of great interest and requires further investigation. A closer examination of the morphological development of the CaCO$_3$ crystals at different crystallization times will be undertaken.

4. Conclusion

In this study, modeling, simulation, and experimental results describing the carbonation of leachates from oil shale ash are presented. This work is part of our effort to develop a promising calcium carbonate production process employing an abundant waste material.

A mathematical model of the multi-step PCC formation process incorporating mechanisms of CO$_2$ dissolution and CaCO$_3$ and CaSO$_4$ precipitation was introduced. The model provided results that were in good agreement with experimental data, confirming its accuracy. The modeling algorithm presented in this paper may be applied to design, energetic, and economic assessment of PCC pilot plants using oil shale ash or other lime-containing wastes or calcium-rich wastewaters as feedstock.

Carbonation of oil shale ash leachates resulted in precipitation of high brightness PCC containing up to ∼96% CaCO$_3$ with mean particle sizes ranging from 4 to 10 μm. Depending on the carbonation conditions, formation of rhombohedral calcite crystals or co-precipitation of calcite and spherical vaterite structures occurred, suggesting control over CaCO$_3$ crystallization and the ability to construct crystals with a desired morphology. The PCC morphogenesis will be further investigated to determine the relationship between formation conditions and morphology.

A description of the carbonation reaction mechanism and the properties of the precipitated product are important for understanding and estimating the potential reusability of alkaline wastes associated with oil shale-based power production. According to simplified calculations, 1 tonne of ash (containing ∼20% of free lime on the average) would allow producing near to 360 kg of CaCO$_3$, while via carbonation of 1 m^3 of leachates at least 1.3 kg of CO$_2$ can be captured and up to 3 kg of PCC formed. Due to availability of enormously large amounts (10–15 million m^3) of highly alkaline ash leachates in the proximity of CO$_2$ emission source, the direct capture and storage of CO$_2$-containing flue gas by leachates could further improve the technology. Hence, oil shale energetics could benefit from this innovative process by utilizing and valorizing its own waste-products into a valuable commodity, lowering the environmental impact of deposited waste material, alkaline leachates and CO$_2$ emissions at the same time.

References

[1] Carbon Dioxide Information Analysis Center, Environmental Sciences Division (US), CO$_2$ emissions—Estonia. Available at: http://data.worldbank.org/indicator/EN.ATM.CO2E.PC/countries/EE-7E-XR (accessed May 2011).
[2] A. Ots, Oil Shale Fuel Combustion, Tallinn University of Technology Press, Tallinn, 2006.
[3] O. Velts, M. Hautaniemi, J. Kallas, M. Kuosa, R. Kuusik, Modeling calcium dissolution from oil shale ash: part 2. Continuous washing of the ash layer, Fuel Process. Technol. 91 (5) (2010) 491–495.
[4] R. Mõtlep, T. Sild, E. Puura, K. Kirsimäe, Composition, diagenetic transformation and alkalinity potential of oil shale ash sediments, J. Hazard. Mater. 184 (1–3) (2010) 567–573.

[5] A.S.M. Ribeiro, R.C.C. Monteiro, E.J.R. Davim, M.H.V. Fernandes, Ash from a pulp mill boiler—characterisation and vitrification, J. Hazard. Mater. 179 (1–3) (2010) 303–308.

[6] C. Ferreira, A. Ribeiro, L. Ottosen, Possible applications for municipal solid waste fly ash, J. Hazard. Mater. 96 (2–3) (2003) 201–216.

[7] R. Cioffi, M. Marroccoli, L. Sansone, L. Santoro, Potential application of coal–fuel oil ash for the manufacture of building materials, J. Hazard. Mater. 124 (1–3) (2005) 101–106.

[8] Yu-Fen Yang, Guo-Sheng Gai, Zhen-Fang Cai, Qing-Ru Chen, Surface modification of purified fly ash and application in polymer, J. Hazard. Mater. 133 (1–3) (2006) 276–282.

[9] O. Velts, M. Uibu, J. Kallas, R. Kuusik, Prospects in waste oil shale ash sustainable valorization, World Acad. Sci. Eng. Technol. 76 (2011) 451–455.

[10] M. Uibu, M. Uus, R. Kuusik, CO_2 mineral sequestration in oil-shale wastes from Estonian power production, J. Environ. Manage. 90 (2) (2009) 1253–1260.

[11] M. Uibu, O. Velts, R. Kuusik, Developments in CO_2 mineral carbonation of oil shale ash, J. Hazard. Mater. 174 (1–3) (2010) 209–214.

[12] R. Kuusik, M. Uus, M. Uibu, et al., Method for neutralization of alkaline waste water with carbon dioxide included in flue gas, Patent nr EE05349B1.

[13] O. Velts, M. Hautaniemi, J. Kallas, R. Kuusik, Modeling calcium dissolution from oil shale ash: part 1. Ca dissolution during ash washing in a batch reactor, Fuel Process. Technol. 91 (5) (2010) 486–490.

[14] O. Velts, M. Uibu, I. Rudjak, J. Kallas, R. Kuusik, Utilization of oil shale ash to prepare PCC: leachibility dynamics and equilibrium in the ash–water system, Energy Procedia 1 (1) (2009) 4843–4850.

[15] O. Velts, M. Hautaniemi, M. Uibu, J. Kallas, R. Kuusik, Modelling of CO_2 mass transfer and hydrodynamics in a semi-batch reactor, J. Int. Sci. Publ. Mater. Methods Technol. 4 (2) (2010) 68–79. Available at: http://www.science-journals.eu/mmt/index.html (accessed May 2011).

[16] O. Velts, M. Uibu, J. Kallas, R. Kuusik, CO_2 mineral trapping: modeling of calcium carbonate precipitation in a semi-batch reactor, Energy Procedia 4 (2011) 771–778.

[17] A.H.G. Cents, D.W.F. Brilman, G.F. Versteeg, CO_2 absorption in carbonate/bicarbonate solutions: the Danckwerts-criterion revisited, Chem. Eng. Sci. 60 (2005) 5830–5835.

[18] R. Pohorecki, W. Moniuk, Calculation of the rate constant for the reaction of carbon dioxide with hydroxyl ions in mixed electrolyte solutions, Rep. Inst. Chem. Eng. Warsaw. Tech. Univ. 5 (1976) 179–192.

[19] C. Tsonopoulos, Ionization constants of water pollutants, J. Chem. Eng. Data 21 (1976) 190–193.

[20] T.J. Edwards, G. Maurer, J. Newman, J.M. Prausnitz, Vapor–liquid equilibria in multicomponent aqueous solution of volatile weak electrolytes, AIChE J. 24 (1978) 966–976.

[21] M. Eigen, Protonenübertragung, säure-base-katalyse und enzymatische hydrolyse. teil I: Elementarvorgänge, Angew. Chem. 75 (1963) 489–508.

[22] H. Hikita, S. Asai, T. Takatsuka, Absorption of carbon dioxide into aqueous sodium hydroxide and sodium bicarbonate solutions, Chem. Eng. J. 11 (1976) 131–141.

[23] P.V. Danckwerts, M.M. Sharma, Absorption of carbon dioxide into solutions of alkalis and amines, Chem. Eng. (London) 10 (1966) 244–280.

[24] R. Pohorecki, W. Moniuk, Kinetics of reaction between carbon dioxide and hydroxyl ions in aqueous electrolyte solutions, Chem. Eng. Sci. 43 (1988) 1677–1684.

[25] A.C. Hindmarsh, ODEPACK, a systematized collection of ODE solvers, Sci. Comput. IMACS Trans. Sci. Comput. 1 (1983) 55–64.

[26] H. Haario, Modest user manual, Profmath Oy, Finland, 1994.

PATENT

Kuusik, R., Uibu, M., Uus, M., V*elts, O*., Trikkel, A., Veinjärv, R.

Method for eliminating CO_2 from flue gases by calcium compounds containing industrial wastes.

Patent EE05446B1 (2011), Joint Stock Company Narva Power Plants, Tallinn University of Technology

(12) **PATENDIKIRJELDUS**

(73) Patendiomanikud:

Tallinna Tehnikaülikool
Ehitajate tee 5, 19086 Tallinn, EE

Eesti Energia Narva Elektrijaamad AS
Auvere küla, Vaivara vald,
40101 Ida-Viru maakond, EE

(72) Leiutise autorid:

Rein Kuusik
Lee 28, Muraste küla, Harku vald,
76905 Harju maakond, EE

Mai Uibu
Keskuse 22-53, 12911 Tallinn, EE

Mati Uus
Jahu 10-5, 10415 Tallinn, EE

Olga Velts
Arbu 2-81, 13617 Tallinn, EE

Andres Trikkel
Gonsiori 24-9, 10128 Tallinn, EE

Rain Veinjärv
Järveotsa tee 37-56, 13520 Tallinn, EE

(74) Patendiomaniku ühine esindaja:

Tallinna Tehnikaülikool

(54) Meetod CO_2 kõrvaldamiseks suitsugaasidest kaltsiumiühendeid sisaldavate tööstusheitmete toimel

(57) Leiutis käsitleb meetodit CO_2 kõrvaldamiseks suitsugaasidest kaltsiumiühendeid sisaldavate heitmete toimel Meetod hõlmab tahke tööstusheitme dispergeerimist vees, kaltsiumiühendite osalist lahustamist ning saadud vesisuspensiooni kontakteerimist CO_2 sisaldava suitsugaasiga. Meetod on eriline selle poolest, et see viiakse läbi kahes etapis, millest esimeses kontakteeritakse tööstusheitme vesisuspensiooni suitsugaasiga pH-vahemikus 10 kuni 12 ning teises etapis pH-vahemikus 7 kuni 8

(57) The present invention provides a method for eliminating CO_2 from flue gases by Ca-containing waste material, which includes dispersing the Ca-containing waste material in water in order to partially dissolve the Ca-compounds and contacting the resulting aqueous suspension with CO_2-containing flue gas, characterized in that in the first step the suspension is bubbled with flue gas keeping the pH levels in the range of 10-12 and in the second step keeping the pH levels in the range of 7-8

EE 05446 B1

ELULOOKIRJELDUS

1. Isikuandmed
   Ees- ja perekonnanimi   Olga Velts
   Sünniaeg ja –koht   29.11.1984 Tallinn
   Kodakondsus   Eesti

2. Kontaktandmed
   Aadress   Arbu 2-81, 13617, Tallinn
   Telefon   +372 5283756
   E-posti aadress   olga.velts@ttu.ee

3. Hariduskäik

Õppeasutus (nimetus lõpetamise ajal)	Lõpetamise aeg	Haridus (eriala/kraad)
Tallinna Tehnikaülikool	2007 -...	Keemia- ja materjalitehnoloogia, doktoriõpe
Tallinna Tehnikaülikool	2007	Tehnikateaduste magistrikraad (Cum Laude)
Tallinna Tehnikaülikool	2005	Tehnikateaduste bakalaureusekraad
Lasnamäe Vene Gümnaasium	2002	Keskharidus

4. Keelteoskus (alg-, kesk- või kõrgtase)

Keel	Tase
Eesti keel	Kõrgtase
Vene keel	Kõrgtase
Inglise keel	Kõrgtase
Saksa keel	Kesktase

5. Täiendusõpe

Õppimise aeg	Täiendusõppe läbiviija nimetus
19-23.09.2010	IEA GHG Student Mentoring Program (Holland)
2010, suvi	intensiivkursus"Mixing" Lappeenranta Tehnikaülikool (LUT; Soome)

2009-...	Doktorikool „Funktsionaalsed materjalid ja tehnoloogiad" (Tartu Ülikool ja Tallinna Tehnikaülikool)
2009, talv	Intensiivkursus "Multivariate Methods in Analytical Chemistry" (LUT; Soome)
2009, kevad	tarkvara "MODEST" omandamine (LUT; Soome)
2007-2009	Doktorikool „Uued tootmistehnoloogiad ja protsessid" (Tartu Ülikool ja Tallinna Tehnikaülikool)
2007, talv	intensiivkursus "Crystallization and Filtration" Lappeenranta Tehnoloogiainstituut (Soome)

6. Teenistuskäik

Töötamise aeg	Tööandja nimetus	Ametikoht
06.2007-...	Tallinna Tehnikaülikool, Anorg. materjalide teaduslaboratoorium	insener
2007 – 2008, suvi	Lappeenranta Tehnikaülikool, Separatsiooniprotsesside laboratoorium (Lappeenranta, Soome)	teaduri abiline
2006, suvi	Tervisekaitseinspektsioon (Tallinn, Eesti)	laborant
2005, suvi	VKG Oil AS (Kohtla-Järve, Eesti)	laborant

7. Kaitstud lõputööd

Magistritöö: Ligniini vesilahuse osoonimine. Tallinna Tehnikaülikool, 2007. Juhendaja: I. Kamenev

8. Teadustöö põhisuunad

Reaktsioonid ja muutused põlevkivituha baasil tekkivates heterogeensetes süsteemides: alused ning modelleerimine

9. Teised uurimisprojektid

SF0140082s08 Karbonaat- ja fosfaatpõhiste anorgaaniliste süsteemide keemia ja rakendused (2008 – 2013)
SF0142518s03 Anorgaaniliste mitmekomponentsete süsteemide keemia ja rakendused (2003 – 2007)
Lep7017 Põlevkivituhk kaltsiumkarbonaadi toormena (2007 – 2008)
ETF7379 Süsinikdioksiidi mineraliseerimisprotsesside modelleerimine (2008 – 2011)

CURRICULUM VITAE

1. Personal data

    Name   Olga Velts
    Date and place of birth   29.11.1984 Tallinn

2. Contact information

    Address   Arbu 2-81, 13617, Tallinn
    Phone   +372 5283756
    E-mail   olga.velts@ttu.ee

3. Education

Educational institution	Graduation year	Education (field of study/degree)
Tallinn University of Technology	2007-...	Chemical and Materials Technology, doctoral studies
Tallinn University of Technology	2007	M. Sc. in Engineering (Cum Laude)
Tallinn University of Technology	2005	B. Sc. in Engineering
Lasnamäe High School	2002	High school education (silver medal)

4. Language competence/skills (fluent; average, basic skills)

Language	Level
Estonian	fluent
Russian	fluent
English	fluent
German	average

5. Special Courses

Period	Educational or other organisation
19-23.09.2010	IEA GHG Student Mentoring Program (The Nederlands)
2010, summer	intensive course „Mixing" (LUT, Finland)
2009-...	Graduate school „Functional Materials and Processes" (University of Tartu and Tallinn University of Technology)
2009, winter	intensive course "Multivariate Methods in Analytical Chemistry" (LUT; Finland)

2009, spring	Course on modeling software „MODEST" (LUT; Finland)
2007-2009	Graduate school „New Production Technologies and Processes" (University of Tartu and Tallinn University of Technology)
2007, winter	intensive course "Crystallization and Filtration" (LUT; Finland)

6. Professional Employment

Period	Organisation	Position
2007-…	Tallinn University of Technology, Laboratory of Inorganic Materials (Estonia)	Engineer
2007- 2008, summers	Lappeenranta University of Technology, Laboratory of Separation Technology (Finland)	Researcher's assistant
2006, summer	Health inspection facility (Estonia)	Laboratory assistant
2005, summer	VKG Oil AS (Estonia)	Laboratory assistant

7. Defended theses

M. Sc. thesis: Ozonation of lignin aqueous solution. Tallinn University of Technology, 2007. Supervisor: I. Kamenev

8. Main areas of scientific work/Current research topics

Reactions and transformations in oil shale ash based heterogeneous systems: basics and modeling

9. Other research projects

SF0140082s08 Chemistry and applications of carbonate-phosphate-based inorganic systems (2008 – 2013)
SF0142518s03 Chemistry and applications of inorganic multicomponent systems (2003 – 2007)
ETF7379 Modeling of carbon dioxide mineralization processes (2008 – 2011)
Lep7017 PCC from oil shale ash (2007 – 2008)

DISSERTATIONS DEFENDED AT
TALLINN UNIVERSITY OF TECHNOLOGY ON
CHEMISTRY AND CHEMICAL ENGINEERING

1. **Endel Piiroja**. Oxidation and Destruction of Polyethylene. 1993.

2. **Meili Rei**. Lihatehnoloogia teaduslikud alused. Fundamentals of Food Technology. 1995.

3. **Meeme Põldme**. Phase Transformations in Hydrothermal Sintering Processing of Phosphate Rock. 1995.

4. **Kaia Tõnsuaadu**. Thermophosphates from Kovdor and Siilinjärvi Apatites. 1995.

5. **Anu Hamburg**. The Influence of Food Processing and Storage on the N-Nitrosamines Formation and Content in Some Estonian Foodstuffs. 1995.

6. **Ruth Kuldvee**. Computerized Sampling in Ion Chromatography and in Capillary Electrophoresis. 1999.

7. **Külliki Varvas**. Enzymatic Oxidation of Arachidonic Acid in the Coral *Gersemia fruticosa*. 1999.

8. **Marina Kudrjašova**. Application of Factor Analysis to Thermochromatography and Promotion Studies. 2000.

9. **Viia Lepane**. Characterization of Aquatic Humic Substances by Size Exclusion Chromatography and Capillary Electrophoresis. 2001.

10. **Andres Trikkel**. Estonian Calcareous Rocks and Oil Shale Ash as Sorbents for SO_2. 2001.

11. **Marina Kritševskaja**. Photocatalytic Oxidation of Organic Pollutants in Aqueous and Gaseous Phases. 2003.

12. **Inna Kamenev**. Aerobic Bio-Oxidation with Ozonation in Recalcitrant Wastewater Treatment. 2003.

13. **Janek Reinik**. Methods for Purification of Xylidine-Polluted Water. 2003.

14. **Andres Krumme**. Crystallisation Behaviour of High Density Polyethylene Blends with Bimodal Molar Mass Distribution. 2003.

15. **Anna Goi**. Advanced Oxidation Processes for Water Purification and Soil Remediation. 2005.

16. **Pille Meier**. Influence of Aqueous Solutions of Organic Substances on Structure and Properties of Pinewood (*Pinus sylvestris*). 2007.

17. **Kristjan Kruusement**. Water Conversion of Oil Shales and Biomass. 2007.

18. **Niina Kulik**. The Application of Fenton-Based Processes for Wastewater and Soil Treatment. 2008.

19. **Raul Järviste**. The Study of the Changes of Diesel Fuel Properties a its Long Term Storage. 2008.

20. **Mai Uibu**. Abatement of CO_2 Emissions in Estonian Oil Shale-Based Power Production. 2008.

21. **Valeri Gorkunov**. Calcium-Aluminothermal Production of Niobium and Utilization of Wastes. 2008.

22. **Elina Portjanskaja**. Photocatalytic Oxidation of Natural Polymers in Aqueous Solutions. 2009.

23. **Karin Reinhold**. Workplace Assessment: Determination of Hazards Profile using a Flexible Risk Assessment Method. 2009.

24. **Natalja Savest**. Solvent Swelling of Estonian Oil Shales: Low Temperature Thermochemical Conversion Caused Changes in Swelling. 2010.

25. **Triin Märtson**. Methodology and Equipment for Optical Studies of Fast Crystallizing Polymers. 2010.

26. **Deniss Klauson**. Aqueous Photocatalytic Oxidation of Non-Biodegradable Pollutants. 2010.

27. **Oliver Järvik**. Intensification of Activated Sludge Process – the Impact of Ozone and Activated Carbon. 2011.

28. **Triinu Poltimäe**. Thermal Analysis of Crystallization Behaviour of Polyethylene Copolymers and Their Blends. 2011.

29. **Mariliis Sihtmäe**. (Eco)toxicological Information on REACH-Relevant Chemicals: Contribution of Alternative Methods to *in vivo* Approaches. 2011.